



UNIVERSITÀ
DI SIENA 1240

University of Siena

Department of Molecular Medicine and Development

Doctoral Research in Molecular Medicine

XXXV Cycle

Coordinator Professor Vincenzo Sorrentino

**Retinopathy of Prematurity and Glaucoma: possible strategies to
prevent Neovascularization and Neurodegeneration**

SCIENTIFIC-DISCIPLINARY SECTOR: BIO/09

PhD Candidate

Martina Lucchesi

Martina Lucchesi

Tutor

Massimo Dal Monte

Academic Year 2022/2023

Abstract

A variety of pathological processes can disrupt the sophisticated and delicate retina architecture, leading to a broad-spectrum of vision-threatening diseases. Retinopathy of prematurity (ROP) is a multifactorial neovascular disease which causes perturbation of the physiological vascular development in the retina of preterm infants, often leading to blindness. ROP progresses in two phases. Of them, the second hypoxic-proliferative phase causes pathological hyper-vascularisation in the superficial plexus, causing functional impairments. Vascular endothelial growth factor (VEGF) plays a crucial role in promoting angiogenesis, both in physiological and in pathological conditions. A growing body of evidence is progressively highlighting the involvement of β -adrenoceptors (BAR) in VEGF production and retinal neovascularization.

Another pathological condition able to alter retinal architecture is glaucoma. Indeed, although the term glaucoma refers to a group of lifelong progressive optic neuropathies that differ cause, risk factors, demographics, symptoms, duration, treatment, and prognosis, the common features of all glaucoma forms are excavation (*cupping*) of the optic disc, apoptotic degeneration of retinal ganglion cells (RGC) and thinning of the nerve fibre layer (NFL). Glaucoma is the leading cause of irreversible blindness worldwide.

Here, we investigated the effects of hypoxia on BAR expression using human Müller cells, the major source of retinal VEGF and human retinal endothelial cells, the main receivers of VEGF within the retina. Subsequently, we tested the effects of BAR3 antagonism in hypoxic condition and/or nitric oxide synthase induction/blocking on VEGF production. We also evaluated the effects of BAR3 agonism/antagonism and BAR2 agonism in a murine model of oxygen-induced retinopathy (OIR) widely used to study ROP.

Then, we used a murine model of induced high-tension glaucoma to investigate the putative beneficial effects of an Achebuche (ACE) oil enriched diet against the deleterious consequences of glaucoma. In particular, within the retina of the model, we evaluated glia reactivity, the inflammatory status, the oxidative stress markers expression, the ischemic damage, the apoptosis activation, and RGC functionality.

List of scientific findings

ROP project:

- *In vitro* findings
- *In vivo* findings

Glaucoma project:

- The beneficial properties of Acebuche oil exert a retinoprotective effect in a murine model of high-tension glaucoma

Published manuscripts not included in the main thesis body:

- Neurosensory Alterations in Retinopathy of Prematurity: A Window to Neurological Impairments Associated to Preterm Birth. Lucchesi M, Marracci S, Amato R, Filippi L, Cammalleri M, Dal Monte M. *Biomedicines*. 2022;10(7):1603.
- HIF-1-Dependent Induction of β 3 Adrenoceptor: Evidence from the Mouse Retina. Amato R, Pisani F, Laudadio E, Cammalleri M, Lucchesi M, Marracci S, Filippi L, Galeazzi R, Svelto M, Dal Monte M, Bagnoli P. *Cells*. 2022;11(8):1271.
- *In vitro* models of retinal diseases. Lucchesi M, Marracci S. *Ann Eye Sci* 2022;7:9.

Index

Introduction

1. Retina structure
2. Retinopathy of prematurity
 - 2.1 A brief history
 - 2.2 Risk factors
 - 2.3 Physiological retinal vessels development
 - 2.3.1 Oxygen tension and VEGF production
 - 2.4 Pathogenesis of ROP
 - 2.5 BAR
 - 2.5.1 BAR and VEGF
 - 2.6 Principal ROP models
 - 2.6.1 OIR models
 - 2.6.2 In vitro models
3. Glaucoma
 - 3.1 A brief history
 - 3.2 Aqueous humour and glaucoma
 - 3.3 Optic nerve damage
 - 3.4 Classification
 - 3.5 Risk factors
 - 3.6 Principal glaucoma models
 - 3.7 Nutraceuticals and glaucoma

Aims

Results and discussion

1. ROP Project: *in vitro* findings
 - Overview
 - Outcomes
 - Conclusion
2. ROP Project: *in vivo* findings
 - Overview
 - Outcomes
 - Conclusion
3. Glaucoma Project
 - Overview
 - Outcomes
 - Conclusion

References

Acknowledgments

Appendix: Published manuscripts not included in the main thesis body

List of abbreviations

ACE = Acebuche
ACG = angle closure glaucoma
BAR = β adrenoceptors
BAR1 = β 1 adrenoceptor
BAR2 = β 2 adrenoceptor
BAR3 = β 3 adrenoceptor
cAMP = cyclic adenosine monophosphate
CO₂ = Carbon Dioxide
eNOS = endothelial nitric oxide synthase
GCL = ganglion cell layer
GFAP = glial fibrillary acidic protein
Gi = inhibitory G protein
GPCR = G protein-coupled receptor
GRK = G protein-coupled receptor kinases
Gs = stimulatory G protein
HBS = HIF-1 binding sequence
HIF-1 = hypoxia inducible factor 1
HIF-1 α = α subunit of HIF-1
HIF-1 β = β subunit of HIF-1
HO-1 = hemeoxygenase-1
HRE = hypoxia responsive element
hREC = human retinal endothelial cells
IBA-1 = ionized calcium-binding adapter molecule 1
IL-6 = interleukin 6
IL-10 = interleukin 10
INL = inner nuclear layer
iNOS = inducible nitric oxide synthase
IOP = intraocular pressure
IPL = inner plexiform layer
KO = knock out
LGN = lateral geniculate nucleus
MAPK = mitogen-activated protein kinase
MCE = methylcellulose
MIO-M1 = Moorfields/Institute of Ophthalmology-Müller 1
mRNA = messenger ribonucleic acid
NFL = nerve fibre layer
NRF2 = nuclear factor erythroid 2-related factor 2
NF- κ B = nuclear factor kappa-light-chain-enhancer of activated B cells
nNOS = neuronal nitric oxide synthase
NOS = nitric oxide synthase
NQO1 = nicotinamide adenine dinucleotide phosphate quinone oxidoreductase 1
OAG = open angle glaucoma

oBRB = outer retinal blood barrier
OIR = oxygen induced retinopathy
ONC = optic nerve crush
OPL = outer plexiform layer
OPP = ocular perfusion pressure
P = post-natal day
PHD = prolyl hydroxylase domain
PKA = protein kinase A
RGC = retinal ganglion cells
RLF = retrolental fibroplasia
ROP = retinopathy of prematurity
RPE = retinal pigment epithelium
TNF α = tumour necrosis factor
VEGF = vascular endothelial growth factor
WT = wild type

Introduction

1. Retina structure

The retina is a delicate and sophisticated multilayer structure derived from the neuroectoderm, with a huge heterogeneity in cell components that form morphologically and functionally distinct circuits. These latter work in parallel and in combination, in order to produce a complex visual output (Hoon et al., 2014). Indeed, the retina exerts the critical function of receiving, modulating and transmitting visual stimuli coming from the external world to the optic nerve and, finally, to the visual cortex of the brain.

In the vertebrate retina, the photoreceptors, i.e. rods and cones, localize in the outer nuclear layer (ONL), differently from invertebrates' retinæ. Thus, light must traverse many layers before initiating signal transduction in rods and cones. Rods are very sensitive to light stimuli and, indeed, can detect even a single photon, allowing vision in the dim-light (Rieke, 2000). Cones account for about 5% of photoreceptors. The maximum cones density is observed into the rod-free region called foveola, responsible for very high visual acuity (Ahnelt, 1998). Cones are less sensitive to light compared to rods, but exhibit faster response kinetics during the process of phototransduction and are responsible for bright-light, high acuity colour vision (Hoon et al., 2014).

Photoreceptors outer segments are wrapped into the apical membrane extensions of retinal pigment epithelium (RPE) cells. RPE consists in a monolayer of cuboidal cells resting upon the underlying Bruch membrane, attached to the choroid. RPE is involved in many fundamental processes within the retina, such as providing nutrients to photoreceptors, phagocytosis and degradation of membrane disks of the photoreceptor outer segments, recycling of vitamin A, absorbance of stray light thanks to melatonin pigments and maintenance of the outer retinal blood barrier (oBRB) (Lakkaraju et al., 2020). Indeed, oBRB is composed by tight junctions between neighbouring RPE cells; moreover, the Bruch membrane separates the retina from the fenestrated choriocapillaries and gives a fundamental contribution in regulating traffic of nutrients from the blood flow to the photoreceptors, as well as in maintaining retinal adhesion (Cunha-Vaz et al., 2011).

In the outer plexiform layer (OPL), synapses between axons of the photoreceptor cells and dendrites of bipolar cells occur. Bipolar cells are neurons that connect the photoreceptors with the dendrites of retinal ganglion cells (RGC) in the inner layers (Kolb, 2005). These neurons form two functional subclasses: the bipolar cells that depolarize (ON) and those that, instead, hyperpolarize (OFF) in response to increments in light intensity. Rod bipolar cells are ON-bipolar cells while cone bipolar cells can either be ON or OFF (Hoon et al., 2014).

These layers made up the so-called outer retina, while the following ones account for the inner retina. In the inner nuclear layer (INL), we can find the cell bodies of Müller cells, the major glial components of the retina. We can also find amacrine and horizontal cells, that are laterally and vertically interconnecting neurons that can influence and integrate the signal (Bertalmío, 2020).

The axons of the bipolar cells connect to the dendrites of the RGC and amacrine cells in the inner plexiform layer (IPL). The ganglion cell layer (GCL) contains the nuclei of the RGC and displaced amacrine cells. RGC axons form the retinal nerve fibre layer (NFL) and converge to the optic nerve head. The same axons go on through the optic tract until they synapse with the neurons located in the lateral geniculate nucleus (LGN). Importantly, not all fibers from the optic tract synapse in the LGN: some of them connect with other nuclei situated in the midbrain, which are related to autonomic functions. From the LGN, the second neurons of the optic nerve send their axons to the visual cortex (De Moraes, 2013).

A variety of pathological processes can disrupt this delicate structure and lead to a broad-spectrum of retinal diseases. Indeed, retinal pathologies often result from a disruption of its sophisticated architecture and are among the most common causes of visual impairment and blindness (Pascolini et al., 2012). The first part of the work of this thesis focuses on Retinopathy of prematurity (ROP), a pathology which disrupts the superficial retinal vascular network, searching for new players that could contribute to neovascularization. The second part concentrates on prevention of the deleterious consequences of high-tension glaucoma on the retina, a condition that alters retinal structure starting from the excavation of the optic disk and leading to RGC death.

2. Retinopathy of prematurity

ROP is one of the main vision-threatening ocular disorders affecting infants born prematurely and the major cause of visual impairment in childhood (Quinn, 2016). The number of preterms affected by ROP has remarkably risen during the last few years. Particularly, 50% of extremely preterm infants show clinical signs of ROP, although this percentage varies widely. In 2008, it was estimated that more than 50,000 babies worldwide were blind due to ROP (Gilbert et al, 2008). Subsequent data suggests that this could have been an underestimation. Indeed, a study evaluated that in 2010 alone, approximately 185,000 preterm infants developed any form of ROP, and that more than 20,000 became blind because of it (Blencowe et al., 2010).

2.1 A brief history

ROP was first observed in a series of preterm infants in 1942 by Terry, who initially coined the term retrolental fibroplasia (RLF) to indicate it (Terry, 1942). He described it as an overgrowth of the developing retinal vessels which invade the vitreous and give rise to a fibrovascular white plaque behind the lens (Cook, 1957). The white appearance was due to retinal detachment (Terry, 1946). In those years, clinical studies by Wilson et al. (1942) found improved respiration rate in premature newborns who were given high oxygen concentrations (Wilson et al., 1942); therefore, the use of supplemental oxygen therapy for preterm babies became routine treatment (Miller, 1956). Together with this increase in the use of oxygen in neonatal care, however, a well-documented rise in the incidence of RLF occurred. In the mid-1950s, different clinical trials showed a significant decrease in the incidence of RLF by limiting the amount of inspired oxygen by premature infants; therefore, it was suggested that oxygen delivery might cause or worsen the disease (Campbell, 1951). Some years later a national multicentre clinical trial in the USA was able to demonstrate that limiting oxygen given to the preterm babies was essential for reducing the risk of development of the disease (Patz, 1957). Since then, controlling oxygen therapy has been the first-line preventative measure concerning this pathology which, successively, took the name of ROP (Bedrossian et al., 1954; Lanman, 1955).

2.2 Risk factors

So far, the greatest predictors for developing ROP are the low gestational age and the low birth weight. Indeed, ROP usually affects preterm infants born before the 31st week of gestation and with very low birth weight, meaning less than 1500 g. Consistently, the vast majority of severe ROP cases have been found in infants with lower gestational age and weight at birth (Quinn et al., 2018). In countries with high quality neonatal care, sight-threatening ROP is mainly confined to infants with birth weight <1000 g and is very rare in babies with birth weight >1250 g (Fielder et al., 2014).

Oxygen tension is a crucial factor in determining ROP initiation, since the vascularization in the human retina needs a physiologically hypoxic environment in order to properly develop (Hughes et al., 2000). Thus, the issue of the correct balance between (i) high oxygen supplementation in the early postnatal period to reduce the risk of life-threatening complications and (ii) lower oxygen to prevent ROP development is critical (Aguilar et al., 2008; Hellstrom et al., 2013; Askie et al., 2018).

2.3 Physiological development of retinal vessels

The mature retina is supplied by two different vascular systems. Particularly, the central retinal artery enters the eye through the centre of the optic nerve and then branches through the inner retina to form three capillary layers. On the other hand, the avascular photoreceptor layer relies on the choriocapillaris lying beneath the RPE to supply oxygen by diffusion. (Netter, 2006).

In human beings the process of inner retinal vasculature development occurs primarily during the latter half of gestation; indeed, it starts in utero by about the 16th week of gestation and is completed by approximately the 40th week of gestation, right before birth. Prior to the formation of the definitive retinal vasculature, a transient network of vessels, called the hyaloid vascular system, develops to nourish the still immature lens (Penn et al., 2008). The hyaloid vasculature originates from the central hyaloid artery, and it runs from the centre of the optic disc, through the vitreous, to the posterior lens and drains into the choroidal veins. The regression of hyaloid vasculature begins approximately by the 13th week of gestation and the concomitant formation of the superficial (or primary) plexus starts around the 16th week of gestation, at the NFL/GCL interface. The superficial plexus emerges from an existing capillary ring located at level of the optic nerve head and spreads across the inner surface of the retina in four main lobes. The superficial plexus reaches the retinal periphery nasally at the 36th week and temporally around the 40th week of gestation (Selvam et al., 2018). Astrocytes provide a template serving as a scaffolding guide to form retinal vessels of the superficial plexus (Dorrel et al., 2002; Penn et al., 2008; Mezu-Ndubuisi et al., 2020). Indeed, the embryonic and foetal vascular development depends on the modulation of a series of proangiogenic factors, such as vascular endothelial growth factor (VEGF); astrocytes do express VEGF, which promotes endothelial cell proliferation and migration within this superficial plane (Stone et al., 1995). The “physiologic hypoxia” created by the increasing metabolic demands of the developing neural components of a largely avascular retina is the driving mechanism for VEGF overexpression and, therefore, angiogenic growth. This results in angiogenic sprouting from the superficial vessel network and, thus, the development of an additional plexus, called the deep plexus. In the human foetus, the deep plexus starts to form by the 25th–26th week of gestation, and it is located at the border of the INL/OPL (Penn et al., 2008). Müller glial cells are believed to guide the growth of this plexus (Stone et al., 1995). The deep plexus penetrates the retina and establishes two networks on either side of the INL; the one located at the border INL/IPL is called intermediate plexus and forms last (Selvam et al., 2018; Fu et al., 2020). Increased blood vessel growth and capillary density relieves the physiologic hypoxia, matching tissue oxygen demand to vessel formation. In normoxia, VEGF is produced by retinal cells at a level adequate to support existing blood vessels (Penn et al., 2008). Particularly, in physiological

conditions, Müller cells provide a permanent antiproliferative environment for retinal vascular endothelial cells, exerting an angiostatic effect (Eichler et al., 2004).

2.3.1 Oxygen tension and VEGF production

Vascular growth is closely regulated by supply and demand of oxygen. This mainly depends on the activity of hypoxia-inducible factor 1 (HIF-1) (Wang et al., 1995). HIF-1 is a transcription factor that binds DNA on specific hypoxia responsive element (HRE), thereby promoting the expression of hundreds of genes involved in the processes of metabolic adaptation to oxygen scarcity (Hammarlund et al., 2020). HIF-1 is composed by two subunits: the α subunit (HIF-1 α) and the β subunit (HIF-1 β) (Wang et al., 1995). Both of these subunits are constitutively expressed, and only HIF-1 α is sensible to oxygen pressure level. Indeed, prolyl hydroxylase domain (PHD) proteins are able to hydroxylate HIF-1 α but they require the presence of molecular oxygen to exert their catalytic activity. Prolyl hydroxylated HIF-1 α is recognized by the von Hippel-Lindau tumour suppressor, ubiquitinated and then degraded by proteasome (Maxwell et al., 1999). On the other hand, in hypoxic conditions, i.e. when molecular oxygen levels are low, PHD cannot hydroxylate HIF-1 α , resulting in the rescue of HIF-1 α from proteolytic degradation. Therefore, HIF-1 α complexes with HIF-1 β , forming dimeric HIF-1. This latter translocates into the nucleus where it can bind DNA as a heterodimer (Yang et al., 2021).

Among the several genes HIF-1 promotes the expression of, there is VEGF, one of the main targets of this transcription factor. VEGF plays a crucial role in promoting angiogenesis as an adaptive response to low oxygen availability, since its expression results in local formation of new blood vessels starting from pre-existing ones (Elen et al., 2020). On the other hand, high oxygen tension suppresses hypoxia-induced VEGF production because of destabilization of HIF-1 α ; lower levels of VEGF result in reduced blood vessel growth (**Figure 1**).

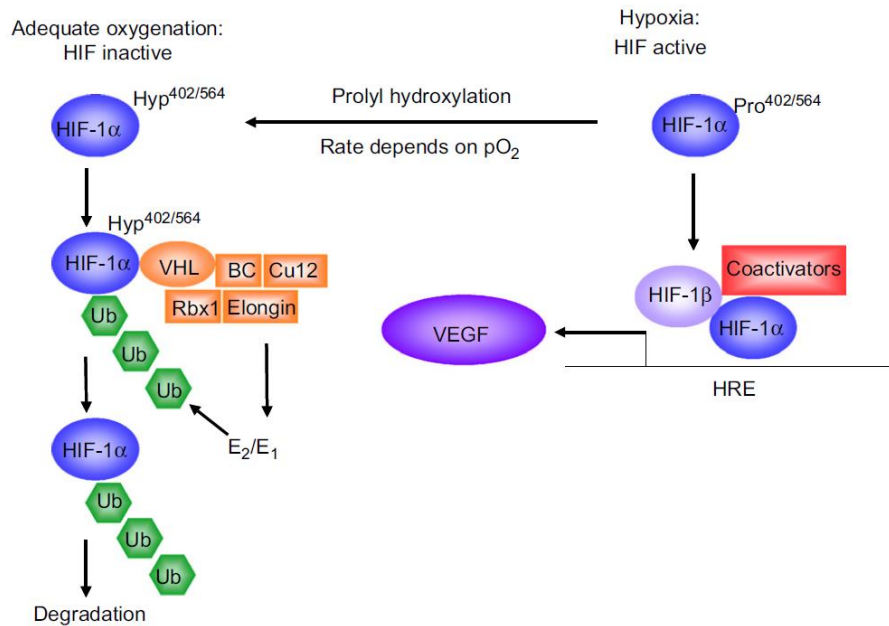


Figure 1. Hypoxia-induced factor 1 (HIF-1) α pathway. In normoxic conditions, HIF-1 α is hydroxylated on a proline residue and von Hippel-Lindau tumour suppressor binds it. This results in ubiquitin attachment and proteasomal degradation. In hypoxic conditions, HIF-1 α dimerizes with HIF-1 β leading to transcription of hypoxia-inducible genes, such as vascular endothelial growth factor (VEGF) (Penn et al., 2008).

2.4 Pathogenesis of ROP

Oxygen-dependent angiogenesis acquires deeper relevance in tissues characterized by elevated oxygen consumption levels, as the case of the retina. If, on one hand, hypoxia-triggered angiogenesis is necessary and fundamental for the development of the definitive retinal vascularization, on the other hand it is also implied in the pathogenesis of proliferative retinopathies, such as ROP (Usui et al., 2015). ROP is a vision-threatening retinal disorder that involves cessation of normal retinal vascular development in the preterm infant, with the instauration of pathological compensatory mechanisms that result in aberrant neovascularization of the retina.

The retina is one of the last organs to be vascularized in the human foetus. In physiologic conditions the process of retinal vascular development occurs within the hypoxic uterine environment (Hughes et al., 2000) where the mean oxygen pressure is less than 50 mmHg during the second half of pregnancy (Nicolaidis et al., 1989); nevertheless, in the case of prematurely born infants it must occur in the relatively hyperoxic extra-uterine environment (Penn et al., 2008). This rise in oxygen pressure triggers the first one of the two ROP phases, called hyperoxic-ischemic phase. Following the premature birth, relative hyperoxia causes suppression of different angiogenesis promoting factors, such as VEGF, leading to retinal vessel growth cessation and vaso-obliteration. This results in the formation of a peripheral avascular area within the human retina (Wood et al., 2021). The second

phase of ROP, called hypoxic-proliferative phase, begins when the poor and incomplete retinal vascularization cannot meet anymore the increasingly metabolically demand of the developing neural retina. This imbalance results in pathological hypoxia and increased release of pro-angiogenic factors, such as VEGF, which promote neovascularization. In contrast to physiological vasculature, these pathological neovessels exhibit excessive, uncontrolled and misdirected growth, with tufts presence and hemorrhages. They poorly perfuse the retina and are leaky, causing plasma extravasation. Eventually, they invade the vitreous. This can result in a fibrous scar, partial or complete retinal detachment and, respectively, partial or complete blindness (Cavallaro et al., 2014).

The aggressiveness of ROP depends on the retinal area progressively affected by aberrant proliferating neovessels, on the vascularization stage (classified from stage 1 to 5), and on the presence of dilatation and tortuosity of the vessels (ROP plus disease). Particularly, from a clinical point of view, stages 1, 2 and 3 describe the acute phases of the disease, while stages 4 and 5 are considered aggressive ROP (**Figure 2**) (Chiang et al., 2021).

- Stage 1 is characterized by the formation of a white, thin and flat demarcation line between the vascular and the avascular zones of the retina.
- In stage 2, the flat demarcation line evolves in a ridge whose thickness can vary. Its colour can range from white to pink. Small, isolated tufts lying on the retina surface can be observed posterior to the ridge.
- In stage 3 extraretinal neovascular proliferation arise towards the vitreous.
- Stage 4 aggressive ROP is characterized by partial retinal detachment, which may either spare or involve the fovea. Stage 4 can be exudative or tractional. In the first situation, partial detachments look convex, sometimes localized, and self-limited. In the second case, partial detachments are associated with progressive fibrovascular organization and vitreous haze. They might be associated with lipid and/or subretinal haemorrhages.
- Stage 5 describes total retinal detachment (Chiang et al., 2021).

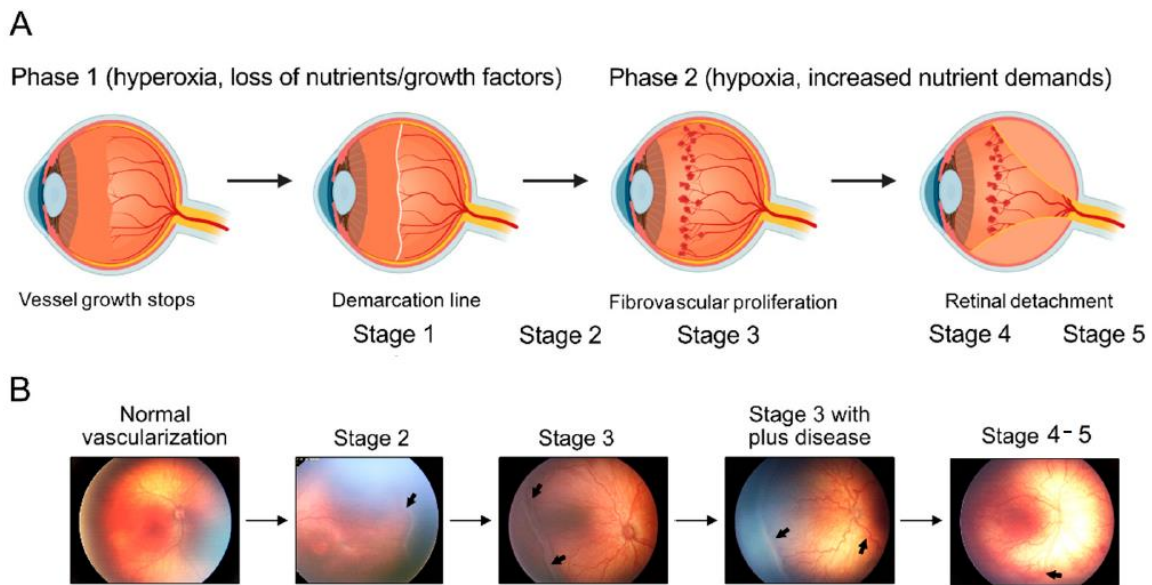


Figure 2. Progression of retinopathy of prematurity (ROP). (A) Loss of essential nutrients and pro-angiogenic growth factors after birth, possibly in combination with oxygen supply, leads to hyperoxia that suppresses retinal vascularization (Phase 1). In the second phase of ROP (Phase 2), relative hypoxia and increased nutrient demands of the mainly avascular retina cause fibrovascular proliferation. ROP anatomic changes begin with the appearance of a demarcation line between the vascular and the avascular area (stage 1), which gets thick and at this point is called ridge (stage 2); extraretinal fibrovascular proliferation occurs (stage 3) resulting in partial retinal detachment (stage 4) and complete retinal detachment (stage 5). (B) ROP progression, from normal retinal neuro-vascular development, via stage 2 with ridge (arrow), stage 3 characterized by neovascularization and haemorrhages (arrows), stage 3 with plus disease (arrow) and retinal detachment which occurs in stage 4-5 (modified from Tomita et al., 2021).

The rate of progression towards the most severe stages of the disease has been reported to be approximately a quarter of ROP infants (Chang, 2019; Filippi et al., 2019; Prakalapakorn et al., 2021). Most of the ROP cases regresses spontaneously through a process of involution/evolution from a vasoproliferative disease to a fibrotic phase (International Committee for the Classification of Retinopathy of Prematurity, 2005). Particularly, spontaneous regression of ROP and/or complete vascularization of the retina might occur by 40–45th week of postmenstrual age or 3 to 4 months after birth (Dogra et al., 2017). The more advanced or the more posterior the active disease, the worse the fibrotic cicatricial sequelae, as the disease enters the so-called “cicatricial phase” (International Committee for the Classification of Retinopathy of Prematurity, 2005).

Despite either the spontaneous regression or even effectiveness of treatments, many children with a clinical history of ROP experience persistent vision impairment, such as astigmatism and myopia (O’Connor et al., 2002), reduced visual acuity and deficient subtle colour vision (Pétursdóttir et al., 2019), constricted visual field and contrast sensitivity (Hansen ad Fulton, 2000), and increased dark-adapted thresholds (Bowl et al., 2019) along with structural abnormalities (Fielder et al., 2014). The

patients who underwent vitrectomy either initially or later in ROP progression have poor post-operative visual acuity and can also experience retinal re-detachment, besides the high care costs (Terasaki et al., 2003). Anti-VEGF drugs proved to be effective in counteracting neovascularization in ROP; however, VEGF and its receptors play an important role in the development of the neural retina, and potential adverse effects of anti-VEGF drugs cannot be excluded on developing neurons in the immature retina (Penn et al., 2008). Therefore, there is an urgent need to develop diverse approaches which can prevent ROP blindness. In this sense, β -adrenoceptors (BAR) have recently risen more and more attention.

2.5 BAR

BAR belong to the 7-transmembrane family of receptors. They are guanine nucleotide regulatory protein (G protein) coupled receptors (GPCR) and mediate many effects of the endogenous catecholamines adrenaline and noradrenaline (Wachter et al., 2012). To date three subtypes of BAR have been identified: BAR1, BAR2 and the last discovered member of this receptor family, BAR3. The first two subtypes of BAR are encoded by two distinct intronless genes located, respectively, on human chromosomes 10q24-26 and 5q31-32 (Dixon et al., 1986; Kobilka et al., 1987; Yang-Feng et al., 1990). The human gene encoding human for BAR3 receptor subtype was cloned for the first time in 1989, and it is localized on chromosome 8p11-12 (Emorine et al., 1989).

BAR1 and BAR2 subtypes couple primarily to the stimulatory G protein (Gs) to induce adenylyl cyclase signal transduction pathways. Adenylyl cyclase catalyses the conversion of adenosine triphosphate to the second messenger cyclic adenosine monophosphate (cAMP), which in turn binds to the regulatory subunits of protein kinase A (PKA), resulting in the release of the active catalytic PKA subunits. PKA phosphorylates serine and threonine residues on a variety of proteins, thereby affecting a wide spectrum of molecular pathways (Wachter et al., 2012). PKA activity can be either increased or reduced by oxygen deprivation in different experimental models. Particularly, in hypoxic mouse retina explants and mouse hypoxic retinae, PKA activity results decreased (Martini et al., 2011). In hypoxic retinae BAR3 can also modulate PKA activity; indeed, BAR3 blockade increases its activity (Martini et al., 2011), while BAR3 pharmacological activation has no effect on its phosphorylation level (Dal Monte et al., 2015). Although most functions of BAR2 are mediated through Gs proteins and the cAMP-dependent PKA system, BAR2 can also couple to G inhibitory (Gi) proteins (Daaka et al., 1997) resulting in stimulation of the extracellular signal-regulation kinase and p38 mitogen-activated protein kinase (MAPK) pathways. Activation of MAPK pathway by BAR2 requires the receptor to be phosphorylated by PKA. This mechanism might serve to uncouple

BAR2 from Gs and, therefore, can represent a means of terminating BAR2 signal and response (Johnson, 2006). Similarly, BAR3 is not coupled only to Gs proteins, but also to Gi ones (Schena et al., 2019). Gi proteins activation mediated by BAR3, rather than inhibit adenylyl cyclase, activates nitric oxide (NO) synthesis pathway, both through the endothelial nitric oxide synthase (eNOS) (Rozec et al., 2006) and the inducible nitric oxide synthase (iNOS) (Dal Monte et al., 2014).

GPCR can be desensitized, meaning uncoupled from G proteins. This desensitization process depends on receptor phosphorylation, which happens at the phosphorylation sites (serine and threonine residues) in the C-terminal tails. This phosphorylation can be induced by several kinases, including GPCR kinases (GRK) (Reiter et al., 2006). Of them, GRK2 is deeply involved in BAR desensitization (Hansen et al., 2006). GPCR desensitization is a protective mechanism against excessive sympathetic transmission that initiates with the phosphorylation of multiple serine residues by kinases and involves the coordinated action of β -arrestins and GRK (Tsao et al., 2000). In fact, GRK-mediated phosphorylation of GPCR results in a receptor conformational change. This creates a high-affinity binding site for β -arrestin1 and β -arrestin2, two distinct members of the four-member protein family of arrestins (Noor et al., 2011; Reiter et al., 2006). β -arrestin1 and β -arrestin2 bind to BAR1 and BAR2, therefore regulating their desensitization. Notably, they play a crucial role especially in BAR2 desensitization (Hall 2004), with β -arrestin2 more efficiently involved than β -arrestin1 (Kohout et al., 2000).

Interestingly, the phosphorylation sites on the C-terminus are absent on BAR3 (Emorine et al., 1989). In fact, β -arrestins are able to act on BAR1 and BAR2, but not on BAR3 that, consequently, is resistant to short-term agonist-induced desensitization (Liggett et al., 1993; Hall, 2004). In a similar way, BAR1 (Freedman et al., 1995) and BAR2 (Hausdorff et al., 1989), but not BAR3 (Strosberg, 1997), can be phosphorylated by PKA, leading to feedback desensitization of BAR signalling (Freedman et al., 1996).

2.5.1 BAR and VEGF

The earliest information regarding the role of BAR in hypoxia-induced neovascularization originates from the fortuitous demonstration that the progression of infantile hemangiomas is efficiently reduced by treatments with propranolol, an unselective BAR1 and BAR2 antagonist (Léauté-Labrèze et al., 2008). The powerful antiangiogenic effects of propranolol aroused interest regarding the putative involvement of the BAR system in the pathogenesis of other human neonatal disorders characterized by angiogenic processes triggered by hypoxia, like the second phase of ROP. The great similarities between the pathogenesis of infantile hemangiomas and ROP, including the role played by hypoxia-

induced proangiogenic factors, encouraged to explore the effect of a treatment with propranolol also for reducing ROP progression. Studies in C57BL/6J oxygen-induced retinopathy (OIR) mice (see the section 2.6.1 “OIR models” for more details about this animal ROP model) revealed that, during the hypoxic-proliferative phase of ROP, there is an upregulation of noradrenaline (Dal Monte et al., 2012), which was already known to stimulate VEGF production *in vitro* (Guo et al., 2009; Yang et al., 2009). Interestingly, BAR blockade with propranolol downregulates VEGF and reduces the proangiogenic effects of hypoxia, while exerting no effects on normoxic tissues (Ristori et al. 2011). Particularly, these data revealed that propranolol reduces VEGF upregulation through destabilization of HIF-1 α (Ristori et al., 2011). Moreover, BAR1/BAR2 knock-out (KO) OIR mice displayed almost complete protection from retinal neovascularization induced by hypoxia (Dal Monte et al., 2015), suggesting a major role of one or both of these subtypes in hypoxia-driven retinal neovascularization. Nonetheless, the efficacy of propranolol treatment appears to be attributable to BAR2 blockade alone rather than to BAR1 antagonism. Indeed, BAR2 selective blockade with ICI 118,551 or desensitization after prolonged isoproterenol administration mimic the effects of propranolol in OIR mice, reducing VEGF upregulation and retinal neovascularization in response to hypoxia (Martini et al., 2011; Dal Monte et al., 2012). On the other hand, BAR1 selective blockade with atenolol does not result in VEGF reduction, suggesting a major role of BAR2 in hypoxia-induced retinal angiogenesis (Martini et al., 2011). In line with this, it has been reported that BAR2 antagonism prevents VEGF upregulation via BAR2/HIF-1/VEGF axis in human pancreatic tumour cells (Shan et al., 2013). Based on the encouraging preclinical results regarding propranolol efficacy in reducing neovascularization, either when systemically or topically administered (Ristori et al., 2011; Dal Monte et al., 2013), the efficacy and the safety of this drug was tested in human preterm newborns. Unfortunately, propranolol systemic administration results to be not sufficiently safe in human infants (Filippi et al., 2013). However, propranolol 0.2% eye micro-drops formulation shows an optimal safety and tolerability profile and efficiently counteracts ROP progression (Filippi et al., 2017; Filippi et al., 2019). Another trial with propranolol 0.4% eye micro-drops is planned (EudraCT number 2021-000131–31). It is noteworthy that propranolol seems also to exert a neuroprotective effect in human patients (Filippi et al., 2022a and references therein). Propranolol exerts protective effects only if administered during the second hypoxic-proliferative phase when VEGF is upregulated and supports neovascularization, and not during the first, hyperoxic-ischemic phase, when VEGF levels are extremely low. Contrarily, in this situation, it leads to the development of a dramatically severe ROP. This might be due to a BAR-blockage dependent further reduction of VEGF during the ischemic phase when, on the contrary, an increase of VEGF would be needed (Filippi et al., 2019).

The efficacy of propranolol administered in the second phase of ROP in reducing the progression of the disease is about 60% (Kaempfen et al., 2018; Strizke et al., 2019; Kong et al., 2021). Given the high percentage of non-responding patients (40%), it is allowed to wonder whether only BAR1 and BAR2 are implicated in ROP neovascularization, or whether other receptors activated by noradrenaline increase could be involved in hypoxia-induced neovascularization (Filippi et al., 2015; Filippi et al., 2022a).

In this respect, it is important to notice that, of the three isoforms of BAR, BAR3 is the only one responsive to oxygen tension within the mouse retina. Indeed, in the retinae of OIR mice, hypoxia results in BAR3 mRNA (Amato et al., 2022) and protein (Ristori et al., 2011; Amato et al., 2022) overexpression, highly localized to engorged vascular tufts of the inner capillary network; on the other hand, BAR1 and BAR2 display no changes in protein nor mRNA levels (Ristori et al., 2011). It has been recently identified a HIF-binding site (HBS), defined as HBS#1, on the mouse *Adrb3* gene that could account for *BAR3* mRNA upregulation in mice (Amato et al., 2022). Interestingly, HBS#1 is located in corresponding regions in the human and mouse *ADRB3* genes (Amato et al., 2022). This suggest that, in human as well as in mouse, *BAR3* mRNA could be regulated by hypoxia through a HIF-1 dependent way. In this respect, it was recently shown that pharmacological abolishment of hyperoxia-induced HIF-1 α degradation prevents not only VEGF, but also BAR3 downmodulation in mice (Amato et al., 2022).

On the other hand, in both humans and mouse (and also in rat), BAR3 protein shows 7 to 8 proline residues, which are hydroxylated in normoxia and stabilized by hypoxia (Dal Monte et al., 2020). This, together with the translation of the increased level of mRNA, and its possible regulation by HIF-1 α (Amato et al., 2022) could explain why BAR3 protein is remarkably upregulated by hypoxia in the mouse retina (Ristori et al., 2011; Amato et al., 2022) and leaves open the possibility to observe such an effect in the human expression level of this receptor. Moreover, differently from mouse, the human *ADRB3* gene displays a canonical HRE localized at position 3546 relative to the transcription start site (Dal Monte et al., 2020). This corroborates the hypothesis that also human *BAR3* mRNA expression level could be modulated by oxygen deprivation.

Furthermore, a recent study in murine lymphocytes demonstrated that restoring normoxic condition following hypoxic treatment reduces upregulated BAR3 protein level to normoxic control (Calvani et al., 2019). This suggests an overall responsiveness to oxygen fluctuations by this receptor that does not exist only within the retina.

BAR3 has a role in VEGF production. Indeed, BAR3 signalling stimulates Gi proteins, resulting in eNOS and iNOS activation and thus promoting the synthesis of NO (Rozec et al., 2006; Dal Monte et al., 2014). NO, in turn, is an important modulator of VEGF expression (Ziche et al., 2009). BAR3

regulation of VEGF mediated through NO has been demonstrated in mouse retinal explants (Dal Monte et al., 2013), murine melanoma cells (Dal Monte et al., 2014), human umbilical vein endothelial cells (Bueno-Pereira et al., 2022) and the endothelium of human coronary arteries (Dessy et al., 2004).

Nevertheless, in OIR mice the selective BAR3 antagonist SR59230A is not effective in reducing retinal neovascularization (Martini et al., 2011), even though BAR3 activation with BRL37344 during the hypoxic-proliferative phase in both wild type (WT) and BAR1/BAR2 KO OIR mice results in enhanced neovascular responses, with increased levels of VEGF (Dal Monte et al., 2015). This is in line with the fact that BAR3 activation requires higher concentrations of catecholamines compared to BAR1 and BAR2 and that, therefore, BAR3 mediated response can be appreciated when BAR1 and BAR2 mediated effects are diminished (Gauthier et al., 2000; Yang et al., 2019) or when BAR3-signalling is potentiated by hypoxia-dependent BAR3 overexpression. To sum up, the role of BAR3 in VEGF production and its contribution to retinal neovascularization is still under debate.

However, considering that HIF-1 α , BAR3 and catecholamines as noradrenaline are concomitantly activated in different hypoxic contexts, including the intrauterine environment, it is legitimate to speculate that an early exposure to relative hyperoxia at birth might induce vascular regression through a coordinated action of these three players (Filippi et al., 2022a).

2.6 Principal ROP models

At the present day, different ROP models exist. Here, the most commonly used one will be briefly summarized, starting from the well-known *in vivo* ones and presenting the *in vitro* ones.

2.6.1 OIR models

Ashton et al. were among the first researchers to investigate the effect of changing oxygen tension on retinal vascular development in kittens, realizing a first model of OIR. Particularly, OIR was obtained in kittens using 40% oxygen (Ashton et al., 1953; Ashton et al., 1954). Kitten retinal vascular development shows similarities to the human one (Flower et al., 1985); however, this model has some important disadvantages such as costs and problems regarding reagents availability. Rabbits were used to study ROP, as well; nevertheless, rabbit retinal vessels are limited to a small area and do not mimic the retinal vascular human development (Madan et al., 2003). Regarding the first attempts to create an OIR model in rodents, it was noticed that, differently from kittens, in mice 70% oxygen was insufficient to appreciate the induction of retinopathy (Bischoff et al., 1983). Indeed, at least 80%

oxygen was necessary to obtain a suitable model (Patz et al., 1953). This data led to the generalization that OIR model can only be reliably and effectively reproduced using near complete oxygen saturation level (Gole et al., 1990). Several subsequent advancements, as improved retinal vascular imaging, and a better understanding of the angiogenetic process, paved the way for establishing a more rigorous and reliable mouse model of OIR, up to the one described by Smith et al (1994). Nowadays, this latter is the most exploited *in vivo* model to study ROP. This model depicted in **Figure 3** exploits the plasticity of neonatal mouse retinal blood vessels. Indeed, in rodents the hyaloid system regresses 2 or 3 weeks postnatally, coinciding with the period of retinal definitive vascular system development (Penn et al., 2008). Indeed, in C57Bl/6 mice, the superficial vascular plexus forms during the first week after birth by radial outgrowth of vessels, from the optic nerve towards the periphery, reaching the retinal borders around postnatal day 8 (P8). From P7 onward, the superficial capillaries start sprouting vertically to form first the deep and subsequently the intermediate vascular plexi. The deep plexus reaches the retinal periphery by approximately P12, while the intermediate plexus reaches it by P12-P15. By the end of the third postnatal week, all the three vascular plexi are fully mature and it is possible to appreciate multiple interconnecting vessels between them (Stahl et al., 2010).

The immature retinal blood vessels undergo regression when the animal is exposed to high oxygen concentrations. Particularly, in this model, in order to mimic the hyperoxic-ischemic phase of ROP, mice pups are placed to 75% oxygen pressure at P7, when there is an optimal balance between the regression of hyaloid vessels and immature retinal vasculature development (Ashton et al., 1970; Smith et al., 1994). Hyperoxia in murine OIR model leads to obliteration of central retinal vessels while ROP in premature babies results from the failure of vascularization of the peripheral retina (Aguilar et al., 2008; O'Bryhim et al., 2012). Loss of vessels correlates with the concentration of inhaled oxygen (Claxton et al., 2005; Lange et al., 2009). In contrast to the central loss of retinal capillaries, the peripheral vascular network (though decelerated) continues to spread centrifugally (Lange et al., 2009). Mice pups are let in this hyperoxic chamber for five days, after which, at P12, they are returned to normal room air. This latter is perceived as a hypoxic condition by the retina, partially because of the previous condition of hyperoxia and partially because of the inadequate vascular supply. This situation, which resembles the second phase of ROP, leads to retinal tissue ischemia and hypoxia, which results in increased levels of hypoxia-induced growth factors, including VEGF, that stimulate abnormal neovascularization at the junction between vascularized and avascular areas (Smith et al., 1994; Liu et al., 2017). These neovessels are hyperpermeable and protrude into the vitreous. Neovascularization level reaches its peak at P17. After P17, aberrant neovascularization

spontaneously starts to regress in a gradual way, and it completely disappears by about P25 (Smith et al., 1994; Connor et al., 2009).

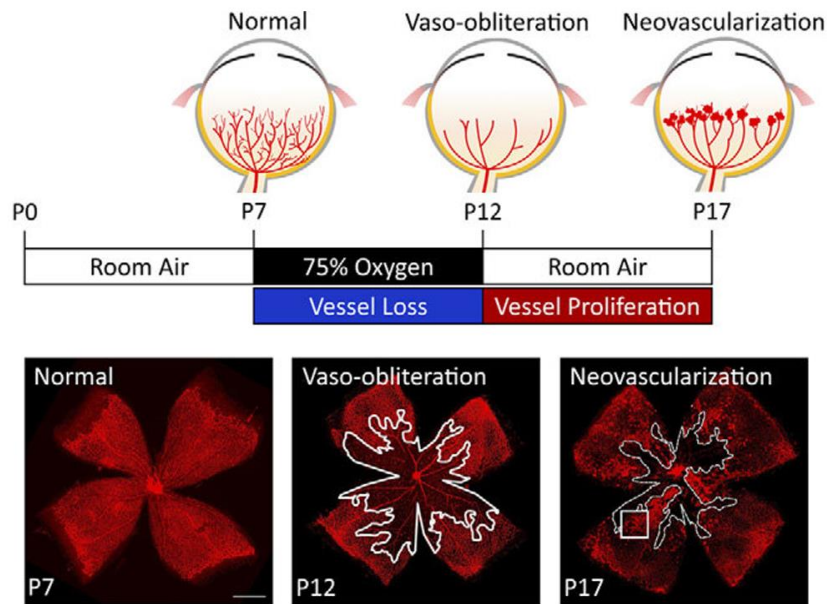


Figure 3. Mouse model of OIR. (A) Schematic representation of the mouse OIR procedure. Mice pups and their mother are exposed to 75% oxygen from P7 to P12. Hyperoxia suppresses the development of the retinal vasculature and leads to obliteration of the existing immature retinal vessels, which results in a central avascular zone. At P12, mice are returned to room air, and the relative hypoxia triggers neovascularization. The levels of neovascularization reach maximum severity at P17. (B) Images of retinal flat mounts with isolectin staining in the normoxic and OIR retinas showing the normal retinal vasculature at P7, vaso-obliteration at P12 (the avascular area is indicated with white outline), and pathologic neovascularization at P17 (the vessel avascular area is highlighted with white dashed line). Scale bar, 1 mm (Liu et al., 2017).

A similar *in vivo* model of ROP is represented by rat OIR. Rat retinal development follows a pattern similar to the human one. The retinal vasculature derives from mesenchymal precursor cells of the hyaloid artery, and vascularization starts at the optic disk and spreads until vessels reach the retinal periphery. In rat this process is completed by about P15 (Barnett et al., 2013). The rat OIR model was established in 1990, when Ricci showed that exposing new-born rats (P0) to 80% oxygen level and then to 40% oxygen tension causes more pronounced neovascularization rather than keeping rat pups under constant 80% oxygen (Ricci, 1990). Later, it was discovered that the exposure to alternative daily hyperoxia (50% oxygen pressure) and hypoxia (10% oxygen pressure) cycles for two weeks, followed by 6 days at room air results in higher level of neovascularization compared to the 80/40% oxygen model (Vähätupa et al., 2020). In the rat OIR model, like in humans, the retinal peripheral vessels are obliterated upon neonatal exposure to hyperoxia (Aguilar et al., 2008).

However, although the rat model of OIR produces a more human-like pathology, the mouse model of OIR is the most widely used model to mimic ROP, as it very closely recapitulates the pathologic events that occur in ROP (Aguilar et al., 2008).

In rodent OIR models, lactating mothers are exposed to oxygen variation together with their pups, so they can feed them. Occasionally, mothers expire because of oxygen toxicity but this problem can be solved letting them at normal oxygen tension for 5-10 minutes every day. However, they usually get stressed after OIR protocol and they can even eat their next litter.

Notably, the OIR model is commonly used to study angiogenesis in general, not only retinal vessel development (Selvam et al., 2018 and references therein).

2.6.2 *In vitro* models

Continuous and primary *in vitro* cultures are largely used to study cellular mechanisms occurring in several pathologic-like conditions as ROP. Due to the relevance of VEGF in ROP disease progression, human Müller cells (MIO-M1) and hREC can be very useful to study ROP. Indeed, Müller glial cells are the major VEGF producer within the retina, particularly during hypoxia (Pierce et al., 1995; Kaur et al., 2008) while, on the other hand, retinal endothelial cells are the main VEGF receivers, even though they are also able to produce it (Tugues et al., 2011). MIO-M1 cells represent a continuous (or stabilized) cell line isolated from healthy human retina which behave like human Müller glia (Limb et al., 2002). Instead, hREC represent a primary human cell line which is a mixture of venous and arterial cell populations (Su et al., 1992).

These two *in vitro* species can be useful tools to investigate the physiological and pathological events that occur within the retina under the different phases of ROP progression. Indeed, the hyperoxic phase of the pathology can be mimicked maintaining these cells at 75% oxygen and 5% carbon dioxide (CO₂). On the other hand, ROP hypoxic phase can be mimicked maintaining cells at 1% oxygen and 5% CO₂. Viability assays and various molecular analyses can be performed after 24h exposure to altered oxygen tension.

3. Glaucoma

The term glaucoma refers to a wide group of lifelong progressive optic neuropathies that differ in their cause, risk factors, demographics, symptoms, duration, treatment, and prognosis (Jonas et al., 2017). The common features of all glaucoma forms are excavation or *cupping* of the optic disc,

apoptotic degeneration of RGC and thinning of the NFL. The so-damaged optic nerve sends signals from the eyes to the brain resulting in patch loss of vision, usually starting from peripheral vision. Glaucoma progressively affects also central vision and narrowing of vision is a symptom that can occur in both eyes (Flaxman et al., 2017; Kishore et al., 2020). At the present, glaucoma is the leading cause of irreversible blindness worldwide (Flaxman et al., 2017) and the second most common cause of blindness globally, after cataract (Kingman, 2004). Glaucoma is currently considered as an age-dependent disease with pathogenetic mechanisms common to those of additional neurodegenerative pathologies of the elderly; because of the growing proportion of older persons in the world population, it is predicted that more than 110 million people will suffer from glaucoma by 2040 (Tham et al., 2014).

3.1 A brief history

Glaucoma was known since ancient times when around 400 bC, the Greek physician Hippocrates described the ocular deterioration of “glaucois,” as the condition in which elderly patients suffered from blindness with a characteristic clouding of the pupil. Subsequently, it was described as “hardness of the eyeball” (Killer et al., 2018 and references therein). The English ophthalmologist Banister was the first to understand the connection between the increased tension of the eyeball and the pathology of glaucoma. The invention of the ophthalmoscope by von Helmholtz in 1850 made it possible to observe glaucoma-related changes in the fundus (Grewe, 1986). The first evidence that high intraocular pressure (IOP) can lead to blindness was found in 1862 by Donders, and the related disease was initially called “Glaukoma simplex” (Killer et al., 2018 and references therein). Further progress in the diagnosis of glaucoma was made by the invention of the tonometer. In 2000, the Advanced Glaucoma Intervention Study officially recognized that lowering of the IOP can be correlated with reduced progression of visual field loss (The AGIS Investigators, 2000).

3.2 Aqueous humour and glaucoma

The pathophysiology of glaucoma-related neurodegeneration is not completely understood. The level of IOP is undoubtedly related to the loss of RGC and optic nerve fibres in some, if not all, patients with primary open-angle glaucoma (see the section 3.4 “Classification”) (Weinreb et al., 2004). IOP directly depends on proper aqueous humour outflow (Goel et al., 2010). Indeed, there is an equilibrium between production and drainage of aqueous humour; alteration of humour aqueous outflow results in elevation of IOP (Kass et al., 1980). The aqueous humour is a transparent and

colourless fluid that fills and helps form the anterior and posterior chambers of the eye. It is analogous to a blood surrogate for the lens and cornea, which must remain avascular in order to allow light transmission. In fact, aqueous humour provides these structures with nutrients and removes metabolic debris; it also transports neurotransmitters, stabilizes the ocular structure, contributes to the regulation of homeostasis and allows inflammatory cells and mediators to circulate in the eye under pathological conditions (Goel et al., 2010). The aqueous humour is produced by the processes of the ciliary body in the posterior chamber. Then, it flows around the lens and through the pupil into the anterior chamber where a temperature gradient creates a convective flow pattern. This flow results in an average IOP of approximately 15mmHg, which is necessary to maintain the proper shape and optical properties of the eye globe (Millar et al., 1995). The upper limit of physiological IOP in humans is considered 21mmHg (Kang et al., 2021). The aqueous humour leaves the eye by passive flow via two pathways localized to the anterior chamber angle. One of them is the so-called conventional pathway and the other one is called non-conventional one. Following the conventional pathway depicted in **Figure 4**, the aqueous humour passes through the trabecular meshwork, across the inner wall of Schlemm's canal, into its lumen, and into draining collector channels, i.e. the aqueous veins and the episcleral veins. The non-conventional route, instead, is composed of the uveal meshwork and the anterior face of the ciliary muscle (Goel et al., 2010 and references therein).

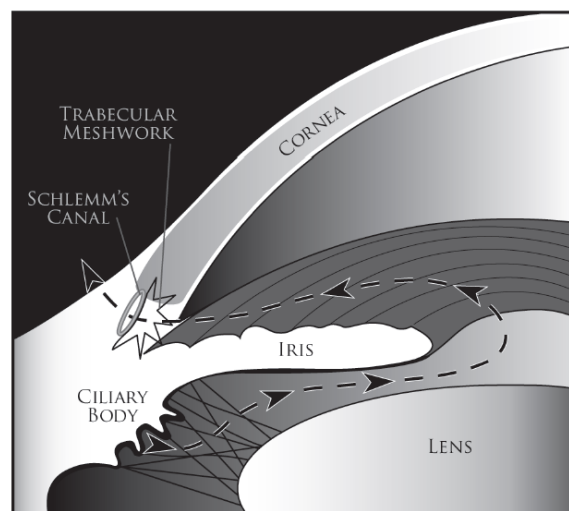


Figure 4. Schematic image describing the trabecular meshwork conventional outflow pathway of the aqueous humour. Aqueous humour is produced by the processes of the ciliary body, and it flows (dashed line shown with arrowheads) from the posterior chamber through the pupil into the anterior chamber. From there it flows out through the trabecular meshwork into the Schlemm's canal and then, it is absorbed into the episcleral veins through the collector channels (Goel et al., 2010).

Aqueous humour drainage can be facilitated through contraction of the ciliary muscle, which pushes aqueous humour through the chambers and decreases outflow resistance through the trabecular meshwork and Schlemm's canal (Marshall et al., 2018). Disruption of aqueous humour outflow usually occurs through the conventional pathway, and it leads to increased IOP (Kass et al., 1980).

3.3 Optic nerve damage

The lamina cribrosa is a highly organized, multi-layered, connective tissue, where the sclera is perforated in order to allow the optic nerve fibres (i.e. RGC axons) to exit the eye. Thus, it is also the weakest point in the wall of the pressurized eye. Hence, it is not surprising that when IOP increases above physiological levels, it may cause compression, deformation, and remodelling of the lamina cribrosa (Bellezza et al., 2003). All these alterations of the lamina cribrosa structure, can cause loss of the normal neural structure and disruption of axonal transport, with interruption of retrograde delivery of essential trophic factors to RGC from their brainstem target (Weinreb et al., 2014). Decreased neurotrophic signalling to the RGC likely results in the initiation of apoptosis (Kang et al., 2021).

The cup is the depression in the centre of the optic disc which, in glaucoma, progressively enlarges because of damage to the lamina cribrosa and loss of RGC axons (Kang et al., 2021) resulting in *cupping*, a characteristic appearance of the optic disc, and visual loss (**Figure 5**) (Weinreb et al., 2004).

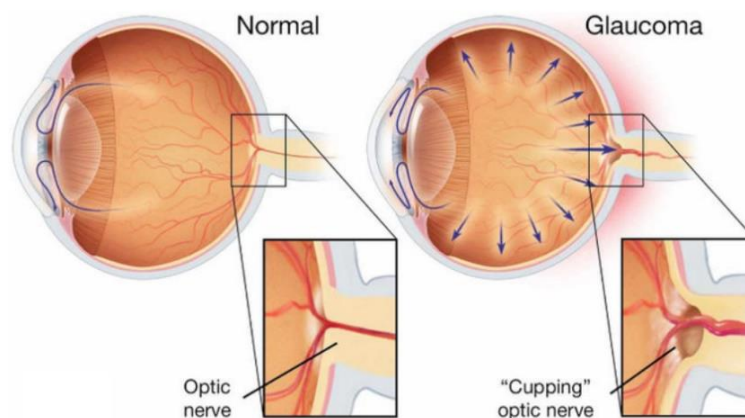


Figure 5. Normal and glaucoma affected eyes. Cupping of the optic disc is a pathological feature of glaucoma. Elevated intraocular pressure (IOP) causes compression, deformation and remodelling of the lamina cribrosa, resulting in typical excavation of the optic disc, which is absent in normal healthy eyes. Cupping of the optic disc can damage retinal ganglion cells (RGC) axons leading to apoptotic degeneration of RGC and, eventually, vision loss (Balakrishnan, 2017).

3.4 Classification

According to the morphology of the anterior chamber angle, glaucoma can be divided into angle-closure glaucoma (ACG) and open-angle glaucoma (OAG). The anterior chamber angle contains Schlemm's canal, that is collocated between the peripheral cornea and the peripheral iris (Jonas et al., 2017).

ACG is characterized by the fact that the site of humour aqueous outflow is obstructed by apposition of the iris, resulting in an anatomically closed angle (Weinreb et al., 2014). Particularly, in ACG the peripheral iris is in contact with the trabecular meshwork, thereby obstructing outflow of aqueous humour (Pan et al., 2011). Glaucoma is defined ACG if at least 270° of the angle is occluded (Weinreb et al., 2014). Pupillary block is the most common mechanism of ACG and is caused by resistance to aqueous humour flow from the posterior to anterior chambers through the pupil. Aqueous humour accumulates behind the iris increasing its convexity causing angle closure. ACG patients can complain of ocular pain, nausea, vomiting and acute visual loss (Weinreb et al., 2014). However, ACG is predominantly an asymptomatic disease with individuals often unaware of the disorder until advanced visual loss occurs (Quigley, 2011).

OAG, instead, is characterized by increased resistance of humour aqueous outflow, usually through the trabecular meshwork, although no obstruction is clinically visible. OAG patients are typically asymptomatic until evidence of severe damage (Pan et al., 2011; Marshall et al., 2018). OAG is a chronic condition, usually bilateral, often with each eye being affected to a different degree (Marshall et al., 2018).

Both ACG and OAG are further divided into primary or secondary glaucoma, indicating, respectively, the lack or the presence of other clinically identifiable ocular or systemic disorders to account for glaucoma onset as, for example, traumatic glaucoma, uveitic glaucoma, drug-induced glaucoma, advanced cases of cataract or diabetes, and others (Greco et al., 2004).

The normal tension glaucoma is a condition in which patients experience glaucomatous deleterious changes despite normal IOP. These represent approximately one-third of all primary OAG cases (Greco et al., 2004). Normal tension glaucoma patients might display an abnormally low cerebrospinal fluid pressure in the optic nerve subarachnoid space, resulting in a large pressure gradient across the lamina. Indeed, from a pathogenic point of view, a low cerebrospinal fluid pressure in normal tension glaucoma could exert the same effects as high IOP in high tension glaucoma (Ren et al., 2010).

Finally, the pathological conditions of congenital and juvenile glaucoma exist, as well, but they will not be discussed in this thesis.

3.5 Risk factors

The mechanisms initiating glaucomatous optic nerve damage are still unclear; elevated IOP is currently seen as a major risk factor for glaucoma rather than its cause (Pan et al., 2011; Gallego et al., 2012; Nickells et al., 2012). Indeed, the definition of glaucoma has progressively evolved from an eye pressure-disease to an optic neuropathy (Pan et al., 2011). Ocular perfusion pressure (OPP) is an important factor in determining IOP level, as it is calculated as the difference between systemic blood pressure and IOP. OPP is relevant for glaucoma since poor perfusion of the optic nerve may contribute to disease development and progression (Kang et al., 2021 and references therein). Besides OPP, circadian rhythms and the episcleral vein pressure contribute to determine IOP level; however, the main player affecting IOP is the balance between secretion and drainage of the aqueous humour (Brubaker, 1991). IOP is currently the solely modifiable risk factor for glaucoma and different medications are available to control it (Guglielmi et al., 2019; Sheybani et al., 2020). However, there are glaucomatous patients in which the neurodegeneration process progresses despite IOP under control (Cockburn 1983; Brubaker 1996; Heijl et al., 2002) Moreover, normotensive glaucoma progresses despite the absence of any IOP increase (Kamal 1998; Mallick et al., 2016; Killer et al., 2018; Kang et al., 2021). Thus, even though IOP is an important risk factor for glaucoma development, it is clear that a normal IOP value does not rule out this pathology (Hollands et al., 2013).

Another well-known risk factor for glaucoma condition is age. Indeed, glaucoma risk increases with age and, particularly, people older than 60 years are 6 times more likely to develop glaucoma compared to younger ones (Greco et al., 2004). In these patients, glaucoma can be expected to be associated with other age-related diseases (McMonnies, 2017).

Risk of OAG development increases when medical examinations reveal an increased cup-disk ratio, cup-disk ratio asymmetry, or disc haemorrhage (Hollands et al., 2013). The ethnic group is also relevant. Indeed, in 2003 Racette et al. estimated the prevalence of primary OAG in black American population to be six times higher compared to whites (Racette et al., 2003). Moreover, the pathologic condition of ACG is prevalent in Asian or Inuit descents (Kang et al., 2021).

In 2002, the Ocular Hypertension Treatment study reported male gender as a useful predictor for the onset of primary OAG (Gordon et al., 2002). However, a more recent review showed that there is no correlation between gender and OAG while, regarding ACG, women seem to be more affected than man (Vajaranant et al., 2010). Other relevant risk factor for ACG development deal with ocular structure features (Weinreb et al., 2014 and references therein).

3.6 Principal glaucoma models

The mouse strain DBA/2J represents the most commonly used congenital mouse model of chronic secondary angle-closure glaucoma, and it was first described in 1995 by Sheldon et al (Sheldon et al., 1995). The DBA/2J mice spontaneously develop anterior segment anomalies, iris atrophy, peripheral anterior synechiae and pigment dispersion, leading to raised IOP. The IOP is usually reported to start increasing by 7th–9th months of life and it is known to be very different in the two eyes (Turner et al., 2017). However, there are many complications to consider when using the DBA/2J mice. Indeed, their eyes undergo many changes that makes techniques like IOP measurement, electrophysiology, and fundus imaging very difficult to perform. Likely, high numbers of mice will be needed since, often, DBA/2J mice die because of systemic complications leading to cardiovascular dysfunctions (Turner et al., 2017).

A different kind of glaucoma paradigm is represented by rodent models in which an artificial occlusion of the aqueous outflow pathway is realized, leading to acute IOP elevation. These models mimic the elevated IOP-induced damages relative to the optic nerve and to the retina. The blockade of the aqueous humour outflow can be obtained either by intracamera injection of occluding materials or by sclerotic damage of the outflow structures/vasculatures (Pang et al., 2020). One example of this kind of models is the methylcellulose (MCE) one, that was initially developed in rabbits (Zhu et al., 1992) and subsequently applied in rats (Pescosolido et al., 2015) and mice (Cammalleri et al., 2020). In the MCE model the aqueous outflow pathway is occluded by MCE injection into the anterior chamber of the eye. MCE is a viscoelastic substance that, when injected into the anterior chamber, accumulates in the trabecular meshwork and Schlemm's canal, thus mechanically blocking the aqueous humour outflow and leading to elevated IOP (Pang et al., 2020). Compared to other models that mimic the human acute ACG – as in the case of the ischemia/reperfusion model, characterized by a transient acute IOP elevation (Russo et al., 2016) – the prolonged IOP elevation characterizing the MCE model more closely simulates the human hypertensive glaucoma (Cammalleri et al., 2020). A synchronous approach to study RGC injury in many mouse strains is represented by the optic nerve crush (ONC) model (McKinnon et al., 2009). This model can be used to examine central nervous system injuries in general or as a model of glaucoma (Yoles et al., 1998; Cho et al., 2005; Cai et al., 2012; Sullivan et al., 2012). Indeed, the ONC experimental model produces an insult mimicking many molecular changes that occur in murine models of glaucoma characterized by either an induced or an intrinsic elevation of IOP (Schlamp et al., 2001; Steele et al., 2006; Libby et al., 2007; Howell et al., 2011; Panagis et al., 2011). ONC is realised in anesthetized mice, making a small incision in the

conjunctiva and rotating the globe to expose the optic nerve. The so-exposed optic nerve is grasped about 1–3 mm from the globe for 10 seconds, with the only pressure from the self-clamping action to press on the nerve. During the clamping, depending on the mouse strain and the aesthetic, it is possible to see mydriasis (Templeton et al., 2012). The different methods and timing variations of the procedure are determined based on the animal, the injury being simulated, as well as the method of analysis post crush. For example, a variety of techniques can be used to injure the optic nerve in rodents: physically transecting the nerve (Sun et al., 2011), using clips to crush the nerve (Feng et al., 2010), or using forceps to crush the nerve (Templeton et al., 2009). In addition to the studies crushing the nerve, the duration of the crush varies considerably, ranging from 3 to 5 s (Li et al., 1999; Ohlsson et al., 2004; Cho et al., 2005; Vázquez-Chona et al., 2007; Ma et al., 2009; Templeton et al., 2009).

3.7 Nutraceuticals and glaucoma

Up to date, despite promising pre-clinical results (Husain et al., 2012; Can et al., 2015; Krishnan et al., 2019), the usage of neuroprotective treatments in clinical trials has not been fruitful to manage glaucoma (Yadav et al., 2020 and references therein). Moreover, the scarce tolerability of most neuroprotective compounds poses several concerns about their usage (Almasieh et al., 2017). On the other hand, the possibility to exploit nutritional intervention in glaucoma to preserve vision has recently risen a lot of interest. Nutraceuticals are often referred to as supplements derived from botanicals or other natural products including regular food, that contain active ingredients able to exert medical benefits (Kalra, 2003). Several nutraceuticals have proven to be effective in preventing RGC degeneration in glaucoma, both at the preclinical and clinical levels (Rusciano et al., 2017; Morrone et al., 2018). For instance, two distinct epidemiological studies found out that high rates consumption of green leaves, vegetables, fruits and fruit juices reduced the risk of developing glaucoma (Coleman et al., 2008; Giaconi et al., 2012). Moreover, it was shown that dietary resveratrol or α lipoic acid are able to counteract RGC loss in glaucoma models (Inman et al., 2013; Lindsay et al., 2015).

Nutraceuticals may confer protection in glaucoma interfering with its molecular pathways, including oxidative stress, inflammation, mitochondrial dysfunction, apoptosis, and vascular dysregulation. Their action in glaucoma could range from protecting undamaged RGC and their axons to the prevention of apoptosis in deeply damaged cells (Osborne, 2008). Consistently, an antioxidant-enriched diet efficiently counteracted glaucomatous-related pathologies by increasing the rate of blood circulation to the optic nerve and promoting RGC survival (Loskutova et al., 2019). Moreover, Lisosan G, a nutritional supplement derived from whole grains containing metabolites with

antioxidant properties, was able to ameliorate RGC function in DBA/2J mice and to decrease oxidative stress and inflammation levels, RGC death, and macroglial activation (Amato et al., 2021). Triterpene acids are compounds with antioxidant and neuroprotective properties (Qian et al., 2016; Wang et al., 2018) and their efficacy against glaucoma-related dysfunctions is progressively emerging from literature in different glaucoma models as ONC (Kyung et al., 2015), trabecular laser photocoagulation (Gu et al., 2018) and microspheres injection (Huang et al., 2018).

Vitamins are natural compounds that can be found both in plants and in animals, characterized by antioxidant and neuroprotective activity (Veach, 2004; West et al., 2006; Lawler et al., 2019; Scuteri et al., 2020). Particularly, vitamin E, i.e. alpha-tocopherol, is a powerful fat-soluble antioxidant able to prevent the oxidation of polyunsaturated fatty acids in cell membranes; deficiency of vitamin E increased RGC death ratio in a rat model of elevated IOP glaucoma, leading to higher levels of retinal lipid peroxidation (Ko et al., 2010). Moreover, a neuroprotective effect of oral supplement of alpha-tocopherol acetate was reported in a nonrandomized placebo-controlled study conducted on 30 glaucomatous patients (Engin et al., 2007).

Due to their antioxidant properties, nutraceuticals might also be effective in reducing glaucoma-related inflammation. Indeed, oxidative stress plays a pivotal role in the development of inflammation (Gill et al., 2010; Reuter et al., 2010) since it activates the redox-sensitive transcription factor nuclear factor kappa-light-chain-enhancer of activated B cells (NF- κ B), which is known to regulate the expression of several inflammatory molecules – including interleukin-6 (IL-6) and tumour necrosis factor alpha (TNF- α) – and apoptosis inhibiting factors, such as B-cell lymphoma 2 (Kabe et al., 2005; Harari, 2010). This leads to detrimental consequences on RGC survival, promoting neurodegeneration (Tezel, 2013).

The ameliorative cascade triggered by some dietary supplementations does not appear to depend on IOP reduction – rather it seems to activate IOP-unrelated mechanisms of action (Inman et al., 2013; Cammalleri et al., 2020; Amato et al., 2021) – although experimental evidence of efficacy of nutraceuticals and anti-oxidants in the reduction of IOP exists (Scuteri et al., 2020). Yet, a few prospective randomized clinical trials have been performed and results of association studies and systematic reviews are still controversial and not conclusive (Scuteri et al., 2020; Garcia-Medina et al., 2020). On the other hand, the neuroprotective efficacy of nutritional compounds has been clearly shown in glaucoma patients regardless of their efficacy in lowering IOP (Shen et al., 2015; Ju et al., 2018). Indeed, several IOP-independent mechanisms can contribute to RGC death, such as oxidative stress, excitotoxicity, neuroinflammation, impaired ocular blood flow, trophic factor deprivation and mitochondrial dysfunction (Alqawlaq et al., 2019; Adornetto et al., 2020).

The possibility to exploit nutritional supplements in order to counteract the detrimental effects of glaucoma, possibly promoting RGC survival and preserving their functionality, is very attractive, especially when irreversible damage of RGC has not appeared yet.

Aims

Once retinal atrophy, the end stage of most retinal pathologies, has occurred or when RGC have already died, pharmacological intervention and/or surgery might not be effective. For this reason, preventive treatments should be taken into account.

Herein, we exploited *in vitro* and/or *in vivo* models to investigate the main effects of two main pathologies affecting retinal homeostasis and functionality, that is to say ROP and high-tension glaucoma.

- (i) Retinal neovascularization of ROP is characterized by an excessive and aberrant growth of blood vessels which can lead to retinal detachment. This thesis explored new strategies (i) to counteract VEGF increase characterizing the second disruptive ROP phase, in order to prevent neovascularization (ii) and also to rise VEGF level when needed, i.e. during the hyperoxic-ischemic phase of ROP.

Particularly, we sought to understand whether VEGF overexpression could be attenuated treating the hypoxic cell lines MIO-M1 and hREC with the BAR3 antagonist SR59230A. We then investigated the putative effect of the drug in modulating NOS isoforms expression, since NOS could be involved in BAR3-dependent modulation of VEGF.

We also exploited the murine OIR model, analysing retinal vasculature development when mice were administered with SR59230A during the hypoxic phase. Finally, we evaluated the effects of administering Salbutamol and BRL37344, respectively BAR2 and BAR3 specific agonists, during the OIR hyperoxic phase in terms of alterations in VEGF expression.

- (ii) RGC loss of function and death characterizing glaucoma represent the final steps of a wider molecular pathway involving oxidative stress, glia reactivity, inflammation and many other factors, on which it could be advantageous to act prior to RGC degeneration. In the present work, we investigated whether a special nutraceutical-based diet could be effective in preventing some of these deleterious outcomes characterizing glaucoma. Specifically, MCE-injected mice were fed either a standard commercial pellet diet or the same food supplemented with an Acebuche (ACE) oil obtained from the wild olive tree (*Olea europaea* var. *sylvestris*). The putative efficacy of the special diet was evaluated in terms of prevention of glia activation, suppression of inflammation, decrease of oxidative

stress, protection against ischemic damage, reduction of apoptosis rate and counteraction of RGC loss of function.

Results and discussion

1. ROP Project: *in vitro* findings

Overview

During normal retinal development, physiological hypoxia stimulates retina vascularization, especially through HIF-1 α stabilization and VEGF expression (Penn et al., 2008). In premature newborns, the relative hyperoxia of the extra-uterine environment inhibits VEGF production resulting in suppression of retinal blood vessel growth and partial regression of existing vessels. This is the first phase of ROP, i.e. the hyperoxic-ischemic one. During this phase the formation of an avascular area within the retina can be appreciated. The imbalance between the poorly developed retinal vessel network and the increasing metabolic demand of the neural retina leads to the second, disruptive, phase of ROP, i.e. the hypoxic-proliferative phase. In this second phase, VEGF is overexpressed and vessels growth is misfolded and uncontrolled (Chen et al., 2007). Neovascularization occurs on the surface of the retina and causes functional impairments and severe vision loss (Zou et al., 2010). Several anti-VEGF drugs (such as bevacizumab, ranibizumab...) are currently used in the management of ROP, although off target (Sankar et al., 2018). However, undesirable consequences due to these anti-VEGF treatments can occur since VEGF and its receptors play an important role in the development of the neural retina (Penn et al., 2008). Consequently, new pharmacological approaches for the treatment or even for the prevention of ROP are urgently needed.

A huge amount of evidence is progressively highlighting the role played by BAR in angiogenesis via modulation of proangiogenic factors such as VEGF (Pérez-Sayáns et al., 2010; Tugues et al., 2011; Martini et al., 2011; Dal Monte et al., 2013a; Dal Monte et al., 2013b). Within the retina, Müller glia is the main source of VEGF (Pierce et al., 1995; Kaur et al., 2008), while endothelial cells represent the main target of VEGF, although they are also able to produce it (Tugues et al., 2011). Thus, we chose one Müller and one endothelial cell lines, both of human origin, to analyse the effects of hypoxia especially on BAR expression, but also on VEGF and HIF-1 α one. Then, we assessed NOS expression in hypoxic cells to investigate its putative involvement in BAR3-dependent VEGF modulation.

Outcomes

BAR3 is the most responsive BAR subtype to oxygen deprivation

The expression of BAR1, BAR2 and BAR3 was evaluated in hREC and MIO-M1 cells exposed to normoxia or hypoxia for 24h. We showed that, among BAR, the most responsive one to oxygen tension is BAR3 (**Figure 1**). Indeed, it is the only BAR isoform overexpressed in hypoxia, in both cell lines, both at mRNA and protein level.

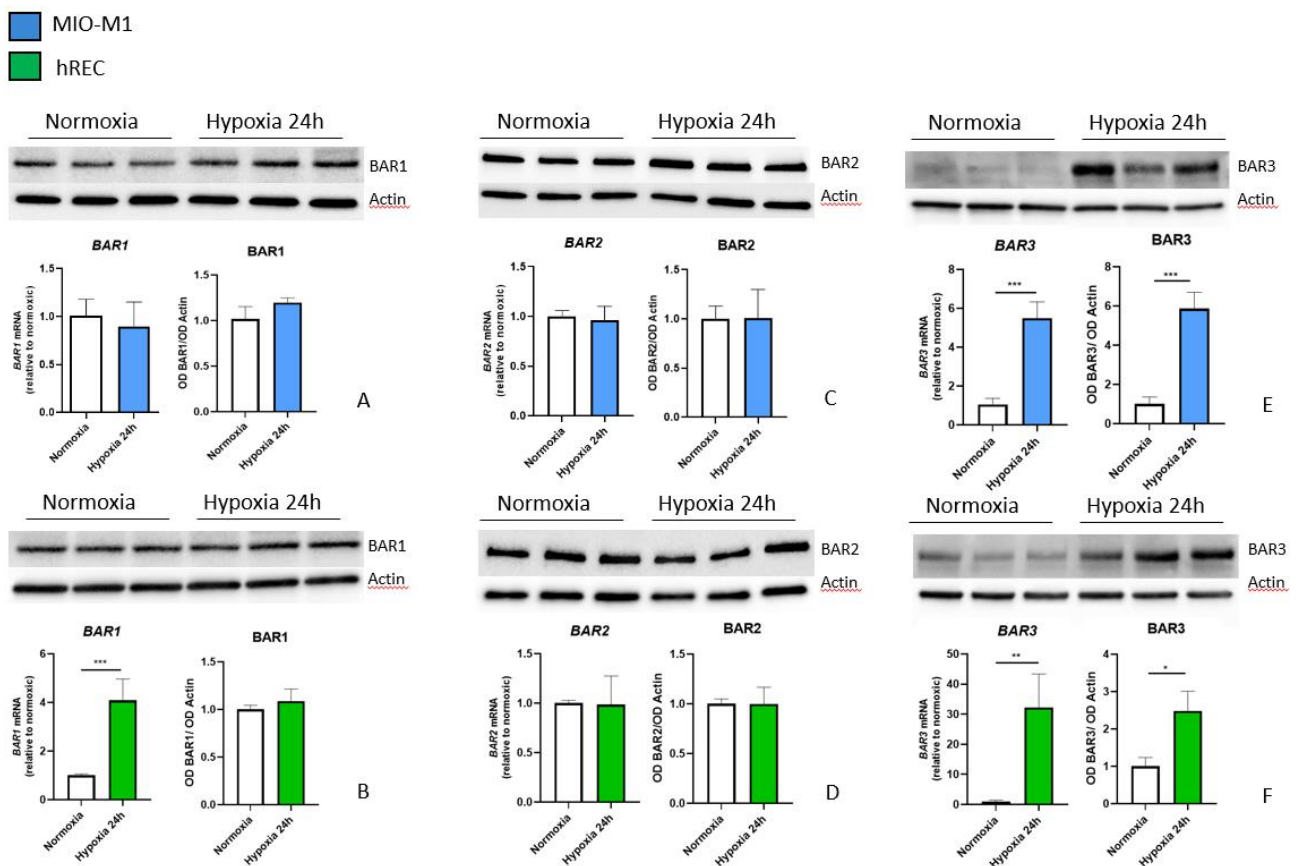


Figure 1. BAR expression in MIO-M1 cells and hREC in normoxic or hypoxic conditions. (A) In MIO-M1 cells, neither mRNA nor protein levels of BAR1 were affected by oxygen deprivation. (B) BAR1 mRNA level in hREC was increased by hypoxia, while BAR1 protein level was not. Similarly, hypoxia did not alter BAR2 mRNA or protein level neither in MIO-M1 cells (C) nor in hREC (D). In both cell lines hypoxia increased both mRNA and protein expression of BAR3 compared to normoxic cells (E, F). The values reported in the mRNA graphs represent the *BAR1,2,3* mean values of relative expression versus β -actin ones, \pm S.D. Each column in these graphs represents the mean of data from three independent samples. The values reported in the protein graphs represent the *BAR1,2,3* bands optical density mean values normalized versus β -actin ones, \pm SD. Each column in these graphs represents the mean of data from three independent samples. Statistical significance was evaluated through unpaired t-test. * $p < 0.05$; ** $p < 0.01$; *** $p < 0.001$.

Immunocytochemistry was performed on normoxic and hypoxic MIO-M1 cells (**Figure 2**). The experiments provided additional qualitative data about the expression level of these targets following 24h hypoxic treatment.

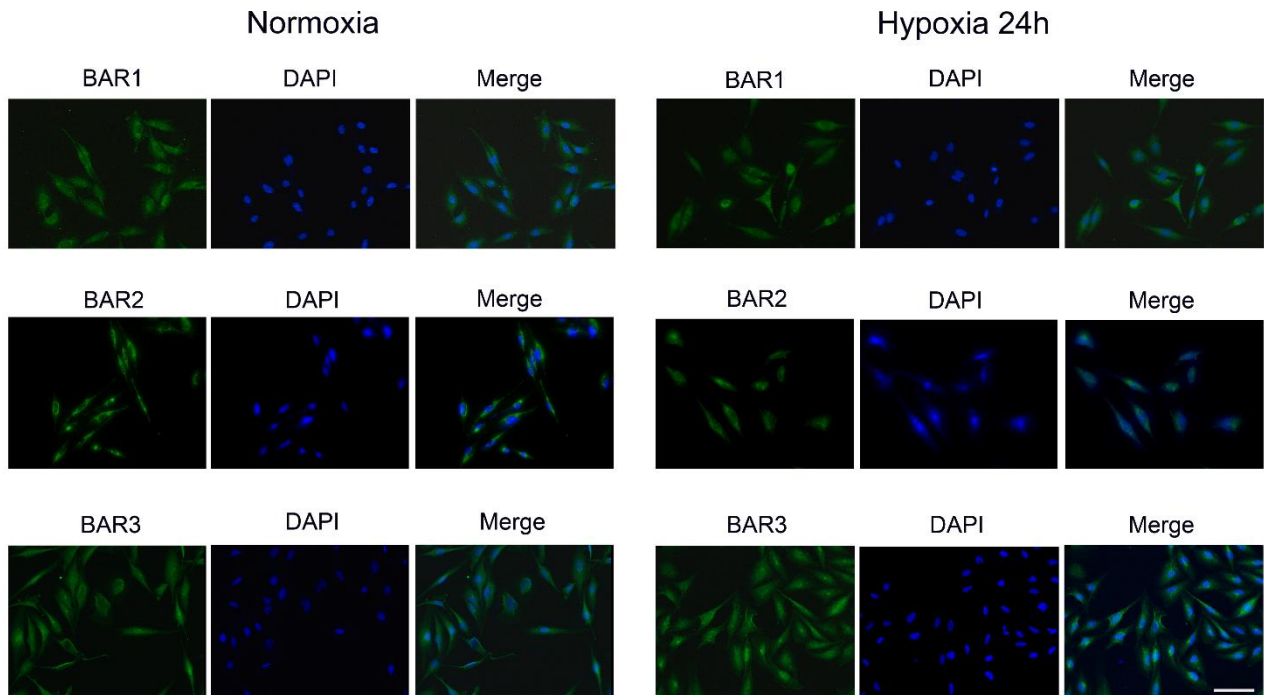


Figure 2. BAR staining in MIO-M1 cells and hREC in normoxic or hypoxic conditions. BAR1, BAR2 and BAR3 were stained on MIO-M1 cells following 24h or 24h hypoxic exposures. Cell nuclei were visualized by DAPI staining. Scale bar = 50 μ m.

The canonical HRE localized at position 3546 relative to the transcription start site in the human ADRB3 gene (Dal Monte et al., 2020) could account for oxygen-dependent BAR3 regulation at the transcriptional level. Moreover, it was recently demonstrated that BAR3 can be regulated by HIF-1 α (Amato et al., 2022) and that BAR3 protein shows 7 to 8 proline residues, which are hydroxylated in normoxia and stabilized by hypoxia (Dal Monte et al., 2020). These data could explain the strong oxygen-dependent modulation of BAR3 protein. Furthermore, BAR3 response to hypoxia is the same as the one of HIF-1 α and VEGF expression, which significantly increased in both cell lines, as shown in **Figure 3**.

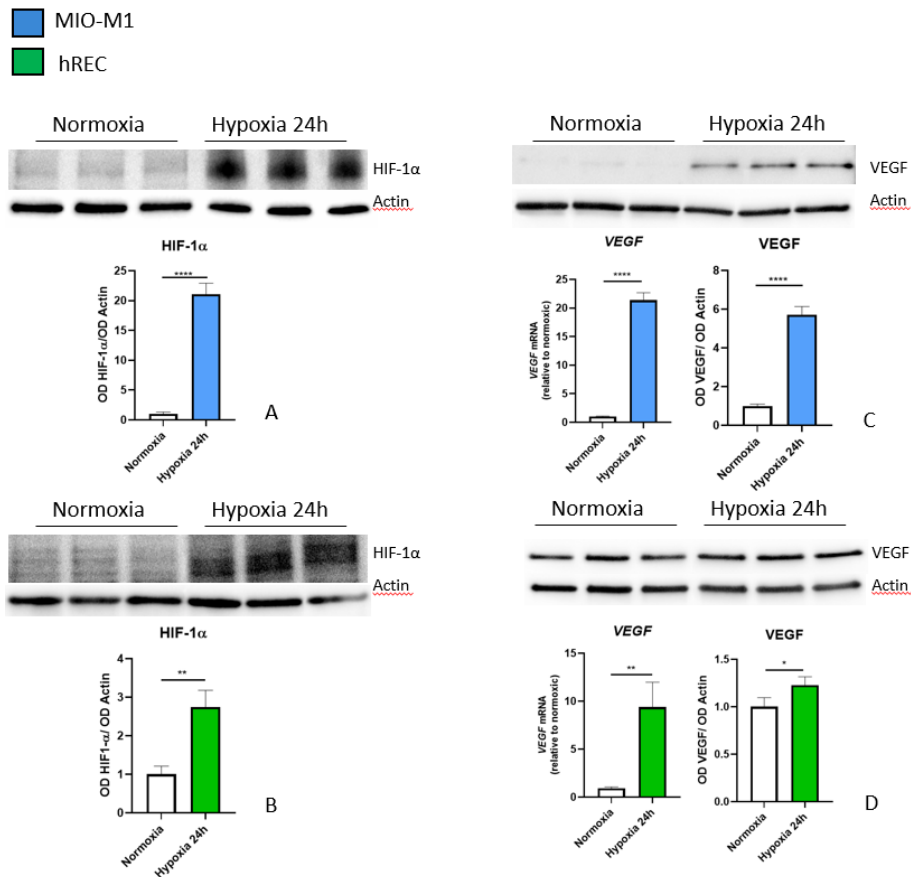


Figure 3. HIF-1 α and VEGF were upregulated by hypoxia in MIO-M1 cells and hREC. Hypoxic treatment increased protein level of HIF-1 α in both MIO-M1 cells (A) and hREC (B). VEGF mRNA and protein levels were increased by the treatments in both cell lines (C, D). The values reported in the mRNA graphs represent the *VEGF* mean values of relative expression versus β -actin ones, \pm S.D. Each column in these graphs represents the mean of data from three independent samples. The values reported in the protein graphs represent the VEGF and HIF-1 α bands optical density mean values normalized versus β -actin ones, \pm S.D. Each column in these graphs represents the mean of data from three independent samples. Statistical significance was evaluated through unpaired t-test. * $p < 0.05$; ** $p < 0.01$; **** $p < 0.0001$.

BAR3 antagonism prevents VEGF upregulation in hypoxic cells, having no effect on HIF-1 α

Importantly, we demonstrated for the first time that BAR3 selective antagonism is able to efficiently prevent VEGF protein overexpression in both hypoxic MIO-M1 cells and hypoxic hREC, without affecting HIF-1 α protein level (**Figure 4**). This strongly suggests that BAR3 signalling pathway can influence angiogenesis.

In both the two cell lines BAR3 blockade exerted no influence on VEGF production in normoxic condition, corroborating the hypothesis proposed by Dal Monte et al. (2015): only an adequate kind of stimulation could activate BAR3 and that, otherwise, this receptor activity would be masked by the one of other BAR isoforms (Dal Monte et al., 2015). The present results support this view and thus the existence of a no-tonic role for BAR3 in VEGF production, probably aimed to maintain VEGF homeostasis within a given tissue in physiological conditions. These findings suggest that

BAR3 activity is necessary to sustain VEGF production in MIO-M1 cells and hREC during hypoxia, since, in condition of oxygen deprivation, its blockage significantly reduces VEGF expression not only compared to vehicle treated hypoxic cells but also to normoxic controls.

Notably, SR59230A was able to efficiently counteract VEGF increase despite the strong upregulation of HIF-1 α and despite the recently demonstrated positive influence of HIF-1 on BAR3 expression (Amato et al., 2022). This suggests the existence of a very robust impact of BAR3 blockade on VEGF production.

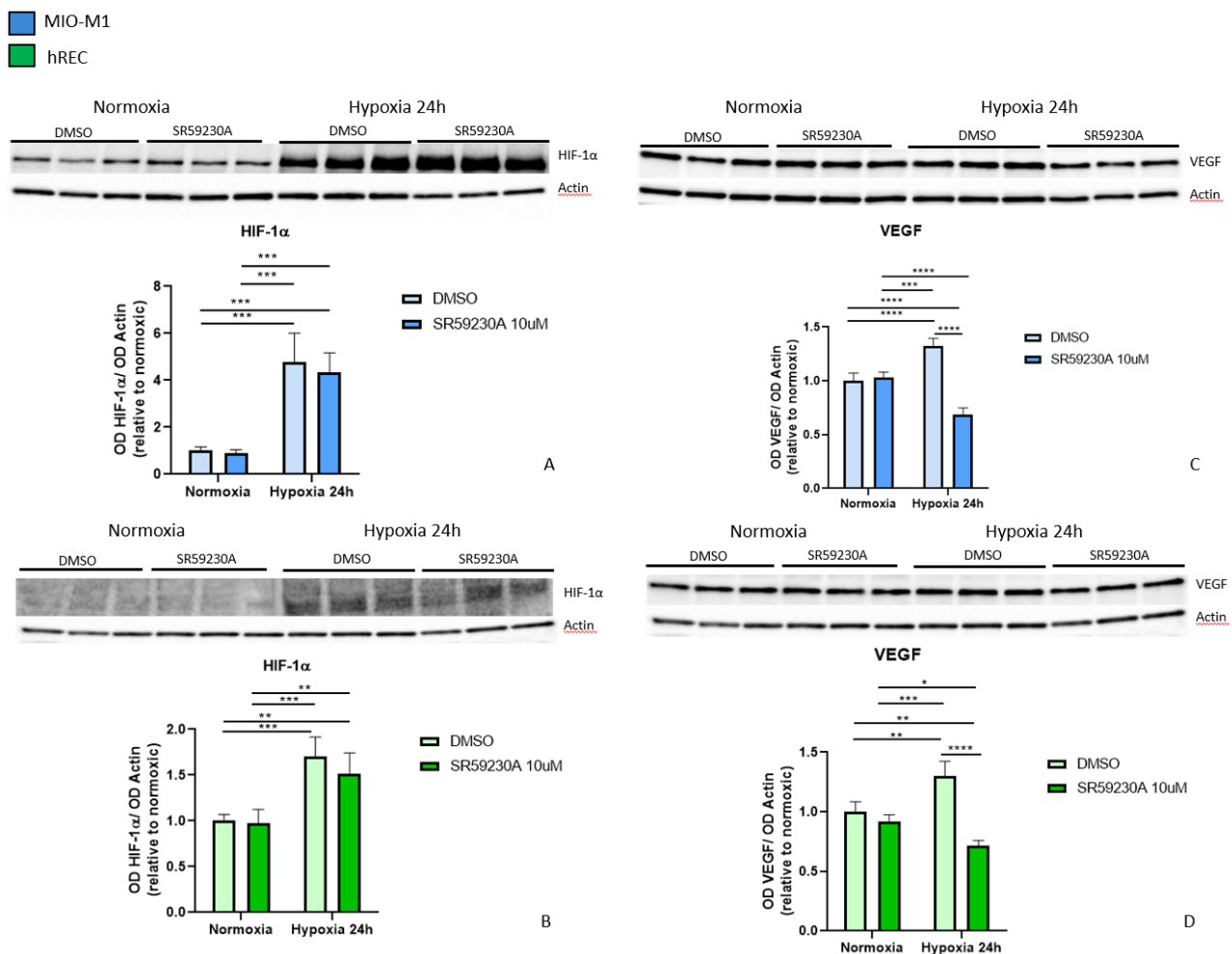


Figure 4. VEGF hypoxic overexpression was prevented by BAR3 antagonism, with no effect on HIF-1 α .

Hypoxic increase of HIF-1 α protein level was not affected by the BAR3 antagonist SR59230A neither in MIO-M1 cells (A) nor in hREC (B). On the other hand, VEGF protein level hypoxia-dependent upregulation was prevented by pharmacologic treatment with SR59230A (C, D). The values reported in the graphs represent the VEGF and HIF-1 α bands optical density mean values normalized versus β -actin ones, \pm SD. Each column in these graphs represents the mean of data from three independent samples. Statistical significance was evaluated through Two-way ANOVA followed by Tukey's post-hoc multiple comparison test. * $p < 0.05$; ** $p < 0.01$; *** $p < 0.001$; **** $p < 0.0001$.

BAR3 antagonism reduces iNOS expression in hypoxic cells

Subsequently, we investigated NOS protein expression levels in MIO-M1 cells and hREC in normoxic or hypoxic conditions (**Figure 5**). There is an HRE in the murine and in the human iNOS gene promoters; this identifies iNOS as a HIF-1 target in both species (Melillo et al., 1995; Lee et al., 2019). Consistently, different studies demonstrated that hypoxia is able to induce the expression of iNOS in A549 human lung epithelial cells (Lee et al., 2019), in rat cardiac myocytes and rat myocardium (Jung et al., 2000) and in the retina of hypoxic OIR mice (He et al., 2007), even though another work disagreed (Jantsch et al., 2011). We showed here that iNOS is significantly upregulated by hypoxia in MIO-M1 cells and in hREC. Interestingly, lack of BAR3 activity in hypoxic Müller cells and hREC significantly reduced iNOS protein level. Indeed, in both cell lines, even though hypoxia caused a strong upregulation of HIF-1 α , iNOS was downmodulated or returned to a control-like situation in the hypoxic SR59230A-treated cells. This might suggest that, together with HIF-1 α stabilization, strong BAR3 activity is necessary to sustain iNOS protein expression in oxygen deprivation.

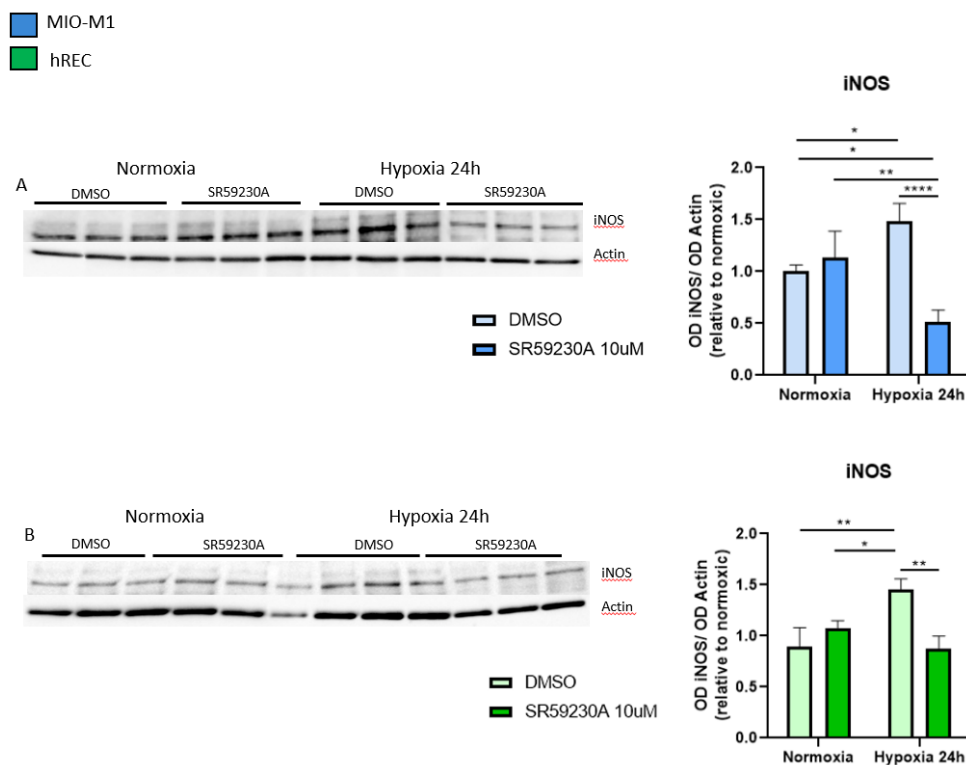


Figure 5. iNOS hypoxic overexpression was prevented by BAR3 antagonism. Western blot results show that iNOS hypoxic-dependent upregulation was prevented by pharmacologic treatment with SR59230A in both MIO-M1 cells (A) and hREC (B). The values reported in the graphs represent iNOS bands optical density mean values normalized versus β -actin ones, \pm SD. Each column in these graphs represents the mean of data from three independent samples. Statistical significance was evaluated through Two-way ANOVA followed by Tukey's post-hoc multiple comparison test. * $p < 0.05$; ** $p < 0.01$; **** $p < 0.0001$.

BAR3 antagonism reduces eNOS expression in hypoxic hREC

Western blot experiments revealed that eNOS is not expressed in human Müller cells (**Figure 6A**). In 1999 Haverkamp et al. (1999) claimed that eNOS isoform is expressed in all vertebrates' Müller cells. However, they did not investigate eNOS expression in human Müller cells. A careful search of the literature revealed absence of data regarding eNOS expression in human Müller cells.

In literature there are contradictory results regarding the effect of hypoxia on eNOS expression, likely due to the different cell types and the different hypoxia exposure times (McQuillan et al., 1994; Fish et al., 2007; Ho et al., 2013; Janaszak-Jasiecka et al., 2018). Nevertheless, our results showed a significant increase of eNOS protein level following 24h hypoxia in hREC, concomitant with HIF-1 α upregulation. Interestingly, despite this strong overexpression of HIF-1 α , BAR3 antagonism was able to restore a control-like situation of eNOS protein expression level in hypoxic condition (**Figure 6B**). These results suggest that, despite the role of HIF-1 α in eNOS synthesis, BAR3 signalling might deeply affect eNOS protein expression in hypoxic hREC.

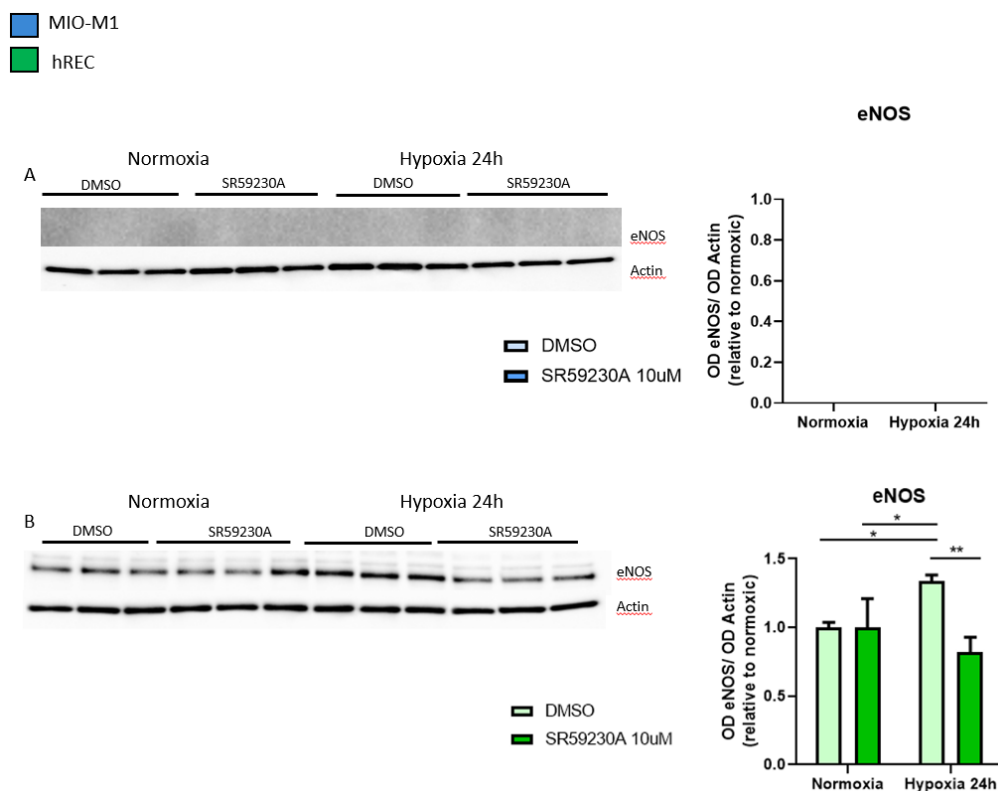


Figure 6. eNOS was not expressed in MIO-M1 cells, while its hypoxic upregulation was prevented by SR59230A in hREC. Western blot results show that eNOS is not expressed in MIO-M1 cells (A). In hREC (B), its hypoxic-dependent upregulation was prevented by pharmacologic treatment with SR59230A. The values reported in the graph represent eNOS bands optical density mean values normalized versus β -actin ones, \pm SD. Each column in this graph represents the mean of data from three independent samples. Statistical significance was evaluated through Two-way ANOVA followed by Tukey's post-hoc multiple comparison test. * $p < 0.05$; ** $p < 0.01$.

BAR3 antagonism reduces nNOS expression in hypoxic MIO-M1 cells with no effect in hREC

Our results reported in **Figure 7** show that nNOS in MIO-M1 is remarkably increased by hypoxia, in line with previous evidence obtained in astrocytes of human corpus callosum (Lorenzi et al., 2021). Interestingly, BAR3 antagonism in oxygen deprivation condition restored a control-like expression level of nNOS. This suggests that BAR3 signalling might play a role in nNOS production in MIO-M1, especially in low oxygen tension.

We found nNOS expression in hREC in line with several previous studies showing that nNOS is present in the vascular endothelium and contributes to the maintenance of the homeostasis of the cardiovascular system (Capettini et al., 2008; Costa et al., 2016 and references therein). However, differently from MIO-M1 cells, in hREC, neither hypoxia nor BAR3 antagonism appear to affect nNOS protein expression level. This might suggest that nNOS expression, depending on the cell type, could undergo a different regulation although the “conditioning” factor is the same. In line with this, it has been previously shown that leptin is able to induce nNOS expression in murine and human vessels and human endothelium but not in human smooth muscle cells (Benkhoff et al., 2012).

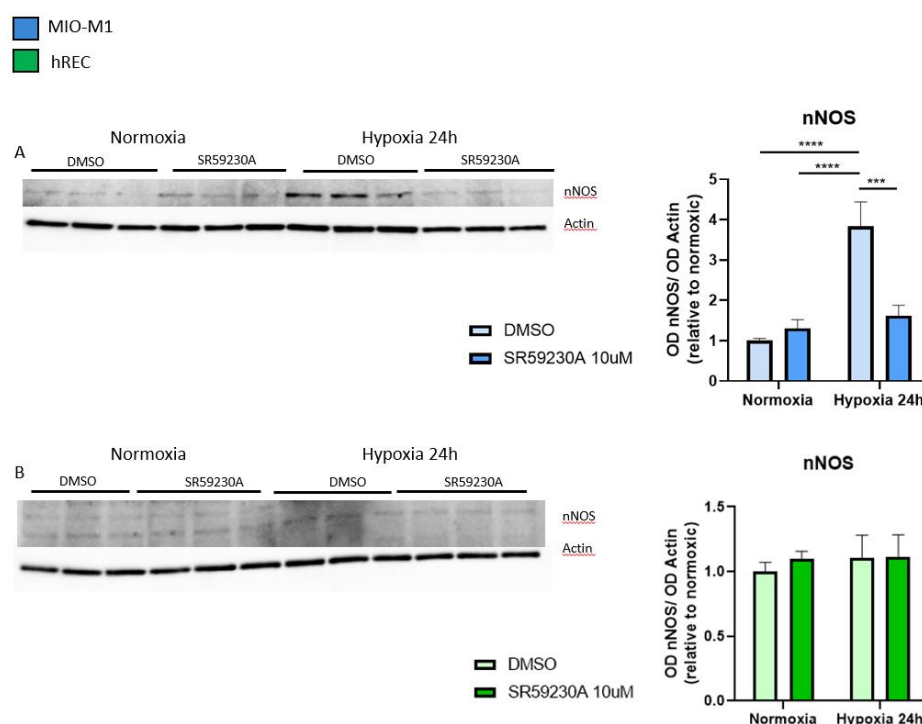


Figure 7. nNOS hypoxic overexpression was prevented by BAR3 antagonism in MIO-M1 cells, while it is not altered by the treatments in hREC. Western blot results show that nNOS hypoxic-dependent upregulation was prevented by SR59230A in MIO-M1 cells (A). On the other hand, in hREC nNOS protein expression level was affected neither by hypoxia nor by the drug (B). The values reported in the graphs represent nNOS bands optical density mean values normalized versus β -actin ones, \pm SD. Each column in these graphs represents the mean of data from three independent samples. Statistical significance was evaluated through Two-way ANOVA followed by Tukey's post-hoc multiple comparison test. *** $p < 0.001$; **** $p < 0.0001$.

Conclusions

These data suggest that in MIO-M1 and hREC the protein levels of VEGF are deeply affected by BAR3 signalling in hypoxic condition. Indeed, blockage of this receptor activity in oxygen deprivation condition resulted in a decreased expression of VEGF, despite the strong upregulation of HIF-1 α . This occurs only under hypoxic condition, when this receptor is overexpressed, corroborating the hypothesis of a non-tonic role for BAR3 activity. Moreover, hypoxia-dependent upregulation of iNOS in both cell lines and of nNOS or eNOS in Müller cells and hREC, respectively, is prevented by SR59230A. This might suggest a possible involvement of NOS in BAR3-mediated regulation of VEGF, in line with previous literature (Dessy et al., 2004; Rozec et al., 2006; Ziche et al., 2009; Dal Monte et al., 2013; Dal Monte et al., 2014; Bueno-Pereira et al., 2022). However, further investigations would be needed to dissect this point.

Even though a correlation of these *in vitro* findings to ROP condition is difficult, they represent a first step in evaluating β -adrenergic system responses to oxygen deficiency, as well as BAR3 involvement in VEGF production through NOS signalling pathway.

2. ROP Project: *in vivo* findings

Overview

Currently, the murine OIR model is the most exploited *in vivo* model to study ROP. This model exploits the plasticity of neonatal mouse retinal blood vessels (Smith et al., 1994). It is well known that in the hypoxic retinae of OIR mice, the expression levels of BAR1 and BAR2 do not vary significantly, whereas the expression levels of BAR3 are remarkably increased compared to normoxic controls (Ristori et al., 2011; Amato et al., 2022). BAR3-mediated regulation of VEGF through NO has been demonstrated in different models (Dessy et al., 2004; Dal Monte et al., 2013a; Dal Monte et al., 2014; Bueno-Pereira et al., 2022). Importantly, in OIR mice, BAR3 activation with the specific agonist BRL37344 during the hypoxic phase in both WT and BAR1/BAR2 KO animals, results in enhanced pathological neovascularization, and increased VEGF expression (Dal Monte et al., 2015). However, *in vivo* administration of 5-20 mg/kg of the BAR3 antagonist SR59230A in hypoxic OIR mice was not effective in reducing neovascularization and tufts formation (Martini et al., 2011). Differently from BAR3, BAR2 is not much responsive to oxygen tension (Ristori et al., 2011).

Nevertheless, in OIR mice, BAR1/2 blockade with propranolol efficiently downregulates VEGF through destabilization of HIF-1 α (Ristori et al. 2011) and additional results suggest that the efficacy of this treatment relies on BAR2 blockade alone rather than on BAR1 one (Martini et al., 2011; Dal Monte et al., 2012). In line with this, it has been shown that BAR2 blocking prevents VEGF upregulation via BAR2/HIF-1/VEGF axis in human pancreatic tumour cells (Shan et al., 2013). Due to this evidence, we chose to evaluate the possible contribution of both BAR3 and BAR2 to VEGF synthesis and/or neovascularization in OIR mice.

First of all, we investigated the possible efficacy of the *in vivo* administration of a higher dose of the BAR3 antagonist SR59230A in hypoxic OIR mice compared to the one previously used by Martini et al. (2011). Particularly, we administered three times per day, from P12 to P17, through intraperitoneal injection, 40 mg/kg of the BAR3 blocker. The putative effects of BAR3 antagonism were then evaluated through immunohistochemistry in terms of counteracting neovascularization and tufts formation at P17.

Next, we investigated whether stabilisation of VEGF levels during the hyperoxic phase through BAR agonism might led to a reduction in VEGF overexpression that occurs during the hypoxic phase. To this aim, we evaluated for the first time the effects of BAR3 and BAR2 agonism administration during the hyperoxic-ischemic phase of OIR, i.e., when VEGF levels are low. Daily administrations through intraperitoneal injection of 0,4 mg/Kg, 2 mg/Kg or 10 mg/Kg of BRL37344 or Salbutamol (a specific BAR2 agonist) were carried out from P5 to P12. The efficacy of both these agonist-based treatments was evaluated in terms of alterations, if any, in VEGF protein levels at P12 and P17. These timings were chosen since they represent crucial phases in the OIR mouse model. Indeed, at P12 the hyperoxic phase ends, and VEGF levels are extremely low and an increase would be needed; on the other hand, P17 is characterised by the highest degree of tuft density, neovascularization, and VEGF overexpression. In this latter phase, a downmodulation of VEGF would be desirable.

Outcomes

SR59230A is not effective in counteracting neovascularization

To investigate whether BAR3 antagonism could reduce retinal neovascularization and tuft formation, OIR mice were treated with high dosage (40 mg/Kg) of SR59230A during the hypoxic phase, from P12 to P17. At P17, immunohistochemistry on the whole retina was performed to visualize retinal blood vessels. In accordance with existing literature (Smith et al., 1994), hyperoxia exposure led to the formation of an avascular area in the central murine retina, that subsequently, during the hypoxic phase underwent incomplete revascularization. This was associated with pronounced

neovascularization at the conjunction between the vascular and the avascular areas and also in the periphery of the retina, with tufts formation.

As shown in **Figure 1**, BAR3 antagonism with SR59230A was not able to counteract the progression of neovascularization, not even using a higher dose compared to the one used by Martini et al. (2011). This result appears to exclude that BAR3 had a role in modulating angiogenesis in the retina of OIR mice. However, the encouraging *in vitro* results discussed in the previous section, as well as the remarkable amount of existing literature (Dessy et al., 2004; Dal Monte et al., 2013a; Calvani et al., 2015; Dal Monte et al., 2015; Bueno-Pereira et al., 2022), seem to indicate the existence of a role for BAR3 in VEGF synthesis and angiogenesis modulation in hypoxic conditions.

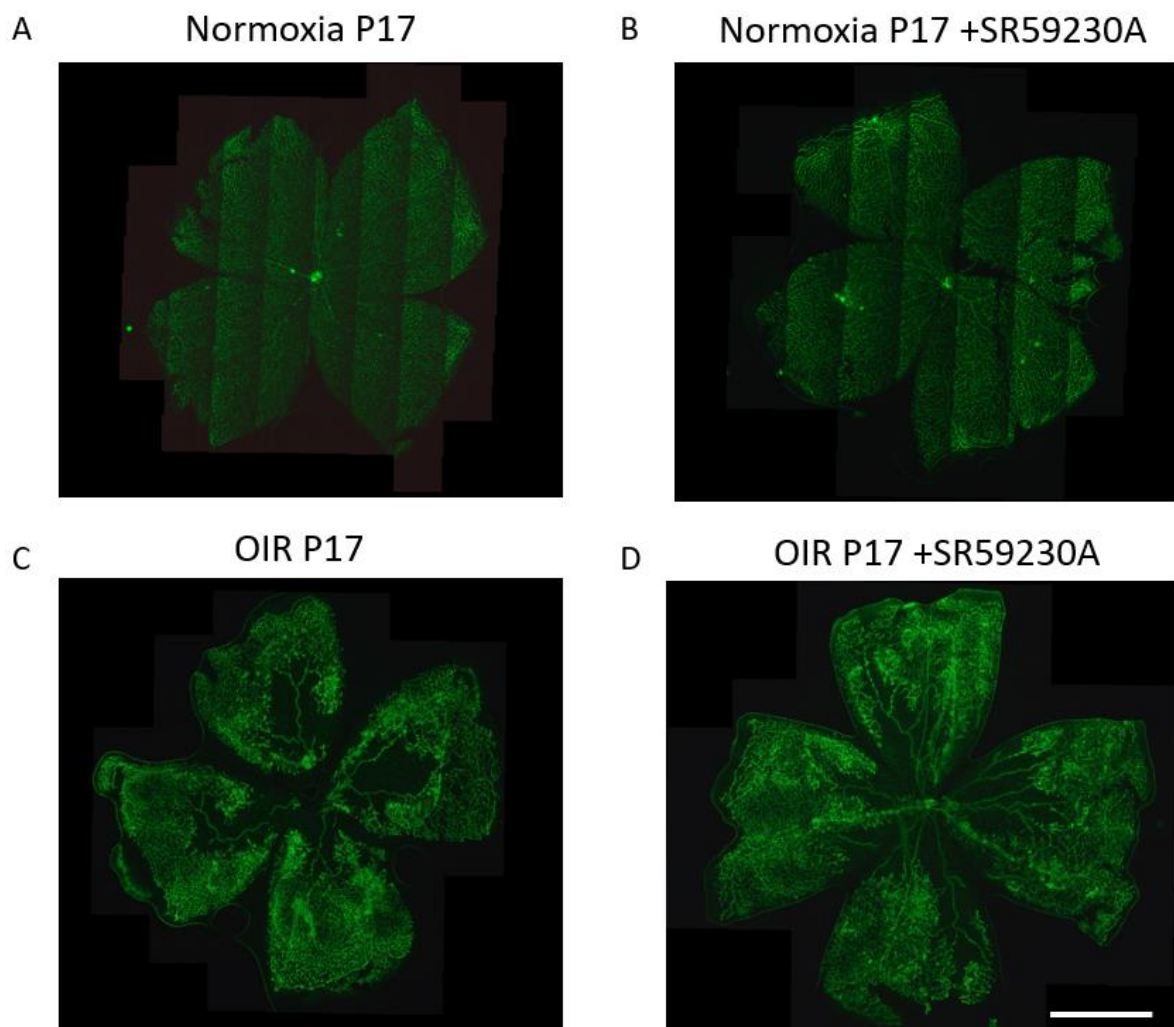


Figure 1. BAR3 antagonism was not able to prevent neovascularization in OIR mice. Representative images of retinal whole mounts immunostained for isolectin B4. Normoxic and OIR mice were treated with 40 mg/Kg SR59230A from P12 to P17. Neovascularization was assessed at P17 in untreated normoxic (A), SR59230A-treated normoxic (B), untreated OIR (C) and SR59230A-treated OIR (D) mice. Pharmacologic treatment with SR59230A did not affect neovascularization. Three mice were used for each experimental condition. Scale bar = 1mm.

BRL37344 does not increase VEGF production during the hyperoxic phase

To explore the possibility to rise VEGF production level during the hyperoxic phase of ROP through BAR3 agonism, we treated OIR mice from P5 to P12 with different doses (0,4 mg/Kg, 2 mg/Kg, 10 mg/Kg) of BRL37344. Subsequently, we analysed VEGF protein expression at P12 and P17 and the results are described in **Figure 2**.

VEGF levels in OIR mice at P12 remained significantly lower than those in normoxic mice, despite BAR3 agonism. In fact, none of the three dosages of BRL37344 used in the experiments was able to increase VEGF protein levels to restore a control-like situation at P12. There was also no reduction of VEGF hypoxic OIR mice compared to controls at P17, which could possibly have occurred following a stabilisation of its levels during the hyperoxic phase. This does not exclude the possibility that BAR3 contributes to VEGF modulation. In fact, the actual dose of agonist that reached the retina after systemic administration is unknown and could have been too low to be effective. Moreover, BAR3 is strongly downregulated in OIR during hyperoxia (Amato et al., 2022) and, therefore, the drug dose needed to produce an appreciable effect might have been higher than expected. It is worth noticing that 2 mg/Kg BRL37344 subcutaneously administered during the hypoxic-proliferative phase of OIR mice was able to worsen VEGF production (Dal Monte et al., 2015). However, during hypoxia, BAR3 is overexpressed rather than downmodulated, and vessels permeability, especially BRB permeability, is increased (Kaur et al., 2008; Deissler et al., 2008; Li et al., 2009). Thus, drug delivery to the retina in such conditions can be facilitated compared to hyperoxia and the dose required to obtain an appreciable effect could be lower due to BAR3 upregulation.

To sum up, due to its high sensitivity to the partial pressure of oxygen, BAR3 remains a very interesting target in the study of ROP.

BRL37344

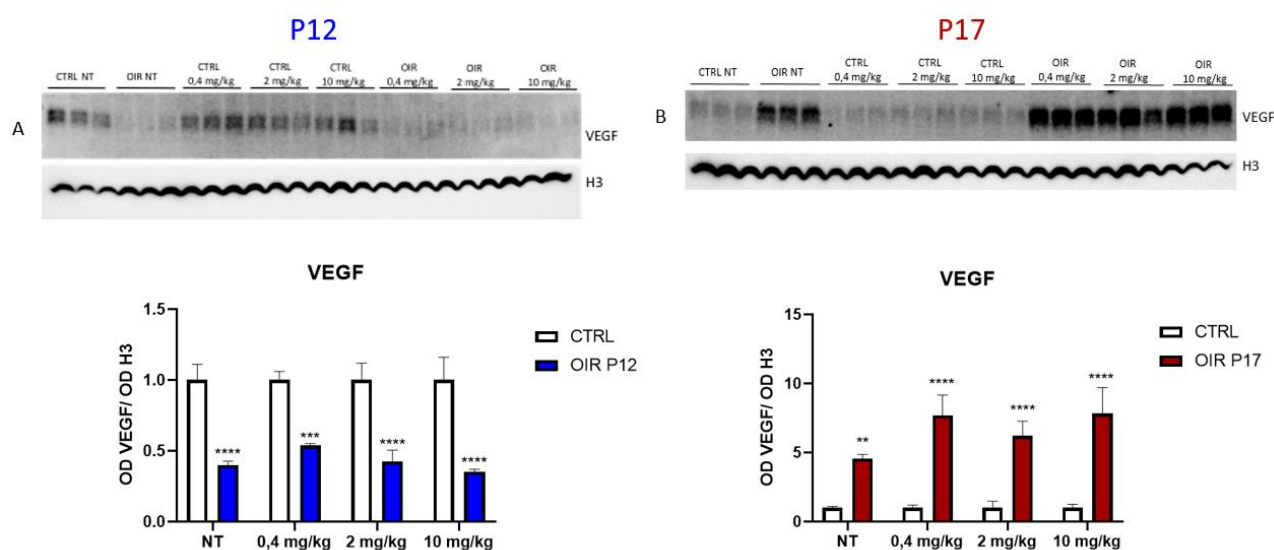


Figure 2. BAR3 agonism was not able to modulate VEGF level in OIR mice. Immunoblot of proteins coming from mice retinae. Normoxic and OIR mice were treated with different doses (0,4 mg/Kg, 2 mg/Kg, 10 mg/Kg) of the BAR3 agonist BRL37344 from P5 to P12. Retinae were collected at P12 (A) and P17 (B) and analysed for VEGF protein content. Pharmacologic treatment with BRL37344 failed to rescue VEGF protein level. NT = no treatment with BRL37344. Three mice were used for each experimental condition. The values reported in the protein graphs represent the VEGF bands optical density mean values normalized versus histone 3 (H3) ones, \pm SD. Each column in the graphs represents the mean of data from three independent samples. Statistical significance was evaluated through Two-way ANOVA followed by Šidák's post-hoc multiple comparison test. ** $p < 0.01$; *** $p < 0.001$; **** $p < 0.0001$.

Salbutamol does not increase VEGF production during the hyperoxic phase

Next, we investigated the possibility to rise VEGF level during the hyperoxic phase of ROP through BAR2 agonism. Therefore, we treated OIR mice from P5 to P12 with different doses (0,4 mg/Kg, 2 mg/Kg, 10 mg/Kg) of Salbutamol and then we analysed VEGF protein expression at P12 and P17. The results are shown in **Figure 3**.

BAR2 agonism was not able to modulate VEGF levels which remained significantly lower in hyperoxic OIR mice than in normoxic controls. In fact, none of the three dosages of Salbutamol used in the experiment was able to increase VEGF protein expression levels in order to restore a control-like situation at P12. There was also no reduction of VEGF in hypoxic OIR mice compared to normoxic controls at P17. This does not rule out the possibility that BAR2 contributes to VEGF modulation. Indeed, the actual dose of Salbutamol that reached the retina after systemic administration is unknown, and could have been too low to be effective. On the other hand, even if the actual drug dose within the retina was enough, it has been demonstrated that BAR2 is downmodulated by prolonged agonist exposure (Dal Monte et al., 2012). Thus, decreased receptor functional activity might be responsible for lack of efficacy of Salbutamol.

Salbutamol

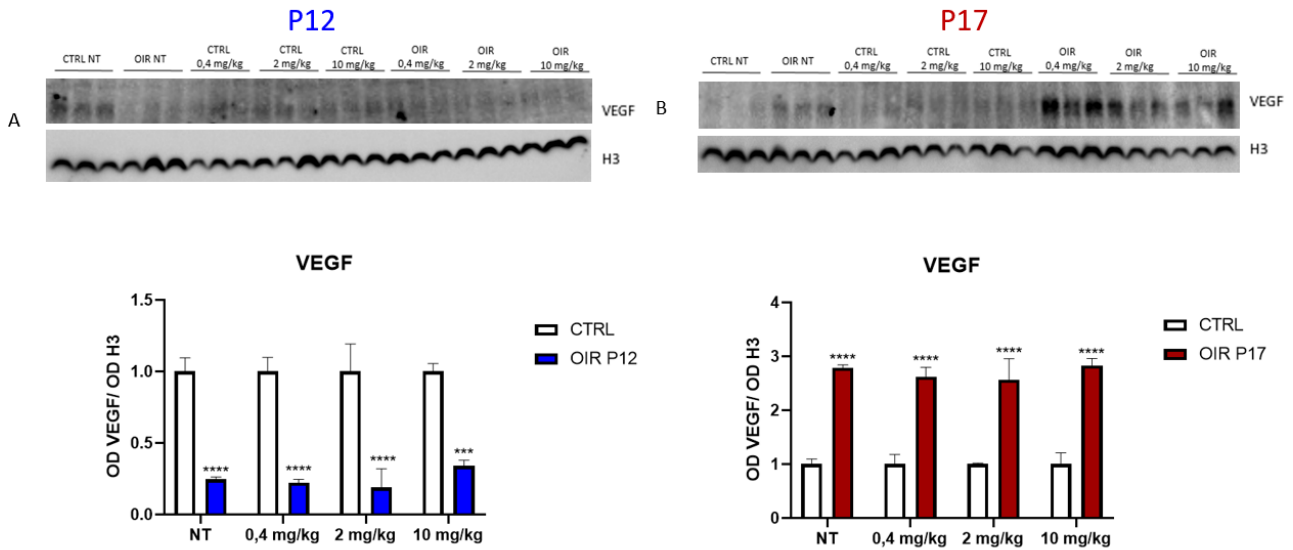


Figure 3. BAR2 agonism was not able to modulate VEGF level in OIR mice. Immunoblot of proteins coming from mice retinæ. Normoxic and OIR mice were treated with different doses (0,4 mg/Kg, 2 mg/Kg, 10 mg/Kg) of the BAR2 agonist Salbutamol from P5 to P12. Retinæ were collected at P12 (A) and P17 (B) and analysed for VEGF protein content. Pharmacologic treatment with Salbutamol failed to rescue VEGF protein level. NT = no treatment with Salbutamol. Three mice were used for each experimental condition. The values reported in the protein graphs represent the VEGF bands optical density mean values normalized versus histone 3 (H3) ones, \pm SD. Each column in the graphs represents the mean of data from three independent samples. Statistical significance was evaluated through Two-way ANOVA followed by Šidák's post-hoc multiple comparison test. *** $p < 0.001$; **** $p < 0.0001$.

Conclusion

Previous results demonstrated the protective effects of BAR2 blockage or KO in hypoxic OIR mice (Dal Monte et al., 2015), as well as the inefficacy of BAR3 antagonism through SR59230A to reduce neovascularization (Martini et al., 2011). Even tested at a higher dosage, the BAR3 blocker SR59230A exerted no protective effect on neovascularization. Moreover, any modulation of VEGF by BAR3 and BAR2 agonism seems unlikely. Nevertheless, this lack of efficacy might also be due to insufficient local drug concentration as well as to downmodulation/desensitization of the receptors.

3. Glaucoma Project

Overview

Glaucoma is an optic neuropathy which leads to blindness due to RGC loss of function and death (Flaxman et al., 2017; Kishore et al., 2020). Hypertensive glaucoma is characterized by elevated IOP (Weinreb et al., 2014). IOP increase usually originates from disruption of aqueous humour outflow through the conventional route (Kass et al., 1980).

The possible usage of nutraceutical to protect eyes and vision from the deleterious outcomes of glaucoma is rising more and more interest, especially for those nutritional supplements able to prevent RGC degeneration, both at the preclinical and at the clinical levels (Coleman et al., 2008; Giaconi et al., 2012; Rusciano et al., 2017; Morrone et al., 2018; Loskutova et al., 2019).

The wild olive tree (*Olea europaea* var. *Sylvestris*) also called ACE is one of the oldest trees worldwide (Kassa et al., 2019) and the oil derived from it contains tocopherols (e.g., vitamin E), sterols, triterpene acids and secoiridoid compounds in higher quantity compared to the classic extra virgin olive oil. Moreover, it was demonstrated that an ACE oil-enriched diet exerted anti-inflammatory, antioxidant and retinoprotective effects in a mouse model of arterial hypertension (Santana-Garrido et al., 2020; Santana-Garrido et al., 2021).

Therefore, we investigated whether ACE oil could reduce ocular hypertension, gliosis, inflammation level, oxidative stress, ischemia, apoptosis rate and RGC loss of function within the retinae of a murine model of hypertensive glaucoma. To this aim, we fed mice either an ACE oil-enriched diet or a regular diet for four weeks, and then induced IOP elevation through intraocular injection of MCE. The putative retinoprotective effects of the ACE oil-enriched diet were evaluated assessing whether high IOP-associated glia reactivity, inflammatory processes, oxidative stress, ischemic injury, apoptosis and RGC functionality were ameliorated by the diet.

Outcomes

ACE oil enriched diet does not prevent IOP elevation

ACE oil enriched diet did not affect IOP compared to animals fed normal diet. Indeed, the IOP increase in MCE-injected mice was only slightly attenuated by ACE oil enriched diet in the first 24 hours after the injection, but this difference was not preserved afterwards (**Figure 1**).

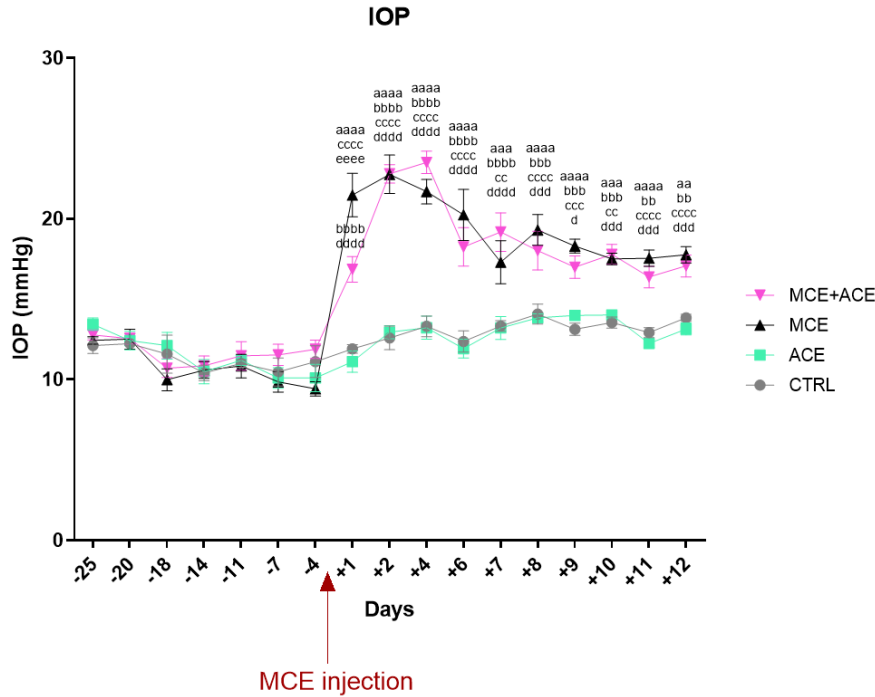


Figure 1. IOP is not affected by ACE oil enriched diet. The injection of MCE in the anterior chamber occurred at day 0 (arrow). Both regular and ACE oil enriched diet did not affect IOP in glaucomatous mice. Data are shown as mean \pm SEM (n = 6 for each group). Grey circles and line: control mice (CTRL); green squares and line: non-injected mice fed ACE oil enriched diet (ACE); black triangles and line: mice intraocularly injected with MCE fed regular diet (MCE); pink triangle and line: mice intraocularly injected with MCE fed ACE oil enriched diet (MCE+ACE). ^a=CTRL vs MCE; ^b=CTRL vs MCE+ACE; ^c=ACE vs MCE; ^d=ACE vs MCE+ACE; ^e=MCE vs MCE+ACE. Statistical significance was evaluated through Two-way ANOVA followed by Tukey's post-hoc multiple comparison test. ^{aa} p < 0.01; ^{aaa} p < 0.001; ^{aaaa} p < 0.0001; ^{bb} p < 0.01; ^{bbb} p < 0.001; ^{bbbb} p < 0.0001; ^{cc} p < 0.01; ^{ccc} p < 0.001; ^{cccc} p < 0.0001; ^d p < 0.05; ^{ddd} p < 0.001; ^{dddd} p < 0.0001; ^{eeee} p < 0.0001.

ACE oil enriched diet suppresses glia activation and retina inflammation

Dysfunctions in glaucoma mouse models are associated to reactive gliosis, usually measured by increases in glial fibrillary acidic protein (GFAP) (Inman et al., 2007; Sun et al., 2017; Wang et al., 2017) and ionized calcium-binding adapter molecule 1 (IBA-1) (Hoogland et al., 2015; Ramirez et al., 2017) expression levels. Therefore, we evaluated GFAP and IBA-1 mRNA and protein expression levels. As described in **Figure 2**, intraocular injection of MCE dramatically increased GFAP and IBA-1 expression compared to not injected animals. Notably, ACE oil enriched diet completely suppressed Müller cells reactivity in MCE glaucoma model in terms of protein expression and allowed a partially recover of mRNA levels.

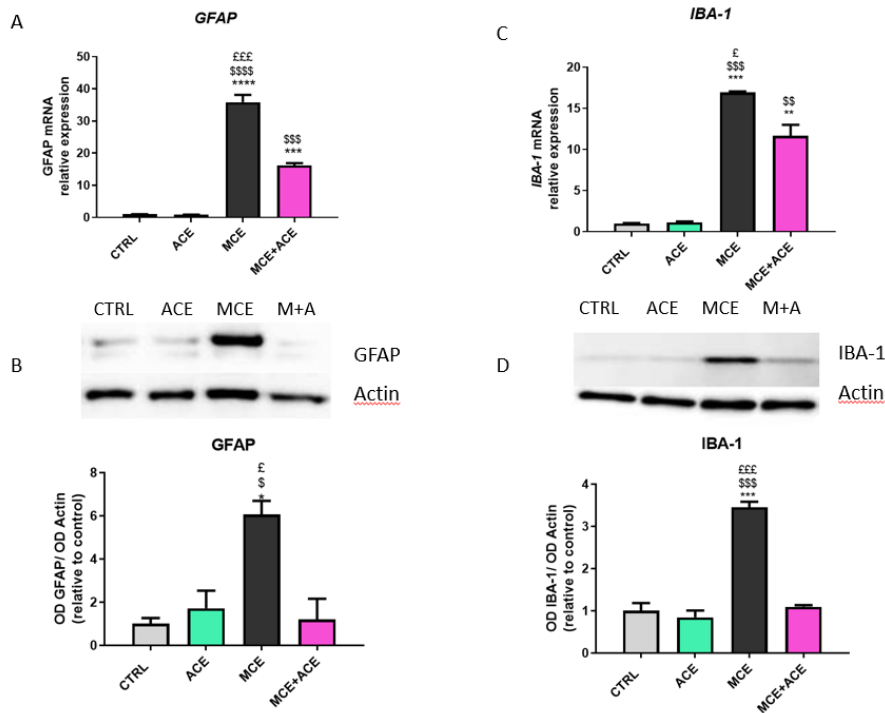


Figure 2. Effects of ACE oil enriched diet on glia activation. (A) Retinal mRNA expression levels of *GFAP* from control mice (CTRL), mice fed with ACE oil enriched diet (ACE) mice that received MCE injection fed with either regular food (MCE) or special diet (M+A). (B) Representative western blots showing immunoreactive bands and optical density analysis of GFAP protein levels in the same groups. (C) Retinal protein expression levels of *IBA-1* from CTRL, ACE, MCE or M+A experimental groups. (D) Representative western blots showing immunoreactive bands and optical density analysis of IBA-1 protein levels in the same groups. The values reported in the mRNA graphs represent the *GFAP* and *IBA-1* mean values of relative expression versus *RPL13a* ones, \pm SEM. Each column in these graphs represents the mean of data from three independent samples. The values reported in the protein graphs represent the GFAP and IBA-1 bands optical density mean values normalized versus β -actin ones, \pm SEM. Each column in these graphs represents the mean of data from three independent samples. Statistical significance was evaluated through One-way ANOVA followed by post-hoc Tukey's multiple comparisons test. * = vs CTRL; \S = vs ACE; £ = vs MCE+ACE. * $p < 0.05$; \S $p < 0.05$; £ $p < 0.05$; ** $p < 0.01$; §§ $p < 0.01$; *** $p < 0.001$; §§§ $p < 0.001$; £££ $p < 0.001$; **** $p < 0.0001$; §§§§ $p < 0.0001$.

According to literature, as a consequence of glaucoma-related harmful stimuli reactive glial cells start producing inflammation mediators (Tezel, 2013). Indeed, as shown in **Figure 3**, gliosis promotes the expression of inflammatory cytokines as IL-6 and TNF- α . In line with this, we found that in the MCE glaucoma model there was an enhanced mRNA and protein expression of IL-6 and TNF- α compared to control. Interestingly, ACE oil enriched diet prevented this upregulation, restoring a control-like situation. Moreover, the anti-inflammatory cytokine interleukin 10 (IL-10) was upregulated in the MCE injected animals fed ACE oil enriched diet, both at the transcript and protein level. These results are in line with the well-demonstrated anti-inflammatory properties of ACE oil (Santana-Garrido et al., 2021).

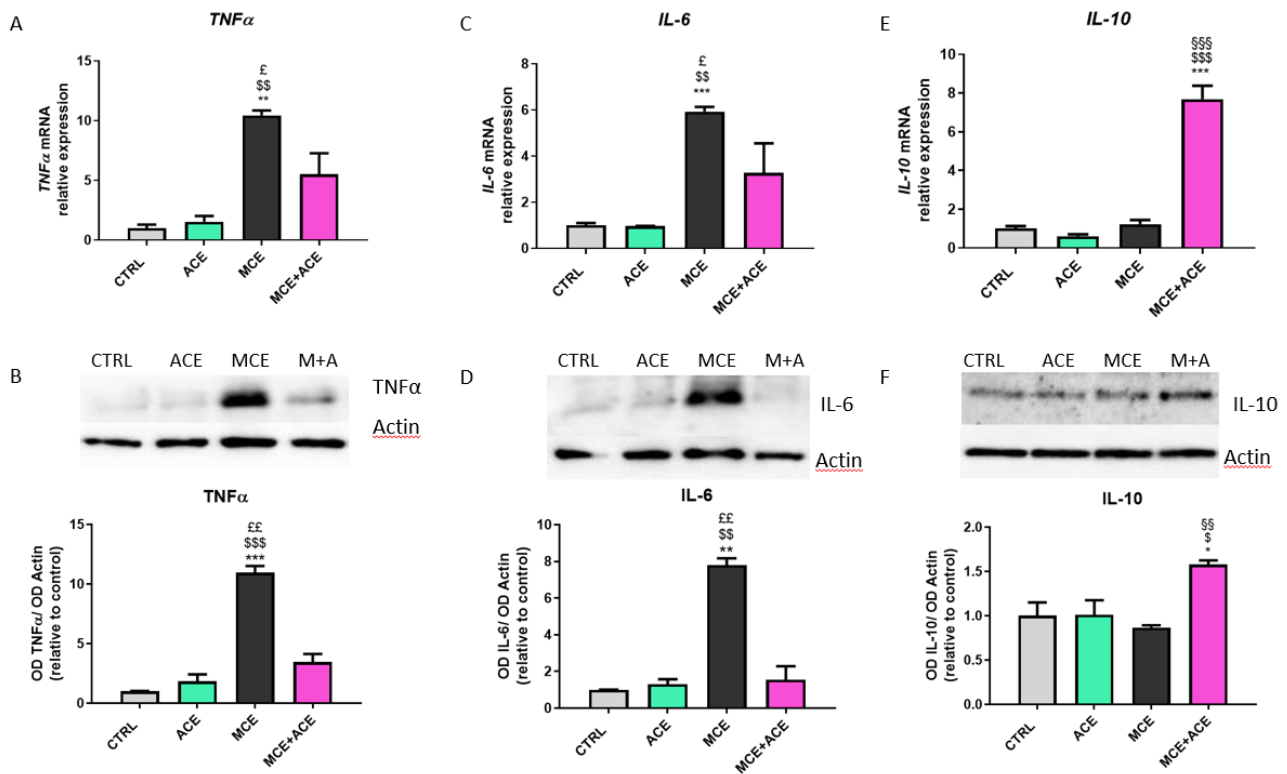


Figure 3. Effects of ACE oil enriched diet on inflammatory cytokines expression. The mRNA and protein expression levels of TNF- α (A,B), IL-6 (C,D) and IL-10 (E,F) were evaluated in retinae coming from control mice (CTRL), mice fed with ACE oil enriched diet (ACE) mice that received MCE injection fed with either regular food (MCE) or special diet (M+A). The values reported in the mRNA graphs represent the TNF- α , IL-6 and IL-10 mean values of relative expression versus *RPL13a* ones, \pm SEM. Each column in these graphs represents the mean of data from three independent samples. The values reported in the protein graphs represent the TNF- α , IL-6 and IL-10 bands optical density mean values normalized versus β -actin ones, \pm SEM. Each column in these graphs represents the mean of data from three independent samples. Statistical significance was evaluated through One-way ANOVA followed by post-hoc Tukey's multiple comparisons test. * = vs CTRL; \$ = vs ACE; § = vs MCE; £ = vs MCE+ACE. * p < 0.05; \$ p < 0.05; £ p < 0.05; ** p < 0.01; §§ p < 0.01; §§ p < 0.01; €€ p < 0.01; *** p < 0.001; §§§ p < 0.001; §§§§ p < 0.001.

ACE oil enriched diet restores a control-like expression of oxidative stress markers

Oxidative stress crucially contributes to apoptotic RGC death in glaucoma (Kabe et al., 2005; Harari, 2010; Chrysostomou et al., 2013). The transcription factor nuclear factor erythroid-2 related factor 2 (Nrf2) is involved in antioxidant responses and it controls the expression of antioxidant enzymes such as hemoxygenase-1 (HO-1) and nicotinamide adenine dinucleotide phosphate quinone oxidoreductase 1 (NQO1) (Jung et al., 2010; Wu et al., 2011; Xu et al., 2014; Deliyanti et al., 2016). Although there is several evidence reporting an inhibition of Nrf2 signalling pathway in glaucoma (Ahmed et al., 2017; Wang et al., 2020), we found no difference in *Nrf2* mRNA expression and Nrf2 total protein level among the experimental groups (Figure 4A, B). However, we cannot know whether the whole amount of Nrf2 protein was kept inactive in the cytoplasm or whether it translocated to the nucleus becoming active in some of the groups. What we can appreciate is an overall increased

antioxidant response in MCE-injected animals, based on HO-1 and NQO1 mRNA and protein expression levels (**Figure 4C-F**). This is in accordance with the data recently presented by Wang et al., showing that the retinal expression of HO-1 and NQO1 is upregulated during the acute phase of glaucoma and up to 6 weeks after high IOP induction (Wang et al., 2019). The overexpression of HO-1 and NQO1 in the MCE glaucoma model was almost completely prevented by the ACE oil enriched diet. Indeed, we obtained a total protein recovery and a partial mRNA recovery in the expression of these enzymes. These results could depend on the action of ACE oil exerted within the retina during the four weeks of special diet prior to MCE injection, which might have allowed to buffer the glaucoma-triggered increase in free radical species formation, thus decreasing the upstream oxidative stress-driven expression of HO-1 and NQO1.

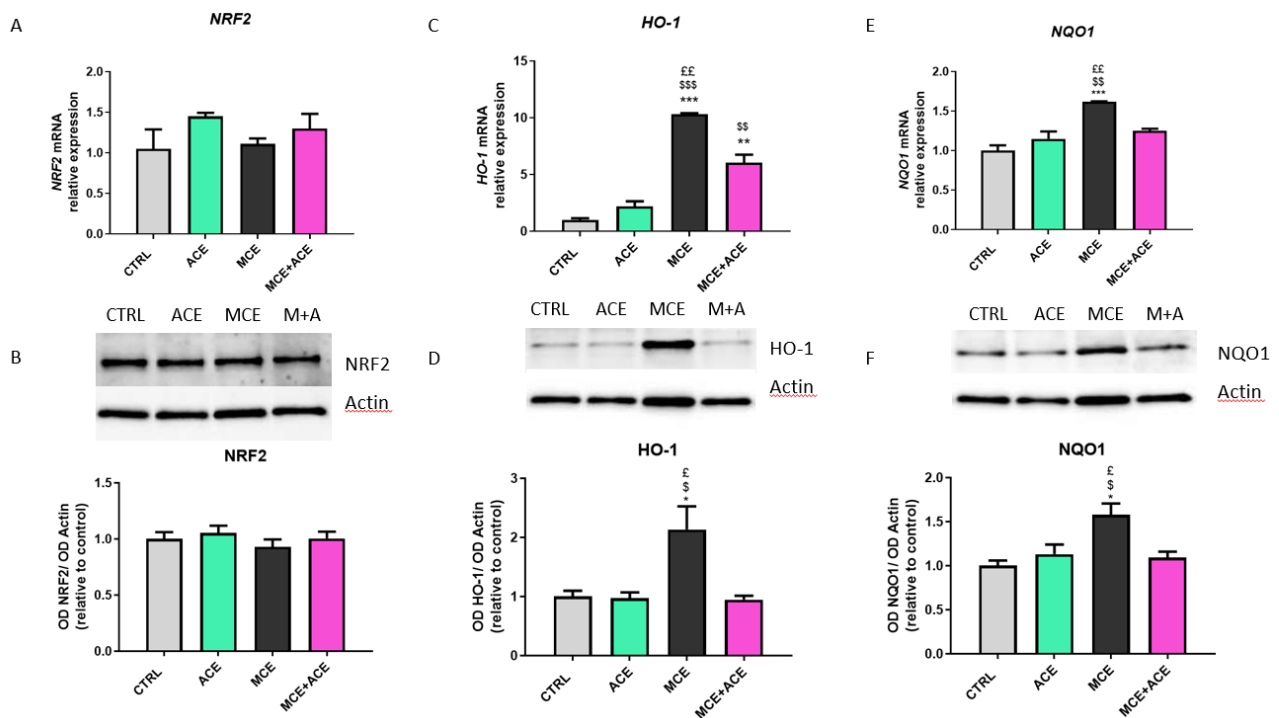


Figure 4. Effects of ACE oil enriched diet on oxidative stress markers. The mRNA and protein expression levels of NRF2 (A,B), HO-1 (C,D) and NQO1 (E,F) were evaluated in retinæ coming from control mice (CTRL), mice fed with ACE oil enriched diet (ACE) mice that received MCE injection fed with either regular food (MCE) or special diet (M+A). The values reported in the mRNA graphs represent the *NRF2*, *HO-1* and *NQO1* mean values of relative expression versus *RPL13a* ones, \pm SEM. Each column in these graphs represents the mean of data from three independent samples. The values reported in the protein graphs represent the NRF2, HO-1 and NQO1 bands optical density mean values normalized versus β -actin ones, \pm SEM. Each column in these graphs represents the mean of data from three independent samples. Statistical significance was evaluated through One-way ANOVA followed by post-hoc Tukey's multiple comparisons test. * = vs CTRL; \$ = vs ACE; £ = vs MCE+ACE. * $p < 0.05$; \$ $p < 0.05$; £ $p < 0.05$; ** $p < 0.01$; \$\$ $p < 0.01$; ££ $p < 0.01$; *** $p < 0.001$; \$\$\$ $p < 0.001$.

ACE oil enriched diet alleviates ischemia within glaucomatous retinae

Glaucoma is characterized by reduced ocular perfusion in both early and late stages; tissue ischemia/hypoxia in the optic nerve head and/or retina can develop either because of or independently from the elevated IOP and is associated to optic nerve degeneration (Flammer et al., 2002; Tezel et al., 2004). Indeed, within the retina, RGC are the most sensitive and vulnerable cells to ischemic injury, which promotes their death by apoptosis (Osborne et al., 1999; Pan et al., 2021). HIF-1 α is a key regulator of the response to ischemic damage (Zhang et al., 2018) and is upregulated in the retina and in the optic nerve head of glaucoma patients (Tezel et al., 2004). Suppression of HIF-1 α upregulation characterizing a high-tension rat glaucoma model, exerts a protective action against retinal ischemia and reduces retinal apoptosis (Chao et al., 2013). In the present work, the MCE-induced overexpression of HIF-1 α was completely suppressed by ACE oil enriched diet (**Figure 5A**). Although not significant, MCE injection caused also a slight increase in VEGF protein, a well-known target of HIF-1 α deeply involved in physiological and pathological angiogenesis (Melincovici et al., 2018). The trend is inhibited by the special diet (**Figure 5B**). These results suggest that ACE oil might exert protective functions against retinal ischemic damage characterizing glaucoma.

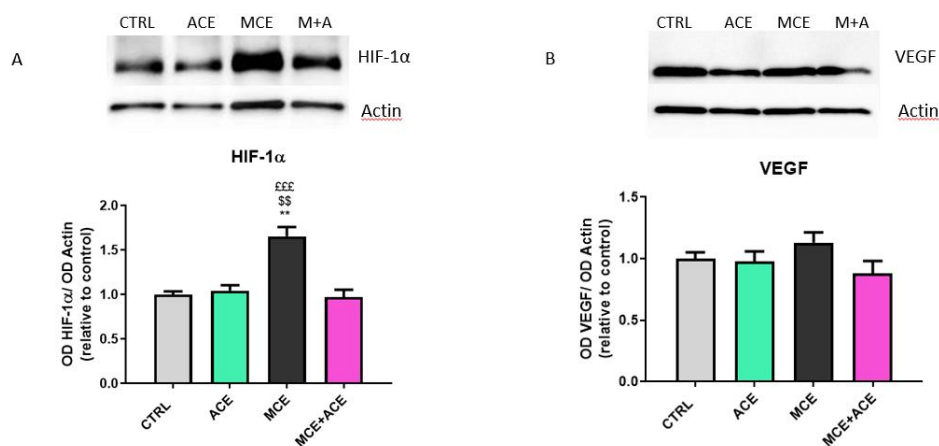


Figure 5. ACE oil enriched diet ameliorates ischemia. The protein expression levels of HIF-1 α (A) and VEGF1 (B) were evaluated through western blot experiments in retinae coming from control mice (CTRL), mice fed with ACE oil enriched diet (ACE), mice that received MCE injection fed with either regular food (MCE) or special diet (M+A). The values reported in the graphs represent the HIF-1 α , and VEGF bands optical density mean values normalized versus β -actin ones, \pm SEM. Each column in these graphs represents the mean of data from three independent samples. Statistical significance was evaluated through One-way ANOVA followed by post-hoc Tukey's multiple comparisons test. * = vs CTRL; $\text{\$}$ = vs ACE; $\text{\text{f}}$ = vs MCE+ACE. ** $p < 0.01$; $\text{\text{S}}$ $p < 0.01$; $\text{\text{f f f}}$ $p < 0.001$.

ACE oil enriched diet exerts protective effects against apoptosis

Inflammation, oxidative stress and ischemia/hypoxia represent a vicious circle where any of these elements can trigger the activation of the others and sustain in time the neurodegenerative processes

(Merelli et al., 2020). Indeed, ischemic/hypoxic injury triggers the initiation of innate inflammatory response with the expression of proinflammatory cytokines (Li et al., 2007; Eltzschig et al., 2011) and, although HIF-1 signalling can exert protective effects, it is well known that it contributes to cellular death and tissue damage when its activation is sustained over time (Zhang et al., 2018 and references therein). Oxidative stress promotes mitochondrial failure and inflammation leading to retinal neuronal morphological and functional alterations, which result in neurodegeneration (Pinazo-Durán et al., 2015; Ahmad et al., 2020). The severe and/or prolonged activation of the inflammatory process, whose aim in the early stages is to counteract an insult and its damaging effects, leads to deleterious outcomes when prolonged over time, with implication in both induction and progression of pathologies. Particularly, in glaucoma, this promotes RGC degeneration (Tezel, 2013). Consistently, as shown in **Figure 6**, MCE-induced IOP elevation, the consequent gliosis triggering, oxidative stress, ischemia and inflammation lead to increased level of the apoptosis effector cleaved caspase 3 within the whole retina. Interestingly, caspase 3 activation in glaucomatous animals was completely prevented by ACE-oil enriched diet, suggesting a reduction of apoptosis triggering within the retinae of these animals.

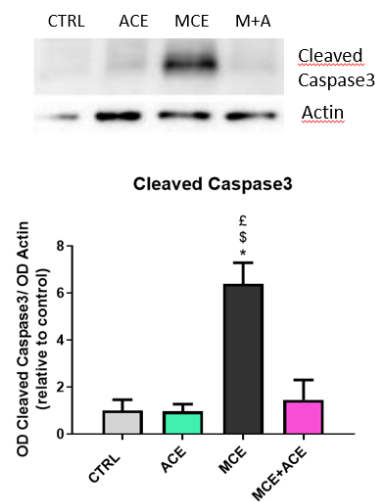


Figure 6. ACE oil enriched diet prevents apoptosis within the retina. The protein expression levels of Cleaved Caspase 3 were evaluated in retinae coming from control mice (CTRL), mice fed with ACE oil enriched diet (ACE) mice that received MCE injection fed with either regular food (MCE) or special diet (M+A). The values reported in the graph represent the Cleaved Caspase 3 bands optical density mean values normalized versus β -actin ones, \pm SEM. Each column in these graphs represents the mean of data from three independent samples. Statistical significance was evaluated through One-way ANOVA followed by post-hoc Tukey's multiple comparisons test. * = vs CTRL; $\text{\$}$ = vs ACE; $\text{\text{€}}$ = vs MCE+ACE. * $p < 0.05$; $\text{\$}$ $p < 0.05$; $\text{\text{€}}$ $p < 0.05$.

ACE oil enriched diet partially rescues RGC functionality

In glaucoma, RGC death precedes RGC loss of function (Fortune et al., 2004; Howell et al., 2007; Saleh et al., 2007; Buckingham et al., 2008; Luo et al., 2014). Therefore, RGC, although still alive,

may no longer be functional. Thus, we decided to analyse electroretinogram (ERG) responses, in particular full field photopic ERG and Pattern ERG (PERG). PERG is generated by central RGC and it is currently recognized as the most specific technique for electrophysiological evaluation of RGC function in primate and rodent models of glaucoma (Porciatti, 2015). On the other hand, photopic ERG is used to verify that the procedure to increase IOP has not induced a generalized retinal damage (Bui et al., 2013) even though alteration of the photopic negative response (PhNR) in the photopic ERG can occur, since this negative wave is generated by the activity of peripheral RGC (Prencipe et al., 2020). As shown in **Figure 7**, both PhNR and PERG are reduced in amplitude by MCE injection, in line with previous reports (Saleh et al., 2007; Cvenkel et al., 2017; Huang et al., 2018; Locri et al., 2019; Cammalleri et al., 2020). ACE oil enriched diet, although not effective in restoring PERG latency, preserved the amplitude of both PhNR and PERG, possibly suggesting a partial recovery of glaucoma-related retinal dysfunctions.

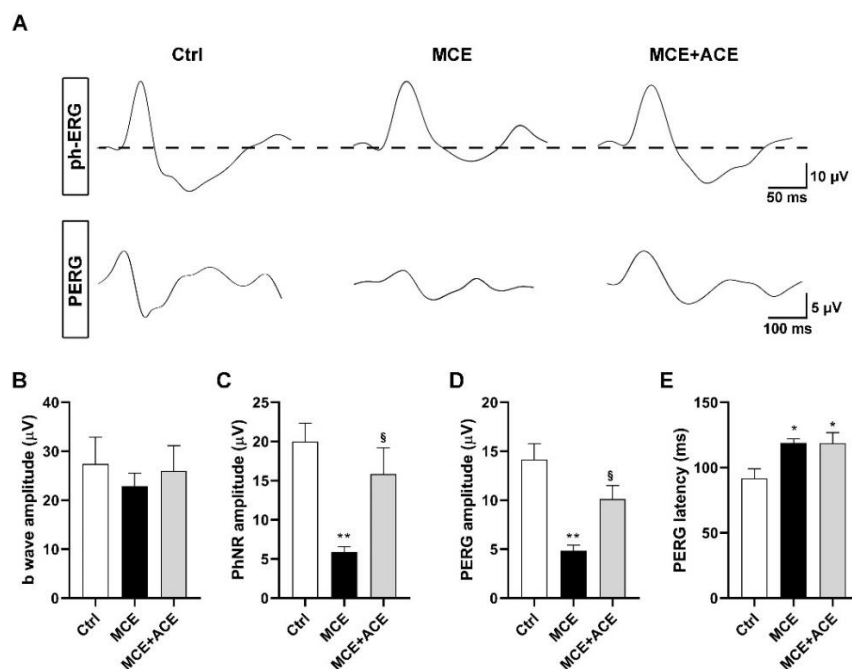


Figure 7. Effects of dietary supplementation on RGC function were evaluated by photopic full field ERG and PERG. Representative photopic ERG (A, upper part) traces showing photopic b-waves with PhNR; PERG (A, lower part) traces showing the two negative peaks (N35 and N95) and the positive peak P50 in control mice and in mice injected with MCE fed ACE-oil enriched diet. (B,C) Mean amplitudes of photopic ERG responses evaluated as changes from baseline, normalized to the amplitude measured in control animals. MCE did not affect the amplitude of the photopic b-wave, while it reduced the amplitude of PhNR. Dietary supplementation partially prevented the reduction in PhNR amplitude. (D) PERG amplitude was reduced by MCE, an effect that was partially prevented by dietary supplementation. (E) Mean implicit time of PERG was increased by MCE, an effect that was not abolished by dietary supplementation. Data are shown as mean of the groups \pm SEM (n = 4 for each group). Statistical significance was evaluated through One-way ANOVA followed by the Newman-Keuls multiple comparison post-hoc test. * = vs CTRL; § = vs MCE. *p < 0.05; §p < 0.05; **p < 0.01.

Conclusion

The possible usage of nutraceuticals characterised by antioxidant, anti-inflammatory, and anti-apoptotic properties to prevent neurodegeneration in glaucoma models is becoming more and more interesting. We added to the list of putative effective natural compounds the ACE oil. The inner composition of ACE oil is quite peculiar, with high quantity of sterols, vitamin E and triterpene acids (Carnés-Sánchez et al., 2002; Zarrouk et al., 2019). Particularly, vitamin E is a powerful antioxidant, and there are some indications about its neuroprotective effect (Engin et al., 2007; Ko et al., 2010). Triterpene acids show anti-inflammatory, antioxidant and neuroprotective properties, as well (Qian et al., 2016; Wang et al., 2018). Their efficacy against glaucoma related dysfunctions is progressively emerging from literature in different glaucoma models (Kyung et al., 2015; Gu et al., 2018; Huang et al., 2018). Thus, the unique composition of ACE oil can account for its strong anti-inflammatory, antioxidant, antiapoptotic and neuroprotective effects. Indeed, as shown in the present study, due to its special properties and composition, ACE oil was able to restore homeostasis in high tension glaucoma through mitigation of glial cells reactivity of the consequent inflammatory response, of oxidative stress and of ischemic damage. This resulted in inhibition of apoptosis within the retina and partial recover of the electrophysiological retinal functions. These ameliorative effects exerted by ACE oil were IOP-independent. The finding of novel compounds able to counteract other risk factors than IOP that contribute to RGC loss, would be invaluable, especially in those cases in which neurodegeneration progression goes on in patients with pharmacologically controlled IOP (Cockburn 1983; Brubaker 1996; Heijl et al., 2002), as well as in normotensive glaucoma (Kamal 1998; Mallick et al., 2016; Killer et al., 2018).

Despite any clinical effectiveness of this oil is yet to be demonstrated, what can be extrapolated from these preliminary data is that nutritional supplementation with ACE oil could represent an interesting coadjuvant in the management of glaucoma.

References

- Adornetto A, Rombolà L, Morrone LA, Nucci C, Corasaniti MT, Bagetta G, Russo R. Natural Products: Evidence for Neuroprotection to Be Exploited in Glaucoma. *Nutrients*. 2020;12(10):3158.
- Aguilar E, Dorrell MI, Friedlander D, Jacobson RA, Johnson A, Marchetti V, Moreno SK, Ritter MR, Friedlander M. Chapter 6. Ocular models of angiogenesis. *Methods Enzymol*. 2008;444:115-58.
- Ahmad A, Ahsan H. Biomarkers of inflammation and oxidative stress in ophthalmic disorders. *J Immunoassay Immunochem*. 2020 May 3;41(3):257-271.
- Ahmed SM, Luo L, Namani A, Wang XJ, Tang X. Nrf2 signaling pathway: Pivotal roles in inflammation. *Biochim Biophys Acta Mol Basis Dis*. 2017;1863(2):585-597.
- Ahnelt PK. The photoreceptor mosaic. *Eye (Lond)*. 1998;12:531-40.
- Almasieh M, Levin LA. Neuroprotection in Glaucoma: Animal Models and Clinical Trials. *Annu Rev Vis Sci*. 2017;3:91-120.
- Alqawlaq S, Flanagan JG, Sivak JM. All roads lead to glaucoma: Induced retinal injury cascades contribute to a common neurodegenerative outcome. *Exp Eye Res*. 2019;183:88-97.
- Amato R, Rossino MG, Cammalleri M, Timperio AM, Fanelli G, Dal Monte M, Pucci L, Casini G. The Potential of Lisosan G as a Possible Treatment for Glaucoma. *Front Pharmacol*. 2021;12:719951.
- Amato R, Pisani F, Laudadio E, Cammalleri M, Lucchesi M, Marracci S, Filippi L, Galeazzi R, Svelto M, Dal Monte M, Bagnoli P. HIF-1-Dependent Induction of β_3 Adrenoceptor: Evidence from the Mouse Retina. *Cells*. 2022;11(8):1271.
- Ashton N, Ward B, Serpell G. Role of oxygen in the genesis of retrolental fibroplasia; a preliminary report. *Br J Ophthalmol*. 1953;37(9):513-20.
- Ashton N, Ward B, Serpell G. Effect of oxygen on developing retinal vessels with particular reference to the problem of retrolental fibroplasia. *Br J Ophthalmol*. 1954;38(7):397-432.
- Askie LM, Darlow BA, Finer N, Schmidt B, Stenson B, Tarnow-Mordi W, Davis PG, Carlo WA, Brocklehurst P, Davies LC, Das A, Rich W, Gantz MG, Roberts RS, Whyte RK, Costantini L, Poets C, Asztalos E, Battin M, Halliday HL, Marlow N, Tin W, King A, Juszczak E, Morley CJ, Doyle LW, Gebiski V, Hunter KE, Simes RJ; Neonatal Oxygenation Prospective Meta-analysis (NeOProm) Collaboration. Association Between Oxygen Saturation Targeting and Death or Disability in Extremely Preterm Infants in the Neonatal Oxygenation Prospective Meta-analysis Collaboration. *JAMA*. 2018;319(21):2190-2201.
- Balakrishnan. NDC-IVM: An automatic segmentation of optic disc and cup region from medical images for glaucoma detection. *J Innov Opt Health Sci*. 2017;10(3):1750007.
- Barnett JM, Yanni SE, Penn JS. The development of the rat model of retinopathy of prematurity. *Doc Ophthalmol*. 2010;120(1):3-12.

- Bedrossian RH, Carmichael P, Ritter J. Retinopathy of prematurity (retrolental fibroplasia) and oxygen. I. Clinical study. II. Further observations on the disease. *Am J Ophthalmol*. 1954;37(1):78-86.
- Bellezza AJ, Rintalan CJ, Thompson HW, Downs JC, Hart RT, Burgoyne CF. Deformation of the lamina cribrosa and anterior scleral canal wall in early experimental glaucoma. *Invest Ophthalmol Vis Sci*. 2003;44(2):623-37.
- Bertalmío M. Chapter 2 -The biological basis of vision: the retina. *Vision Models for High Dynamic Range and Wide Colour Gamut Imaging*. 2020: 11-46.
- Bischoff PM, Wajer SD, Flower RW. Scanning electron microscopic studies of the hyaloid vascular system in newborn mice exposed to O₂ and CO₂. *Graefes Arch Clin Exp Ophthalmol*. 1983;220(6):257-63.
- Blencowe H, Lawn JE, Vazquez T, Fielder A, Gilbert C. Preterm-associated visual impairment and estimates of retinopathy of prematurity at regional and global levels for 2010. *Pediatr Res*. 2013;74 Suppl 1(Suppl 1):35-49.
- Bowl W, Lorenz B, Stieger K, Schweinfurth S, Holve K, Andrassi-Darida M. Fundus-Controlled Dark Adaptometry in Young Children Without and With Spontaneously Regressed Retinopathy of Prematurity. *Transl Vis Sci Technol*. 2019;8(3):62.
- Brubaker RF. Delayed functional loss in glaucoma. LII Edward Jackson Memorial Lecture. *Am J Ophthalmol*. 1996;121(5):473-83.
- Buckingham BP, Inman DM, Lambert W, Oglesby E, Calkins DJ, Steele MR, Vetter ML, Marsh-Armstrong N, Horner PJ. Progressive ganglion cell degeneration precedes neuronal loss in a mouse model of glaucoma. *J Neurosci*. 2008;28(11):2735-44.
- Bueno-Pereira TO, Nunes PR, Matheus MB, Vieira da Rocha AL, Sandrim VC. Nebivolol Increases Nitric Oxide Synthase via β_3 Adrenergic Receptor in Endothelial Cells Following Exposure to Plasma from Preeclamptic Patients. *Cells*. 2022;11(5):883.
- Bui BV, He Z, Vingrys AJ, Nguyen CT, Wong VH, Fortune B. Using the electroretinogram to understand how intraocular pressure elevation affects the rat retina. *J Ophthalmol*. 2013;2013:262467.
- Cai X, Yuan R, Hu Z, Chen C, Yu J, Zheng Z, Ye J. Expression of PirB protein in intact and injured optic nerve and retina of mice. *Neurochem Res* 2012; 37:647-54.
- Calvani M, Pelon F, Comito G, Taddei ML, Moretti S, Innocenti S, Nassini R, Gerlini G, Borgognoni L, Bambi F, Giannoni E, Filippi L, Chiarugi P. Norepinephrine promotes tumor microenvironment reactivity through β_3 -adrenoreceptors during melanoma progression. *Oncotarget*. 2015;6(7):4615-32.
- Calvani M, Bruno G, Dal Monte M, Nassini R, Fontani F, Casini A, Cavallini L, Becatti M, Bianchini F, De Logu F, Forni G, la Marca G, Calorini L, Bagnoli P, Chiarugi P, Pupi A, Azzari C, Geppetti P, Favre C, Filippi L. β_3 -Adrenoceptor as a potential immuno-suppressor agent in melanoma. *Br J Pharmacol*. 2019;176(14):2509-2524.

Cammalleri M, Dal Monte M, Amato R, Bagnoli P, Rusciano D. A Dietary Combination of Forskolin with Homotaurine, Spearmint and B Vitamins Protects Injured Retinal Ganglion Cells in a Rodent Model of Hypertensive Glaucoma. *Nutrients*. 2020;12(4):1189.

Campbell K. Intensive oxygen therapy as a possible cause of retrolental fibroplasia; a clinical approach. *Med J Aust*. 1951;2(2):48-50.

Can N, Catak O, Turgut B, Demir T, Ilhan N, Kuloglu T, Ozercan IH. Neuroprotective and antioxidant effects of ghrelin in an experimental glaucoma model. *Drug Des Devel Ther*. 2015;9:2819-29.

Carnés Sánchez J, Iraola VM, Sastre J, Florido F, Boluda L, Fernández-Caldas E. Allergenicity and immunochemical characterization of six varieties of *Olea europaea*. *Allergy*. 2002;57(4):313-8.

Cavallaro G, Filippi L, Bagnoli P, La Marca G, Cristofori G, Raffaeli G, Padrini L, Araimo G, Fumagalli M, Groppo M, Dal Monte M, Osnaghi S, Fiorini P, Mosca F. The pathophysiology of retinopathy of prematurity: an update of previous and recent knowledge. *Acta Ophthalmol*. 2014;92(1):2-20.

Chang JW. Risk factor analysis for the development and progression of retinopathy of prematurity. *PloS One*. 2019;14(7):e0219934.

Chao HM, Chuang MJ, Liu JH, Liu XQ, Ho LK, Pan WH, Zhang XM, Liu CM, Tsai SK, Kong CW, Lee SD, Chen MM, Chao FP. Baicalein protects against retinal ischemia by antioxidation, antiapoptosis, downregulation of HIF-1 α , VEGF, and MMP-9 and upregulation of HO-1. *J Ocul Pharmacol Ther*. 2013;29(6):539-49.

Chen J, Smith LE. Retinopathy of prematurity. *Angiogenesis*. 2007;10(2):133-40.

Chen PP, Kalina RE. Chronic angle-closure mimicking rubeotic glaucoma in an adult with retinopathy of prematurity. *Arch Ophthalmol*. 1998;116(9):1248.

Chiang MF, Quinn GE, Fielder AR, Ostmo SR, Paul Chan RV, Berrocal A, Binenbaum G, Blair M, Peter Campbell J, Capone A Jr, Chen Y, Dai S, Ells A, Fleck BW, Good WV, Elizabeth Hartnett M, Holmstrom G, Kusaka S, Kychenthal A, Lepore D, Lorenz B, Martinez-Castellanos MA, Özdek Ş, Ademola-Popoola D, Reynolds JD, Shah PK, Shapiro M, Stahl A, Toth C, Vinekar A, Visser L, Wallace DK, Wu WC, Zhao P, Zin A. International Classification of Retinopathy of Prematurity, Third Edition. *Ophthalmology*. 2021;128(10):e51-e68.

Cho KS, Yang L, Lu B, Feng Ma H, Huang X, Pekny M, Chen DF. Re-establishing the regenerative potential of central nervous system axons in postnatal mice. *J Cell Sci* 2005; 118:863-72.

Chrysostomou V, Rezanian F, Trounce IA, Crowston JG. Oxidative stress and mitochondrial dysfunction in glaucoma. *Curr Opin Pharmacol*. 2013;13(1):12-5.

Claxton S, Fruttiger M. Role of arteries in oxygen induced vaso-obliteration. *Exp Eye Res*. 2003;77(3):305-11.

Cockburn DM. Does reduction of intraocular pressure (IOP) prevent visual field loss in glaucoma? *Am J Optom Physiol Opt*. 1983;60(8):705-11.

Coleman AL, Stone KL, Kodjebacheva G, Yu F, Pedula KL, Ensrud KE, Cauley JA, Hochberg MC, Topouzis F, Badala F, Mangione CM; Study of Osteoporotic Fractures Research Group. Glaucoma risk and the consumption of fruits and vegetables among older women in the study of osteoporotic fractures. *Am J Ophthalmol*. 2008;145(6):1081-9.

Connor KM, Krah NM, Dennison RJ, Aderman CM, Chen J, Guerin KI, Sapielha P, Stahl A, Willett KL, Smith LE. Quantification of oxygen-induced retinopathy in the mouse: a model of vessel loss, vessel regrowth and pathological angiogenesis. *Nat Protoc*. 2009;4(11):1565-73.

Cook C. Retrolental fibroplasia. *Postgrad Med J*. 1957;33(380):260-5.

Cunha-Vaz J, Bernardes R, Lobo C. Blood-retinal barrier. *Eur J Ophthalmol*. 2011;21 Suppl 6:S3-9.

Cvenkel B, Sustar M, Perovšek D. Ganglion cell loss in early glaucoma, as assessed by photopic negative response, pattern electroretinogram, and spectral-domain optical coherence tomography. *Doc Ophthalmol*. 2017;135(1):17-28.

Daaka Y, Luttrell LM, Lefkowitz RJ. Switching of the coupling of the beta2-adrenergic receptor to different G proteins by protein kinase A. *Nature*. 1997;390(6655):88-91.

Dal Monte M, Martini D, Latina V, Pavan B, Filippi L, Bagnoli P. Beta-adrenoreceptor agonism influences retinal responses to hypoxia in a model of retinopathy of prematurity. *Invest Ophthalmol Vis Sci*. 2012;53(4):2181-92.

Dal Monte M, Filippi L, Bagnoli P. Beta3-adrenergic receptors modulate vascular endothelial growth factor release in response to hypoxia through the nitric oxide pathway in mouse retinal explants. *Naunyn Schmiedebergs Arch Pharmacol*. 2013a;386(4):269-78.

Dal Monte M, Casini G, la Marca G, Isacchi B, Filippi L, Bagnoli P. Eye drop propranolol administration promotes the recovery of oxygen-induced retinopathy in mice. *Exp Eye Res*. 2013b;111:27-35.

Dal Monte M, Fornaciari I, Nicchia GP, Svelto M, Casini G, Bagnoli P. β 3-adrenergic receptor activity modulates melanoma cell proliferation and survival through nitric oxide signaling. *Naunyn Schmiedebergs Arch Pharmacol*. 2014;387(6):533-43.

Dal Monte M, Cammalleri M, Mattei E, Filippi L, Bagnoli P. Protective effects of β 1/2 adrenergic receptor deletion in a model of oxygen-induced retinopathy. *Invest Ophthalmol Vis Sci*. 2015;56(1):59-73.

Dal Monte M, Evans BA, Arioglu-Inan E, Michel MC. Upregulation of β 3-adrenoceptors-a general marker of and protective mechanism against hypoxia? *Naunyn Schmiedebergs Arch Pharmacol*. 2020;393(2):141-146.

De Moraes CG. Anatomy of the visual pathways. *J Glaucoma*. 2013;22 Suppl 5:S2-7.

Deissler H, Deissler H, Lang S, Lang GE. VEGF-induced effects on proliferation, migration and tight junctions are restored by ranibizumab (Lucentis) in microvascular retinal endothelial cells. *Br J Ophthalmol*. 2008;92(6):839-43.

- Deliyanti D, Lee JY, Petratos S, Meyer CJ, Ward KW, Wilkinson-Berka JL, de Haan JB. A potent Nrf2 activator, dh404, bolsters antioxidant capacity in glial cells and attenuates ischaemic retinopathy. *Clin Sci (Lond)*. 2016;130(15):1375-87.
- Dessy C, Moniotte S, Ghisdal P, Havaux X, Noirhomme P, Balligand JL. Endothelial beta3-adrenoceptors mediate vasorelaxation of human coronary microarteries through nitric oxide and endothelium-dependent hyperpolarization. *Circulation*. 2004;110(8):948-54.
- Dhillon B, Butt Z, Fleck B. Rubeotic glaucoma and retinopathy of prematurity: a case report. *J Pediatr Ophthalmol Strabismus*. 1992;29(2):123-5.
- Dixon RA, Kobilka BK, Strader DJ, Benovic JL, Dohlman HG, Frielle T, Bolanowski MA, Bennett CD, Rands E, Diehl RE, Mumford RA, Slater EE, Sigal IS, Caron MG, Lefkowitz RJ, Strader CD. Cloning of the gene and cDNA for mammalian beta-adrenergic receptor and homology with rhodopsin. *Nature*. 1986;321(6065):75-9.
- Dorrell MI, Aguilar E, Friedlander M. Retinal vascular development is mediated by endothelial filopodia, a preexisting astrocytic template and specific R-cadherin adhesion. *Invest Ophthalmol Vis Sci*. 2002;43(11):3500-10.
- Eelen G, Treps L, Li X, Carmeliet P. Basic and Therapeutic Aspects of Angiogenesis Updated. *Circ Res*. 2020;127(2):310-329.
- Eichler W, Yafai Y, Keller T, Wiedemann P, Reichenbach A. PEDF derived from glial Müller cells: a possible regulator of retinal angiogenesis. *Exp Cell Res*. 2004;299(1):68-78.
- Eltzschig HK, Carmeliet P. Hypoxia and inflammation. *N Engl J Med*. 2011;364(7):656-65.
- Emorine LJ, Marullo S, Briend-Sutren MM, Patey G, Tate K, Delavier-Klutchko C, Strosberg AD. Molecular characterization of the human beta 3-adrenergic receptor. *Science*. 1989;245(4922):1118-21.
- Engin KN, Engin G, Kucuksahin H, Oncu M, Engin G, Guvener B. Clinical evaluation of the neuroprotective effect of alpha-tocopherol against glaucomatous damage. *Eur J Ophthalmol*. 2007;17(4):528-33.
- Feng DF, Chen ET, Li XY, Liu Y, Wang Y. Standardizing optic nerve crushes with an aneurysm clip. *Neurol Res* 2010; 32:476-81.
- Fielder A, Blencowe H, O'Connor A, Gilbert C. Impact of retinopathy of prematurity on ocular structures and visual functions. *Arch Dis Child Fetal Neonatal Ed*. 2015 Mar;100(2):F179-84.
- Filippi L, Cavallaro G, Bagnoli P, Dal Monte M, Fiorini P, Donzelli G, Tinelli F, Araimo G, Cristofori G, la Marca G, Della Bona ML, La Torre A, Fortunato P, Furlanetto S, Osnaghi S, Mosca F. Oral propranolol for retinopathy of prematurity: risks, safety concerns, and perspectives. *J Pediatr*. 2013;163(6):1570-1577.e6.
- Filippi L, Dal Monte M, Casini G, Daniotti M, Sereni F, Bagnoli P. Infantile hemangiomas, retinopathy of prematurity and cancer: a common pathogenetic role of the β -adrenergic system. *Med Res Rev*. 2015 May;35(3):619-52.

Filippi L, Cavallaro G, Bagnoli P, Dal Monte M, Fiorini P, Berti E, Padrini L, Donzelli G, Araimo G, Cristofori G, Fumagalli M, la Marca G, Della Bona ML, Pasqualetti R, Fortunato P, Osnaghi S, Tomasini B, Vanni M, Calvani AM, Milani S, Cortinovis I, Pugi A, Agosti M, Mosca F. Propranolol 0.1% eye micro-drops in newborns with retinopathy of prematurity: a pilot clinical trial. *Pediatr Res.* 2017;81(2):307-314.

Filippi L, Cavallaro G, Berti E, Padrini L, Araimo G, Regiroli G, Raffaelli G, Bozzetti V, Tagliabue P, Tomasini B, Mori A, Buonocore G, Agosti M, Bossi A, Chirico G, Aversa S, Fortunato P, Osnaghi S, Cavallotti B, Suzani M, Vanni M, Borsari G, Donati S, Nascimbeni G, Nardo D, Piermarocchi S, la Marca G, Forni G, Milani S, Cortinovis I, Calvani M, Bagnoli P, Dal Monte M, Calvani AM, Pugi A, Villamor E, Donzelli G, Mosca F. Propranolol 0.2% Eye Micro-Drops for Retinopathy of Prematurity: A Prospective Phase IIB Study. *Front Pediatr.* 2019;7:180.

Filippi L, Cammalleri M, Amato R, Ciantelli M, Pini A, Bagnoli P, Dal Monte M. Decoupling Oxygen Tension From Retinal Vascularization as a New Perspective for Management of Retinopathy of Prematurity. New Opportunities From β -adrenoceptors. *Front Pharmacol.* 2022;13:835771.

Fish JE, Matouk CC, Yeboah E, Bevan SC, Khan M, Patil K, Ohh M, Marsden PA. Hypoxia-inducible expression of a natural cis-antisense transcript inhibits endothelial nitric-oxide synthase. *J Biol Chem.* 2007;282(21):15652-66.

Flammer J, Orgül S, Costa VP, Orzalesi N, Krieglstein GK, Serra LM, Renard JP, Stefánsson E. The impact of ocular blood flow in glaucoma. *Prog Retin Eye Res.* 2002;21(4):359-93.

Flaxman SR, Bourne RRA, Resnikoff S, Ackland P, Braithwaite T, Cicinelli MV, Das A, Jonas JB, Keeffe J, Kempen JH, Leasher J, Limburg H, Naidoo K, Pesudovs K, Silvester A, Stevens GA, Tahhan N, Wong TY, Taylor HR; Vision Loss Expert Group of the Global Burden of Disease Study. Global causes of blindness and distance vision impairment 1990-2020: a systematic review and meta-analysis. *Lancet Glob Health.* 2017;5(12):e1221-e1234.

Flower RW, McLeod DS, Lutty GA, Goldberg B, Wajer SD. Postnatal retinal vascular development of the puppy. *Invest Ophthalmol Vis Sci.* 1985;26(7):957-68.

Fortune B, Bui BV, Morrison JC, Johnson EC, Dong J, Cepurna WO, Jia L, Barber S, Cioffi GA. Selective ganglion cell functional loss in rats with experimental glaucoma. *Invest Ophthalmol Vis Sci.* 2004;45(6):1854-62.

Freedman, N. J., & Lefkowitz, R. J. (1996). Desensitization of G protein-coupled receptors. *Recent progress in hormone research*, 51, 319–353.

Fu Z, Sun Y, Cakir B, Tomita Y, Huang S, Wang Z, Liu CH, S Cho S, Britton W, S Kern T, Antonetti DA, Hellström A, E H Smith L. Targeting Neurovascular Interaction in Retinal Disorders. *Int J Mol Sci.* 2020 Feb 22;21(4):1503.

Gallego BI, Salazar JJ, de Hoz R, Rojas B, Ramírez AI, Salinas-Navarro M, Ortín-Martínez A, Valiente-Soriano FJ, Avilés-Trigueros M, Villegas-Perez MP, Vidal-Sanz M, Triviño A, Ramírez JM. IOP induces upregulation of GFAP and MHC-II and microglia reactivity in mice retina contralateral to experimental glaucoma. *J Neuroinflammation.* 2012;9:92.

Garcia-Medina JJ, Rubio-Velazquez E, Lopez-Bernal MD, Cobo-Martinez A, Zanon-Moreno V, Pinazo-Duran MD, Del-Rio-Vellosillo M. Glaucoma and Antioxidants: Review and Update. *Antioxidants (Basel)*. 2020;9(11):1031.

Gauthier C, Langin D, Balligand JL. Beta3-adrenoceptors in the cardiovascular system. *Trends Pharmacol Sci*. 2000;21(11):426-31.

Giaconi JA, Yu F, Stone KL, Pedula KL, Ensrud KE, Cauley JA, Hochberg MC, Coleman AL; Study of Osteoporotic Fractures Research Group. The association of consumption of fruits/vegetables with decreased risk of glaucoma among older African-American women in the study of osteoporotic fractures. *Am J Ophthalmol*. 2012;154(4):635-44.

Gilbert C. Retinopathy of prematurity: a global perspective of the epidemics, population of babies at risk and implications for control. *Early Hum Dev*. 2008;84(2):77-82.

Gill R, Tsung A, Billiar T. Linking oxidative stress to inflammation: Toll-like receptors. *Free Radic Biol Med*. 2010;48(9):1121-32.

Goel M, Picciani RG, Lee RK, Bhattacharya SK. Aqueous humor dynamics: a review. *Open Ophthalmol J*. 2010;4:52-9.

Gole GA, Browning J, Elts SM. The mouse model of oxygen-induced retinopathy: a suitable animal model for angiogenesis research. *Doc Ophthalmol*. 1990 Mar;74(3):163-9.

Greco A, Rizzo MI, De Virgilio A, Gallo A, Fusconi M, de Vincentiis M. Emerging Concepts in Glaucoma and Review of the Literature. *Am J Med*. 2016;129(9):1000.e7-1000.e13.

Grewe R. Zur Geschichte des Glaukoms [The history of glaucoma]. *Klin Monbl Augenheilkd*. 1986 Feb;188(2):167-9. German. doi: 10.1055/s-2008-1050606.

Gordon MO, Beiser JA, Brandt JD, Heuer DK, Higginbotham EJ, Johnson CA, Keltner JL, Miller JP, Parrish RK 2nd, Wilson MR, Kass MA. The Ocular Hypertension Treatment Study: baseline factors that predict the onset of primary open-angle glaucoma. *Arch Ophthalmol*. 2002;120(6):714-20; discussion 829-30.

Gu L, Kwong JMK, Yadegari D, Yu F, Caprioli J, Piri N. The effect of celastrol on the ocular hypertension-induced degeneration of retinal ganglion cells. *Neurosci Lett*. 2018;670:89-93.

Guglielmi P, Carradori S, Campestre C, Poce G. Novel therapies for glaucoma: a patent review (2013-2019). *Expert Opin Ther Pat*. 2019;29(10):769-780.

Guo K, Ma Q, Wang L, Hu H, Li J, Zhang D, Zhang M. Norepinephrine-induced invasion by pancreatic cancer cells is inhibited by propranolol. *Oncol Rep*. 2009;22(4):825-30.

Hall RA. Beta-adrenergic receptors and their interacting proteins. *Semin Cell Dev Biol*. 2004;15(3):281-8.

Hammarlund EU, Flashman E, Mohlin S, Licausi F. Oxygen-sensing mechanisms across eukaryotic kingdoms and their roles in complex multicellularity. *Science*. 2020 Oct 23;370(6515):eaba3512.

- Hansen JL, Theilade J, Aplin M, Sheikh SP. Role of G-protein-coupled receptor kinase 2 in the heart-do regulatory mechanisms open novel therapeutic perspectives? *Trends Cardiovasc Med*. 2006;16(5):169-77.
- Hansen RM, Fulton AB. Background adaptation in children with a history of mild retinopathy of prematurity. *Invest Ophthalmol Vis Sci*. 2000;41(1):320-4.
- Harari OA, Liao JK. NF- κ B and innate immunity in ischemic stroke. *Ann N Y Acad Sci*. 2010;1207:32-40.
- Hausdorff WP, Bouvier M, O'Dowd BF, Irons GP, Caron MG, Lefkowitz RJ. Phosphorylation sites on two domains of the beta 2-adrenergic receptor are involved in distinct pathways of receptor desensitization. *J Biol Chem*. 1989;264(21):12657-65.
- Haverkamp S, Kolb H, Cuenca N. Endothelial nitric oxide synthase (eNOS) is localized to Müller cells in all vertebrate retinas. *Vision Res*. 1999;39(14):2299-303.
- He T, Xing YQ, Zhao XH, Ai M. Interaction between iNOS and COX-2 in hypoxia-induced retinal neovascularization in mice. *Arch Med Res*. 2007;38(8):807-15.
- Heijl A, Leske MC, Bengtsson B, Hyman L, Bengtsson B, Hussein M; Early Manifest Glaucoma Trial Group. Reduction of intraocular pressure and glaucoma progression: results from the Early Manifest Glaucoma Trial. *Arch Ophthalmol*. 2002;120(10):1268-79.
- Hellström A, Smith LE, Dammann O. Retinopathy of prematurity. *Lancet*. 2013 Oct 26;382(9902):1445-57.
- Ho JJ, Robb GB, Tai SC, Turgeon PJ, Mawji IA, Man HS, Marsden PA. Active stabilization of human endothelial nitric oxide synthase mRNA by hnRNP E1 protects against antisense RNA and microRNAs. *Mol Cell Biol*. 2013;33(10):2029-46.
- Hollands H, Johnson D, Hollands S, Simel DL, Jinapriya D, Sharma S. Do findings on routine examination identify patients at risk for primary open-angle glaucoma? The rational clinical examination systematic review. *JAMA*. 2013;309(19):2035-42.
- Hoogland IC, Houbolt C, van Westerloo DJ, van Gool WA, van de Beek D. Systemic inflammation and microglial activation: systematic review of animal experiments. *J Neuroinflammation*. 2015;12:114.
- Hoon M, Okawa H, Della Santina L, Wong RO. Functional architecture of the retina: development and disease. *Prog Retin Eye Res*. 2014;42:44-84.
- Howell GR, Libby RT, Jakobs TC, Smith RS, Phalan FC, Barter JW, Barbay JM, Marchant JK, Mahesh N, Porciatti V, Whitmore AV, Masland RH, John SW. Axons of retinal ganglion cells are insulted in the optic nerve early in DBA/2J glaucoma. *J Cell Biol*. 2007;179(7):1523-37.
- Howell GR, Macalinao DG, Sousa GL, Walden M, Soto I, Kneeland SC, Barbay JM, King BL, Marchant JK, Hibbs M, Stevens B, Barres BA, Clark AF, Libby RT, John SW. Molecular clustering identifies complement and endothelin induction as early events in a mouse model of glaucoma. *J Clin Invest* 2011; 121:1429-44.

- Huang W, Gao F, Hu F, Huang J, Wang M, Xu P, Zhang R, Chen J, Sun X, Zhang S, Wu J. Asiatic Acid Prevents Retinal Ganglion Cell Apoptosis in a Rat Model of Glaucoma. *Front Neurosci.* 2018;12:489.
- Hughes S, Yang H, Chan-Ling T. Vascularization of the human fetal retina: roles of vasculogenesis and angiogenesis. *Invest Ophthalmol Vis Sci.* 2000;41(5):1217-28.
- Husain S, Abdul Y, Crosson CE. Preservation of retina ganglion cell function by morphine in a chronic ocular-hypertensive rat model. *Invest Ophthalmol Vis Sci.* 2012;53(7):4289-98.
- Inman DM, Horner PJ. Reactive nonproliferative gliosis predominates in a chronic mouse model of glaucoma. *Glia.* 2007;55(9):942-53.
- Inman DM, Lambert WS, Calkins DJ, Horner PJ. α -Lipoic acid antioxidant treatment limits glaucoma-related retinal ganglion cell death and dysfunction. *PLoS One.* 2013;8(6):e65389.
- International Committee for the Classification of Retinopathy of Prematurity. The international classification of retinopathy of prematurity revisited. *JAMA Ophthalmol* 2005;123:991-9.
- Janaszak-Jasiecka A, Siekierzycka A, Bartoszewska S, Serocki M, Dobrucki LW, Collawn JF, Kalinowski L, Bartoszewski R. eNOS expression and NO release during hypoxia is inhibited by miR-200b in human endothelial cells. *Angiogenesis.* 2018;21(4):711-724.
- Jantsch J, Wiese M, Schödel J, Castiglione K, Gläsner J, Kolbe S, Mole D, Schleicher U, Eckardt KU, Hensel M, Lang R, Bogdan C, Schnare M, Willam C. Toll-like receptor activation and hypoxia use distinct signaling pathways to stabilize hypoxia-inducible factor 1 α (HIF1A) and result in differential HIF1A-dependent gene expression. *J Leukoc Biol.* 2011;90(3):551-62.
- Johnson M. Molecular mechanisms of beta(2)-adrenergic receptor function, response, and regulation. *J Allergy Clin Immunol.* 2006;117(1):18-24; quiz 25.
- Jonas JB, Aung T, Bourne RR, Bron AM, Ritch R, Panda-Jonas S. Glaucoma. *Lancet.* 2017;390(10108):2183-2193.
- Ju WK, Shim MS, Kim KY, Bu JH, Park TL, Ahn S, Weinreb RN. Ubiquinol promotes retinal ganglion cell survival and blocks the apoptotic pathway in ischemic retinal degeneration. *Biochem Biophys Res Commun.* 2018;503(4):2639-2645.
- Jung KA, Kwak MK. The Nrf2 system as a potential target for the development of indirect antioxidants. *Molecules.* 2010;15(10):7266-91.
- Jung F, Palmer LA, Zhou N, Johns RA. Hypoxic regulation of inducible nitric oxide synthase via hypoxia inducible factor-1 in cardiac myocytes. *Circ Res.* 2000;86(3):319-25.
- Kabe Y, Ando K, Hirao S, Yoshida M, Handa H. Redox regulation of NF-kappaB activation: distinct redox regulation between the cytoplasm and the nucleus. *Antioxid Redox Signal.* 2005;7(3-4):395-403.
- Kaempfen S, Neumann RP, Jost K, Schulzke SM. Beta-blockers for prevention and treatment of retinopathy of prematurity in preterm infants. *Cochrane Database Syst Rev.* 2018;3(3):CD011893.

- Kalra EK. Nutraceutical: definition and introduction. *AAPS PharmSci.* 2003;5(3):E25.
- Kamal D, Hitchings R. Normal tension glaucoma: a practical approach. *Br J Ophthalmol.* 1998;82(7):835-40.
- Kang JM, Tanna AP. Glaucoma. *Med Clin North Am.* 2021;105(3):493-510.
- Kass MA, Hart WM Jr, Gordon M, Miller JP. Risk factors favoring the development of glaucomatous visual field loss in ocular hypertension. *Surv Ophthalmol.* 1980;25(3):155-62.
- Kassa A, Konrad H, Geburek T. Molecular diversity and gene flow within and among different subspecies of the wild olive (*Olea europaea* L.): A review. *Flora.* 2019;250:18-26.
- Kaur C, Foulds WS, Ling EA. Blood-retinal barrier in hypoxic ischaemic conditions: basic concepts, clinical features and management. *Prog Retin Eye Res.* 2008;27(6):622-47.
- Killer HE, Pircher A. Normal tension glaucoma: review of current understanding and mechanisms of the pathogenesis. *Eye (Lond).* 2018;32(5):924-930.
- Kingman S. Glaucoma is second leading cause of blindness globally. *Bull World Health Organ.* 2004;82(11):887-8.
- Kishore B, Ananthamoorthy NP. Glaucoma classification based on intra-class and extra-class discriminative correlation and consensus ensemble classifier. *Genomics.* 2020;112(5):3089-3096.
- Ko ML, Peng PH, Hsu SY, Chen CF. Dietary deficiency of vitamin E aggravates retinal ganglion cell death in experimental glaucoma of rats. *Curr Eye Res.* 2010;35(9):842-9.
- Kobilka BK, Dixon RA, Frielle T, Dohlman HG, Bolanowski MA, Sigal IS, Yang-Feng TL, Francke U, Caron MG, Lefkowitz RJ. cDNA for the human beta 2-adrenergic receptor: a protein with multiple membrane-spanning domains and encoded by a gene whose chromosomal location is shared with that of the receptor for platelet-derived growth factor. *Proc Natl Acad Sci U S A.* 1987;84(1):46-50.
- Kohout TA, Lin FS, Perry SJ, Conner DA, Lefkowitz RJ. beta-Arrestin 1 and 2 differentially regulate heptahelical receptor signaling and trafficking. *Proc Natl Acad Sci U S A.* 2001 Feb 13;98(4):1601-6.
- Kolb H. Outer Plexiform Layer. 2005 May 1 [updated 2007 May 1]. In: Kolb H, Fernandez E, Nelson R, editors. *Webvision: The Organization of the Retina and Visual System* [Internet]. Salt Lake City (UT): University of Utah Health Sciences Center; 1995.
- Kong HB, Zheng GY, He BM, Zhang Y, Zhou Q. Clinical Efficacy and Safety of Propranolol in the Prevention and Treatment of Retinopathy of Prematurity: A Meta-Analysis of Randomized Controlled Trials. *Front Pediatr.* 2021;9:631673.
- Krishnan A, Kocab AJ, Zacks DN, Marshak-Rothstein A, Gregory-Ksander M. A small peptide antagonist of the Fas receptor inhibits neuroinflammation and prevents axon degeneration and retinal ganglion cell death in an inducible mouse model of glaucoma. *J Neuroinflammation.* 2019;16(1):184.
- Kyung H, Kwong JM, Bekerman V, Gu L, Yadegari D, Caprioli J, Piri N. Celastrol supports survival of retinal ganglion cells injured by optic nerve crush. *Brain Res.* 2015;1609:21-30.

- Lange C, Ehlken C, Stahl A, Martin G, Hansen L, Agostini HT. Kinetics of retinal vaso-obliteration and neovascularization in the oxygen-induced retinopathy (OIR) mouse model. *Graefes Arch Clin Exp Ophthalmol*. 2009;247(9):1205-11.
- Lanman JT. The control of oxygen therapy for the prevention of retrolental fibroplasia. *J Pediatr*. 1955;46(3):365-8.
- Lakkaraju A, Umapathy A, Tan LX, Daniele L, Philp NJ, Boesze-Battaglia K, Williams DS. The cell biology of the retinal pigment epithelium. *Prog Retin Eye Res*. 2020;24:100846.
- Lawler T, Liu Y, Christensen K, Vajaranant TS, Mares J. Dietary Antioxidants, Macular Pigment, and Glaucomatous Neurodegeneration: A Review of the Evidence. *Nutrients*. 2019;11(5):1002.
- Léauté-Labrèze C, Dumas de la Roque E, Hubiche T, Boralevi F, Thambo JB, Taïeb A. Propranolol for severe hemangiomas of infancy. *N Engl J Med*. 2008;358(24):2649-51.
- Lee M, Wang C, Jin SW, Labrecque MP, Beischlag TV, Brockman MA, Choy JC. Expression of human inducible nitric oxide synthase in response to cytokines is regulated by hypoxia-inducible factor-1. *Free Radic Biol Med*. 2019;130:278-287.
- Li J, Wang JJ, Chen D, Mott R, Yu Q, Ma JX, Zhang SX. Systemic administration of HMG-CoA reductase inhibitor protects the blood-retinal barrier and ameliorates retinal inflammation in type 2 diabetes. *Exp Eye Res*. 2009;89(1):71-8.
- Li L, Huang L, Sung SS, Lobo PI, Brown MG, Gregg RK, et al. NKT cell activation mediates neutrophil IFN-gamma production and renal ischemia-reperfusion injury. *J Immunol* 2007;178(9):5899–5911.
- Li Y, Schlamp CL, Nickells RW. Experimental induction of retinal ganglion cell death in adult mice. *Invest Ophthalmol Vis Sci* 1999; 40:1004-8.
- Libby RT, Howell GR, Pang IH, Savinova OV, Mehalow AK, Barter JW, Smith RS, Clark AF, John SW. Inducible nitric oxide synthase, *Nos2*, does not mediate optic neuropathy and retinopathy in the DBA/2J glaucoma model. *BMC Neurosci* 2007; 8:108.
- Liggett SB, Freedman NJ, Schwinn DA, Lefkowitz RJ. Structural basis for receptor subtype-specific regulation revealed by a chimeric beta 3/beta 2-adrenergic receptor. *Proc Natl Acad Sci U S A*. 1993;90(8):3665-9.
- Limb GA, Salt TE, Munro PM, Moss SE, Khaw PT. In vitro characterization of a spontaneously immortalized human Müller cell line (MIO-M1). *Invest Ophthalmol Vis Sci*. 2002;43(3):864-9.
- Lindsey JD, Duong-Polk KX, Hammond D, Leung CK, Weinreb RN. Protection of injured retinal ganglion cell dendrites and unfolded protein response resolution after long-term dietary resveratrol. *Neurobiol Aging*. 2015;36(5):1969-81.
- Liu CH, Wang Z, Sun Y, Chen J. Animal models of ocular angiogenesis: from development to pathologies. *FASEB J*. 2017;31(11):4665-4681.

- Locri F, Cammalleri M, Dal Monte M, Rusciano D, Bagnoli P. Protective Efficacy of a Dietary Supplement Based on Forskolin, Homotaurine, Spearmint Extract, and Group B Vitamins in a Mouse Model of Optic Nerve Injury. *Nutrients*. 2019;11(12):2931.
- Loskutova E, O'Brien C, Loskutov I, Loughman J. Nutritional supplementation in the treatment of glaucoma: A systematic review. *Surv Ophthalmol*. 2019;64(2):195-216.
- Lulli M, Cammalleri M, Granucci I, Witort E, Bono S, Di Gesualdo F, Lupia A, Loffredo R, Casini G, Dal Monte M, Capaccioli S. In vitro and in vivo inhibition of proangiogenic retinal phenotype by an antisense oligonucleotide downregulating uPAR expression. *Biochem Biophys Res Commun*. 2017;490(3):977-983.
- Luo X, Patel NB, Rajagopalan LP, Harwerth RS, Frishman LJ. Relation between macular retinal ganglion cell/inner plexiform layer thickness and multifocal electroretinogram measures in experimental glaucoma. *Invest Ophthalmol Vis Sci*. 2014;55(7):4512-24.
- Ma K, Xu L, Zhang H, Zhang S, Pu M, Jonas JB. Effect of brimonidine on retinal ganglion cell survival in an optic nerve crush model. *Am J Ophthalmol* 2009; 147:326-31.
- Madan A, Penn JS. Animal models of oxygen-induced retinopathy. *Front Biosci*. 2003;8:d1030-43.
- Mallick J, Devi L, Malik PK, Mallick J. Update on Normal Tension Glaucoma. *J Ophthalmic Vis Res*. 2016;11(2):204-8.
- Mariani AP. Multiaxonal horizontal cells in the retina of the tree shrew, *Tupaia glis*. *J Comp Neurol*. 1985;233(4):553-63.
- Marshall LL, Hayslett RL, Stevens GA. Therapy for Open-Angle Glaucoma. *Consult Pharm*. 2018;33(8):432-445.
- Martini D, Monte MD, Ristori C, Cupisti E, Mei S, Fiorini P, Filippi L, Bagnoli P. Antiangiogenic effects of β_2 -adrenergic receptor blockade in a mouse model of oxygen-induced retinopathy. *J Neurochem*. 2011;119(6):1317-29.
- Maxwell PH, Wiesener MS, Chang GW, Clifford SC, Vaux EC, Cockman ME, Wykoff CC, Pugh CW, Maher ER, Ratcliffe PJ. The tumour suppressor protein VHL targets hypoxia-inducible factors for oxygen-dependent proteolysis. *Nature*. 1999;399(6733):271-5.
- McKinnon SJ, Schlamp CL, Nickells RW. Mouse models of retinal ganglion cell death and glaucoma. *Exp Eye Res* 2009; 88:816-24.
- McMonnies CW. Glaucoma history and risk factors. *J Optom*. 2017;10(2):71-78.
- McQuillan LP, Leung GK, Marsden PA, Kostyk SK, Kourembanas S. Hypoxia inhibits expression of eNOS via transcriptional and posttranscriptional mechanisms. *Am J Physiol*. 1994;267(5 Pt 2):H1921-7.
- Melillo G, Musso T, Sica A, Taylor LS, Cox GW, Varesio L. A hypoxia-responsive element mediates a novel pathway of activation of the inducible nitric oxide synthase promoter. *J Exp Med*. 1995;182(6):1683-93.

- Melincovici CS, Boşca AB, Şuşman S, Mărginean M, Mişu C, Istrate M, Moldovan IM, Roman AL, Mişu CM. Vascular endothelial growth factor (VEGF) - key factor in normal and pathological angiogenesis. *Rom J Morphol Embryol*. 2018;59(2):455-467.
- Merelli A, Repetto M, Lazarowski A, Auzmendi J. Hypoxia, Oxidative Stress, and Inflammation: Three Faces of Neurodegenerative Diseases. *J Alzheimers Dis*. 2021;82(s1):S109-S126.
- Mezu-Ndubuisi OJ, Macke EL, Kalavacherla R, Nwaba AA, Suscha A, Zaitoun IS, Ikeda A, Sheibani N. Long-term evaluation of retinal morphology and function in a mouse model of oxygen-induced retinopathy. *Mol Vis*. 2020;26:257-276.
- Millar C, Kaufman PL. Aqueous humour: secretion and dynamics. In: Tasman W, Jaeger EA, Eds. *Duane's foundations of clinical ophthalmology*. Philadelphia: Lippincott-Raven 1995.
- Miller HC. Survival of premature infants; classification according to respiration rate and need for oxygen therapy. *Obstet Gynecol*. 1956;8(4):459-64.
- Morrone LA, Rombola L, Adornetto A, Corasaniti MT, Russo R. Rational Basis for Nutraceuticals in the Treatment of Glaucoma. *Curr Neuropharmacol*. 2018;16(7):1004-1017.
- Netter FH. 2006. *Atlas of Human Anatomy*. Philadelphia: Elsevier Health Sci.
- Nickells RW, Howell GR, Soto I, John SW. Under pressure: cellular and molecular responses during glaucoma, a common neurodegeneration with axonopathy. *Annu Rev Neurosci*. 2012;35:153-79.
- Nicolaides KH, Economides DL, Soothill PW. Blood gases, pH, and lactate in appropriate- and small-for-gestational-age fetuses. *Am J Obstet Gynecol*. 1989;161(4):996-1001.
- Noor N, Patel CB, Rockman HA. B-arrestin: a signaling molecule and potential therapeutic target for heart failure. *J Mol Cell Cardiol*. 2011;51(4):534-41.
- O'Bryhim BE, Radel J, Macdonald SJ, Symons RC. The genetic control of avascular area in mouse oxygen-induced retinopathy. *Mol Vis*. 2012;18:377-89.
- O'Connor AR, Stephenson T, Johnson A, Tobin MJ, Moseley MJ, Ratib S, Ng Y, Fielder AR. Long-term ophthalmic outcome of low birth weight children with and without retinopathy of prematurity. *Pediatrics*. 2002;109(1):12-8.
- Ohlsson M, Mattsson P, Svensson M. A temporal study of axonal degeneration and glial scar formation following a standardized crush injury of the optic nerve in the adult rat. *Restor Neurol Neurosci* 2004; 22:1-10.
- Olivares-González L, Martínez-Fernández de la Cámara C, Hervás D, Millán JM, Rodrigo R. HIF-1 α stabilization reduces retinal degeneration in a mouse model of retinitis pigmentosa. *FASEB J*. 2018;32(5):2438-2451.
- Osborne NN, Ugarte M, Chao M, Chidlow G, Bae JH, Wood JP, Nash MS. Neuroprotection in relation to retinal ischemia and relevance to glaucoma. *Surv Ophthalmol*. 1999;43 Suppl 1:S102-28.
- Osborne NN. Pathogenesis of ganglion "cell death" in glaucoma and neuroprotection: focus on ganglion cell axonal mitochondria. *Prog Brain Res*. 2008;173:339-52.

- Pan L, Cho KS, Yi I, To CH, Chen DF, Do CW. Baicalein, Baicalin, and Wogonin: Protective Effects against Ischemia-Induced Neurodegeneration in the Brain and Retina. *Oxid Med Cell Longev*. 2021;2021:8377362.
- Pan Y, Varma R. Natural history of glaucoma. *Indian J Ophthalmol*. 2011;59 Suppl(Suppl1):S19-23.
- Panagis L, Zhao X, Ge Y, Ren L, Mittag TW, Danias J. Retinal gene expression changes related to IOP exposure and axonal loss in DBA/2J mice. *Invest Ophthalmol Vis Sci* 2011; 52:7807-16.
- Pang IH, Clark AF. Inducible rodent models of glaucoma. *Prog Retin Eye Res*. 2020;75:100799.
- Pascolini D, Mariotti SP. Global estimates of visual impairment: 2010. *Br J Ophthalmol*. 2012;96(5):614-8.
- Patz A, Eastham A, Higginbotham DH, Kleh T. Oxygen studies in retrolental fibroplasia. II. The production of the microscopic changes of retrolental fibroplasia in experimental animals. *Am J Ophthalmol*. 1953;36(11):1511-22.
- Penn JS, Madan A, Caldwell RB, Bartoli M, Caldwell RW, Hartnett ME. Vascular endothelial growth factor in eye disease. *Prog Retin Eye Res*. 2008 Jul;27(4):331-71.
- Pérez-Sayáns M, Somoza-Martín JM, Barros-Angueira F, Diz PG, Gándara Rey JM, García-García A. Beta-adrenergic receptors in cancer: therapeutic implications. *Oncol Res*. 2010;19(1):45-54.
- Pescosolido N, Scarsella G, Rusciano D. Oral administration of forskolin decreases retinal damage after experimental induction of ocular hypertension in the rat. In *Forskolin – Sources, Mechanisms of Action and Health Effects*; Walker, M.H., Ed.; Novinka: New York, NY, USA, 2015;31–50.
- Pétursdóttir D, Holmström G, Larsson E. Visual function is reduced in young adults formerly born prematurely: a population-based study. *Br J Ophthalmol*. 2020;104(4):541-546.
- Pierce EA, Avery RL, Foley ED, Aiello LP, Smith LE. Vascular endothelial growth factor/vascular permeability factor expression in a mouse model of retinal neovascularization. *Proc Natl Acad Sci U S A*. 1995;92(3):905-9.
- Pinazo-Durán MD, Zanón-Moreno V, Gallego-Pinazo R, García-Medina JJ. Oxidative stress and mitochondrial failure in the pathogenesis of glaucoma neurodegeneration. *Prog Brain Res*. 2015;220:127-53.
- Porciatti V. Electrophysiological assessment of retinal ganglion cell function. *Exp Eye Res*. 2015;141:164-70.
- Prakalapakorn SG, Greenberg L, Edwards EM, Ehret DEY. Trends in Retinopathy of Prematurity Screening and Treatment: 2008-2018. *Pediatrics*. 2021;147(6):e2020039966.
- Prencipe M, Perossini T, Brancoli G, Perossini M. The photopic negative response (PhNR): measurement approaches and utility in glaucoma. *Int Ophthalmol*. 2020;40(12):3565-3576.

- Qian Y, Tang X, Guan T, Li Y, Sun H. Neuroprotection by Combined Administration with Maslinic Acid, a Natural Product from *Olea europaea*, and MK-801 in the Cerebral Ischemia Model. *Molecules*. 2016;21(8):1093.
- Quigley HA. Glaucoma. *Lancet*. 2011;377(9774):1367-77.
- Quinn GE. Retinopathy of prematurity blindness worldwide: phenotypes in the third epidemic. *Eye Brain*. 2016;8:31-36.
- Quinn GE, Ying GS, Bell EF, Donohue PK, Morrison D, Tomlinson LA, Binenbaum G; G-ROP Study Group. Incidence and Early Course of Retinopathy of Prematurity: Secondary Analysis of the Postnatal Growth and Retinopathy of Prematurity (G-ROP) Study. *JAMA Ophthalmol*. 2018;136(12):1383-1389.
- Racette L, Wilson MR, Zangwill LM, Weinreb RN, Sample PA. Primary open-angle glaucoma in blacks: a review. *Surv Ophthalmol*. 2003;48(3):295-313.
- Ramirez AI, de Hoz R, Salobarra-Garcia E, Salazar JJ, Rojas B, Ajoy D, López-Cuenca I, Rojas P, Triviño A, Ramírez JM. The Role of Microglia in Retinal Neurodegeneration: Alzheimer's Disease, Parkinson, and Glaucoma. *Front Aging Neurosci*. 2017;9:214.
- Reiter E, Lefkowitz RJ. GRK and beta-arrestins: roles in receptor silencing, trafficking and signaling. *Trends Endocrinol Metab*. 2006;17(4):159-65.
- Ren R, Jonas JB, Tian G, Zhen Y, Ma K, Li S, Wang H, Li B, Zhang X, Wang N. Cerebrospinal fluid pressure in glaucoma: a prospective study. *Ophthalmology*. 2010;117(2):259-66.
- Reuter S, Gupta SC, Chaturvedi MM, Aggarwal BB. Oxidative stress, inflammation, and cancer: how are they linked? *Free Radic Biol Med*. 2010;49(11):1603-16.
- Ricci B. Oxygen-induced retinopathy in the rat model. *Doc Ophthalmol*. 1990;74(3):171-7.
- Rieke F. Mechanisms of single-photon detection in rod photoreceptors. *Methods Enzymol*. 2000;316:186-202.
- Ristori C, Filippi L, Dal Monte M, Martini D, Cammalleri M, Fortunato P, la Marca G, Fiorini P, Bagnoli P. Role of the adrenergic system in a mouse model of oxygen-induced retinopathy: antiangiogenic effects of beta-adrenoreceptor blockade. *Invest Ophthalmol Vis Sci*. 2011;52(1):155-70.
- Rozec B, Gauthier C. beta3-adrenoceptors in the cardiovascular system: putative roles in human pathologies. *Pharmacol Ther*. 2006;111(3):652-73.
- Rusciano D, Pezzino S, Mutolo MG, Giannotti R, Librando A, Pescosolido N. Neuroprotection in Glaucoma: Old and New Promising Treatments. *Adv Pharmacol Sci*. 2017;2017:4320408.
- Russo R, Varano GP, Adornetto A, Nucci C, Corasaniti MT, Bagetta G, Morrone LA. Retinal ganglion cell death in glaucoma: Exploring the role of neuroinflammation. *Eur J Pharmacol*. 2016;787:134-42.

- Saleh M, Nagaraju M, Porciatti V. Longitudinal evaluation of retinal ganglion cell function and IOP in the DBA/2J mouse model of glaucoma. *Invest Ophthalmol Vis Sci.* 2007;48(10):4564-72.
- Sankar MJ, Sankar J, Chandra P. Anti-vascular endothelial growth factor (VEGF) drugs for treatment of retinopathy of prematurity. *Cochrane Database Syst Rev.* 2018;1(1):CD009734.
- Santana-Garrido Á, Reyes-Goya C, Pérez-Camino MC, André H, Mate A, Vázquez CM. Retinoprotective Effect of Wild Olive (Acebuche) Oil-Enriched Diet against Ocular Oxidative Stress Induced by Arterial Hypertension. *Antioxidants (Basel).* 2020;9(9):885.
- Santana-Garrido Á, Reyes-Goya C, Milla-Navarro S, de la Villa P, André H, Vázquez CM, Mate A. Anti-Inflammatory Action of Dietary Wild Olive (Acebuche) Oil in the Retina of Hypertensive Mice. *Foods.* 2021;10(9):1993.
- Schena G, Caplan MJ. Everything You Always Wanted to Know about β 3-AR * (* But Were Afraid to Ask). *Cells.* 2019;8(4):357.
- Schlamp CL, Johnson EC, Li Y, Morrison JC, Nickells RW. Changes in Thy1 gene expression associated with damaged retinal ganglion cells. *Mol Vis* 2001; 7:192-201.
- Scuteri D, Rombolà L, Watanabe C, Sakurada S, Corasaniti MT, Bagetta G, Tonin P, Russo R, Nucci C, Morrone LA. Impact of nutraceuticals on glaucoma: A systematic review. *Prog Brain Res.* 2020;257:141-154.
- Selvam S, Kumar T, Fruttiger M. Retinal vasculature development in health and disease. *Prog Retin Eye Res.* 2018;63:1-19.
- Shan T, Ma J, Ma Q, Guo K, Guo J, Li X, Li W, Liu J, Huang C, Wang F, Wu E. β 2-AR-HIF-1 α : a novel regulatory axis for stress-induced pancreatic tumor growth and angiogenesis. *Curr Mol Med.* 2013;13(6):1023-34.
- Sheldon, W. G., Warbritton, A. R., Bucci, T. J., & Turturro, A. (1995). Glaucoma in food-restricted and ad libitum-fed DBA/2Nnia mice. *Laboratory animal science*, 45(5), 508–518.
- Shen C, Chen L, Jiang L, Lai TY. Neuroprotective effect of epigallocatechin-3-gallate in a mouse model of chronic glaucoma. *Neurosci Lett.* 2015;600:132-6.
- Sheybani A, Scott R, Samuelson TW, Kahook MY, Bettis DI, Ahmed IIK, Stephens JD, Kent D, Ferguson TJ, Herndon LW. Open-Angle Glaucoma: Burden of Illness, Current Therapies, and the Management of Nocturnal IOP Variation. *Ophthalmol Ther.* 2020;9(1):1-14.
- Smith LE, Wesolowski E, McLellan A, Kostyk SK, D'Amato R, Sullivan R, D'Amore PA. Oxygen-induced retinopathy in the mouse. *Invest Ophthalmol Vis Sci.* 1994;35(1):101-11.
- Stahl A, Hellstrom A, Smith LE. Insulin-like growth factor-1 and anti-vascular endothelial growth factor in retinopathy of prematurity: has the time come? *Neonatology.* 2014;106(3):254-60.
- Steele MR, Inman DM, Calkins DJ, Horner PJ, Vetter ML. Microarray analysis of retinal gene expression in the DBA/2J model of glaucoma. *Invest Ophthalmol Vis Sci* 2006; 47:977-85.

- Stone J, Itin A, Alon T, Pe'er J, Gnessin H, Chan-Ling T, Keshet E. Development of retinal vasculature is mediated by hypoxia-induced vascular endothelial growth factor (VEGF) expression by neuroglia. *J Neurosci.* 1995;15(7 Pt 1):4738-47.
- Stritzke A, Kabra N, Kaur S, Robertson HL, Lodha A. Oral propranolol in prevention of severe retinopathy of prematurity: a systematic review and meta-analysis. *J Perinatol.* 2019;39(12):1584-1594.
- Strosberg AD. Structure and function of the beta 3-adrenergic receptor. *Annu Rev Pharmacol Toxicol.* 1997;37:421-50.
- Su T, Gillies MC. A simple method for the in vitro culture of human retinal capillary endothelial cells. *Invest Ophthalmol Vis Sci.* 1992 Sep;33(10):2809-13.
- Sullivan TA, Geisert EE, Templeton JP, Rex TS. Dosedependent treatment of optic nerve crush by exogenous systemic mutant erythropoietin. *Exp Eye Res* 2012;96:36-41.
- Sun D, Moore S, Jakobs TC. Optic nerve astrocyte reactivity protects function in experimental glaucoma and other nerve injuries. *J Exp Med.* 2017;214(5):1411-1430.
- Sun MH, Chen KJ, Tsao YP, Kao LY, Han WH, Lin KK, Pang JH. Down-regulation of matrix metalloproteinase-9 by pyrrolidine dithiocarbamate prevented retinal ganglion cell death after transection of optic nerve in rats. *Curr Eye Res* 2011; 36:1053-63.
- Templeton JP, Nassr M, Vazquez-Chona F, Freeman- Anderson NE, Orr WE, Williams RW, Geisert EE. Differential response of C57BL/6J mouse and DBA/2J mouse to optic nerve crush. *BMC Neurosci* 2009; 10:90.
- Templeton JP, Geisert EE. A practical approach to optic nerve crush in the mouse. *Mol Vis.* 2012;18:2147-52.
- Terasaki H, Hirose T. Late-onset retinal detachment associated with regressed retinopathy of prematurity. *Jpn J Ophthalmol.* 2003;47(5):492-497.
- Terry TL. Fibroblastic Overgrowth of Persistent Tunica Vasculosa Lentis in Infants Born Prematurely: II. Report of Cases-Clinical Aspects. *Trans Am Ophthalmol Soc.* 1942;40:262-84.
- Terry TL. Retrolental fibroplasia. *J Pediatr.* 1946;29(6):770-3.
- Tezel G, Wax MB. Hypoxia-inducible factor 1alpha in the glaucomatous retina and optic nerve head. *Arch Ophthalmol.* 2004;122(9):1348-56.
- Tezel G. Immune regulation toward immunomodulation for neuroprotection in glaucoma. *Curr Opin Pharmacol.* 2013;13(1):23-31.
- Tham YC, Li X, Wong TY, Quigley HA, Aung T, Cheng CY. Global prevalence of glaucoma and projections of glaucoma burden through 2040: a systematic review and meta-analysis. *Ophthalmology.* 2014;121(11):2081-90.

- The AGIS Investigators. The Advanced Glaucoma Intervention Study (AGIS): 7. The relationship between control of intraocular pressure and visual field deterioration. *Am J Ophthalmol.* 2000;130(4):429-40.
- Tomita Y, Usui-Ouchi A, Nilsson AK, Yang J, Ko M, Hellström A, Fu Z. Metabolism in retinopathy of Prematurity. *Life (Basel).* 2021;11(11):1119.
- Tsao P, von Zastrow M. Downregulation of G protein-coupled receptors. *Curr Opin Neurobiol.* 2000;10(3):365-9.
- Tugues S, Koch S, Gualandi L, Li X, Claesson-Welsh L. Vascular endothelial growth factors and receptors: anti-angiogenic therapy in the treatment of cancer. *Mol Aspects Med.* 2011;32(2):88-111.
- Turner AJ, Vander Wall R, Gupta V, Klistorner A, Graham SL. DBA/2J mouse model for experimental glaucoma: pitfalls and problems. *Clin Exp Ophthalmol.* 2017;45(9):911-922.
- Usui Y, Westenskow PD, Murinello S, Dorrell MI, Schepke L, Bucher F, Sakimoto S, Paris LP, Aguilar E, Friedlander M. Angiogenesis and Eye Disease. *Annu Rev Vis Sci.* 2015;1:155-184.
- Vähätupa M, Jääskeläinen N, Cerrada-Gimenez M, Thapa R, Järvinen T, Kalesnykas G, Uusitalo-Järvinen H. Oxygen-Induced Retinopathy Model for Ischemic Retinal Diseases in Rodents. *J Vis Exp.* 2020;(163).
- Vajaranant TS, Nayak S, Wilensky JT, Joslin CE. Gender and glaucoma: what we know and what we need to know. *Curr Opin Ophthalmol.* 2010;21(2):91-9.
- Vázquez-Chona FR, Lu L, Williams RW, Geisert EE. Genomic loci modulating the retinal transcriptome in wound healing. *Gene Regul Syst Bio.* 2007; 1:327-48.
- Veach J. Functional dichotomy: glutathione and vitamin E in homeostasis relevant to primary open-angle glaucoma. *Br J Nutr.* 2004;91(6):809-29.
- Wachter SB, Gilbert EM. Beta-adrenergic receptors, from their discovery and characterization through their manipulation to beneficial clinical application. *Cardiology.* 2012;122(2):104-12.
- Wang GL, Semenza GL. Purification and characterization of hypoxia-inducible factor 1. *J Biol Chem.* 1995;270(3):1230-7.
- Wang M, Li J, Zheng Y. The Potential Role of Nuclear Factor Erythroid 2-Related Factor 2 (Nrf2) in Glaucoma: A Review. *Med Sci Monit.* 2020;26:e921514.
- Wang R, Seifert P, Jakobs TC. Astrocytes in the Optic Nerve Head of Glaucomatous Mice Display a Characteristic Reactive Phenotype. *Invest Ophthalmol Vis Sci.* 2017;58(2):924-932.
- Wang X, Yuan ZL. Activation of Nrf2/HO-1 pathway protects retinal ganglion cells from a rat chronic ocular hypertension model of glaucoma. *Int Ophthalmol.* 2019;39(10):2303-2312.
- Wang ZH, Mong MC, Yang YC, Yin MC. Asiatic acid and maslinic acid attenuated kainic acid-induced seizure through decreasing hippocampal inflammatory and oxidative stress. *Epilepsy Res.* 2018;139:28-34.

- Weinreb RN, Khaw PT. Primary open-angle glaucoma. *Lancet*. 2004;363(9422):1711-20.
- West AL, Oren GA, Moroi SE. Evidence for the use of nutritional supplements and herbal medicines in common eye diseases. *Am J Ophthalmol*. 2006;141(1):157-66.
- Wilson JL, Long SB, Howard PJ. Respiration of premature infants. *Am J Dis Child*. 1942;63(6):1080.
- Wu KC, Cui JY, Klaassen CD. Beneficial role of Nrf2 in regulating NADPH generation and consumption. *Toxicol Sci*. 2011;123(2):590-600.
- Xu Z, Wei Y, Gong J, Cho H, Park JK, Sung ER, Huang H, Wu L, Eberhart C, Handa JT, Du Y, Kern TS, Thimmulappa R, Barber AJ, Biswal S, Duh EJ. NRF2 plays a protective role in diabetic retinopathy in mice. *Diabetologia*. 2014;57(1):204-13.
- Yadav KS, Sharma S, Londhe VY. Bio-tactics for neuroprotection of retinal ganglion cells in the treatment of glaucoma. *Life Sci*. 2020;243:117303.
- Yang C, Zhong ZF, Wang SP, Vong CT, Yu B, Wang YT. HIF-1: structure, biology and natural modulators. *Chin J Nat Med*. 2021;19(7):521-527.
- Yang EV, Kim SJ, Donovan EL, Chen M, Gross AC, Webster Marketon JI, Barsky SH, Glaser R. Norepinephrine upregulates VEGF, IL-8, and IL-6 expression in human melanoma tumor cell lines: implications for stress-related enhancement of tumor progression. *Brain Behav Immun*. 2009;23(2):267-75.
- Yang LK, Tao YX. Physiology and pathophysiology of the β ₃-adrenergic receptor. *Prog Mol Biol Transl Sci*. 2019;161:91-112.
- Yang-Feng TL, Xue FY, Zhong WW, Cotecchia S, Frielle T, Caron MG, Lefkowitz RJ, Francke U. Chromosomal organization of adrenergic receptor genes. *Proc Natl Acad Sci U S A*. 1990;87(4):1516-20.
- Yoles E, Schwartz M. Degeneration of spared axons following partial white matter lesion: implications for optic nerve neuropathies. *Exp Neurol* 1998; 153:1-7.
- Zarrouk A, Martine L, Grégoire S, Nury T, Meddeb W, Camus E, Badreddine A, Durand P, Namsi A, Yammine A, Nasser B, Mejri M, Bretillon L, Mackrill JJ, Cherkaoui-Malki M, Hammami M, Lizard G. Profile of Fatty Acids, Tocopherols, Phytosterols and Polyphenols in Mediterranean Oils (Argan Oils, Olive Oils, Milk Thistle Seed Oils and Nigella Seed Oil) and Evaluation of their Antioxidant and Cytoprotective Activities. *Curr Pharm Des*. 2019;25(15):1791-1805.
- Zhang Z, Yao L, Yang J, Wang Z, Du G. PI3K/Akt and HIF-1 signaling pathway in hypoxia-ischemia (Review). *Mol Med Rep*. 2018;18(4):3547-3554.

Zhu MD, Cai FY. Development of experimental chronic intraocular hypertension in the rabbit. *Aust N Z J Ophthalmol.* 1992;20(3):225-34.

Ziche M, Morbidelli L. Molecular regulation of tumour angiogenesis by nitric oxide. *Eur Cytokine Netw.* 2009;20(4):164-70.

Zou H, Otani A, Oishi A, Yodoi Y, Kameda T, Kojima H, Yoshimura N. Bone marrow-derived cells are differentially involved in pathological and physiological retinal angiogenesis in mice. *Biochem Biophys Res Commun.* 2010;391(2):1268-73.

Acknowledgments

Prof. Massimo Dal Monte
Prof. Maurizio Cammalleri
Prof. Giovanni Casini
Prof. Alfonso Mate-Barrero
Prof. Carmen Maria Vasqu ez-Cueto
Dr. Silvia Marracci
Dr. Dominga Lapi
Dr. Rosario Amato
Dr. Matteo Lulli
Dr. Maria Grazia Rossino
Dr. Alessio Canovai
Dr. Alberto Melecchi
Dr. Lorenzo Guidotti
Dr. Veronica Rodriguez
Dr.  lvvaro Santana-Garrido
Dr. Pablo Espinosa-Mart n



Appendix: Published manuscripts not included in the main thesis body

The manuscripts I have contributed to during my PhD period and that are not part of the thesis discussion, have been reported in the following section.



Review

Neurosensory Alterations in Retinopathy of Prematurity: A Window to Neurological Impairments Associated to Preterm Birth

Martina Lucchesi ^{1,†}, Silvia Marracci ^{1,†} , Rosario Amato ¹ , Luca Filippi ² , Maurizio Cammalleri ¹ and Massimo Dal Monte ^{1,*}

¹ Department of Biology, University of Pisa, 56127 Pisa, Italy; martina.lucchesi@student.unipi.it (M.L.); silvia.marracci@unipi.it (S.M.); rosario.amato@biologia.unipi.it (R.A.); maurizio.cammalleri@unipi.it (M.C.)
² Department of Clinical and Experimental Medicine, Division of Neonatology and NICU, University of Pisa, 56126 Pisa, Italy; luca.filippi@unipi.it
* Correspondence: massimo.dalmonete@unipi.it; Tel.: +39-050-2211426
† These authors contributed equally to this work.

Abstract: Retinopathy of prematurity (ROP) is one of the main blinding diseases affecting preterm newborns and is classically considered a vascular disorder. The premature exposure to the extrauterine environment, which is hyperoxic in respect to the intrauterine environment, triggers a cascade of events leading to retinal ischemia which, in turn, makes the retina hypoxic thus setting off angiogenic processes. However, many children with a history of ROP show persistent vision impairment, and there is evidence of an association between ROP and neurosensory disabilities. This is not surprising given the strict relationship between neuronal function and an adequate blood supply. In the present work, we revised literature data evidencing to what extent ROP can be considered a neurodegenerative disease, also taking advantage from data obtained in preclinical models of ROP. The involvement of different retinal cell populations in triggering the neuronal damage in ROP was described along with the neurological outcomes associated to ROP. The situation of ROP in Italy was assessed as well.

Keywords: neurodegeneration; photoreceptors; retinal ganglion cells; retinal glia



Citation: Lucchesi, M.; Marracci, S.; Amato, R.; Filippi, L.; Cammalleri, M.; Dal Monte, M. Neurosensory Alterations in Retinopathy of Prematurity: A Window to Neurological Impairments Associated to Preterm Birth. *Biomedicines* **2022**, *10*, 1603. <https://doi.org/10.3390/biomedicines10071603>

Academic Editors: Amedeo Amedei and Jessica Mandrioli

Received: 22 April 2022

Accepted: 4 July 2022

Published: 6 July 2022

Publisher's Note: MDPI stays neutral with regard to jurisdictional claims in published maps and institutional affiliations.



Copyright: © 2022 by the authors. Licensee MDPI, Basel, Switzerland. This article is an open access article distributed under the terms and conditions of the Creative Commons Attribution (CC BY) license (<https://creativecommons.org/licenses/by/4.0/>).

1. Introduction

In the latest decades, the survival rate of extremely preterm and low birth-weight infants has drastically improved [1]. Although this could represent an important achievement reflecting the advanced efficacy in the clinical management of preterm infants, it also increases the risk of short- or long-term complications deriving from preterm birth.

Among them, retinopathy of prematurity (ROP) is one of the main ocular disorders affecting preterm newborns that may result in a significant loss of vision or even blindness [2]. Extremely preterm infants are at high risk of developing ROP. In particular, about 50% of them show clinical signs of ROP, although this percentage may vary. In 2010, a study evaluated that over approximately 185,000 preterm infants were affected by ROP and more than 20,000 were affected by complete loss of visual function [3]. So far, the greatest risk predictors of ROP are a low gestational age and a low birth weight. In this respect, in countries with high-quality neonatal care, sight-threatening ROP is mainly confined to infants with a birth weight lower than 1000 g and is very rare in babies with a birth weight higher than 1250 g [4].

The common denominator of preterm birth complications, including ROP, is represented by drastic changes in physiochemical parameters due to the precocious passage from the intrauterine to external environment, which influences the development of immature tissues and organs. In the case of the retina, its organogenesis occurs relatively late in the gestational period. Therefore, the preterm birth drastically impairs the morphofunctional organization of the still immature organ, creating a wide range of structural and

functional changes in both neural and vascular components. Since the early discovery of ROP, its pathogenesis has been mainly attributed to the change in oxygen tension when passing from a hypoxic condition, as in the intrauterine environment, to a relative hyperoxic condition, as in the extrauterine environment.

The hypoxia physiologically present in the pregnant uterus represents the ideal environment where retinal vascularization of the fetus can develop [5]. The early retinal vasculature originates from spindle-shaped precursor endothelial cells, that migrate by 14–15 weeks of the postmenstrual age from the optic disk towards the ora serrata, and the early networks of capillaries are formed from 17–18 weeks of the postmenstrual age [5]. The relative hypoxia promotes the vascular development through the production of a dimeric nuclear transcription factor, the hypoxia inducible factor 1 (HIF-1), which modulates a plethora of oxygen-sensing genes including a series of proangiogenic factors, such as a vascular endothelial growth factor (VEGF) [6]. Under hypoxia, the subunit HIF-1 α accumulates into the cell, migrates into the nucleus and, after dimerization with the subunit HIF-1 β , activates the transcription of VEGF [7]. In the developing retina, which becomes physiologically hypoxic after the onset of neuronal activity, VEGF is mainly (but transiently) produced by neuroglial cells, to stimulate in a paracrine fashion growth, and migration of endothelial cells that organize to form the retinal vessel network [8]. The formation of a functional retinal circulation relieves the retina from hypoxia and, under oxygen exposure, HIF-1 α subunit is hydroxylated, ubiquitinated and finally degraded, thus reducing the transcription of HIF-1 target genes [7]. Through such a mechanism the exposure of the immature retina to atmospheric oxygen leads to the interruption of the vascularization processes, which normally occur within the intrauterine hypoxic environment, thus leaving the peripheral retina avascular until an approximate gestational age of 32 weeks. The interruption or even the regression of the vascularization process establishes an ischemic condition (ischemic phase of ROP), which gradually worsens together with the increasing metabolic demand of the developing retina. The persistent ischemia and the deriving hypoxia drive the switch to the proliferative phase of ROP, which is characterized by the abnormal activation of angiogenic processes leading to the outgrowth of dysfunctional and disorganized new vessels. In addition to further exacerbating the ischemic condition, the proliferation of aberrant neovessels may also induce the development of intravitreal fibrosis with consequent retinal traction and detachment [9]. Considering that vascular abnormalities manifest the most pathological hallmarks in ROP, the location and the appearance of the vascular aberrations are currently considered as the main parameters for the classification of disease progression and severity from stage 1 to stage 5 (Figure 1). Stages 1–3 describe the acute phases of the disease characterized by the formation of a demarcation line between the vascular and the avascular retina (stage 1) that will evolve in a ridge (stage 2) from which extraretinal neovascular proliferation will arise towards the vitreous (stage 3). From the acute stages of ROP, vascular abnormalities can either spontaneously regress turning to a regular retinal vascularization, or further evolve in stages 4 and 5 defined as severe ROP, characterized by partial and total retinal detachment, respectively [10].

The importance of oxygen in the pathogenesis and in the progression of ROP has become evident with clinical trials demonstrating that limiting oxygen delivery to preterm newborns reduces the risk of the disease but increases their mortality [11]. Therefore, although the fine control of oxygen delivery to preterm infants is currently the first line of prevention of ROP progression, a saturation target lower than 90% is not acceptable, and the persistence of a certain ROP incidence is considered an unavoidable consequence of a reduced mortality [12]. Conversely, significant steps forward have been made in the characterization of the oxygen-dependent mechanisms contributing to the vascular abnormalities.

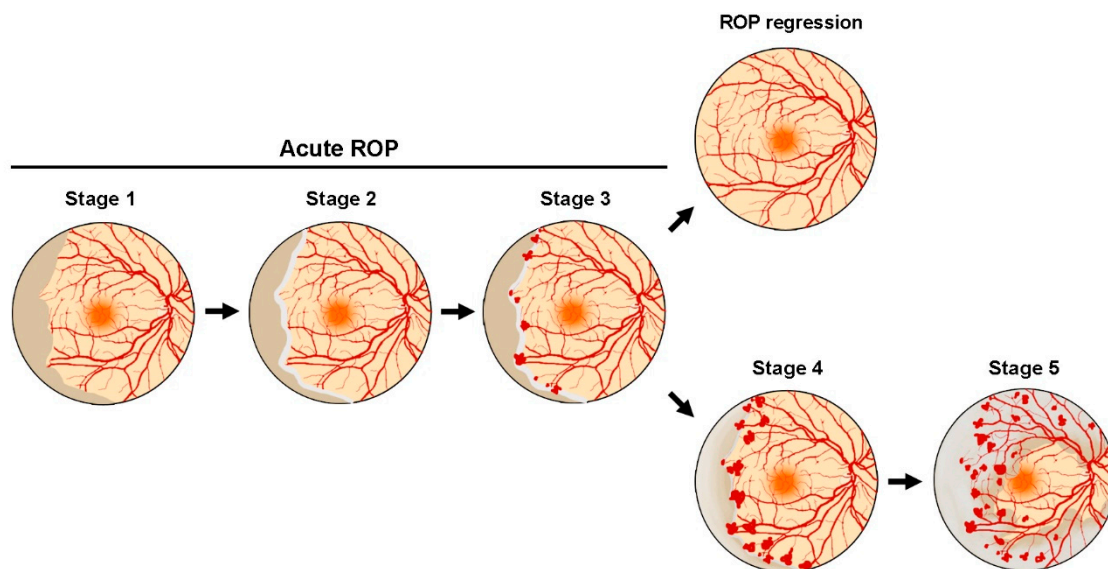


Figure 1. Schematic representation of retinopathy of prematurity (ROP) stages. Stage 1 is characterized by the appearance of a demarcation line between the vascular and the avascular zone of the retina, which may evolve in a visible ridge in stage 2. In stage 3, proliferating retinal vessels depart from the ridge to gradually occupy extraretinal spaces towards the vitreous. Stages 1–3 represent the acute phase of ROP, which could resolve in a spontaneous regression of the abnormal neovascularization or could further evolve in the more severe stages 4 and 5, characterized by partial and total retinal detachment, respectively.

Fundamental contributions in the study of ROP pathophysiology have derived from the use of the *in vivo* model of oxygen-induced retinopathy (OIR) in rodents [13]. This model exploits the plasticity of retinal vessels typical of neonatal mice and rats, whose vascular plexa physiologically develop after birth [14]. The OIR model firstly consists of the exposure of pups to hyperoxia, which interferes with the process of retinal vascularization and induces a wide vaso-obliteration (around the optic nerve head in mice; in the peripheral retina in rats). Then, newborn pups are returned to a normoxic environment, with a sudden reduction in retinal oxygenation that is perceived as a relative hypoxia. As is the case of ROP, the ischemia/hypoxia in the OIR retina triggers a dramatic increment in angiogenesis causing abnormal vessel sprouts along with hemorrhages and vitreous edema due to the vascular hyperpermeability [13].

The primary players in the mechanisms linking the alterations in retinal oxygenation with the abnormal vascular sprout, in ROP as well as in the OIR model, are HIF-1 and VEGF. Indeed, the HIF-1-dependent dramatic downregulation of VEGF occurring under hyperoxia drives the interruption of vascularization and the vaso-obliteration, while VEGF overexpression under hypoxia is the leading mechanism causing vascular hyperpermeability and proliferation [7]. With VEGF having a relevant role in ROP pathogenesis, it has been identified as a useful target in treating ROP. In fact, cryotherapy or the less painful laser photocoagulation, for a long time, were used as the gold standard treatment for infants with severe ROP, aimed at destroying the hypoxic peripheral retina, thus reducing VEGF production [15]. However, this approach is burdened by serious adverse effects (need of anesthesia, non negligible risk of repeated intervention, and visual dysfunction) [16] and complications (corneal burns, band keratopathy, cataract) [17]. The currently available alternative treatment that avoids retinal destruction is the intravitreal injection of neutralizing anti-VEGF drugs. In respect to laser photocoagulation, anti-VEGF drugs have been recently reported to display a decreased incidence of retinal detachment, probably thanks to a faster decrease in VEGF levels [18], a reduced rate of optic atrophy and amblyopia [19], and less eye complications even if burdened by a higher retreatment incidence [20]. However,

the short- or long-term safety of anti-VEGF drugs still arouses some concern, and further investigations are required to evaluate their effects on retinal developmental processes [21].

2. ROP in Italy

The birth rate in Italy, calculated using the birth rate of 2020 [22], is approximately 410,000/year and 1% of these newborns are born with a birth weight lower than 1500 g or at a gestational age lower than 30 weeks, thus indicating that about 4000 infants are at risk for ROP. Borroni et al. [23] analyzed the incidence and the associated risk factors of ROP and aggressive posterior-ROP (AP-ROP), a severe form of ROP, in 25 Italian neonatal intensive care units through a prospective multicenter observational study examining 421 infants born with a birth weight lower than 750 g and/or a gestational age shorter than 27 weeks. Starting the ophthalmologic screening at about 30 weeks of gestational age, ROP was diagnosed in 62.9% of the preterm infants, while AP-ROP was diagnosed in 24.2% of them. At a univariate analysis, ROP was significantly associated with gestational age, body weight, intraventricular hemorrhage, patent ductus arteriosus, bronchopulmonary dysplasia, erythropoietin therapy and sepsis, while AP-ROP was significantly associated with gestational age, bronchopulmonary dysplasia, and sepsis. Performing a multivariate analysis, ROP was found to be associated only to intraventricular hemorrhage and erythropoietin therapy, while AP-ROP was found to be associated to gestational age and sepsis. The incidence data of this Italian study does not match with those of the CRYO-ROP and of the ETROP studies [24,25], possibly because these studies were performed before the introduction of the guidelines for ROP prevention [26], which were applied in the Italian study. On the other hand, the results of the work of Borroni et al. [23] are in agreement with those of other studies and of the Vermont–Oxford Network, which is a non-profit organization of health care professionals collaborating to improve neonatal care [27–30]. The finding that the use of erythropoietin may be associated with the development of ROP has been confirmed by another Italian study [31]. This study found that in preterm infants with a body weight lower than 1000 g receiving erythropoietin therapy, the occurrence of ROP was double than that of preterm infants that did not receive erythropoietin, suggesting this therapy as an independent risk factor for ROP development. More recently, the incidence and risk factors for ROP were examined in 2 Italian neonatal intensive care units, through a retrospective study involving 178 infants with a gestational age lower than 29 weeks [32]. This study found an occurrence of ROP of 38%, similar to that found in other studies [33–40], and an association between red blood cell transfusion and the risk of ROP. The finding that red blood cell transfusion may represent a risk factor for ROP development is in agreement with other studies [41–46]. However, red blood cell transfusion is often essential to treat anemia in preterm neonates (very common due to the prematurity itself and to repeated blood sampling). In this respect, a retrospective study involving neonates with a gestational age lower than 32 weeks demonstrated that the risk for developing ROP carried by blood products is likely to depend on the gestational age. In particular, the gestational age at the second transfusion seems to be even more useful to determine the risk for severe ROP development, outperforming all other variables in predicting severe ROP [47].

There are premature infants with apparent similar characteristics, sharing similar clinical features (gestational age, birth weight, oxygen support), who have a completely different ROP evolution, with some of them needing treatment, and others experiencing spontaneous regression of the pathology. Therefore, there is an urgent need of standardizing evaluation criteria and identifying early indicators for ROP development. In this respect, a recent retrospective Italian study reported that early platelet counts were significantly reduced in newborns who later developed severe ROP which required treatment, but not in those who never developed ROP [48,49] suggesting that platelet count may be used to detect in advance premature infants prone to ROP development. Recently, a new prediction model for ROP, the Postnatal Growth and ROP (G-ROP), which was originally developed in 2018 and validated in a North American cohort of preterm infants [50], has been also validated in Italy [51]. G-ROP is based on birth weight, gestational age and weight gain, and

allows to reduce the number of infants undergoing ROP examinations by about 30% while maintaining 100% sensitivity for ROP when compared to the criteria currently in use, thus being very promising for future clinical adaptation. Its validation in the Italian population lays the foundation for the introduction of G-ROP criteria in all European countries.

If on the one hand, the list of ROP risk factors is becoming longer, on the other, a growing body of evidence is progressively highlighting the ability of a variety of compounds, both naturals and pharmacological, to prevent ROP or to reduce its progression towards later and more deleterious stages. For example, Garofoli et al. [52] demonstrated in a cohort of preterm infants with birth weight lower than 1500 g that orally administered vitamin A is effective in attenuating ROP incidence and severity. Moreover, Filippi et al. widely demonstrated that propranolol, a usually well-tolerated non-selective beta adrenoceptor antagonist is able to counteract the progression of ROP [53–55]. These clinical trials followed preclinical studies performed in OIR mice in which systemic or topic propranolol administered during the hypoxic phase of the disease reduced retinal neovascularization by preventing HIF-1 α upregulation and its proangiogenic cascade [56,57].

Although in preterm infants oral propranolol is not sufficiently safe [54], propranolol 0.2% eye micro-drops showed an optimal safety and tolerability profile and efficiently reduced ROP progression [58,59]. It is noteworthy that propranolol seems to exert a neuroprotective effect in the OIR retina, suggesting that beta adrenoceptor blockade may be useful in human patients not only to prevent neovascularization but also to limit the neural damage evidenced by impaired ERG [60]. Indeed, OIR mice showed an altered ERG profile due to neuronal cell death, while the propranolol treatment protected retinal cells enhancing pro-survival pathways such as autophagy while inhibiting apoptosis, thus finally resulting in recovered retinal function [61]. However, clinical trials performed to date are not large enough to draw definitive conclusions about propranolol efficacy in treating ROP nor on its supposed neuroprotective effect [60]. In the meantime, the results obtained in ROP infants treated with propranolol so far, especially related to its antiangiogenic effects, are very promising.

3. The Impact of ROP in the Central Nervous System

Preterm children are at risk of developing poor visual outcomes with respect to children born at full term, independently to the presence of ROP. Indeed, there is a large cohort of studies indicating that a reduced visual acuity, defined as the capacity of the central visual system to discriminate contrast variation, can be associated to preterm-born children with or without ROP, with visual impairment lasting into adulthood. Therefore, this suggests that a poor visual outcome may be considered a long-term functional consequence of preterm birth [4,62–66]. On the other hand, ROP development in preterm infants impacts on visual outcomes, and acuity deficits in patients with a history of ROP are typical, even though the pathology has resolved completely [64]. For instance, a Swedish population-based prospective study conducted in children of 10 years who had been born preterm, found that visual impairments were present in 26% of those with no ROP and in 64% of those with severe ROP, while they occurred in 8% of controls born at term [67]. In the same line, a population-based prospective study, made in New Zealand on young adults born preterm before ROP treatment was available, reached the conclusion that adults who had developed ROP had reduced visual acuity when compared to adults with no ROP, indicating that ROP increases the risk of developing poor long-term visual outcomes [68]. In this respect, both the CRYO-ROP and the ET-ROP studies found a correlation between severity of acute-phase ROP and development of visual acuity [24,25]. Notably, an examination over a period of 18 years of adolescents and adult patients with previously regressed ROP showed a late reactivation of ocular deficits together with a reduced visual acuity, highlighting that a decreased visual acuity can occur as a long-term outcome in patients with resolved ROP [69]. Treatment for ROP became available after the publication of the results of the CRYO-ROP study [24] and there is evidence that treating ROP ameliorates visual outcomes, with anti-VEGF agents giving better results on visual acuity than laser

photocoagulation. For instance, a study published by Rodriguez and colleagues in 2020 evaluated visual acuity in children aged over 4 years treated with anti-VEGF, comparing their visual acuity with that measured in the ET-ROP study published in 2010 [70]. This study revealed that 85% of eyes treated with anti-VEGF had normal visual acuity with respect to 35% of eyes receiving laser photocoagulation, suggesting that different ROP treatments may have different impacts on visual outcomes over the years [71], a conclusion shared with other works as, for instance, a recent study performed at the UCLA Medical Centers [19]. In this context, it would be important to clarify whether anti-VEGF may actually have greater effects over laser photocoagulation, in order to maximize preterm newborn visual outcomes, since they could affect, at least in part, the everyday activities in adult life.

Although ROP may be associated with later visual impairments, it may also impact on non-visual abilities. In fact, besides ocular injuries, infants with ROP may exhibit further neurodevelopmental impairments. Given the common embryonic derivation of eye and brain, it has been hypothesized that pathological processes associated to ROP (such as oxygen fluctuations, oxidative stress, inflammation) could also have harmful effects on the development of different regions of the central nervous system (CNS) [72–74].

Notably, cerebral cortex and cerebellum development occurs during the gestational third trimester and are vulnerable to detrimental environmental factors. Thus, the early exposition to extrauterine environments as well as damage to the vascular and neuronal pathways during maturation, could alter CNS development. As an example, ROP disease is characterized by the dysregulation of insulin-like growth factor 1 (IGF-1) and VEGF and it is known that both these factors play an important role in neurogenesis, neural differentiation, axon maturation, and neuroplasticity [75–77]. In particular, based on the fundamental roles of IGF-1 on neurodevelopment, it is possible to speculate that altered IGF-1 levels may affect the correct development of CNS regions. In line with these hypotheses, the postnatal decrease in circulating IGF-1 observed in very preterm infants has been found to associate with a low brain volume at term age, suggesting that normalizing IGF-1 levels may result in the neuroprotection of these patients [78]. Similarly, changes of VEGF levels may lead to improper CNS development. For instance, the use of intravitreal bevacizumab injections induces a risk of neurodevelopmental delay in ROP infants, suggesting that anti-VEGF therapies may introduce a risk of developmental impairments [79].

However, it remains to be determined whether ROP and any neurological alterations in the CNS may depend on a shared etiological origin and further studies will be necessary to elucidate this point. From another point of view and considering that the retina itself is an anatomical and functional portion of the CNS, all the interventions that may have an impact on ROP and reduce the risk factors associated to the disease may also have a beneficial effect on the development of those CNS structures altered as a consequence of premature birth.

3.1. Neurological Outcomes Associated with ROP

Studies investigating possible associations between ROP and neurological outcomes are in progress. Presently, there is a general agreement that severe ROP may represent a risk factor for neurosensory impairments in childhood, although studies exploring possible connections between ROP severity and neurodevelopmental disorders have led to controversial conclusions. For instance, a study performed in extremely preterm infants with a gestational age lower than 26 weeks suggested that severe ROP is a good predictor for major neurosensory disabilities, including cerebral palsy, severe visual impairment, and hearing loss. In particular, preterm infants with severe ROP have been reported to display a significantly poorer outcome at 11 years than preterm infants without ROP, with neurosensory impairments detected in 50% of the infants who had suffered from severe ROP [80]. Similar conclusions have been reached in other studies relative to cohorts of premature children suffering from severe ROP evaluated at age 1.5 or 5 years [81–83]. In addition, in a Swedish study performed on 27 preterm children totally blind due to ROP

stage 5, the authors found that 75% of them had major neurological impairments, including mental retardation, cerebral palsy and epilepsy, indicating an association between severe ROP and worsened neurodevelopment [84]. In this respect, at the beginning of this century, two studies aimed to assess the relationship between ROP and neurodevelopmental functions in the same cohort of preterm children, evaluated at 5.5 and 8 years, reached the conclusion that severe ROP may be considered a marker for functional disabilities developed in very low birth weight infants [85,86]. In the same period, a study enrolling 115 preterm infants, none of which were suffering from severe ROP, associated moderate ROP with worsened motor and cognitive disabilities, an association that, however, was found borderline after correction for gestational age [87]. In 2014, Allred et al. reported that preterm children with severe ROP followed up at 2 years corrected age (that is the chronological age minus the number of months the preterm infant is born early), showed a higher probability of impaired neurodevelopment characterized, for instance, by brain lesions and cerebral palsies [88]. In 2018, Drost et al. performed a study to compare the volumes of different brain structures and the cortical morphology of preterm infants with severe ROP with those of control infants with the same gestational age, birth weight and sex. This analysis, carried out using magnetic resonance imaging (MRI), indicated that preterm infants with severe ROP have smaller cerebellar volumes and reduced cortical gyrification. Cognitive and motor abilities at 15 months corrected age, were shown to be worse in infants with severe ROP than in controls [75]. In addition, a cohort study using MRI analysis carried out by Sveinsdóttir et al. in infants of 2 years corrected age, showed that infants with ROP had lower unmyelinated white matter and cerebellar volume as well as reduced mental and psychomotor developmental indices with respect to infants without ROP. However, infants with less severe ROP exhibited a reduction in brain volume and a neurodevelopmental impairment similar to those observed in infants with more severe ROP, suggesting that any stage of ROP may result in neurodevelopmental deficits and that preventing ROP, also in its less severe stages, may positively impact brain development [89]. In the same line, Glass et al. found that severe ROP is associated with white matter alterations and with a delayed maturation of brain regions involved in visual and motor processing [90], suggesting that severe ROP may be associated to neurodevelopmental outcomes. In an additional cohort study on ROP-diagnosed children, 68.4% of ROP infants showed neurodevelopmental disabilities, including blindness, cerebral palsy, cognitive, motor, speech and hearing problems. However, approximately half of ROP children with normal visual capacities exhibited neurodevelopmental disabilities, thus suggesting that preterm ROP infants have a high risk for developing neurodevelopmental anomalies even when their visual abilities are normal and underscoring the importance to prevent ROP not only to avoid blindness but also to hamper neurodevelopmental disorders [91].

Different from the studies discussed above, some other works suggest that neurodevelopmental alterations may be more strongly associated to preterm birth than to ROP. For instance, two studies comparing preterm infants with ROP stage 3 with those with ROP stage 2 and ROP stage 1/no ROP and evaluating their developmental outcome, found that preterm children in all groups have reduced neural development that was not associated with ROP severity, suggesting that neurodevelopmental disabilities are most likely associated with premature birth instead of ROP severity [92,93]. In 2007, Stephenson et al. performed a retrospective study on 505 subjects of 11–14 years that were born prematurely, of whom 49% had developed ROP, and assessing visual and cognitive outcomes. The study concluded that neither poor ophthalmic nor poor cognitive outcomes results were associated to previous stage 1 or stage 2 ROP, and that stage 3 ROP is associated to poor visual acuity but not to cognitive impairment, suggesting that unexplored factors in addition to ROP may explain the poor cognitive performance [94]. Ahn et al., using MRI, evaluated the microstructural integrity of brain white matter in preterm infants with and without ROP and in full-term infants. The results demonstrated alterations in 15–17 of the 23 predefined regions in which the brain was divided. Fewer differences were instead observed comparing preterm infants with and without ROP, limited to 2 of the 23 predefined regions, thus

suggesting that alterations of white matter maturation could be associated with preterm birth rather than with ROP [95]. The same research group reached the same conclusions in a more recent work showing that ROP or severe ROP were not associated with white matter abnormalities in preterm infants of 18 months corrected age with or without ROP. Particularly, developmental outcomes, including cognitive, language and motor functions, were similar between preterm infants with or without ROP and independent from ROP severity [96]. In line with these studies, Altendahl et al. examined cognition, language, and motor scores of premature neonates at 0–36 months corrected age, screened for ROP, and found that ROP severity was not associated with worse neurodevelopmental scores [97]. Similar results were obtained in a recent study evaluating the presence of hearing loss in a large cohort of preterm infants at 18 months corrected age, revealing no significant associations between ROP and hearing impairments [98]. Overall, these studies suggest that negative neurodevelopmental outcomes in preterm neonates are plausibly related to prematurity-associated factors more than to ROP severity and that ROP, *per se*, does not seem to contribute significantly to neurodevelopmental diseases.

The controversial correlation between ROP (and, eventually, its severity) and neurodevelopmental outcomes made evident by the studies cited in the present paragraph, highlights the necessity of extensive studies investigating brain development and its alterations in infants suffering from ROP in order to reach more robust and accurate conclusions.

3.2. Neurodegeneration in the Retina of ROP Patients

From a clinical point of view, ROP is classified as a vascular disorder. In line with this, most literature focuses on the mechanisms leading to neovascularization and the current therapeutic treatments are directed to the normalization of the retinal vasculature [99]. However, despite the effectiveness of these treatments or the spontaneous regression of the pathology, many children with a history of ROP experience persistent vision impairment, such as astigmatism and myopia [100], reduced visual acuity and deficient subtle color vision [101], constricted visual field and contrast sensitivity [102], and increased dark-adapted thresholds [103], along with structural retinal abnormalities [4,104]. Overall, these data suggest that some form of alteration in the development, viability, and function of neuroretinal cells (photoreceptors, retinal neurons and glia), may occur during ROP progression (Figure 2). This is not surprising, given the existence of a strict functional relationship between neurons, glia and blood vessels known as neurovascular unit, in which chemical signals released by neurons and/or glial cells regulate the surrounding blood vessels to adequately support the metabolism of neuronal cells [105]. However, in retinopathies the relationships between vascular abnormalities and neurodegeneration can be of various types. For instance, in diabetic retinopathy, a retinal disease that develops years after the diagnosis of diabetes, neurodegeneration occurs early during disease development and, at least in part, precedes the vascular damage [106]. On the contrary, in ROP the disease progresses in a short time and the damage to the neural part of the retina is likely to be secondary to the development of vascular abnormalities.

Relevant insights about the neuroretinal alterations in ROP derive from functional analyses performed by means of electroretinography. An electroretinogram (ERG) is classically composed of a biphasic waveform displaying an early negative component (a-wave), elicited by the light-induced response of the photoreceptors, followed by a positive component (b-wave) generated by post receptor cells [107]. Depending on retinal light adaptation, the ERG may reflect the activity of rod-mediated (dark-adapted scotopic ERG) or cone-mediated (light-adapted photopic ERG) pathways. ERG analyses in patients with ROP or in animals with OIR have revealed significant functional abnormalities in both the inner and outer retina. In patients with ROP, ERG response results are significantly attenuated and are accompanied by impaired contrast sensitivity and decreased scotopic visual thresholds [13,100,108–110]. ERG deficits are also evident in OIR animals [111,112], in which both a- and b-wave alterations generally correlate with structural deficits. Although the attenuation of the a-wave in OIR animals has been reported to occur without the

apparent loss of photoreceptors [113], it seems to be related with a thinner photoreceptor outer segment layer, which is more disorganized than in normal controls [114]. Animals with OIR also exhibit a reduced thickness of the inner plexiform layer (IPL) and of the inner nuclear layer (INL), with a concomitant increase of apoptosis in the inner retina [113]. These changes might affect the ERG due to loss of retinal neurons and disruption of synaptic transmission, which involve largely, but not exclusively, the regions of vascular dysfunction [115].

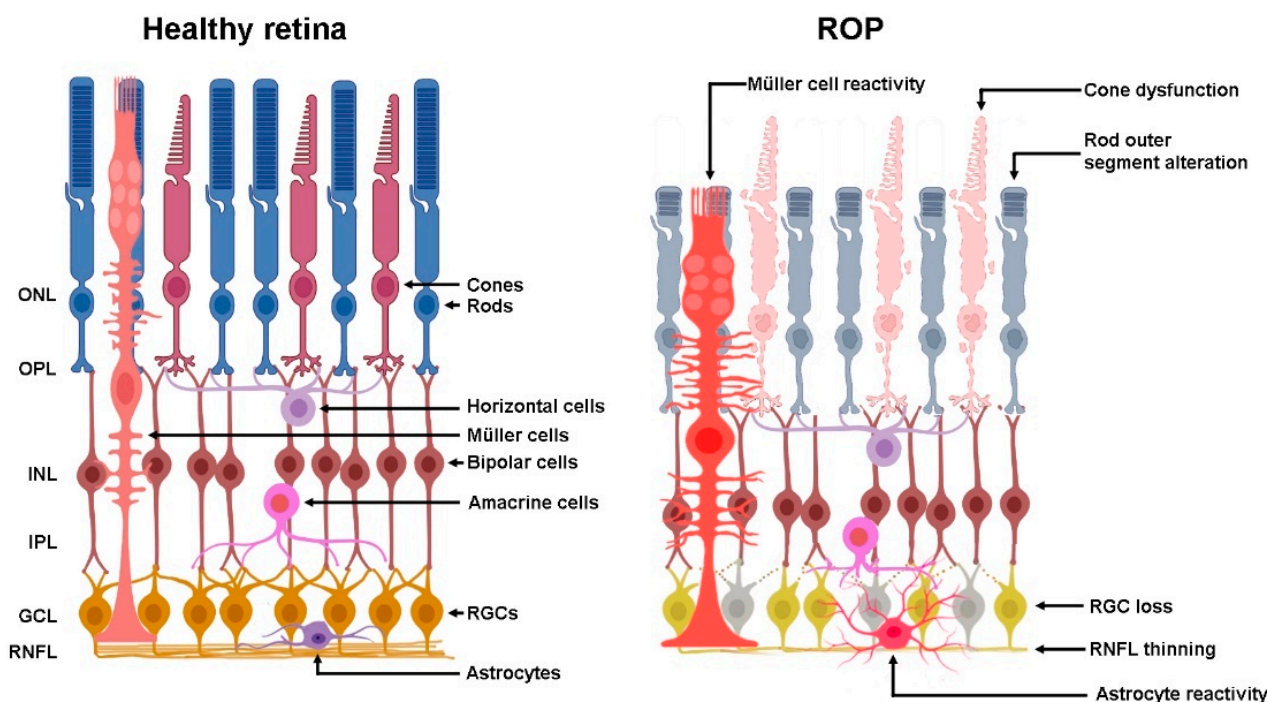


Figure 2. Schematic representation of neuroretinal alterations in ROP according to evidence from preterm infants and experimental model of oxygen-induced retinopathy. ONL, outer nuclear layer; OPL, outer plexiform layer; INL, inner nuclear layer; IPL, inner plexiform layer; GCL, ganglion cell layer; RNFL, retinal nerve fiber layer; RGCs, retinal ganglion cells.

3.2.1. Photoreceptors

The photoreceptors are the last cells to complete maturation, with the increase of outer segment elongation and the escalation of photopigment content occurring in the last 8 weeks of gestation. Therefore, alterations of the photoreceptor maturation due to the preterm birth might cover a relevant role in the onset of long-term visual dysfunctions in ROP [116].

Rods

Rods are the last retinal cell subtype to reach maturity, with their rhodopsin content in the outer segment appearing and increasing from approximately 32 weeks of gestational age [108,114]. Together with their maturation, the energy demand of rods rises due to the increased turnover of the light transduction-related molecules in the outer segment and to the increment in rod electrical activity. Alterations in oxygen supply due to a still incomplete and insufficient retinal vasculature, as it occurs in ROP, produce significant abnormalities in the maturation of rod outer segments. Indeed, they could be shorter, containing a low amount of rhodopsin and consequently showing diminished quantum catch, impaired mobility of the transduction cascade proteins in the disc membranes. Accordingly, infants affected by ROP display significant alterations in retinal activity demonstrated by the ERG analysis [110]. In this respect, although the abnormal ERG response may derive from an overall damage of the whole neuroretina, as demonstrated

in the OIR model, strong evidence supports the possibility that alterations in the outer segments of rods may have a primary counterpart in the ERG dysfunction [114]. This is even more evident in parafoveal rods, in which the developmental elongation of outer segments is physiologically delayed compared to peripheral rods. Thus, rods in the late-maturing parafovea are more vulnerable to the effects of ROP. In fact, the development of rod-mediated scotopic threshold is prolonged in infants with ROP compared to controls, more so in the parafoveal than in the peripheral retina. The precise underlying mechanisms remain to be defined, but they could include a slower rate of rod outer segment elongation, delayed packing of parafoveal rods (along with the delay in the foveal pit—see the section below), or disorganization of rod outer segments [117].

Cones

Primate cone maturation occurs earlier than that of rod outer segments, thus implying a higher resistance to the alterations caused by premature birth [109]. In addition, cones appear to be more resistant to metabolic insults, having twice as many mitochondria and three times the surface area of mitochondrial cristae compared to rods [118]. However, a recent study [119] has underlined the possibility that, together with the rods, cones might also undergo some form of functional alteration that manifests years after birth. Using multifocal ERG (mfERG), which allows to concomitantly measure the light-adapted activity of cones and that of post receptor cells in different areas of the retina, a significant dysfunction of the cone pathway in the central retina, characterized by low-cone sensitivity and slower recovery of cone responses, has been reported in subjects with a history of severe ROP [119]. Importantly, the magnitude of mfERG alterations varied together with the severity of the antecedent ROP but, notably, did not completely match with the canonical categorization of ROP based on the vascular abnormalities, as the case of no differences in mfERG amplitudes were detected between children with a history of mild ROP and children with no ROP. Therefore, this would suggest that the current ROP categorization, exclusively based on the characteristics of the retinal vasculature at the time of examination in the nursery, is quite reductive, since it does not take into account the important effects observed in the neurosensory retina.

The Foveal Pit

Macula lutea development is a sophisticated process which is not completed until at least the third or fourth year of life; particularly, the fovea centralis is the last retinal structure to reach complete maturity and it mediates the excellent visual acuity in healthy adults [120,121]. Within the macula lutea, the foveal pit (or fovea centralis) is an avascular zone formed by the centrifugal displacement of inner nuclear cells and retinal ganglion cells (RGCs) toward the periphery [122].

ROP significantly delays foveal development [123]. It also alters the foveal structure, although data on this point are not univocal. Indeed, Hammer et al. [120] reported that the foveal pit of subjects with a history of spontaneously regressed ROP appears broad and shallow, while some years later Wang et al., studying a slightly wider group of subjects, observed a diminished depth and a reduced shallow slope of the ROP foveal pit compared to controls [124].

Certainly, ROP determines the presence of retinal capillaries intertwined with the neural cells that cover the fovea [120] and increases foveal thickness [121]. This latter outcome is mainly due to the presence of inner retinal layers overlying the fovea, probably due to a failure of the inner retinal neurons to migrate away from the pit [124]. In line with this, studies on preterm children with or without a history of ROP reported that the thickness of both the RGC layer (GCL) and the IPL was remarkably higher at fovea centralis compared with full-term controls, while no differences were observed at more peripheral retinal locations [124–126].

Wang et al. found that the increased foveal thickness did not result in any changes in visual acuity [124]. However, other studies demonstrated the existence of a correlation

between inner retinal layer thickness and worsening of the best-corrected visual acuity (BCVA) in extremely preterm infants [127,128], while there was no correlation between altered BCVA and the thickness of outer retinal layers. Moreover, worsened BCVA is associated with an increased GCL thickness in extremely preterm infants, possibly as a consequence of the arrest of GCL maturation due to preterm birth, which prevents RGC death, a major event in retinal development [127].

3.2.2. Retinal Ganglion Cells

RGCs are particularly sensitive to changing oxygen levels. In this respect, hypoxia has been established to severely impact RGC survival and RGC axon outgrowth [129,130]. The significant damage to RGCs in the developing retina under altered oxygenation has mainly been demonstrated in the OIR model, in which the hypoxic phase is primarily responsible for inducing RGC degeneration and subsequent decrement in RGC density [130]. In this model, the alteration in RGC survival has been established to depend on the imbalance between apoptosis and autophagy during the hypoxic phase, resulting in the degeneration not only of RGCs, but also of bipolar and amacrine cells [61]. In this respect, there is evidence from our group that treatments based on natural antioxidant/anti-inflammatory compounds may prevent RGC death in several models of RGC degeneration [131–134], suggesting that such an approach may be useful also in counteracting neurodegeneration of RGCs in ROP. The use of nutraceuticals as a non-invasive approach in preventing ROP and in its management has been recently reviewed and discussed [135].

Evidence about the altered neural pro-survival signalling also derives from preterm infants affected by severe ROP, which display serum levels of neurotrophin-4 and brain-derived neurotrophic factor (BDNF) during the first 3 weeks of life that are lower than those in preterm infants who did not develop severe ROP. In the same cohort of patients, specific gene variations of BDNF were associated with threshold ROP [136,137], indicating the possibility that a possible alteration in neural trophism could concur to RGC degeneration during ROP progression. Besides their overt loss, evidence of a significant RGC damage is represented by structural alterations of their axons within the retinal nerve fiber layer (RNFL).

Studies of optical coherence tomography or spectral-domain optical coherence tomography revealed that RNFL thickness is altered in premature newborns compared to full-term children. In this respect, the RNFL resulted in a greater thickness on the temporal side of the optic disc in preterm infants than in full-term controls, whereas all other RNFL sectors were thinner. Such alterations in RNFL thickness were correlated with gestational age and birth weight, two key factors related with the risk of ROP development [138–140], as well as with the stage of ROP progression [141].

Whether RNFL alterations would correlate with visual function is still under debate. In this respect, Park et al. found no association between RNFL thickness and visual function [141]. On the contrary, Wang et al. in an analysis of 25 preterm and 54 full-term infants, reported an association between RNFL thickness in the retinal temporal sector and visual acuity [139]. Similarly, Fieß et al. demonstrated that decreased RNFL thickness in all retinal sectors is associated with reduced visual function in both preterm infants and full-term neonates, underscoring the high risk of preterm infants to develop alterations in the RNFL in association with a decrease in visual function [140].

3.2.3. Müller Cells and Astrocytes

Müller cells are the main retinal glial cells. From their soma, located in the INL, two major projections extend towards the GCL and the photoreceptor layer. Processes generated from these projections reach and surround neurons, synapses, and blood vessels creating physical and chemical relationships that allow intimate communications of central importance for physiological retinal functions [142]. Among the functions Müller cells accomplish, they: i. provide neurons with trophic factors and antioxidants; ii. uptake and recycle neurotransmitters including glutamate, thus avoiding excitotoxic insults to

neural cells; iii. transport water, ions and metabolites through channels and transporters participating, for instance, to K⁺ buffering and to the control of the composition of the retinal milieu; iv. participate to the formation of the blood-retinal barrier by secreting factors that enhance the barrier function of the surrounding endothelium [143].

Astrocytes, star-shaped glial cells mainly located in the GCL and in the RNFL, also play important roles in retinal physiology. For instance, astrocytes provide metabolic support to RGCs, thus controlling their ionic and metabolic homeostasis, and regulate neurovascular coupling. They also have a paramount role in the development of retinal vasculature; astrocytes are indeed the earliest glial cell type in the optic nerve of the embryo and, migrating into the neuroretina and releasing proangiogenic factors including VEGF, critically contribute to the formation of retinal blood vessels. They also act as a scaffold on which retinal vessels develop from the centre of the retina to the periphery. In this respect, astrocytes are lacking within the avascular foveal pit and are present only in the vascularized retina, a finding that highlights astrocyte importance in the development of retinal vasculature. In addition to inducing the formation of retinal blood vessels, similarly to Müller cells astrocytes contribute to the formation and maintenance of the blood retinal barrier [144].

When retinal homeostasis is challenged, glial cells undergo morphological and functional changes (gliosis or glial activation) with the attempt to avoid conditions potentially leading to a diseased state; however, gliosis may have not only beneficial but also detrimental effects on retinal function [145]. In Müller cells, the upregulation of proteins contributing to the formation of intermediate filaments, including glial fibrillary acidic protein (GFAP), is a hallmark of gliosis; in fact, in the healthy retina GFAP is only minimally expressed by Müller cells, which, on the contrary, dramatically increase GFAP expression in retinal diseases [146]. After their activation, glial cells secrete trophic factors to support neuronal and vascular function; however, if gliosis becomes chronic, direct and indirect damage to neurons and vessels may occur. For instance, the overproduction of VEGF leads to blood retinal barrier leakage, while the release of inflammatory cytokines may result in neuronal degeneration [147–149].

In humans, massive retinal gliosis is a rare, benign, intraocular condition that develops in association with other ocular diseases and is mainly constituted by Müller cell activation [150]. There are only a couple, not very recent, case reports describing the association between massive retinal gliosis and ROP [151,152]. One of them reported the presence of bilateral massive gliosis in a 39-year-old man born prematurely that developed severe ROP with retinal detachment [151], suggesting that severe ROP may have deleterious effects during the patient life. Although no clinical evidence indicates that gliosis may participate in ROP pathogenesis, results in preclinical models suggest this possibility. In fact, it has been demonstrated that gliosis, and in particular Müller cell activation, is a feature of OIR rodents [13] and that in these animals, maneuvers attenuating Müller cell gliosis reduce retinal neurovascular degeneration and preserve retinal function [153–155].

4. Future Perspectives

Although ROP has long been considered a vascular disorder, there is evidence raising the question on how this disease may be linked to neurodegenerative processes that may involve higher brain functions (Figure 3). Therefore, future studies will be necessary to investigate whether long-term neurodevelopmental outcomes can be considered associated to functional alterations characterizing ROP pathology. The involvement of the neural components in ROP, and not only of the vascular ones, should be taken into account when considering the resulting retinal structural and visual abnormalities. Such an approach could identify new targets for interventions in order to give children affected by ROP the best possible visual outcome.

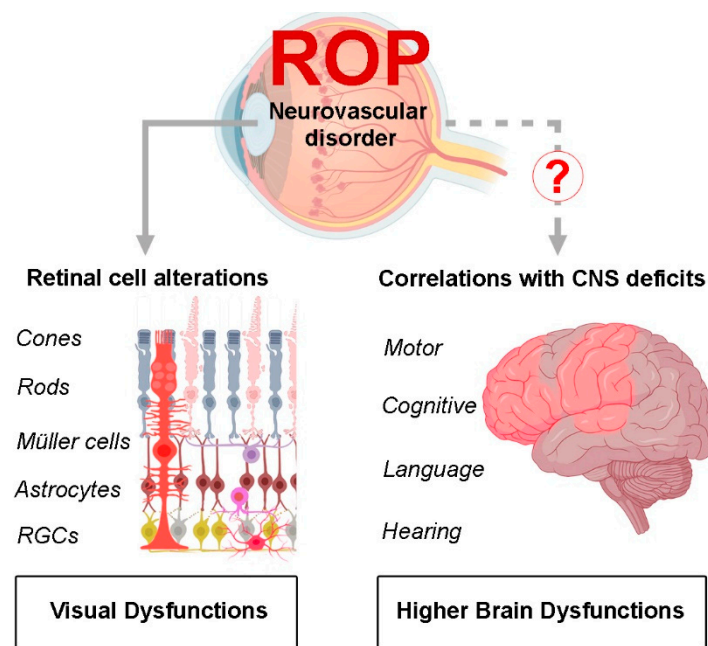


Figure 3. ROP, as neurovascular disorder, leads to retinal cell alterations finally resulting in visual dysfunctions. Further studies are required to evaluate whether long-term neurological outcomes observed in patients that had developed ROP are actually related to the disease or are instead a consequence of premature birth. CNS, central nervous system.

Author Contributions: Conceptualization, M.L., S.M. and M.D.M.; writing—original draft preparation, M.L. and S.M.; writing—review and editing, R.A., L.F., M.C. and M.D.M.; supervision, M.D.M. All authors have read and agreed to the published version of the manuscript.

Funding: This study was supported by fundings from the Italian Ministry of University and Research (FRA-2019/2021) to L.F., M.C. and M.D.M., and the Meyer Children’s University Hospital, Florence, Italy to M.D.M.

Institutional Review Board Statement: Not applicable.

Informed Consent Statement: Not applicable.

Data Availability Statement: Not applicable.

Acknowledgments: The authors thank Giovanni Casini for critical reading of the manuscript.

Conflicts of Interest: The authors declare no conflict of interest.

References

- AlQurashi, M.A. Survival rate of very low birth weight infants over a quarter century (1994–2019): A single-institution experience. *J. Neonatal Perinatal. Med.* **2021**, *14*, 253–260. [[CrossRef](#)] [[PubMed](#)]
- Chen, J.; Smith, L.E. Retinopathy of prematurity. *Angiogenesis* **2007**, *10*, 133–140. [[CrossRef](#)] [[PubMed](#)]
- Blencowe, H.; Lawn, J.E.; Vazquez, T.; Fielder, A.; Gilbert, C. Preterm-associated visual impairment and estimates of retinopathy of prematurity at regional and global levels for 2010. *Pediatr. Res.* **2013**, *74* (Suppl. S1), 35–49. [[CrossRef](#)] [[PubMed](#)]
- Fielder, A.; Blencowe, H.; O’Connor, A.; Gilbert, C. Impact of retinopathy of prematurity on ocular structures and visual functions. *Arch. Dis. Child Fetal Neonatal* **2015**, *100*, F179–F184. [[CrossRef](#)] [[PubMed](#)]
- Hughes, S.; Yang, H.; Chan-Ling, T. Vascularization of the human fetal retina: Roles of vasculogenesis and angiogenesis. *Investig. Ophthalmol. Vis. Sci.* **2000**, *41*, 1217–1228.
- Krock, B.L.; Skuli, N.; Simon, M.C. Hypoxia-induced angiogenesis: Good and evil. *Genes Cancer* **2011**, *2*, 1117–1133. [[CrossRef](#)]
- Wang, G.L.; Semenza, G.L. Characterization of hypoxia-inducible factor 1 and regulation of DNA binding activity by hypoxia. *J. Biol. Chem.* **1993**, *268*, 21513–21518. [[CrossRef](#)]
- Stone, J.; Itin, A.; Alon, T.; Pe’er, J.; Gnessin, H.; Chan-Ling, T.; Keshet, E. Development of retinal vasculature is mediated by hypoxia-induced vascular endothelial growth factor (VEGF) expression by neuroglia. *J. Neurosci.* **1995**, *15*, 4738–4747. [[CrossRef](#)]
- Hellström, A.; Smith, L.E.; Dammann, O. Retinopathy of prematurity. *Lancet* **2013**, *382*, 1445–1457. [[CrossRef](#)]

10. Chiang, M.F.; Quinn, G.E.; Fielder, A.R.; Ostmo, S.R.; Paul Chan, R.V.; Berrocal, A.; Binenbaum, G.; Blair, M.; Peter Campbell, J.; Capone, A., Jr.; et al. International Classification of Retinopathy of Prematurity, Third Edition. *Ophthalmology* **2021**, *128*, e51–e68. [CrossRef]
11. Askie, L.M.; Darlow, B.A.; Finer, N.; Schmidt, B.; Stenson, B.; Tarnow-Mordi, W.; Davis, P.G.; Carlo, W.A.; Brocklehurst, P.; Davies, L.C.; et al. Association Between Oxygen Saturation Targeting and Death or Disability in Extremely Preterm Infants in the Neonatal Oxygenation Prospective Meta-analysis Collaboration. *JAMA* **2018**, *319*, 2190–2201. [CrossRef] [PubMed]
12. Cummings, J.J.; Polin, R.A. Committee on Fetus and Newborn. Oxygen Targeting in Extremely Low Birth Weight Infants. *Pediatrics* **2016**, *138*, e20161576. [CrossRef]
13. Smith, L.E.; Wesolowski, E.; McLellan, A.; Kostyk, S.K.; D’Amato, R.; Sullivan, R.; D’Amore, P.A. Oxygen-induced retinopathy in the mouse. *Investig. Ophthalmol. Vis. Sci.* **1994**, *35*, 101–111.
14. Caprara, C.; Grimm, C. From oxygen to erythropoietin: Relevance of hypoxia for retinal development, health and disease. *Prog. Retin. Eye Res.* **2012**, *31*, 89–119. [CrossRef]
15. Hellström, A.; Hård, A.L. Screening and novel therapies for retinopathy of prematurity—A review. *Early Hum. Dev.* **2019**, *138*, 104846. [CrossRef] [PubMed]
16. Hurley, B.R.; McNamara, J.A.; Fineman, M.S.; Ho, A.C.; Tasman, W.; Kaiser, R.S.; Vander, J.F.; Regillo, C.D.; Brown, G.C. Laser treatment for retinopathy of prematurity: Evolution in treatment technique over 15 years. *Retina* **2006**, *26*, S16–S17. [CrossRef]
17. Kieselbach, G.F.; Ramharter, A.; Baldissera, I.; Kralinger, M.T. Laser photocoagulation for retinopathy of prematurity: Structural and functional outcome. *Acta Ophthalmol. Scand.* **2006**, *84*, 21–26. [CrossRef]
18. Barry, G.P.; Yu, Y.; Ying, G.S.; Tomlinson, L.A.; Lajoie, J.; Fisher, M.; Binenbaum, G. Retinal Detachment after Treatment of Retinopathy of Prematurity with Laser versus Intravitreal Anti-Vascular Endothelial Growth Factor. *Ophthalmology* **2021**, *128*, 1188–1196. [CrossRef]
19. Gundlach, B.S.; Kokhanov, A.; Altendahl, M.; Suh, S.Y.; Fung, S.; Demer, J.; Pineles, S.; Khitri, M.; Chu, A.; Tsui, I. Real-world visual outcomes of laser and anti-VEGF treatments for retinopathy of prematurity. *Am. J. Ophthalmol.* **2022**, *238*, 86–96. [CrossRef]
20. Li, Z.; Zhang, Y.; Liao, Y.; Zeng, R.; Zeng, P.; Lan, Y. Comparison of efficacy between anti-vascular endothelial growth factor (VEGF) and laser treatment in Type-1 and threshold retinopathy of prematurity (ROP). *BMC Ophthalmol.* **2018**, *18*, 19. [CrossRef]
21. Sankar, M.J.; Sankar, J.; Chandra, P. Anti-vascular endothelial growth factor (VEGF) drugs for treatment of retinopathy of prematurity. *Cochrane Database Syst. Rev.* **2018**, *1*, CD009734. [CrossRef] [PubMed]
22. Italian Institute of Statistics. Available online: http://dati.istat.it/Index.aspx?DataSetCode=DCIS_INDEMOG1 (accessed on 21 April 2022).
23. Borroni, C.; Carlevaro, C.; Morzenti, S.; De Ponti, E.; Bozzetti, V.; Console, V.; Capobianco, S.; Tagliabue, P.E. Survey on retinopathy of prematurity (ROP) in Italy. *Ital. J. Pediatr.* **2013**, *39*, 43. [CrossRef] [PubMed]
24. Palmer, E.A.; Flynn, J.T.; Hardy, R.J.; Phelps, D.L.; Phillips, C.L.; Schaffer, D.B.; Tung, B. Incidence and early course of retinopathy of prematurity. The Cryotherapy for Retinopathy of Prematurity Cooperative Group. *Ophthalmology* **1991**, *98*, 1628–1640. [CrossRef]
25. Good, W.V.; Hardy, R.J.; Dobson, V.; Palmer, E.A.; Phelps, D.L.; Quintos, M.; Tung, B. Early Treatment for Retinopathy of Prematurity Cooperative Group. The incidence and course of retinopathy of prematurity: Findings from the early treatment for retinopathy of prematurity study. *Pediatrics* **2005**, *116*, 15–23. [CrossRef] [PubMed]
26. Bullard, S.R.; Donahue, S.P.; Feman, S.S.; Sinatra, R.B.; Walsh, W.F. The decreasing incidence and severity of retinopathy of prematurity. *J. AAPOS* **1999**, *3*, 46–52. [CrossRef]
27. Database Summaries and VLBW. Quality Management Report Revised March 2011. Burlington, Vermont: Vermont Oxford Network. Available online: <https://clinicaltrials.gov/ct2/show/NCT01825499> (accessed on 12 April 2022).
28. Austeng, D.; Källén, K.B.; Ewald, U.W.; Jakobsson, P.G.; Holmström, G.E. Incidence of retinopathy of prematurity in infants born before 27 weeks’ gestation in Sweden. *Arch. Ophthalmol.* **2009**, *127*, 1315–1319. [CrossRef] [PubMed]
29. Choo, M.M.; Martin, F.J.; Theam, L.C.; U-Teng, C. Retinopathy of prematurity in extremely low birth weight infants in Malaysia. *J. AAPOS* **2009**, *13*, 446–449. [CrossRef]
30. Teed, R.G.; Saunders, R.A. Retinopathy of prematurity in extremely premature infants. *J. AAPOS* **2009**, *13*, 370–373. [CrossRef]
31. Manzoni, P.; Memo, L.; Mostert, M.; Gallo, E.; Guardione, R.; Maestri, A.; Saia, O.S.; Opramolla, A.; Calabrese, S.; Tavella, E.; et al. Use of erythropoietin is associated with threshold retinopathy of prematurity (ROP) in preterm ELBW neonates: A retrospective, cohort study from two large tertiary NICUs in Italy. *Early Hum. Dev.* **2014**, *90* (Suppl. S2), S29–S33. [CrossRef]
32. Dani, C.; Coviello, C.; Panin, F.; Frosini, S.; Costa, S.; Purcaro, V.; Lepore, D.; Vento, G. Incidence and risk factors of retinopathy of prematurity in an Italian cohort of preterm infants. *Ital. J. Pediatr.* **2021**, *47*, 64. [CrossRef]
33. Holmström, G.; Broberger, U.; Thomassen, P. Neonatal risk factors for retinopathy of prematurity—A population-based study. *Acta Ophthalmol. Scand.* **1998**, *76*, 204–207. [CrossRef] [PubMed]
34. Shah, V.A.; Yo, C.L.; Ling, Y.L.; Ho, L.Y. Incidence, risk factors of retinopathy of prematurity among very low birth weight infants in Singapore. *Ann. Acad. Med. Singap* **2005**, *34*, 169–78. [PubMed]
35. Akkoyun, I.; Oto, S.; Yilmaz, G.; Gurakan, B.; Tarcan, A.; Anuk, D.; Akgun, S.; Akova, Y.A. Risk factors in the development of mild and severe retinopathy of prematurity. *J. AAPOS* **2006**, *10*, 449–453. [CrossRef] [PubMed]

36. Yau, G.S.; Lee, J.W.; Tam, V.T.; Liu, C.C.; Yip, S.; Cheng, E.; Chu, B.C.; Yuen, C.Y. Incidence and Risk Factors of Retinopathy of Prematurity From 2 Neonatal Intensive Care Units in a Hong Kong Chinese Population. *Asia Pac. J. Ophthalmol.* **2016**, *5*, 185–191. [[CrossRef](#)]
37. Bas, A.Y.; Demirel, N.; Koc, E.; Ulubas Isik, D.; Hirfanoglu, İ.M.; Tunc, T. TR-ROP Study Group. Incidence, risk factors and severity of retinopathy of prematurity in Turkey (TR-ROP study): A prospective, multicentre study in 69 neonatal intensive care units. *Br. J. Ophthalmol.* **2018**, *102*, 1711–1716. [[CrossRef](#)]
38. Chang, J.W. Risk factor analysis for the development and progression of retinopathy of prematurity. *PLoS ONE* **2019**, *14*, e0219934. [[CrossRef](#)]
39. Mehner, L.C.; Wagner, B.D.; Bol, K.A.; Singh, J.K.; Oliver, S.C.; Patnaik, J.L.; Palestine, A.G.; McCourt, E.A.; Mandava, N.; Wymore, E.M.; et al. Trends in Retinopathy of Prematurity over 12 Years in a Colorado Cohort. *Ophthalmic Epidemiol.* **2021**, *3*, 220–226. [[CrossRef](#)]
40. Grottenberg, B.G.; Korseth, K.M.; Follestad, T.; Stensvold, H.J.; Støen, R.; Austeng, D. Stable incidence but regional differences in retinopathy of prematurity in Norway from 2009 to 2017. *Acta Ophthalmol.* **2021**, *99*, 299–305. [[CrossRef](#)]
41. Dani, C.; Reali, M.F.; Bertini, G.; Martelli, E.; Pezzati, M.; Rubaltelli, F.F. The role of blood transfusions and iron intake on retinopathy of prematurity. *Early Hum. Dev.* **2001**, *62*, 57–63. [[CrossRef](#)]
42. Valieva, O.A.; Strandjord, T.P.; Mayock, D.E.; Juul, S.E. Effects of transfusions in extremely low birth weight infants: A retrospective study. *J. Pediatr.* **2009**, *155*, 331–337.e1. [[CrossRef](#)]
43. Keir, A.; Pal, S.; Trivella, M.; Lieberman, L.; Callum, J.; Shehata, N.; Stanworth, S.J. Adverse effects of red blood cell transfusions in neonates: A systematic review and meta-analysis. *Transfusion* **2016**, *56*, 2773–2780. [[CrossRef](#)] [[PubMed](#)]
44. Ghirardello, S.; Dusi, E.; Cortinovis, I.; Villa, S.; Fumagalli, M.; Agosti, M.; Milani, S.; Mosca, F. Effects of Red Blood Cell Transfusions on the Risk of Developing Complications or Death: An Observational Study of a Cohort of Very Low Birth Weight Infants. *Am. J. Perinatol.* **2017**, *34*, 88–95. [[CrossRef](#)] [[PubMed](#)]
45. Lust, C.; Vesoulis, Z.; Jackups, R.J.; Liao, S.; Rao, R.; Mathur, A.M. Early red cell transfusion is associated with development of severe retinopathy of prematurity. *J. Perinatol.* **2019**, *39*, 393–400. [[CrossRef](#)]
46. Zhu, Z.; Hua, X.; Yu, Y.; Zhu, P.; Hong, K.; Ke, Y. Effect of red blood cell transfusion on the development of retinopathy of prematurity: A systematic review and meta-analysis. *PLoS ONE* **2020**, *15*, e0234266. [[CrossRef](#)]
47. Teofili, L.; Papacci, P.; Bartolo, M.; Molisso, A.; Orlando, N.; Pane, L.; Giannantonio, C.; Serrao, F.; Bianchi, M.; Valentini, C.G.; et al. Transfusion-Free Survival Predicts Severe Retinopathy in Preterm Neonates. *Front. Pediatr.* **2022**, *10*, 814194. [[CrossRef](#)] [[PubMed](#)]
48. Parrozzani, R.; Nacci, E.B.; Bini, S.; Marchione, G.; Salvadori, S.; Nardo, D.; Midena, E. Severe retinopathy of prematurity is associated with early post-natal low platelet count. *Sci. Rep.* **2021**, *11*, 891. [[CrossRef](#)] [[PubMed](#)]
49. Parrozzani, R.; Marchione, G.; Fantin, A.; Frizziero, L.; Salvadori, S.; Nardo, D.; Midena, G. Thrombocytopenia as Type 1 ROP Biomarker: A Longitudinal Study. *J. Pers. Med.* **2021**, *11*, 1120. [[CrossRef](#)]
50. Binenbaum, G.; Bell, E.F.; Donohue, P.; Quinn, G.; Shaffer, J.; Tomlinson, L.A.; Ying, G.S.; G-ROP Study Group. Development of modified screening criteria for retinopathy of prematurity: Primary results from the postnatal growth and retinopathy of prematurity study. *JAMA Ophthalmol.* **2018**, *136*, 1034–1040. [[CrossRef](#)]
51. Caruggi, S.; Scaramuzzi, M.; Calevo, M.G.; Priolo, E.; Sposetti, L.; Camicione, P.; Ramenghi, L.A.; Serafino, M. Validation of the postnatal growth and retinopathy of prematurity screening criteria: A retrospective Italian analysis. *Eur. J. Ophthalmol.* **2021**, *32*, 1169–1173. [[CrossRef](#)]
52. Garofoli, F.; Barillà, D.; Angelini, M.; Mazzucchelli, I.; De Silvestri, A.; Guagliano, R.; Decembrino, L.; Tziella, C. Oral vitamin A supplementation for ROP prevention in VLBW preterm infants. *Ital. J. Pediatr.* **2020**, *46*, 77. [[CrossRef](#)]
53. Filippi, L.; Cavallaro, G.; Fiorini, P.; Daniotti, M.; Benedetti, V.; Cristofori, G.; Araimo, G.; Ramenghi, L.; La Torre, A.; Fortunato, P.; et al. Study protocol: Safety and efficacy of propranolol in newborns with Retinopathy of Prematurity (PROP-ROP): ISRCTN18523491. *BMC Pediatr.* **2010**, *10*, 83. [[CrossRef](#)] [[PubMed](#)]
54. Filippi, L.; Cavallaro, G.; Fiorini, P.; Malvagia, S.; Della Bona, M.L.; Giocaliere, E.; Bagnoli, P.; Dal Monte, M.; Mosca, F.; Donzelli, G.; et al. Propranolol concentrations after oral administration in term and preterm neonates. *J. Matern. Fetal Neonatal Med.* **2013**, *26*, 833–840. [[CrossRef](#)] [[PubMed](#)]
55. Filippi, L.; Dal Monte, M.; Casini, G.; Daniotti, M.; Sereni, F.; Bagnoli, P. Infantile hemangiomas, retinopathy of prematurity and cancer: A common pathogenetic role of the β -adrenergic system. *Med. Res. Rev.* **2015**, *35*, 619–652. [[CrossRef](#)]
56. Ristori, C.; Filippi, L.; Dal Monte, M.; Martini, D.; Cammalleri, M.; Fortunato, P.; Bagnoli, P. Role of the adrenergic system in a mouse model of oxygen-induced retinopathy: Antiangiogenic effects of beta-adrenoreceptor blockade. *Investig. Ophthalmol. Vis. Sci.* **2011**, *52*, 155–170. [[CrossRef](#)]
57. Dal Monte, M.; Casini, G.; la Marca, G.; Isacchi, B.; Filippi, L.; Bagnoli, P. Eye drop propranolol administration promotes the recovery of oxygen-induced retinopathy in mice. *Exp. Eye Res.* **2013**, *111*, 27–35. [[CrossRef](#)]
58. Filippi, L.; Cavallaro, G.; Berti, E.; Padrini, L.; Araimo, G.; Regiroli, G.; Bozzetti, V.; De Angelis, C.; Tagliabue, P.; Tomasini, B.; et al. Study protocol: Safety and efficacy of propranolol 0.2% eye drops in newborns with a precocious stage of retinopathy of prematurity (DROP-ROP-0.2%): A multicenter, open-label, single arm, phase II trial. *BMC Pediatr.* **2017**, *17*, 165. [[CrossRef](#)] [[PubMed](#)]

59. Filippi, L.; Cavallaro, G.; Berti, E.; Padrini, L.; Araimo, G.; Regiroli, G.; Raffaelli, G.; Bozzetti, V.; Tagliabue, P.; Tomasini, B.; et al. Propranolol 0.2% Eye Micro-Drops for Retinopathy of Prematurity: A Prospective Phase IIB Study. *Front. Pediatr.* **2019**, *7*, 180. [[CrossRef](#)]
60. Filippi, L.; Cammalleri, M.; Amato, R.; Ciantelli, M.; Pini, A.; Bagnoli, P.; Dal Monte, M. Decoupling Oxygen Tension From Retinal Vascularization as a New Perspective for Management of Retinopathy of Prematurity. New Opportunities From β -adrenoceptors. *Front. Pharmacol.* **2022**, *13*, 835771. [[CrossRef](#)]
61. Cammalleri, M.; Locri, F.; Catalani, E.; Filippi, L.; Cervia, D.; Dal Monte, M.; Bagnoli, P. The Beta Adrenergic Receptor Blocker Propranolol Counteracts Retinal Dysfunction in a Mouse Model of Oxygen Induced Retinopathy: Restoring the Balance between Apoptosis and Autophagy. *Front. Cell Neurosci.* **2017**, *11*, 395. [[CrossRef](#)]
62. Leung, M.P.; Thompson, B.; Black, J.; Dai, S.; Alsweiler, J.M. The effects of preterm birth on visual development. *Clin. Exp. Optom.* **2018**, *101*, 4–12. [[CrossRef](#)]
63. Bowl, W.; Lorenz, B.; Stieger, K.; Schweinfurth, S.; Holve, K.; Friedburg, C.; Andrassi-Darida, M. Correlation of central visual function and ROP risk factors in pretermates with and without acute ROP at the age of 6-13 years: The Giessen long-term ROP study. *Br. J. Ophthalmol.* **2016**, *100*, 1238–1244. [[CrossRef](#)]
64. Moskowitz, A.; Hansen, R.M.; Fulton, A.B. Retinal, visual, and refractive development in retinopathy of prematurity. *Eye Brain* **2016**, *20*, 103–111. [[CrossRef](#)] [[PubMed](#)]
65. Geldof, C.J.; Oosterlaan, J.; Vuijk, P.J.; de Vries, M.J.; Kok, J.H.; van Wassenaer-Leemhuis, A.G. Visual sensory and perceptive functioning in 5-year-old very preterm/very-low-birthweight children. *Dev. Med. Child Neurol.* **2014**, *56*, 862–868. [[CrossRef](#)] [[PubMed](#)]
66. Haugen, O.H.; Nepstad, L.; Standal, O.A.; Elgen, I.; Markestad, T. Visual function in 6 to 7 year-old children born extremely preterm: A population-based study. *Acta Ophthalmol.* **2012**, *90*, 422–427. [[CrossRef](#)]
67. Larsson, E.K.; Rydberg, A.C.; Holmström, G.E. A population-based study of the refractive outcome in 10-year-old preterm and full-term children. *Arch. Ophthalmol.* **2003**, *121*, 1430–1436. [[CrossRef](#)] [[PubMed](#)]
68. Darlow, B.A.; Elder, M.J.; Kimber, B.; Martin, J.; Horwood, L.J. Vision in former very low birthweight young adults with and without retinopathy of prematurity compared with term born controls: The NZ 1986 VLBW follow-up study. *Br. J. Ophthalmol.* **2018**, *102*, 1041–1046. [[CrossRef](#)]
69. Uner, O.E.; Rao, P.; Hubbard, G.B., 3rd. Reactivation of Retinopathy of Prematurity in Adults and Adolescents. *Ophthalmol. Retina* **2020**, *4*, 720–727. [[CrossRef](#)]
70. Early Treatment for Retinopathy of Prematurity Cooperative Group; Good, W.V.; Hardy, R.J.; Dobson, V.; Palmer, E.A.; Phelps, D.L.; Tung, B.; Redford, M. Final visual acuity results in the early treatment for retinopathy of prematurity study. *Arch. Ophthalmol.* **2010**, *128*, 663–671. [[CrossRef](#)]
71. Rodriguez, S.H.; Schechet, S.A.; Shapiro, M.J.; Blair, M.P. Late visual outcomes in infants treated with primary bevacizumab for type 1 retinopathy of prematurity. *J. AAPOS* **2020**, *24*, 149.e1–149.e5. [[CrossRef](#)]
72. Graziosi, A.; Perrotta, M.; Russo, D.; Gasparroni, G.; D'Egidio, C.; Marinelli, B.; Di Marzio, G.; Falconio, G.; Mastropasqua, L.; Li Volti, G.; et al. Oxidative Stress Markers and the Retinopathy of Prematurity. *J. Clin. Med.* **2020**, *9*, 2711. [[CrossRef](#)]
73. Holm, M.; Morken, T.S.; Fichorova, R.N.; VanderVeen, D.K.; Allred, E.N.; Dammann, O.; Leviton, A. ELGAN Study Neonatology and Ophthalmology Committees. Systemic Inflammation-Associated Proteins and Retinopathy of Prematurity in Infants Born Before the 28th Week of Gestation. *Investig. Ophthalmol. Vis. Sci.* **2017**, *58*, 6419–6428. [[CrossRef](#)] [[PubMed](#)]
74. Morken, T.S.; Dammann, O.; Skranes, J.; Austeng, D. Retinopathy of prematurity, visual and neurodevelopmental outcome, and imaging of the central nervous system. *Semin. Perinatol.* **2019**, *43*, 381–389. [[CrossRef](#)] [[PubMed](#)]
75. Drost, F.J.; Keunen, K.; Moeskops, P.; Claessens, N.H.P.; van Kalken, F.; Išgum, I.; Voskuil-Kerkhof, E.S.M.; Groenendaal, F.; de Vries, L.S.; Benders, M.J.N.L.; et al. Severe retinopathy of prematurity is associated with reduced cerebellar and brainstem volumes at term and neurodevelopmental deficits at 2 years. *Pediatr. Res.* **2018**, *83*, 818–824. [[CrossRef](#)] [[PubMed](#)]
76. Dumpich, M.; Theiss, C. VEGF in the nervous system: An important target for research in neurodevelopmental and regenerative medicine. *Neural. Regen. Res.* **2015**, *10*, 1725–1726. [[PubMed](#)]
77. Dyer, A.H.; Vahdatpour, C.; Sanfeliu, A.; Tropea, D. The role of Insulin-Like Growth Factor 1 (IGF-1) in brain development, maturation and neuroplasticity. *Neuroscience* **2016**, *325*, 89–99. [[CrossRef](#)]
78. Hansen-Pupp, I.; Löfqvist, C.; Polberger, S.; Niklasson, A.; Fellman, V.; Hellström, A.; Ley, D. Influence of insulin-like growth factor I and nutrition during phases of postnatal growth in very preterm infants. *Pediatr. Res.* **2011**, *69*, 448–453. [[CrossRef](#)]
79. Arima, M.; Akiyama, M.; Fujiwara, K.; Mori, Y.; Inoue, H.; Seki, E.; Nakama, T.; Tsukamoto, S.; Ochiai, M.; Ohga, S.; et al. Neurodevelopmental outcomes following intravitreal bevacizumab injection in Japanese preterm infants with type 1 retinopathy of prematurity. *PLoS ONE* **2020**, *15*, e0230678. [[CrossRef](#)]
80. Farooqi, A.; Hägglöf, B.; Sedin, G.; Serenius, F. Impact at age 11 years of major neonatal morbidities in children born extremely preterm. *Pediatrics* **2011**, *127*, e1247–e1257. [[CrossRef](#)]
81. Schmidt, B.; Roberts, R.S.; Davis, P.G.; Doyle, L.W.; Asztalos, E.V.; Opie, G.; Bairam, A.; Solimano, A.; Arnon, S.; Sauve, R.S. Caffeine for Apnea of Prematurity (CAP) Trial Investigators; Caffeine for Apnea of Prematurity CAP Trial Investigators. Prediction of Late Death or Disability at Age 5 Years Using a Count of 3 Neonatal Morbidities in Very Low Birth Weight Infants. *J. Pediatr.* **2015**, *167*, 982–986.e2. [[CrossRef](#)]










82. Schmidt, B.; Davis, P.G.; Asztalos, E.V.; Solimano, A.; Roberts, R.S. Association between severe retinopathy of prematurity and nonvisual disabilities at age 5 years. *JAMA* **2014**, *311*, 523–525. [[CrossRef](#)]
83. Schmidt, B.; Asztalos, E.V.; Roberts, R.S.; Robertson, C.M.; Sauve, R.S.; Whitfield, M.F. Trial of Indomethacin Prophylaxis in Preterms (TIPP) Investigators. Impact of bronchopulmonary dysplasia, brain injury, and severe retinopathy on the outcome of extremely low-birth-weight infants at 18 months: Results from the trial of indomethacin prophylaxis in preterms. *JAMA* **2003**, *289*, 1124–1129. [[CrossRef](#)] [[PubMed](#)]
84. Jacobson, L.; Fernell, E.; Broberger, U.; Ek, U.; Gillberg, C. Children with blindness due to retinopathy of prematurity: A population-based study. Perinatal data, neurological and ophthalmological outcome. *Dev. Med. Child Neurol.* **1998**, *40*, 155–159. [[CrossRef](#)] [[PubMed](#)]
85. Msall, M.E.; Phelps, D.L.; Hardy, R.J.; Dobson, V.; Quinn, G.E.; Summers, C.G.; Tremont, M.R. Cryotherapy for Retinopathy of Prematurity Cooperative Group. Educational and social competencies at 8 years in children with threshold retinopathy of prematurity in the CRYO-ROP multicenter study. *Pediatrics* **2004**, *113*, 790–799. [[CrossRef](#)] [[PubMed](#)]
86. Msall, M.E.; Phelps, D.L.; DiGaudio, K.M.; Dobson, V.; Tung, B.; McClead, R.E.; Quinn, G.E.; Reynolds, J.D.; Hardy, R.J.; Palmer, E.A. Severity of neonatal retinopathy of prematurity is predictive of neurodevelopmental functional outcome at age 5.5 years. Behalf of the Cryotherapy for Retinopathy of Prematurity Cooperative Group. *Pediatrics* **2000**, *106*, 998–1005. [[CrossRef](#)] [[PubMed](#)]
87. Cooke, R.W.; Foulder-Hughes, L.; Newsham, D.; Clarke, D. Ophthalmic impairment at 7 years of age in children born very preterm. *Arch. Dis. Child Fetal Neonatal Ed.* **2004**, *89*, F249–F253. [[CrossRef](#)]
88. Allred, E.N.; Capone, A., Jr.; Fraioli, A.; Dammann, O.; Droste, P.; Duker, J.; Gise, R.; Kuban, K.; Leviton, A.; O’Shea, T.M.; et al. Retinopathy of prematurity and brain damage in the very preterm newborn. *J. AAPOS* **2014**, *18*, 241–247. [[CrossRef](#)]
89. Sveinsdóttir, K.; Ley, D.; Hövel, H.; Fellman, V.; Hüppi, P.S.; Smith, L.E.H.; Hellström, A.; Hansen-Pupp, I. Relation of Retinopathy of Prematurity to Brain Volumes at Term Equivalent Age and Developmental Outcome at 2 Years of Corrected Age in Very Preterm Infants. *Neonatology* **2018**, *114*, 46–52. [[CrossRef](#)]
90. Glass, T.J.A.; Chau, V.; Gardiner, J.; Foong, J.; Vinall, J.; Zwicker, J.G.; Grunau, R.E.; Synnes, A.; Poskitt, K.J.; Miller, S.P. Severe retinopathy of prematurity predicts delayed white matter maturation and poorer neurodevelopment. *Arch. Dis. Child Fetal Neonatal Ed.* **2017**, *102*, F532–F537. [[CrossRef](#)]
91. Beligere, N.; Perumalsamy, V.; Flora, J.H.; Garska, M.J. Neurodevelopmental Disabilities in Children with Retinopathy of Prematurity: A Report from India. *Int. J. Ophthalmol. Clin. Res.* **2020**, *7*, 114.
92. Todd, D.A.; Goyen, T.A.; Smith, J.; Rochefort, M. Developmental outcome in preterm infants <29 weeks gestation with ≤Stage 3 retinopathy of prematurity (ROP): Relationship to severity of ROP. *J. Dev. Orig. Health Dis.* **2012**, *3*, 116–122. [[CrossRef](#)]
93. Goyen, T.A.; Todd, D.A.; Veddovi, M.; Wright, A.L.; Flaherty, M.; Kennedy, J. Eye-hand co-ordination skills in very preterm infants <29 weeks gestation at 3 years: Effects of preterm birth and retinopathy of prematurity. *Early Hum. Dev.* **2006**, *82*, 739–745. [[CrossRef](#)] [[PubMed](#)]
94. Stephenson, T.; Wright, S.; O’Connor, A.; Fielder, A.; Johnson, A.; Ratib, S.; Tobin, M. Children born weighing less than 1701 g: Visual and cognitive outcomes at 11–14 years. *Arch. Dis. Child Fetal Neonatal Ed.* **2007**, *92*, F265–F270. [[CrossRef](#)] [[PubMed](#)]
95. Ahn, S.J.; Park, H.K.; Lee, B.R.; Lee, H.J. Diffusion Tensor Imaging Analysis of White Matter Microstructural Integrity in Infants with Retinopathy of Prematurity. *Investig. Ophthalmol. Vis. Sci.* **2019**, *60*, 3024–3033. [[CrossRef](#)] [[PubMed](#)]
96. Ahn, S.J.; Lee, J.Y.; Lee, J.Y.; Lee, Y.J.; Lee, J.M.; Lee, B.R.; Kim, J.; Lee, H.J. Brain White Matter Maturation and Early Developmental Outcomes in Preterm Infants with Retinopathy of Prematurity. *Investig. Ophthalmol. Vis. Sci.* **2021**, *62*, 2. [[CrossRef](#)]
97. Altendahl, M.; Sim, M.S.; Kokhanov, A.; Gundlach, B.; Tsui, I.; Chu, A. Severe Retinopathy of Prematurity Is Not Independently Associated with Worse Neurodevelopmental Outcomes in Preterm Neonates. *Front. Pediatr.* **2021**, *9*, 679546. [[CrossRef](#)] [[PubMed](#)]
98. Song, C.M.; Ahn, J.H.; Hwang, J.K.; Kim, C.R.; Kim, M.J.; Lee, K.M.; Lee, H.J.; Ahn, S.J. Retinopathy of Prematurity and Hearing Impairment in Infants Born with Very-Low-Birth-Weight: Analysis of a Korean Neonatal Network Database. *J. Clin. Med.* **2021**, *10*, 4781. [[CrossRef](#)]
99. Fletcher, E.L.; Downie, L.E.; Hatzopoulos, K.; Vessey, K.A.; Ward, M.M.; Chow, C.L.; Pianta, M.J.; Vingrys, A.J.; Kalloniatis, M.; Wilkinson-Berka, J.L. The significance of neuronal and glial cell changes in the rat retina during oxygen-induced retinopathy. *Doc. Ophthalmol.* **2010**, *120*, 67–86. [[CrossRef](#)]
100. O’Connor, A.R.; Stephenson, T.; Johnson, A.; Tobin, M.J.; Moseley, M.J.; Ratib, S.; Ng, Y.; Fielder, A.R. Long-term ophthalmic outcome of low birth weight children with and without retinopathy of prematurity. *Pediatrics* **2002**, *109*, 12–18. [[CrossRef](#)]
101. Pétursdóttir, D.; Holmström, G.; Larsson, E. Visual function is reduced in young adults formerly born prematurely: A population-based study. *Br. J. Ophthalmol.* **2020**, *104*, 541–546. [[CrossRef](#)]
102. Hansen, R.M.; Fulton, A.B. Background adaptation in children with a history of mild retinopathy of prematurity. *Investig. Ophthalmol. Vis. Sci.* **2000**, *41*, 320–324. [[CrossRef](#)]
103. Bowl, W.; Lorenz, B.; Stieger, K.; Schweinfurth, S.; Holve, K.; Andrassi-Darida, M. Fundus-Controlled Dark Adaptometry in Young Children Without and With Spontaneously Regressed Retinopathy of Prematurity. *Transl. Vis. Sci. Technol.* **2019**, *8*, 62. [[CrossRef](#)] [[PubMed](#)]
104. Lee, Y.S.; Chang, S.; Wu, S.C.; See, L.C.; Chang, S.H.; Yang, M.L.; Wu, W.C. The inner retinal structures of the eyes of children with a history of retinopathy of prematurity. *Eye* **2018**, *32*, 104–112. [[CrossRef](#)] [[PubMed](#)]
105. Schaeffer, S.; Iadecola, C. Revisiting the neurovascular unit. *Nat. Neurosci.* **2021**, *24*, 1198–1209. [[CrossRef](#)] [[PubMed](#)]

106. Hernández, C.; Dal Monte, M.; Simó, R.; Casini, G. Neuroprotection as a Therapeutic Target for Diabetic Retinopathy. *J. Diabetes Res.* **2016**, *2016*, 9508541. [[CrossRef](#)] [[PubMed](#)]
107. Creel, D.J. Electroretinograms. *Handb. Clin. Neurol.* **2019**, *160*, 481–493. [[CrossRef](#)]
108. Fulton, A.B.; Hansen, R.M.; Moskowitz, A.; Akula, J.D. The neurovascular retina in retinopathy of prematurity. *Prog. Retin. Eye Res.* **2009**, *28*, 452–482. [[CrossRef](#)]
109. Fulton, A.B.; Hansen, R.M.; Moskowitz, A. The cone electroretinogram in retinopathy of prematurity. *Investig. Ophthalmol. Vis. Sci.* **2008**, *49*, 814–819. [[CrossRef](#)]
110. Fulton, A.B.; Hansen, R.M.; Petersen, R.A.; Vanderveen, D.K. The rod photoreceptors in retinopathy of prematurity: An electroretinographic study. *Arch. Ophthalmol.* **2001**, *119*, 499–505. [[CrossRef](#)]
111. Akula, J.D.; Hansen, R.M.; Martinez-Perez, M.E.; Fulton, A.B. Rod photoreceptor function predicts blood vessel abnormality in retinopathy of prematurity. *Investig. Ophthalmol. Vis. Sci.* **2007**, *48*, 4351–4359. [[CrossRef](#)]
112. Liu, K.; Akula, J.D.; Falk, C.; Hansen, R.M.; Fulton, A.B. The retinal vasculature and function of the neural retina in a rat model of retinopathy of prematurity. *Investig. Ophthalmol. Vis. Sci.* **2006**, *47*, 2639–2647. [[CrossRef](#)]
113. Downie, L.E.; Hatzopoulos, K.M.; Pianta, M.J.; Vingrys, A.J.; Wilkinson-Berka, J.L.; Kalloniatis, M.; Fletcher, E.L. Angiotensin type-1 receptor inhibition is neuroprotective to amacrine cells in a rat model of retinopathy of prematurity. *J. Comp. Neurol.* **2010**, *518*, 41–63. [[CrossRef](#)] [[PubMed](#)]
114. Fulton, A.B.; Reynaud, X.; Hansen, R.M.; Lemere, C.A.; Parker, C.; Williams, T.P. Rod photoreceptors in infant rats with a history of oxygen exposure. *Investig. Ophthalmol. Vis. Sci.* **1999**, *40*, 168–174.
115. Downie, L.E.; Pianta, M.J.; Vingrys, A.J.; Wilkinson-Berka, J.L.; Fletcher, E.L. Neuronal and glial cell changes are determined by retinal vascularization in retinopathy of prematurity. *J. Comp. Neurol.* **2007**, *504*, 404–417. [[CrossRef](#)] [[PubMed](#)]
116. Rivera, J.C.; Holm, M.; Austeng, D.; Morken, T.S.; Zhou, T.E.; Beaudry-Richard, A.; Sierra, E.M.; Dammann, O.; Chemtob, S. Retinopathy of prematurity: Inflammation, choroidal degeneration, and novel promising therapeutic strategies. *J. Neuroinflammation* **2017**, *14*, 165. [[CrossRef](#)]
117. Barnaby, A.M.; Hansen, R.M.; Moskowitz, A.; Fulton, A.B. Development of scotopic visual thresholds in retinopathy of prematurity. *Investig. Ophthalmol. Vis. Sci.* **2007**, *48*, 4854–4860. [[CrossRef](#)]
118. Perkins, G.A.; Ellisman, M.H.; Fox, D.A. Three-dimensional analysis of mouse rod and cone mitochondrial cristae architecture: Bioenergetic and functional implications. *Mol. Vis.* **2003**, *9*, 60–73.
119. Altschwager, P.; Moskowitz, A.; Fulton, A.B.; Hansen, R.M. Multifocal ERG Responses in Subjects with a History of Preterm Birth. *Investig. Ophthalmol. Vis. Sci.* **2017**, *58*, 2603–2608. [[CrossRef](#)]
120. Hammer, D.X.; Iftimia, N.V.; Ferguson, R.D.; Bigelow, C.E.; Ustun, T.E.; Barnaby, A.M.; Fulton, A.B. Foveal fine structure in retinopathy of prematurity: An adaptive optics Fourier domain optical coherence tomography study. *Investig. Ophthalmol. Vis. Sci.* **2008**, *49*, 2061–2070. [[CrossRef](#)]
121. Akerblom, H.; Larsson, E.; Eriksson, U.; Holmström, G. Central macular thickness is correlated with gestational age at birth in prematurely born children. *Br. J. Ophthalmol.* **2011**, *95*, 799–803. [[CrossRef](#)]
122. Jabroun, M.N.; AlWattar, B.K.; Fulton, A.B. Optical Coherence Tomography Angiography in Prematurity. *Semin. Ophthalmol.* **2021**, *36*, 264–269. [[CrossRef](#)]
123. Gursoy, H.; Bilgec, M.D.; Erol, N.; Basmak, H.; Colak, E. The macular findings on spectral-domain optical coherence tomography in premature infants with or without retinopathy of prematurity. *Int. Ophthalmol.* **2016**, *36*, 591–600. [[CrossRef](#)] [[PubMed](#)]
124. Wang, J.; Spencer, R.; Leffler, J.N.; Birch, E.E. Critical period for foveal fine structure in children with regressed retinopathy of prematurity. *Retina* **2012**, *32*, 330–339. [[CrossRef](#)] [[PubMed](#)]
125. Yanni, S.E.; Wang, J.; Chan, M.; Carroll, J.; Farsiu, S.; Leffler, J.N.; Spencer, R.; Birch, E.E. Foveal avascular zone and foveal pit formation after preterm birth. *Br. J. Ophthalmol.* **2012**, *96*, 961–966. [[CrossRef](#)] [[PubMed](#)]
126. Miki, A.; Honda, S.; Inoue, Y.; Yamada, Y.; Nakamura, M. Foveal Depression and Related Factors in Patients with a History of Retinopathy of Prematurity. *Ophthalmologica* **2018**, *240*, 106–110. [[CrossRef](#)]
127. Balasubramanian, S.; Beckmann, J.; Mehta, H.; Sadda, S.R.; Chanwimol, K.; Nassisi, M.; Tsui, I.; Marlow, N.; Jain, S. Relationship between Retinal Thickness Profiles and Visual Outcomes in Young Adults Born Extremely Preterm: The EPICure@19 Study. *Ophthalmol.* **2019**, *126*, 107–112. [[CrossRef](#)]
128. Wu, W.C.; Lin, R.I.; Shih, C.P.; Wang, N.K.; Chen, Y.P.; Chao, A.N.; Chen, K.J.; Chen, T.L.; Hwang, Y.S.; Lai, C.C.; et al. Visual acuity, optical components, and macular abnormalities in patients with a history of retinopathy of prematurity. *Ophthalmology* **2012**, *119*, 1907–1916. [[CrossRef](#)]
129. Kergoat, H.; Hérard, M.E.; Lemay, M. RGC sensitivity to mild systemic hypoxia. *Investig. Ophthalmol. Vis. Sci.* **2006**, *47*, 5423–5427. [[CrossRef](#)]
130. Yang, C.; Lafleur, J.; Mwaikambo, B.R.; Zhu, T.; Gagnon, C.; Chemtob, S.; Di Polo, A.; Hardy, P. The role of lysophosphatidic acid receptor (LPA1) in the oxygen-induced retinal ganglion cell degeneration. *Investig. Ophthalmol. Vis. Sci.* **2009**, *50*, 1290–1298. [[CrossRef](#)]
131. Locri, F.; Cammalleri, M.; Dal Monte, M.; Rusciano, D.; Bagnoli, P. Protective Efficacy of a Dietary Supplement Based on Forskolin, Homotaurine, Spearmint Extract, and Group B Vitamins in a Mouse Model of Optic Nerve Injury. *Nutrients* **2019**, *11*, 2931. [[CrossRef](#)]

132. Amato, R.; Rossino, M.G.; Cammalleri, M.; Locri, F.; Pucci, L.; Dal Monte, M.; Casini, G. Lisosan G Protects the Retina from Neurovascular Damage in Experimental Diabetic Retinopathy. *Nutrients* **2018**, *10*, 1932. [[CrossRef](#)]
133. Dal Monte, M.; Cammalleri, M.; Locri, F.; Amato, R.; Marsili, S.; Rusciano, D.; Bagnoli, P. Fatty Acids Dietary Supplements Exert Anti-Inflammatory Action and Limit Ganglion Cell Degeneration in the Retina of the EAE Mouse Model of Multiple Sclerosis. *Nutrients* **2018**, *10*, 325. [[CrossRef](#)]
134. Locri, F.; Cammalleri, M.; Pini, A.; Dal Monte, M.; Rusciano, D.; Bagnoli, P. Further Evidence on Efficacy of Diet Supplementation with Fatty Acids in Ocular Pathologies: Insights from the EAE Model of Optic Neuritis. *Nutrients* **2018**, *10*, 1447. [[CrossRef](#)] [[PubMed](#)]
135. Tsang, J.K.W.; Wolf, S.A.; Pompoes, I.M.; Jousseaume, A.M.; Lam, W.C.; Yang, D.; Lo, A.C.Y. Potential Effects of Nutraceuticals in Retinopathy of Prematurity. *Life* **2021**, *11*, 79. [[CrossRef](#)] [[PubMed](#)]
136. Sood, B.G.; Madan, A.; Saha, S.; Schendel, D.; Thorsen, P.; Skogstrand, K.; Hougaard, D.; Shankaran, S.; Carlo, W. Perinatal systemic inflammatory response syndrome and retinopathy of prematurity. *Pediatr. Res.* **2010**, *67*, 394–400. [[CrossRef](#)] [[PubMed](#)]
137. Hartnett, M.E. Vascular endothelial growth factor antagonist therapy for retinopathy of prematurity. *Clin. Perinatol.* **2014**, *41*, 925–943. [[CrossRef](#)] [[PubMed](#)]
138. Tariq, Y.M.; Pai, A.; Li, H.; Afsari, S.; Gole, G.A.; Burlutsky, G.; Mitchell, P. Association of birth parameters with OCT measured macular and retinal nerve fiber layer thickness. *Investig. Ophthalmol. Vis. Sci.* **2011**, *52*, 1709–1715. [[CrossRef](#)]
139. Wang, J.; Spencer, R.; Leffler, J.N.; Birch, E.E. Characteristics of peripapillary retinal nerve fiber layer in preterm children. *Am. J. Ophthalmol.* **2012**, *153*, 850–855.e1. [[CrossRef](#)]
140. Fieß, A.; Christian, L.; Janz, J.; Kölb-Keerl, R.; Knuf, M.; Kirchhof, B.; Muether, P.S.; Bauer, J. Functional analysis and associated factors of the peripapillary retinal nerve fibre layer in former preterm and full-term infants. *Br. J. Ophthalmol.* **2017**, *101*, 1405–1411. [[CrossRef](#)]
141. Park, K.A.; Oh, S.Y. Retinal nerve fiber layer thickness in prematurity is correlated with stage of retinopathy of prematurity. *Eye* **2015**, *29*, 1594–1602. [[CrossRef](#)]
142. Reichenbach, A.; Bringmann, A. Glia of the human retina. *Glia* **2020**, *68*, 768–796. [[CrossRef](#)]
143. Reichenbach, A.; Bringmann, A. New functions of Müller cells. *Glia* **2013**, *61*, 651–678. [[CrossRef](#)] [[PubMed](#)]
144. Tao, C.; Zhang, X. Development of astrocytes in the vertebrate eye. *Dev. Dyn.* **2014**, *243*, 1501–1510. [[CrossRef](#)] [[PubMed](#)]
145. Coorey, N.J.; Shen, W.; Chung, S.H.; Zhu, L.; Gillies, M.C. The role of glia in retinal vascular disease. *Clin. Exp. Optom.* **2012**, *95*, 266–281. [[CrossRef](#)]
146. Lewis, G.P.; Fisher, S.K. Up-regulation of glial fibrillary acidic protein in response to retinal injury: Its potential role in glial remodeling and a comparison to vimentin expression. *Int. Rev. Cytol.* **2003**, *230*, 263–290. [[CrossRef](#)] [[PubMed](#)]
147. Maharaj, A.S.; Saint-Geniez, M.; Maldonado, A.E.; D’Amore, P.A. Vascular endothelial growth factor localization in the adult. *Am. J. Pathol.* **2006**, *168*, 639–648. [[CrossRef](#)]
148. Nakazawa, T.; Matsubara, A.; Noda, K.; Hisatomi, T.; She, H.; Skondra, D.; Miyahara, S.; Sobrin, L.; Thomas, K.L.; Chen, D.F.; et al. Characterization of cytokine responses to retinal detachment in rats. *Mol. Vis.* **2006**, *12*, 867–878.
149. Harada, T.; Harada, C.; Kohsaka, S.; Wada, E.; Yoshida, K.; Ohno, S.; Mamada, H.; Tanaka, K.; Parada, L.F.; Wada, K. Microglia-Müller glia cell interactions control neurotrophic factor production during light-induced retinal degeneration. *J. Neurosci.* **2002**, *22*, 9228–9236. [[CrossRef](#)]
150. Jakobiec, F.A.; Thanos, A.; Stagner, A.M.; Grossniklaus, H.E.; Proia, A.D. So-called massive retinal gliosis: A critical review and reappraisal. *Surv. Ophthalmol.* **2016**, *61*, 339–356. [[CrossRef](#)]
151. Houston, S.K.; Bourne, T.D.; Lopes, M.B.; Ghazi, N.G. Bilateral massive retinal gliosis associated with retinopathy of prematurity. *Arch. Pathol. Lab. Med.* **2009**, *133*, 1242–1245. [[CrossRef](#)]
152. Yanoff, M.; Zimmerman, L.E.; Davis, R.L. Massive gliosis of the retina. *Int. Ophthalmol. Clin.* **1971**, *11*, 211–229.
153. Huang, Z.; Ng, T.K.; Chen, W.; Sun, X.; Huang, D.; Zheng, D.; Yi, J.; Xu, Y.; Zhuang, X.; Chen, S. Nattokinase Attenuates Retinal Neovascularization Via Modulation of Nrf2/HO-1 and Glial Activation. *Investig. Ophthalmol. Vis. Sci.* **2021**, *62*, 25. [[CrossRef](#)] [[PubMed](#)]
154. Thounaojam, M.C.; Jadeja, R.N.; Rajpurohit, S.; Gutsaeva, D.R.; Stansfield, B.K.; Martin, P.M.; Bartoli, M. Ursodeoxycholic Acid Halts Pathological Neovascularization in a Mouse Model of Oxygen-Induced Retinopathy. *J. Clin. Med.* **2020**, *9*, 1921. [[CrossRef](#)] [[PubMed](#)]
155. Fu, Z.; Nian, S.; Li, S.Y.; Wong, D.; Chung, S.K.; Lo, A.C. Deficiency of aldose reductase attenuates inner retinal neuronal changes in a mouse model of retinopathy of prematurity. *Graefes Arch. Clin. Exp. Ophthalmol.* **2015**, *253*, 1503–1513. [[CrossRef](#)] [[PubMed](#)]

Article

HIF-1-Dependent Induction of $\beta 3$ Adrenoceptor: Evidence from the Mouse Retina

Rosario Amato ^{1,†} , Francesco Pisani ^{2,†} , Emiliano Laudadio ^{3,†} , Maurizio Cammalleri ¹ , Martina Lucchesi ¹,
Silvia Marracci ¹ , Luca Filippi ⁴ , Roberta Galeazzi ⁵ , Maria Svelto ^{2,6,7}, Massimo Dal Monte ^{1,*} 
and Paola Bagnoli ^{1,‡} 

- ¹ Department of Biology, University of Pisa, 56127 Pisa, Italy; rosario.amato@biologia.unipi.it (R.A.); maurizio.cammalleri@unipi.it (M.C.); martina.lucchesi@student.unisi.it (M.L.); silvia.marracci@unipi.it (S.M.); paola.bagnoli@unipi.it (P.B.)
- ² Department of Biosciences, Biotechnologies and Biopharmaceutics, University of Bari Aldo Moro, 70125 Bari, Italy; francesco.pisani@uniba.it (F.P.); maria.svelto@uniba.it (M.S.)
- ³ Department of Materials, Environmental Sciences and Urban Planning, Polytechnic University of Marche, 60131 Ancona, Italy; e.laudadio@staff.univpm.it
- ⁴ Department of Clinical and Experimental Medicine, Division of Neonatology and NICU, University of Pisa, 56100 Pisa, Italy; luca.filippi@unipi.it
- ⁵ Department of Life and Environmental Sciences, Polytechnic University of Marche, 60131 Ancona, Italy; r.galeazzi@staff.univpm.it
- ⁶ Institute of Biomembranes and Bioenergetics, National Research Council, 70126 Bari, Italy
- ⁷ National Institute of Biostructures and Biosystems (INBB), 00136 Rome, Italy
- * Correspondence: massimo.dalmonete@unipi.it; Tel.: +39-050-2211426
- † These young authors equally contributed to this work.
- ‡ These senior authors contributed equally to this work.



Citation: Amato, R.; Pisani, F.; Laudadio, E.; Cammalleri, M.; Lucchesi, M.; Marracci, S.; Filippi, L.; Galeazzi, R.; Svelto, M.; Dal Monte, M.; et al. HIF-1-Dependent Induction of $\beta 3$ Adrenoceptor: Evidence from the Mouse Retina. *Cells* **2022**, *11*, 1271. <https://doi.org/10.3390/cells11081271>

Academic Editor: George Simos

Received: 23 March 2022

Accepted: 7 April 2022

Published: 8 April 2022

Publisher's Note: MDPI stays neutral with regard to jurisdictional claims in published maps and institutional affiliations.



Copyright: © 2022 by the authors. Licensee MDPI, Basel, Switzerland. This article is an open access article distributed under the terms and conditions of the Creative Commons Attribution (CC BY) license (<https://creativecommons.org/licenses/by/4.0/>).

Abstract: A major player in the homeostatic response to hypoxia is the hypoxia-inducible factor (HIF)-1 that transactivates a number of genes involved in neovessel proliferation in response to low oxygen tension. In the retina, hypoxia overstimulates β -adrenoceptors (β -ARs) which play a key role in the formation of pathogenic blood vessels. Among β -ARs, $\beta 3$ -AR expression is increased in proliferating vessels in concomitance with increased levels of HIF-1 α and vascular endothelial growth factor (VEGF). Whether, similarly to VEGF, hypoxia-induced $\beta 3$ -AR upregulation is driven by HIF-1 is still unknown. We used the mouse model of oxygen-induced retinopathy (OIR), an acknowledged model of retinal angiogenesis, to verify the hypothesis of $\beta 3$ -AR transcriptional regulation by HIF-1. Investigation of $\beta 3$ -AR regulation over OIR progression revealed that the expression profile of $\beta 3$ -AR depends on oxygen tension, similar to VEGF. The additional evidence that HIF-1 α stabilization decouples $\beta 3$ -AR expression from oxygen levels further indicates that HIF-1 regulates the expression of the $\beta 3$ -AR gene in the retina. Bioinformatics predicted the presence of six HIF-1 binding sites (HBS #1-6) upstream and inside the mouse $\beta 3$ -AR gene. Among these, HBS #1 has been identified as the most suitable HBS for HIF-1 binding. Chromatin immunoprecipitation-qPCR demonstrated an effective binding of HIF-1 to HBS #1 indicating the existence of a physical interaction between HIF-1 and the $\beta 3$ -AR gene. The additional finding that $\beta 3$ -AR gene expression is concomitantly activated indicates the possibility that HIF-1 transactivates the $\beta 3$ -AR gene. Our results are indicative of $\beta 3$ -AR involvement in HIF-1-mediated response to hypoxia.

Keywords: oxygen-induced retinopathy; HIF-1 binding site; computational analysis; CHIP-qPCR; gene expression

1. Introduction

Oxygen sensors play a primary role in living organisms as they activate homeostatic responses when oxygen levels decrease. Oxygen availability is sensed by oxygen-sensitive enzymes, which, in turn, regulate the activity of transcription factors. Among these, the

first to be identified was hypoxia-inducible factor (HIF)-1 [1]. HIF-1 is a dimer formed by a labile α and a stable β subunits. In the presence of oxygen, HIF-1 α is hydroxylated by oxygen-sensitive prolyl hydroxylases, ubiquitinated by the von Hippel–Lindau protein and therefore degraded by the proteasome. When oxygen levels drop, HIF-1 α escapes from hydroxylation and stabilizes, migrates into the nucleus, dimerizes with HIF-1 β and binds to the hypoxia-responsive elements (HREs). HREs are composite regulatory elements containing conserved HIF-binding sites (HBSs) and highly variable flanking sequences [2]. HIF-1 promotes the transactivation of hundreds of genes involved in metabolic adaptation to reduced oxygen availability [3]. One of the main HIF-1 target genes is that of VEGF, which plays a major role in triggering angiogenesis as metabolic adaptation to hypoxia consisting in the local formation of new blood vessels from pre-existing ones [4]. Oxygen-dependent angiogenesis is particularly relevant in tissues characterized by high rate of oxygen consumption, as the case of the retina. In effect, hypoxia-driven angiogenesis is crucial for retinal vascularization during development but is also implied in the pathogenesis of several retinal diseases such as proliferative retinopathies [5]. The hypoxia-driven angiogenesis is influenced by several side mechanisms, which could enhance or inhibit the activity of the HIF-1/VEGF axis.

At the retinal level, β -adrenoceptors (β -ARs) have been established to cover a relevant role in the regulation of hypoxia-driven angiogenesis [6]. In particular, hypoxia determines the surge of norepinephrine which drives the overstimulation of β -ARs [7]. Among β -ARs, particular attention has been recently directed to β 3-AR, the third β -AR subtype to be discovered that was cloned and characterized in humans at the end of the eighties [8]. β 3-AR's role in response to hypoxia has been determined in several tissues supporting the hypothesis that reduced oxygen tension may trigger β 3-AR upregulation in hypoxic conditions. In particular, β 3-AR is highly expressed in embryo tissues, which are physiologically hypoxic [9], while showing a restricted expression in adult tissues [10] in which β 3-AR levels increase in conditions associated with hypoperfusion, such as cancer or heart failure [11–13]. In this respect, there is evidence that hypoxia increases β 3-AR expression in endothelial cells lining proliferating vessels, as for instance in the human heart or in the mouse retina. In heart failure in particular, β 3-AR is upregulated in the hypoxic endothelium of coronary arteries where it is involved in vasodilation and re-vascularization through the nitric oxide pathway [14]. In the hypoxic retina, β 3-AR is localized to proliferating vessels where its expression is drastically upregulated when oxygen tension decreases [15]. Assuming that β 3-AR expression is regulated by oxygen tension, then the possibility exists that β 3-AR upregulation in response to hypoxia involves HIF-1-mediated transcriptional mechanisms as it occurs for additional hypoxia-inducible proteins.

In the present study, the hypothesis that HIF-1 may act as a transcription factor involved in the regulation of β 3-AR gene expression was verified taking advantage of the mouse model of oxygen-induced retinopathy (OIR), a model of retinal angiogenesis that is widely used as a paradigm to study angiogenesis in general [16]. This model is characterized by two phases: phase I or a “vaso-obliterative” phase coinciding with hyperoxia and phase II or a “vaso-proliferative” phase coinciding with hypoxia [17]. Therefore, thanks to the alternation of a period of hyperoxia and a period of hypoxia, this model is paramount to study the dependence of gene expression from oxygen levels and HIF-1 activity. Here, we first investigated whether β 3-AR expression varies in concomitance with changing oxygen levels at different stages of OIR. Whether preventing hyperoxia-induced degradation of HIF-1 α may influence β 3-AR expression was also investigated. In order to verify the possibility of HIF-1 interaction with the β 3-AR gene, a theoretical approach based on *in silico* predictive analysis was then performed to search for putative HBSs. As they may be located in genomic regions outside the promoter, as part of transcriptional enhancers [18–20], the DNA sequence upstream and inside the β 3-AR gene was analyzed. In addition, docking analysis and molecular dynamics (MD) simulation were consequently used for reconstructing the complete structure of mouse HIF-1 and to evaluate its feasibility to tightly bind to specific nucleotide sequences as suggested by the prediction analysis.

To demonstrate the direct physical interaction between HIF-1 and the potential HBSs, chromatin immunoprecipitation (ChIP)-qPCR experiments were then performed under hypoxic conditions and timely-dependent β 3-AR mRNA levels were evaluated to check the possibility that β 3-AR expression may be triggered by HIF-1 interaction with HBS.

2. Materials and Methods

2.1. Animals

C57BL/6J mice were purchased from Charles River Laboratories, Italia (Calco, Italy) and mated in our breeding colonies. Experimental animals were housed in a regulated environment (23 ± 1 °C, $50 \pm 5\%$ humidity) with a 12 h light/dark schedule. Overall, 162 mice (6 for each experimental group), either male or female, were used. Of them, 120 mice were used to compare β 3-AR mRNA or protein levels between control (48) and OIR mice (72), without (36 mice) or with (36 mice) dimethylolallylglycine (DMOG) administration; 42 mice, including 12 controls and 30 OIR, were used in ChIP-qPCR experiments and β 3-AR mRNA determination. Animal studies were carried out in compliance with the recommendations in the Guide for the Care and Use of Laboratory Animals of the National Institutes of Health, the ARVO Statement for the Use of Animals in Ophthalmic and Vision Research, the Italian guidelines for animal care (DL 6/14) and the European Communities Council Directive (2010/63/UE). The experimental procedures were approved by the Ethical Committee in Animal Experiments of the University of Pisa (permit number 656/2018-PR, 3 September 2018). All efforts were made to reduce the animal suffering and the animal number based on the rules of replacement, refinement and reduction (the 3Rs).

2.2. OIR Model and DMOG Treatment

In the mouse model of OIR [17], litters of mouse pups with their nursing mothers were exposed to high oxygen concentration ($75 \pm 2\%$; hyperoxia) from postnatal day (PD) 7 to PD12 before returning to room air from PD12 to PD17 (normoxia sensed as relative hypoxia). During the exposure to hyperoxia, 36 mice were treated with DMOG, an inhibitor of prolyl hydroxylases that stabilizes HIF-1 α also in the presence of oxygen by preventing its hydroxylation and the consequent degradation [21]. DMOG (Cayman Chemical, East Ellsworth, MI, USA) was dissolved in dimethyl sulfoxide, diluted in phosphate-buffered saline (PBS) at 1:100 and daily intraperitoneally injected between PD7 and PD12 at 200 mg/kg in line with previous studies of the mouse retina [22,23].

2.3. Western Blotting

After mice euthanasia, eyes were enucleated, and retinas were removed from the eyecups, snap frozen in liquid nitrogen, and stored at -80 °C. Six independent samples, each containing 2 retinas from 2 different mice, were used for each experimental condition. Samples were lysed with RIPA lysis buffer (50 mmol/L Tris, pH 7.4 containing 150 mmol/L NaCl, 1% Triton X-100, 1% sodium deoxycholate, 0.1% SDS, 5 mmol/L EDTA) containing proteinase and phosphatase inhibitor cocktails (Roche Applied Science, Indianapolis, IN, USA). Protein concentration was measured using the Micro BCA Protein Assay (Thermo Fisher Scientific, Waltham, MA, USA). For each sample, 30 μ g of proteins were subjected to SDS-PAGE (4–20%; Bio-Rad Laboratories, Hercules, CA, USA). Gels were transblotted onto a nitrocellulose membrane (Bio-Rad Laboratories). Blots were blocked in 3% skim milk for 1 h at room temperature and then incubated overnight at 4 °C with the following primary antibodies: rabbit polyclonal against HIF-1 α (ab2185; Abcam, Cambridge, UK; 1:500 dilution), rabbit polyclonal against VEGF (ab9570; Abcam; 1:1000 dilution), mouse monoclonal against β 3-AR (sc-515763; Santa Cruz Biotechnologies, Santa Cruz, CA, USA; 1:200 dilution), mouse monoclonal against β -actin (A2228; Sigma Aldrich, St. Louis, MO, USA; 1:2500 dilution). After washing, membranes were incubated for 2 h at room temperature with appropriate HRP-conjugated anti-mouse or anti-rabbit secondary antibodies (1:5000 dilution). Blots were developed using Clarity Western enhanced chemiluminescence substrate (Bio-Rad Laboratories) and images were acquired using ChemiDoc XRS+

(Bio-Rad Laboratories). The quantification of Western blot bands has been performed with the automated software Image Lab 6.0 (Bio-Rad Laboratories) by considering the integrated optical density (OD) that derives from each pixel with given xy coordinates within the band area. The OD for each target protein was normalized to that of β -actin used as loading control.

2.4. Quantitative Real-Time PCR

Six independent samples for each experimental condition, each containing 2 retinas from 2 different mice, were used. Total RNA was extracted (RNeasy Mini Kit; Qiagen, Valencia, CA, USA), purified, resuspended in RNase-free water and quantified. First-strand cDNA was produced from 1 μ g of total RNA (QuantiTect Reverse Transcription Kit; Qiagen). The SsoAdvanced Universal SYBR Green Supermix (Bio-Rad Laboratories) was used to perform real-time PCR amplifications on a CFX Connect Real-Time PCR detection system equipped with the software CFX manager (Bio-Rad Laboratories). Forward and reverse primers were chosen to hybridize to unique regions of the appropriate gene sequence. Their sequences are as follows: β 3-AR forward, 5'-TCTCTGGCTTTGTGGTCGGA-3'; β 3-AR reverse, 5'-GTTGGTTATGGTCTGTAGTCTCG-3'; Rpl13a forward, 5'-CCAGGTATACAAGCAGGTGTGCTC-3'; Rpl13a reverse, 5'-CATCATTAGGCCATCCTGGAC-3'. Primer amplification efficiency was close to 100%. The target gene was run concurrently with Rpl13a, a stable housekeeping gene in the OIR model [24]. Samples were compared using the relative threshold cycle (Ct method) and expressed as fold increase. All reactions were run in triplicate.

2.5. Prediction of HBSs

Mouse β 3-AR gene and its mRNA sequences were obtained from the NCBI Reference Sequence database (gene ID: 11556). The transcription start site (TSS) was mapped by DNA/RNA alignment using Clustal Omega online tool (<https://www.ebi.ac.uk/Tools/msa/clustalo/>; accessed on 12 January 2020) between genomic DNA and the longest β 3-AR mRNA (misc_RNA (XR_004934751.1)) at the position 27230845 of the chromosome 8 (strand-). The DNA sequence of mouse chromosome 8 (UCSC Genome Browser Mouse (GRCm38/mm10)) was analyzed from the absolute position 27237610 to 27226612 to search for potential HBSs using the PROMO software online tool (http://alggen.lsi.upc.es/cgi-bin/promo_v3/promo/promoinit.cgi?dirDB=TF_8.3; accessed on 12 January 2020). To search for the core sequence ACGTG, which is highly conserved inside HBSs [25–27], the Fuzzy Search DNA on-line tool (https://www.genscript.com/sms2/fuzzy_search_dna.html; accessed on 12 January 2020) was used. A comparable evaluation was also performed for the human β 3-AR gene (gene ID: 155) by analyzing the human chromosome 8 sequence (strand-) from the absolute position 37971666 to 37960995 (UCSC Genome Browser on Human (GRCh38/hg38)).

2.6. Computational Modeling of HIF-1 α

The complete structure of the mouse HIF-1 α was reconstructed starting from crystallographic data of protein fragments stored in both Uniprot (code Q61221) and Protein Data Bank (codes 4h6j) using Iterative Threading ASSEMBLY Refinement (I-TASSER) [28]. In addition, ModLoop [29] and GalaxyLoop [30] were used for loop modeling and refinement, respectively. DISULFIND online server [31] was used to predict the disulfide bonding state of cysteines and their disulfide connectivity's. The completely rebuilt HIF-1 α structure was opportunely stabilized creating a simulation box of 22.2 \times 18.02 \times 18.12 nm, and neutralizing the net charge of the protein with 205,981 TIP3P water molecules, 605 Na⁺ ions and 572 Cl⁻ ions to reach a salt concentration of 0.15 M. The protein was minimized with 10,000 cycles steepest descent followed by 5000 steps conjugate gradient thus obtaining a convergence of maximum force to energy threshold of 1000 kJ/mol nm². Then, HIF-1 α was gradually accommodated within the aqueous environment using 6 equilibration steps; the Verlet cutoff scheme was used for neighbor searching [32], combined with particle

mesh Ewald for electrostatics [33]. The cutoff for the Van der Waals forces calculation was settled to 1.2 nm with force smoothly switched to 0 (between 1.0 and 1.2 nm) generating the velocities at 310 K in constant temperature, constant volume (NVT) ensemble using a Maxwell distribution function with random seed (Berendsen thermostat; 2 simulation runs, 25 ps). Then, we shifted to constant temperature, constant pressure (NPT) ensemble maintaining the weak coupling also for pressure control (Berendsen barostat, isotropic conditions, 1 bar, time coupling 5 ps), maintained for 4 equilibration runs (50 ps). In the 200 ns production phase, we shifted to Nosé–Hoover [34] and Parrinello–Rhaman [35] algorithms for temperature control and pressure coupling, respectively; leapfrog algorithm and a time step of 0.002 ps were used. AMBER99-SB-ILDN force field as implemented in GROMACS 5.0.4 software package [36] was also used.

2.7. HIF-1/DNA Docking

HDOCK server for Protein/DNA hybrid docking (<http://hdock.phys.hust.edu.cn/>; accessed on 13 March 2020) was used to assess the configuration and the stability of HIF-1 with specific DNA sequences that were selected on the basis of the known minimum consensus sequences [37–41]. The corresponding HIF-1/DNA 3D structures were built up and minimized using AMBER18 software and AMBER force field [42,43].

2.8. HIF-1/DNA MD Simulation

The HIF-1/DNA models obtained from the docking approach underwent to 100 ns of MD simulation following the MD protocol described above for the HIF-1 α stabilization. Each HIF-1/DNA model included 2 monomers of the entire HIF-1 α protein (monomer-A and monomer-B) together with each of the 6 DNA segments containing predicted HBSs. Since the information about the sequence and the domains of HIF-1 β are scarce and uncertain to operate an efficient modeling of the full protein structure, the homodimeric association of HIF-1 α was considered instead of its heterodimeric form with HIF-1 β . The accuracy of this approach was confirmed by the observation that the coordinates of the heterodimeric HIF-1 α :HIF-1 β DNA binding domain, as provided by 4zpr pdb structure [44], are maintained with maximum accuracy in the homodimeric form. These coordinates were therefore used to create the DNA-binding site and the overall configuration of the dimeric interface. The simulation box for each system was 20.8 \times 20.8 \times 20.8 nm to contain the whole HIF-1 omodimer. Water molecules and ions were opportunely added to solvate the systems and to reach the physiological salt condition. Appropriate optimal salt concentration (267,174 TIP3P water molecules followed by 843 Na⁺ ions and 755 Cl⁻ ions, on average) was then added to each model to neutralize the net charges of proteins and DNA.

With the aim to identify specific bonds formed with the nucleotide sequences, the contacts between HIF-1 and DNA structures were investigated along 200 ns MD simulation using *gmx mindist* gromacs tool, while the analysis of the simulation trajectories was performed by means of the VMD [45] and CHIMERA software [46].

2.9. Chromatin Immunoprecipitation-Quantitative Real-Time PCR (ChIP-qPCR)

ChIP-qPCR was performed in 6 independent samples using the high-sensitivity ChIP kit (ab185913; Abcam) according to the instructions provided by the manufacturer. Six independent samples for each experimental condition, each containing 2 retinas from two different mice, were used. Samples were homogenized and crosslinked using 1% formaldehyde, quenching the reaction with 1.25 M glycine. After centrifugation, the pellet was homogenized with the Working Lysis Buffer and added with the ChIP buffer provided in the kit. Chromatin was then sheared into fragments of about 300 bp by sonication, and fragmentation was verified by agarose gel electrophoresis. Immunoprecipitation was performed using a ChIP-grade antibody against HIF-1 α (ab2185; Abcam; 1:500 dilution) or non-immune IgG as negative control. Immuno-complexes and small aliquots of lysate (for input controls) were treated with DNA Release Buffer and Proteinase K provided

in the kit to reverse crosslinking and to purify DNA. The purified DNA was used as input sample in qPCR using primers (forward 5'-ATGCCTCCTGTCTGTGTG-3'; reverse 5'-ACTCGCCTCTCAAACAGTCA-3') mapping the most probable HBS among the different HBSs as detected by PROMO software online tool (see above). The SsoAdvanced Universal SYBR Green Supermix (Bio-Rad Laboratories) and a CFX Connect Real-Time PCR detection system equipped with the software CFX manager (Bio-Rad Laboratories) were used. Fold enrichment was calculated through the Ct method by using a ratio of amplification efficiency of the ChIP sample over that of non-immune IgG (fold enrichment = $2^{(\text{IgG Ct} - \text{sample Ct})}$).

2.10. Statistics

The Shapiro-Wilk test was used to verify the normal distribution of the data. One-way analysis of variance (ANOVA) followed by Tukey's multiple comparison post-hoc test was used to evaluate statistical significance (Prism 8.0.2, GraphPad Software, Inc., San Diego, CA, USA). Differences with $p < 0.05$ were considered statistically significant. Data are plotted as means \pm SEM of the reported n values. A priori power analysis using the software G*Power 3.0.10 (www.gpower.hhu.de; accessed on 4 December 2019) was carried out to determine the minimum number of animals necessary to obtain a statistical power of at least 0.80, with $\alpha = 0.05$, when considering an expected large effect size.

3. Results

3.1. HIF-1-Regulated β 3-AR Expression

Retinal levels of HIF-1 α , VEGF and β 3-AR were determined at different time points of OIR (before the hyperoxic phase at PD7, during the hyperoxic phase at PD9, at the end of the hyperoxic phase at PD12 or at the end of the hypoxic phase at PD17). In order to assess whether oxygen may regulate β 3-AR levels through HIF-1, protein levels of HIF-1 α , VEGF and β 3-AR were also determined in OIR mice that received DMOG, a chemical widely used as a HIF-1 α stabilizer [21], administered daily during the hyperoxic phase (from PD7 to PD12; Figure 1A). Blots in Figure 1B are representative of the protein levels of HIF-1 α , VEGF and β 3-AR in the different experimental conditions. Densitometric analysis shown in Figure 1C-E demonstrates that proteins levels of HIF-1 α , VEGF and β 3-AR were downregulated during hyperoxia both at PD9 and PD12, while they became upregulated during hypoxia at PD17 compared with their relative levels as determined under normoxia. In respect to untreated mice, DMOG administration prevented downregulation of HIF-1 α , VEGF and β 3-AR in response to hyperoxia as well as their upregulation in response to hypoxia. The finding that the effects of hyperoxia or hypoxia on HIF-1 α and VEGF were abnegated after DMOG administration is in line with previous results [22,47,48]. The additional finding that HIF-1 α stabilization counteracts variations in protein levels of β 3-AR in response to changing oxygen levels supports the hypothesis that oxygen regulates β 3-AR expression through HIF-1. β 3-AR dependence on HIF-1 was also supported by the fact that protein levels of β 3-AR were found to mirror the levels of VEGF, a major oxygen-dependent HIF-1 transcript. Variations in β 3-AR proteins in response to changing oxygen tension were found to correlate with the corresponding variations in β 3-AR mRNA expression in OIR mice either untreated or treated with DMOG further supporting the possibility that β 3-AR is a HIF-1 target gene (Figure 1F).

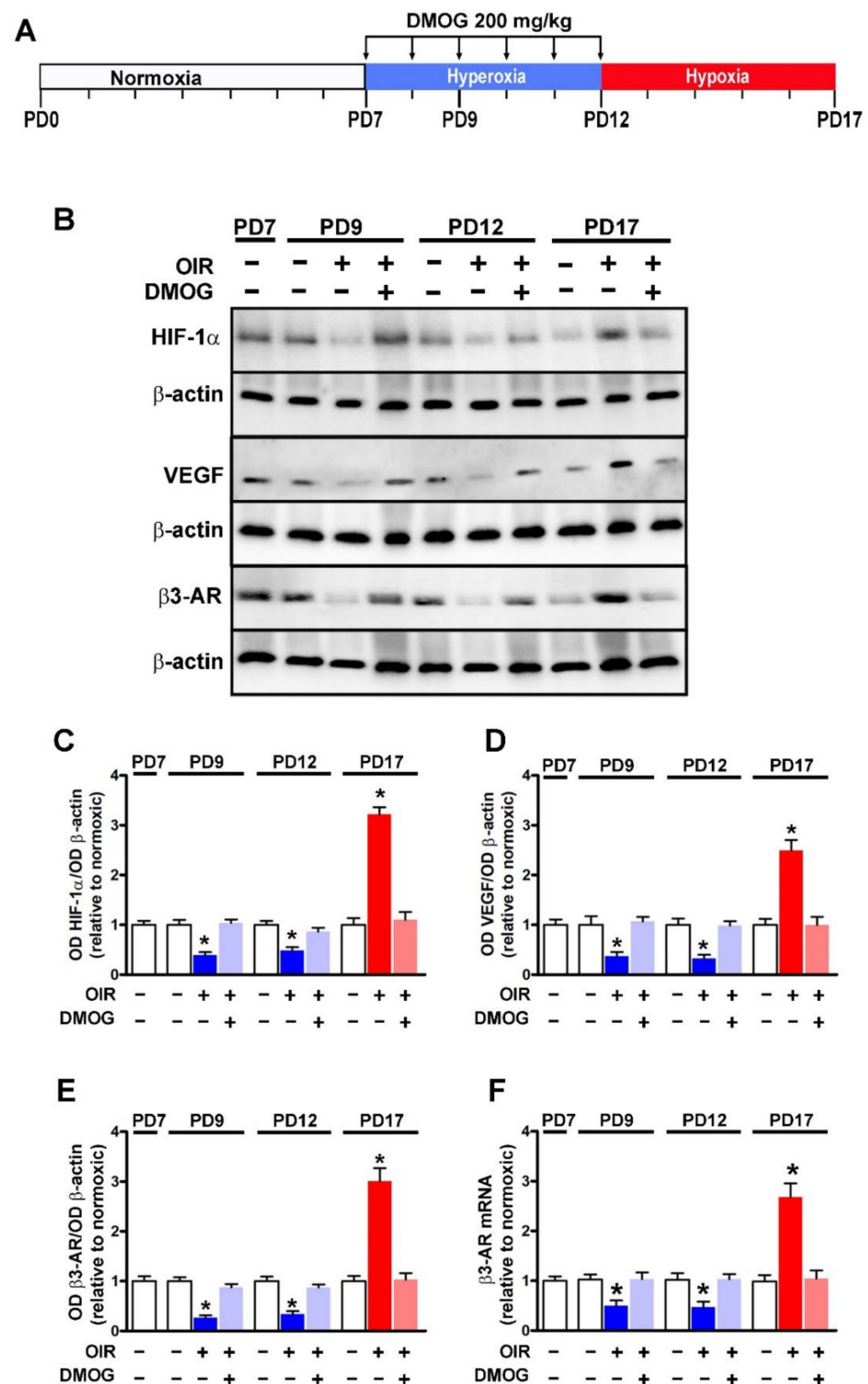


Figure 1. Effects of oxygen tension on retinal levels of HIF-1 α , VEGF and β 3-AR from PD7 to PD17. (A) Schematic diagram of the OIR model including DMOG administration daily from PD7 to PD12. (B) Representative blots showing protein levels of HIF-1 α , VEGF and β 3-AR as evaluated by Western blot in retinal extracts at different times from normoxic controls or OIR mice without or with DMOG administration. β -actin was used as the loading control. (C–E), Relative densitometric analyses of the protein levels of HIF-1 α , VEGF and β 3-AR. (F) Retinal mRNA levels of β 3-AR at different times from controls or OIR mice untreated or treated with DMOG. * $p < 0.05$ vs. normoxic controls. One-way ANOVA followed by Tukey’s multiple comparison post-hoc test. Each histogram represents the mean \pm SEM of data from 6 independent samples.

3.2. Potential HBSs as Revealed by DNA Prediction Analysis

The finding that β 3-AR expression may depend on HIF-1 levels prompted us to verify whether potential HBSs can be present in the region upstream and inside the mouse and the human β 3-AR gene (Figure 2). As reported by NCBI Reference Sequence Database and represented in Figure 2A, the mouse β 3-AR gene contains 5 exons (E1-E5) that may potentially express up to 6 different alternative mRNAs. Of them, 3 codify for the canonical β 3-AR protein (Figure 2A, green mRNAs) while the other 3 may be predicted to codify for an alternative β 3-AR protein with a different C-terminal sequence (Figure 2A, purple mRNAs). Following DNA/RNA alignment between the genomic DNA and the longest β 3-AR mRNA, the TSS was predicted to be localized at the absolute position 27230845 of the mouse chromosome 8. The TSS was taken as a reference for the localization of the potential HBSs. As HBSs can be localized at high distance with respect to the TSS [18] or even inside the transcriptional region [19,20], we searched for potential HBSs by analyzing the DNA sequence from the position -6765 upstream the TSS up to the position $+4234$ downstream the TSS using PROMO software [49,50] and searching for the minimal HBS consensus sequence ACGTG known to be strongly conserved at the HBS level [25–27] using the Fuzzy Search DNA tool. We found 6 different potential HBSs (Figure 2A, HBSs #1–6). HBSs #1, #4 and #5 contain the ACGTG core sequence and were directly predicted by PROMO, while HBSs #2, #3 and #6 contain ACGTG core sequence were not predicted by PROMO as potential HBSs but were identified by Fuzzy Search DNA tool. To complete this analysis, we evaluated the contribution of nucleotides additional to the ACGTG core sequence in all 6 putative HBSs by comparing their sequences with those previously characterized for a wide number of HIF-target genes [25,26,51]. We found that HBSs #1, #4 and #5 contain the G^{-2} and/or the C^{+5} nucleotides (red highlighted in Figure 2A) in respect to the A^0 ACGTG core sequence, two nucleotides demonstrated an ability to increase the probability that HIF-1 binds to the HBS [25]. These nucleotides are absent at level of HBSs #2, #3 and #6, which contain only the core sequence. For these reasons HBSs #1, #4 and #5 were predicted as high-probability HBSs and, among them, the HBS #1 was the only one identified into the DNA region upstream the TSS at -2186 , a position compatible with a classical transcriptional enhancer. As shown in Figure 2B, upstream and inside the human β 3-AR gene, 6 HBSs were also predicted. Of these, HBSs #3–6 are localized inside the β 3-AR gene, while HBSs #1 and #2 are localized upstream the putative TSS. In respect to the data reported for the mouse β 3-AR gene, human HBSs #1, #4, #5 and #6 show the G^{-2} and/or the C^{+5} nucleotides (highlighted in red in Figure 2B) in addition to the conserved core sequence. Beside containing the G^{-2} nucleotide, the human HBS #1 was predicted at -3545 , a position comparable to that of the mouse HBS #1.

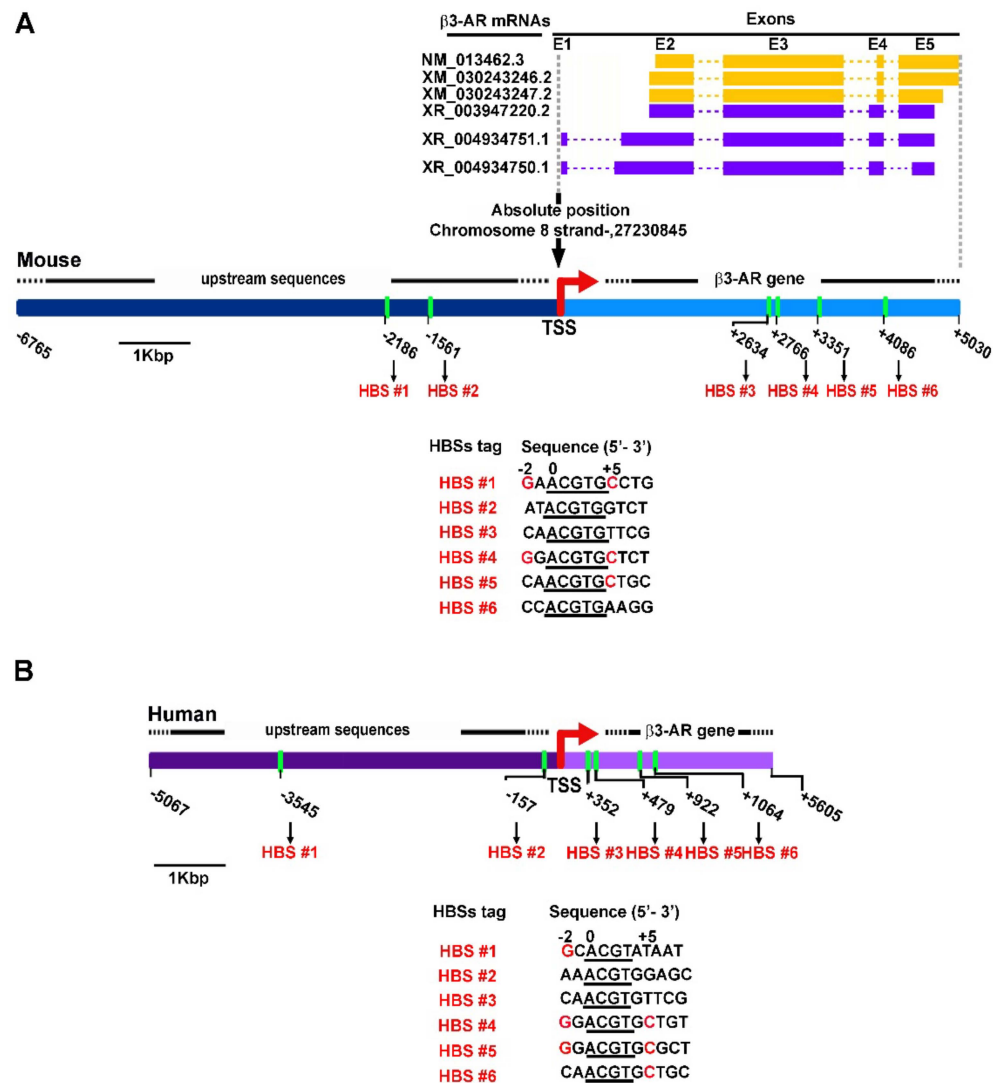


Figure 2. Schematic representation of mouse and human $\beta 3$ -AR genes including their upstream sequences. (A) In the mouse gene, 5 exons (E1–E5; solid boxes) and 4 introns (dashed lines) are depicted. They potentially express up to 6 different alternative mRNAs of which 3 codify for the canonical $\beta 3$ -AR protein (yellow mRNAs) while the other 3 for an alternative $\beta 3$ -AR protein with a different C-terminal sequence (purple mRNAs). The putative transcription-start site (TSS) is indicated by the red arrow. The positions of the 6 potential HBSs relative to the TSS are in green. All of them contain the minimal HBS consensus sequence (underlined sequence 5'-ACGTG-3'). (B) In the human gene, the positions of the 6 potential HBSs relative to the TSS are in green. All of them contain the minimal consensus sequence (underlined sequence 5'-ACGT-3'). The putative TSS is indicated by the red arrow. The highly conserved nucleotides G⁻² and/or C⁺⁵ in the mouse and human HBSs sequence are highlighted in red.

3.3. Stability of the HIF-1 α Protein Model

The stability of the rebuilt structure of HIF-1 α has been monitored using the root-mean-square (RMS) deviation analysis, which represents the average displacement of the atoms over the simulation time relative to a reference structure. This type of analysis allows us to observe when the trajectories of displaced atoms plateau and converge towards an equilibrium state. As shown in Figure 3A, the HIF-1 α protein model stabilizes after 100 ns and remains stable throughout 200 ns of MD simulation. To describe the structural mobility of HIF-1 α protein, the RMS fluctuation analysis has been performed. It consists in a measurement of the displacement of aminoacids relative to the starting structure. The

fluctuation degree of aminoacids plays a key role for specific biological function; for this reason the last 20 ns of MD simulation have been considered to define the RMS fluctuation profile. Figure 3B shows that different HIF-1 α regions, as evidenced by the corresponding colors in Figure 3C, display a different fluctuation trend confirming the presence of flexible domains in the HIF-1 α structure. Since the domains of HIF-1 α dimerization and binding with DNA (Crystal Structure of the Heterodimeric HIF-1 α :ARNT Complex with HRE DNA as determined by Protein Data Bank) are known to correspond to the first portion of the protein (i.e., the yellow domain in Figure 3C), HIF-1 in its dimeric form has been modeled using the coordinates of the heterodimeric HIF-1 α :HIF-1 β DNA binding domain as available from 4zpr pdb file [44]. Thereby, modeling of HIF-1 β has been avoided because of the scarce information in terms of its aminoacid sequence and crystallographic structure. To confirm the reliability of the obtained dimeric interface, a comparison between the present model and the 4zpr interface has allowed us to demonstrate a close superimposition of the helices in the DNA binding domain (Figure S1).

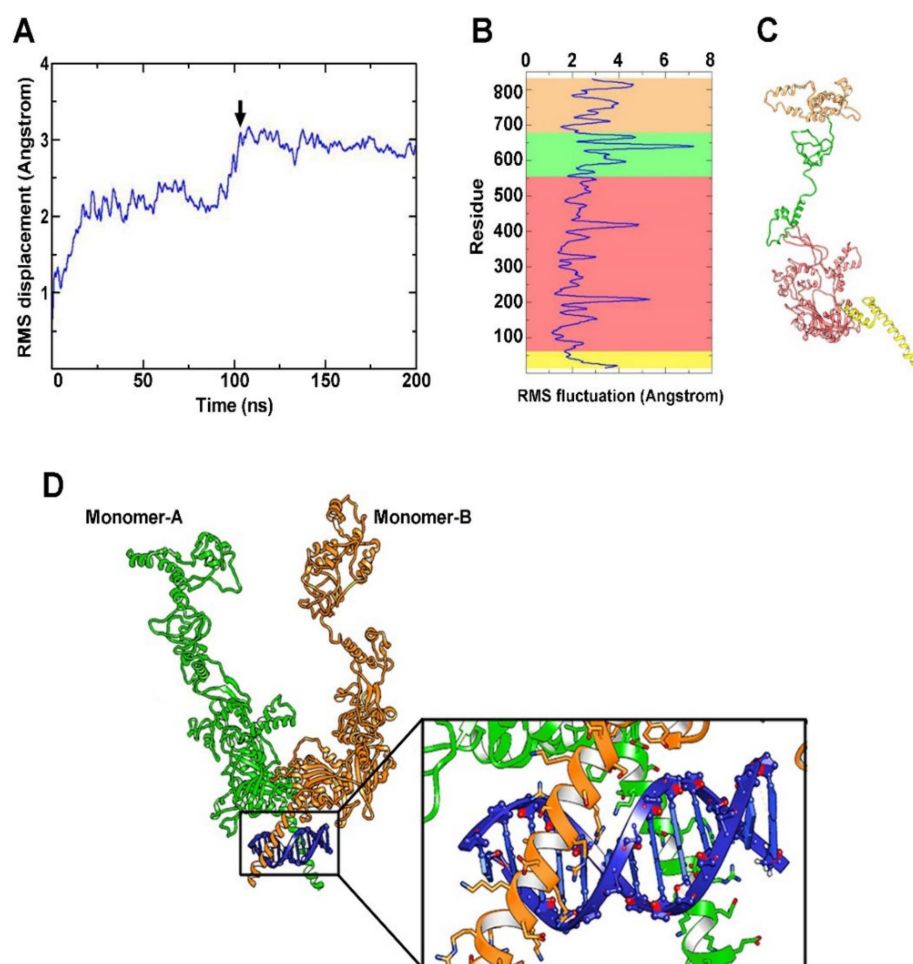


Figure 3. HIF-1 α modeling and HIF-1/DNA docking. (A) Root-mean-square (RMS) displacement of protein backbone (black arrow indicates the time at which the stabilization of the protein structure occurs). (B) RMS fluctuation of aminoacid displacement relative to the starting structure and the principal domains of the HIF-1 α protein, accordingly colored in (C). (D) HIF-1 α protein modeled in its dimeric form showing the correct interaction with the DNA fragment. The two monomers are reported in green and orange respectively, while the DNA fragment is highlighted in blue. The binding site generated by dimerization is better shown in the focus section.

After energy minimization, the final structure of HIF-1 in its dimeric form was recognized as the starting point for the subsequent investigation of affinity and specificity

between HIF-1 and the different HBSs. In the representative model of Figure 3D, the correct interaction between the DNA binding portion of the HIF-1 dimer and the DNA fragment is shown.

3.4. Simulation of HIF-1/DNA Interaction and Binding Stability

The analysis of HIF-1/DNA docking identified 6 possible DNA segments (models 1–6) corresponding to the 6 HBSs found in the mouse β 3-AR genes by computational analysis with additional flanking nucleotides upstream and downstream the HBS (model 1, GAACGTGCCTGGC, containing HBS #1; model 2, AACATACGTGGTCTT, containing HBS #2; model 3, AACCAACGTGTTTCGT, containing HBS #3; model 4, TGGACGTGCTCTGTG, containing HBS #4; model 5, TGGCCAAACGTGCTGCGGCAC, containing HBS #5; model 6, TCCCACGTGAAGG, containing HBS #6). DNA sequences and reconstructions of the models 1–6 are represented in Figure 4. The results are reported according to the docking score for each simulated model. On the basis of the specificity of binding, which involves interactions with the nitrogen-containing bases and not merely with the phosphate skeleton, 2 models have been selected. In particular, among the 6 simulated models, model 1 and model 3 are those that show the highest affinity and specificity for HIF-1 (-276.06 and -292.03 kJ/mol, respectively). For both, the highest scored models bind to the DNA binding domain for HIF-1. The other models, both for their docking score (-261.41 , -254.76 , -239.97 and -251.09 kJ/mol for model 2, model 4, model 5 and model 6, respectively) and for the nature of their interactions do not appear as suitable candidates for HIF-1 binding. The characteristics of the docking models together with their 3-D structure including DNA binding are summarize in Figure 4.

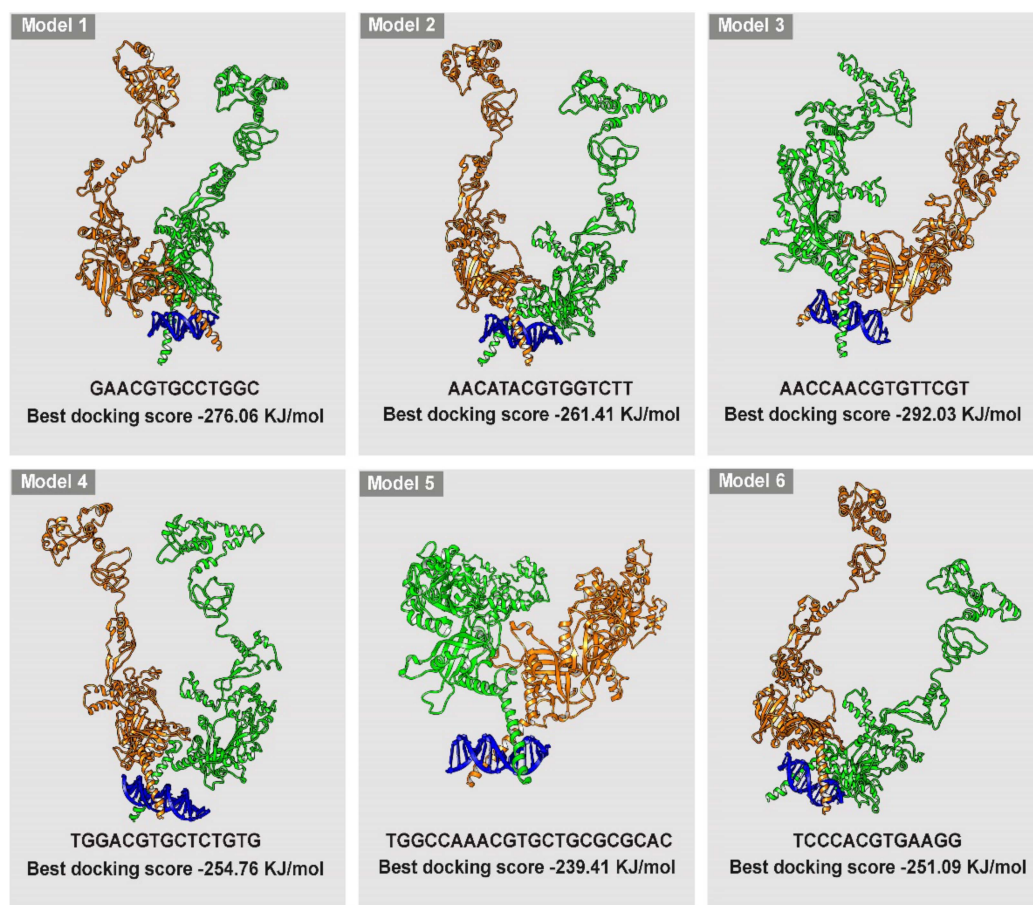


Figure 4. Graphical representation of the 6 HIF-1/DNA models displaying the 3D reconstruction of the HIF-1 docking to each of the nucleotide sequence, including HBS and flanking sequences, and their relative best docking score in kJ/mol.

In order to make a definitive assessment of the binding stability, the selected models underwent 100 ns of MD simulation. Direct interactions between HIF-1 protein and DNA have been extrapolated from MD trajectories, and the results were plotted (Figure 5). The effective amount of the contacts was verified by considering the number of atom pairs that fall within a distance of 0.6 nm from each other. This is the maximum distance required for effective interactions between aminoacids and nucleotides. As shown in Figure 5, model 1 shows a high number of contacts, with an average value of 578 contacts in the last 10 ns. A similar trend was observed for model 3, with 584 contacts in the last 10 ns. In models 4 and 2, the average number of contacts in the last 10 ns are 504 and 476, respectively. Regarding models 5 and 6, the number of contacts in the last 10 ns is 436 and 428, respectively, indicating that their overall structures do not remain stable during MD simulation.

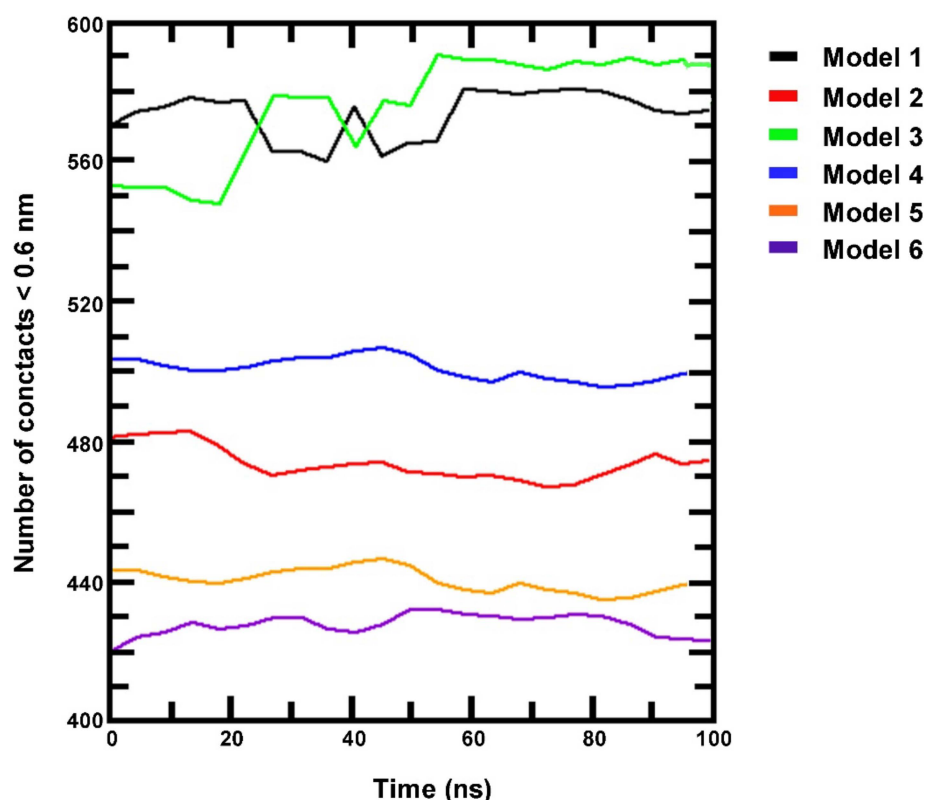


Figure 5. Direct interactions between HIF-1 and the 6 DNA fragments containing the HBSs as extrapolated from 100 ns molecular dynamics trajectory simulation, expressed as number of contacts within 0.6 nm distance between each other.

Docking analysis shown in Figure 6A demonstrates that, in model 1, Asp24 of the monomer-A interacts with T in position 10 of the HBS #1 while the hydroxyl group of Ser22 of the monomer-B interacts with A in position 2 of the flanking nucleotides upstream the HBS #1. On the contrary, in model 3 (Figure 6B), the observed interactions are less specific and only marginally involve the bases in the HBS #3. In particular, the 2 A in position 5 and 6, with A in position 6 being part of the HBS #3, interacts with Arg30 in monomer-A, whereas the other interactions (between A in position 1 and 2 with Arg18 and Ser22 in monomer-B, respectively) involve merely the phosphate skeleton and are electrostatic in nature. Therefore, model 3 although predicted with high affinity in its binding, displays Ser22 and Arg18 interactions mainly with the DNA phosphate skeleton thus resulting in low specificity and less stable binding over time. Model 1, instead, displays a wide number of interactions between aminoacidic residues of HIF-1 and the DNA bases contained in the HBS #1.

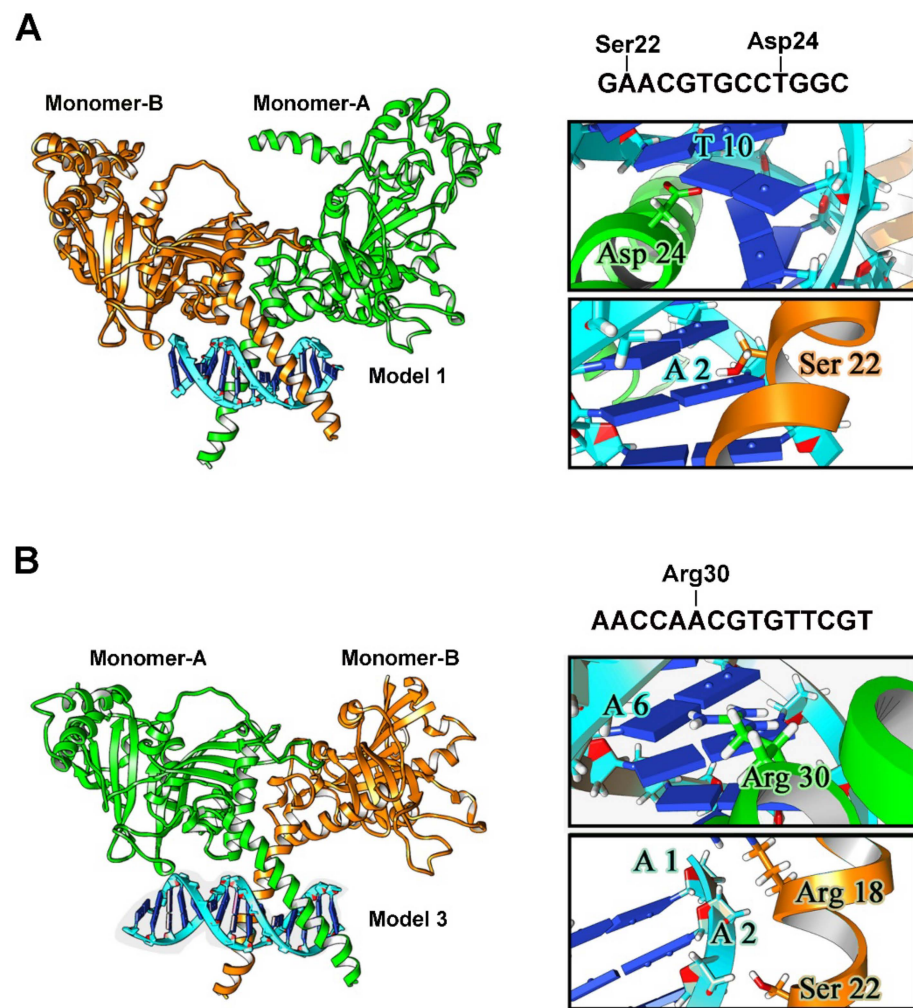


Figure 6. Docking analysis of model 1 and model 3. (A) HIF-1/HBS #1 best association complex: full structure and focus on HIF-1-DNA interactions (boxes). (B) HIF-1/HBS #3 best association complex: full structure and focus on HIF-1-DNA interactions (boxes).

3.5. HIF-1/HBS #1 Interaction and β 3-AR Gene Expression

Overall, docking results and MD simulation point to HBS #1 as the HBS to which HIF-1 is most likely to bind. To explore the interaction between HIF-1 α and HBS #1, HIF-1 α -specific ChIP-qPCR analysis was performed in the mouse retina at PD12 (immediately after the end of hyperoxia as well as at 1, 6 and 12 h after exposure to relative hypoxia) and at PD17 (Figure 7A). These time points were identified as appropriate for the effective detection of HIF-1-dependent VEGF transcription in the OIR model [52]. As shown in Figure 7B, the interactions between HIF-1 and HBS #1, as determined by HBS #1 enrichment relative to the IgG input, are drastically lower at the end of hyperoxia (PD12, time 0) than in normoxic controls to then gradually increase from 1 to 12 h of hypoxia when about 35-fold enrichment is reached. At that time, the HBS #1 enrichment is about 6-fold higher than in normoxic controls. At 5 days of hypoxia (PD17), the interactions between HIF-1 and HBS #1 are lower than after 12 h of hypoxia, but similar to those measured after 6 h of hypoxia. At PD17, the interactions between HIF-1 and HBS #1 are about 3-fold higher in respect to normoxic controls. β 3-AR gene expression was also assessed in order to evaluate whether HIF-1/HBS #1 interaction would be correlated with β 3-AR gene expression. As shown in Figure 7C, β 3-AR mRNA levels gradually increase from 0 to 12 h of hypoxia in close similarity with the HIF-1/HBS #1 interaction profile. In respect to normoxic controls, mRNA levels of β 3-AR are downregulated at the end of hyperoxia to then time-dependently

increase with a peak at 12 h of hypoxia. At PD 17, $\beta 3$ -AR mRNA levels are higher than in normoxic controls but lower than after 12 h of hypoxia.

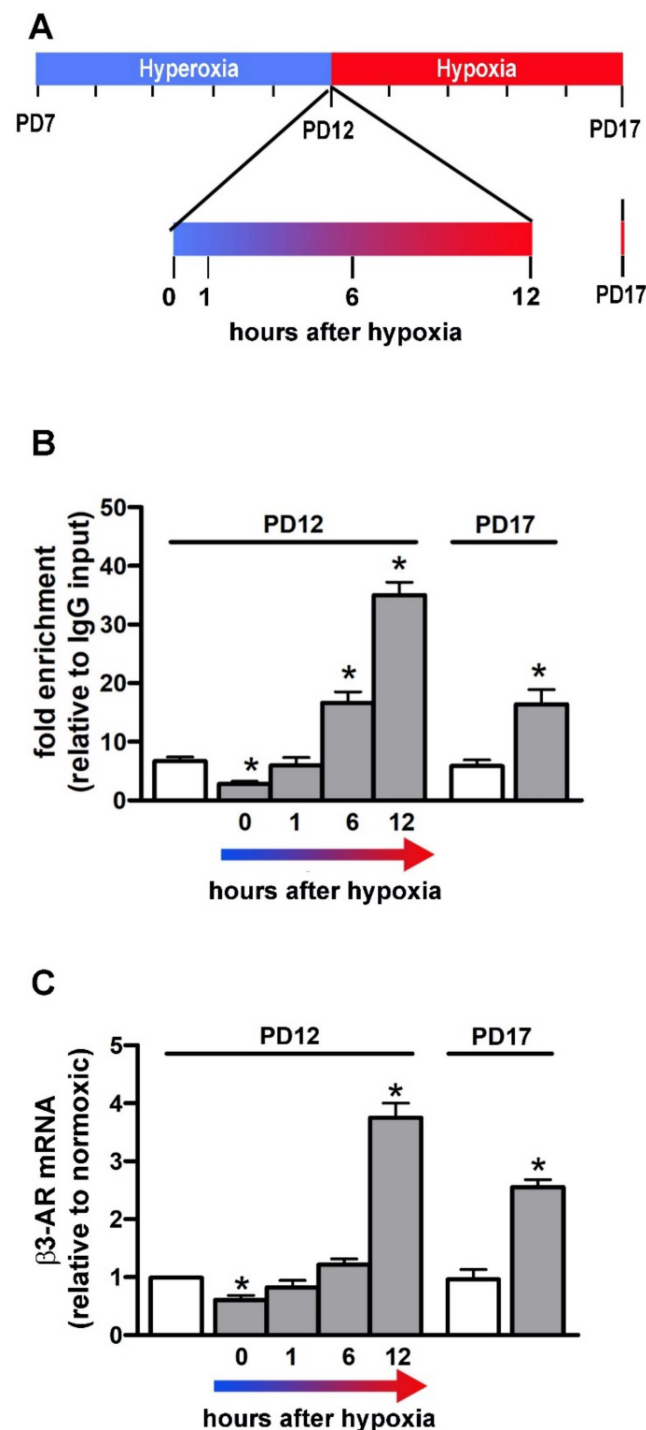


Figure 7. HIF-1 α interaction with HBS #1 and corresponding $\beta 3$ -AR gene expression at PD12 (from 0 to 12 h of hypoxia) or at PD17. (A) Schematic diagram of the OIR model pointing to the specific times under analysis. (B) Data from HIF-1 α chromatin immunoprecipitation and HBS #1-specific qPCR (ChIP-qPCR) represented as fold enrichment relative to IgG input. (C) Corresponding levels of $\beta 3$ -AR mRNA. White bars represent data from retinas of normoxic controls while grey bars represent data from hypoxic mice. One-way ANOVA followed by Tukey's multiple comparison post-hoc test. Each histogram represents the mean \pm SEM of data from 6 independent samples. * $p < 0.05$ vs. normoxic controls ($n = 6$ samples).

4. Discussion

Maintaining oxygen homeostasis is crucial for oxygen-dependent metabolism, and exposure to low oxygen tension needs to be faced by adaptive responses, many of which are triggered by HIF-1. Here, we demonstrate that an active HIF-1 binding site, the HBS #1, is present upstream the mouse β 3-AR TSS and that the physical interaction between HIF-1 and HBS #1 is correlated with β 3-AR transcription. This suggests that HBS #1 might be a transcriptional regulator of β 3-AR gene in the mouse retina thus playing a central role in determining β 3-AR expression when retinal oxygen tension changes.

In a recent review, the possibility that β 3-AR upregulation may be viewed as a general marker of hypoxic conditions has been discussed [13]. In solid tumors, in particular, β 3-AR upregulation occurs in response to tumor cell proliferation leading to oxygen and nutrients deprivation that drives the activation of key transcription factors regulating a large panel of genes that allows the tumor cells to escape from an oxygen-deprived environment. Infantile hemangioma (a benign tumor of childhood), for instance, and a wide range of malignant tumors, which share dedifferentiation and hypoxia as main pathological features are characterized by drastic β 3-AR upregulation. Upregulation of β 3-AR mRNA and protein also characterizes additional ischemic conditions as for instance the failed heart in which β 3-AR ligands have been demonstrated to ameliorate the pathological signs of cardiac injury [12,53,54]. The present findings that β 3-ARs are upregulated in the retina in response to hypoxia in concomitance with HIF-1 α is in line with previous findings indicating the possibility that increased levels of β 3-AR would be coupled to the retinal angiogenic response [15,55]. Upregulated levels of HIF-1 α and β 3-AR would trigger a compensatory response by promoting VEGF accumulation causing the proliferation of new vessels and the vasodilation of existing vessels. The additional finding that retinal β 3-AR is downregulated by hyperoxia in concomitance with lowered levels of HIF-1 α and VEGF opens the question of whether β 3-AR downregulation would be involved in retinal vessel regression in response to high oxygen tension.

β 3-AR downregulation at birth has been recently demonstrated in the ductus arteriosus (DA), a fetal blood vessel connecting the aorta to the pulmonary artery. DA remains open during the hypoxic intrauterine environment, whereas it normally closes soon after birth in concomitance with a drastic decrease of β 3-AR levels suggesting the possibility that β 3-AR participates in DA patency [56]. Additional evidence from peripheral blood mononuclear cells is indicative of β 3-AR downregulation during the switch from hypoxia to normoxia sensed as hyperoxia [57]. The present finding that the expression profile of retinal β 3-ARs depends on changing oxygen tension similarly to HIF-1 α and VEGF is intriguing if one considers that the panel of genes transactivated by HIF-1 plays a central role in cellular adaptation to oxygen deprivation [58].

Although receptor levels may depend on transcriptional and/or post-transcriptional mechanisms, the present finding that β 3-AR mRNA is accordingly regulated by oxygen levels further supports the possibility that changing protein levels might be due to variations in β 3-AR gene expression. The additional finding that abolishing hyperoxia-induced HIF-1 α degradation prevents oxygen-dependent modulation of both β 3-AR and VEGF reinforces the possibility that β 3-AR, similar to VEGF, behaves as a HIF-1 target gene. However, the definitive establishment of HIF-1 role in the transcriptional regulation of β 3-AR would imply the identification of a functional HRE with which HIF-1 could physically interact. In this respect, a previous study failed to demonstrate the presence of HRE consensus sites in the promoter/enhancer region of the mouse β 3-AR gene suggesting that hypoxia-induced β 3-AR upregulation derives exclusively from the post-transcriptional regulation of β 3-AR mRNA and/or from the stabilization of β 3-AR protein [59]. On the other hand, the high variability of the flanking sequences of the HRE might limit its determination which, in contrast, might be facilitated by the identification of the highly conserved cores i.e., the HBSs. Therefore, we investigated the presence of HBSs by analyzing the chromosome 8 sequences spanning upstream and inside the mouse β 3-AR gene since potential HBSs can be distant from the TSS, thus increasing the probability to find them. The present results

reveal 6 different potential HBSs suggesting the presence of multiple sites of interaction through which HIF-1 could actually bind to mouse β 3-AR gene to modulate its expression. In particular, HBS #1 and HBS #2 are localized upstream the TSS in a region containing other established β 3-AR gene enhancers [60] thus increasing the probability for these sites to represent functional HBSs. HIF-1 binding to HBS#1 is further supported by the fact that the nucleotides which are present upstream and downstream the minimal consensus core have been demonstrated to play an important role in the interaction between HIF-1 and HBSs [25]. The additional finding that human and mouse HBS #1 are located in corresponding regions further reinforces the possibility that HBS #1 is the best candidate for potential binding to HIF-1.

Still, the HBS consensus sequence is highly abundant across the genome, but less than 1% of potential sites are actually bound by HIF-1 as demonstrated by genome-wide analyses of HIF chromatin occupancy [25,26,61,62]. Therefore, a computational analysis allowing the simulation of the HIF-1 binding affinity and specificity has been used to assess the actual possibility of HIF-1 physical interaction with each of the identified HBSs. To this aim, the 3D structure of HIF-1 α has been reconstructed using the full HIF-1 α aminoacidic sequence and crystallographic data relative to HIF-1 α fragments. As shown by the present results, the build structure reaches a stable conformation at 100 ns after an initial rise that is indicative of the equilibration of the system. The additional presence of flexible domains confirms that the HIF-1 α structure is stable, but with the flexibility needed to allow for DNA binding. HIF-1 in its dimeric form has been approximated to HIF-1 α homodimer instead of a HIF-1 α /HIF-1 β heterodimer since HIF-1 α and HIF-1 β show similar flexibility patterns in regions close to the dimerization portion [44]. The superimposition between the homodimer and the dimer interface in the 4zpr structure shows that the present model preserves the exact coordinates to generate the DNA binding domain. The analysis of HIF-1/DNA docking has allowed the identification of 6 possible models, each of them including the DNA sequence corresponding to each HBS sequence plus upstream and downstream additional nucleotides. A similar analysis has been previously performed for HIF-1/HBSs docking in the VEGF gene promoter [63]. Among the 6 models identified here, model 1, including HBS #1, and model 3, including HBS #3, have been predicted as the best models based on both docking score and number of contacts. The fact that model 3 displays HIF-1/DNA interactions mainly based on contacts of aminoacidic residues with the phosphate skeleton suggests that, despite the high docking score and the high number of contacts, this model would be devoid of the specificity required for an effective HIF-1 binding. Conversely, together with a high docking score and a high number of contacts, in model 1, HIF-1 interacts exclusively with nucleotides within the consensus sequence suggesting both affinity and specificity compatible with an actual HIF-1 binding.

Overall, the integration of data deriving from the bioinformatic analysis about the localization of HBS #1 and the computational analysis regarding its compatibility for HIF-1 indicate HBS #1 as the most suitable site for HIF-1 binding to the β 3-AR gene.

The validation of the actual HIF-1 physical interaction with the HBS #1 derives from the ChIP-qPCR analysis, which definitively allows us to demonstrate HBS #1 as an effective HIF-1 binding site. In particular, the present findings show a time-dependent increment in HIF-1/HBS #1 physical interaction during the first hours of hypoxia, similar to that demonstrated for the VEGF gene in the OIR model [52]. Although the presence of a specific site for the HIF-1 binding confers hypoxic inducibility to the β 3-AR gene, additional conditions such as the recruitment of coactivators or epigenetic modifications may be required to assemble a fully functional transcription complex [64,65]. Therefore, the physical interaction of HIF-1 with the HBS #1 does not necessarily imply an actual transcriptional regulation of the β 3-AR gene by HIF-1. However, the close correlation between the time-dependent profile of the HIF-1/HBS #1 interaction and the corresponding β 3-AR mRNA expression indicates that, under hypoxia, the HIF-1 binding to the HBS #1 may effectively induce the β 3-AR gene expression and the consequent increase of β 3-AR protein levels.

HIF-1-mediated β 3-AR expression opens the question of whether this event constitutes only a marker of oxygen levels or is functionally related to hypoxia-associated events such as angiogenesis. In this respect, the possibility exists that increased β 3-AR expression may play a functional role during the early phase of oxygen deprivation by promoting the angiogenic drive in support of suffering retinal cells. Although β 3-AR's role in retinal angiogenesis remains so far to be clarified, preliminary findings are indicative of β 3-AR's contribution to massive vessel proliferation in response to hypoxia. In particular, results obtained from retinal explants demonstrate that a β 3-AR blockade or silencing prevents hypoxia-induced VEGF upregulation [66]. In addition, in β 1/ β 2-AR knock out mice undergoing the OIR protocol, β 3-AR agonism results in a dramatic increase in VEGF accumulation in concomitance with retinal vessel proliferation in response to hypoxia [67]. However, the finding that β 3-AR antagonism does not influence hypoxia-associated increase in VEGF levels and retinal vascularization [24], although in contrast with a possible role of β 3-AR in angiogenesis, may be due to the fact that many of β 3-AR antagonists bind β 3-AR with a low affinity and specificity [68,69]. In contrast to β 3-AR antagonism, selective agonists are efficiently used for the treatment of overactive bladder in which β 3-AR activation leads to myorelaxant effects and increases bladder capacity [70]. In addition, the fact that β 3-AR agonism causes angiogenesis and vasodilation in the ischemic heart [14,71] led to new pilot clinical trials assessing β 3-AR agonists as promising therapeutic targets for the treatment of heart failure [12]. In the retina, β 3-AR overstimulation during hyperoxia might serve to prevent vessel regression thus limiting vessel proliferation in response to hypoxia similarly to that which has already been observed through preventing HIF-1 α degradation [47,48], but without the complication derived from the activation of a vast array of genes.

Major constraints to the identifications of β 3-AR's role in ophthalmic diseases originate from the scarce data on β 3-AR expression and function in the posterior segment of the human eye. Although the role of β 3-ARs as a therapeutic target in ophthalmological diseases has been questioned [72], β 3-AR involvement in the control of cell proliferation, migration, invasion and elongation has been demonstrated in human retinal and choroidal endothelial cells. In particular, β 3-AR are expressed by human retinal endothelial cells where their activation promotes cell migration and proliferation both of which characterize vascular responses to altered sympathetic nerve activity [73]. In human choroidal endothelial cells, β 3-AR activation contributes to cell invasion, proliferation and elongation thus suggesting β 3-AR involvement in ocular diseases characterized by choroidal neovascularization [74]. These findings have been confirmed by recent data of Topcuoglu and Aslan [75] who have demonstrated that in patients with an overactive bladder, routinary treatment with mirabegron significantly increases choroidal vascular parameters suggesting that β 3-ARs may have a role in eye diseases associated with choroidal vascularization.

5. Conclusions

Reduced oxygen availability to retinal cells may lead to the progression of hypoxia-induced proliferative diseases in which HIF-1 upregulation plays a major role. Although inhibiting HIF-1 can be considered as an effective treatment of oxygen-dependent ocular diseases, the use of most HIF-1 inhibitors is still debated because of their side effects and toxicities. In contrast, therapies related to HIF-1 target genes may have remarkable impact on counteracting hypoxia-related pathologies as it occurs for anti-VEGF therapies. Here, we suggest the possibility that β 3-AR transcription may depend on HIF-1 thus supporting β 3-AR involvement in HIF-1-mediated responses to hypoxia. In this respect, HIF-1 would transactivate both VEGF and β 3-AR, which has been shown to regulate VEGF levels in response to low oxygen tension. This supports the possibility that β 3-AR participates in the angiogenic response to hypoxia.

In summary, the present study shows an increased β 3-AR expression in the hypoxic retina in which HIF-1 has been demonstrated to directly bind to the β 3-AR enhancer region thus up-regulating β 3-AR at the transcriptional level. Future studies will be required to

clarify β 3-AR's role in hypoxia-driven angiogenesis to lay the ground for novel treatments of proliferative retinal diseases.

Supplementary Materials: The following supporting information can be downloaded at: <https://www.mdpi.com/article/10.3390/cells11081271/s1>, Figure S1: Close superimposition of the heterodimeric interface from 4zpr (orange) with the HIF1 α homodimer model (green): full structure and focus on DNA binding domain (boxes).

Author Contributions: Conceptualization, L.F., R.G., M.S., M.D.M. and P.B.; methodology, F.P., M.C. and R.G.; formal analysis and investigation, R.A., F.P., E.L., M.L. and S.M. Writing—original draft preparation, R.A., F.P. and E.L.; writing—review and editing, R.A., M.C. and P.B.; funding acquisition, M.C., M.S. and M.D.M.; resources, F.P., R.G. and M.D.M.; supervision, R.G., M.S., M.D.M. and P.B. All authors have read and agreed to the published version of the manuscript.

Funding: This study was supported by fundings from the Italian Ministry of University and Research (FRA-2019/2021) to M.D.M. and M.C., the Meyer Children's University Hospital, Florence, Italy to M.D.M., and the Telethon Foundation (GGP15083) to M.S.

Institutional Review Board Statement: This study was performed in line with the recommendations in the Guide for the Care and Use of Laboratory Animals of the National Institutes of Health, the ARVO Statement for the Use of Animals in Ophthalmic and Vision Research, the Italian guidelines for animal care (DL 6/14) and the European Communities Council Directive (2010/63/UE). The experimental procedures were approved by the Ethical Committee in Animal Experiments of the University of Pisa (permit number 656/2018-PR, 3 September 2018).

Informed Consent Statement: Not applicable.

Data Availability Statement: The data presented in this study are available on request from the corresponding author.

Acknowledgments: We thank Tiziana Cintio for the assistance with mouse colonies and CINECA-HPC ISCRA MARCONI-100 computer system (project n. HP10CMPMGP) for the support in molecular dynamics simulations.

Conflicts of Interest: The authors declare no conflict of interest.

References

1. Semenza, G.L.; Wang, G.L. A nuclear factor induced by hypoxia via de novo protein synthesis binds to the human erythropoietin gene enhancer at a site required for transcriptional activation. *Mol. Cell. Biol.* **1992**, *12*, 5447–5454. [[CrossRef](#)] [[PubMed](#)]
2. Kaluz, S.; Kaluzová, M.; Stanbridge, E.J. Regulation of gene expression by hypoxia: Integration of the HIF-transduced hypoxic signal at the hypoxia-responsive element. *Clin. Chim. Acta* **2008**, *395*, 6–13. [[CrossRef](#)] [[PubMed](#)]
3. Hammarlund, E.U.; Flashman, E.; Mohlin, S.; Licausi, F. Oxygen-sensing mechanisms across eukaryotic kingdoms and their roles in complex multicellularity. *Science* **2020**, *370*, eaba3512. [[CrossRef](#)] [[PubMed](#)]
4. Eelen, G.; Treps, L.; Li, X.; Carmeliet, P. Basic and Therapeutic Aspects of Angiogenesis Updated. *Circ. Res.* **2020**, *127*, 310–329. [[CrossRef](#)] [[PubMed](#)]
5. Usui, Y.; Westenskow, P.D.; Murinello, S.; Dorrell, M.I.; Scheppke, L.; Bucher, F.; Sakimoto, S.; Paris, L.P.; Aguilar, E.; Friedlander, M. Angiogenesis and Eye Disease. *Annu. Rev. Vis. Sci.* **2015**, *1*, 155–184. [[CrossRef](#)]
6. Casini, G.; Monte, M.D.; Fornaciari, I.; Filippi, L.; Bagnoli, P. The β -adrenergic system as a possible new target for pharmacologic treatment of neovascular retinal diseases. *Prog. Retin. Eye Res.* **2014**, *42*, 103–129. [[CrossRef](#)]
7. Monte, M.D.; Martini, D.; Latina, V.; Pavan, B.; Filippi, L.; Bagnoli, P. Beta-Adrenoreceptor Agonism Influences Retinal Responses to Hypoxia in a Model of Retinopathy of Prematurity. *Investig. Ophthalmol. Vis. Sci.* **2012**, *53*, 2181–2192. [[CrossRef](#)]
8. Emorine, L.J.; Marullo, S.; Briand-Sutren, M.-M.; Patey, G.; Tate, K.; Delavier-Klutchko, C.; Strosberg, A.D. Molecular Characterization of the Human beta 3-Adrenergic Receptor. *Science* **1989**, *245*, 1118–1121. [[CrossRef](#)]
9. Calvani, M.; Cavallini, L.; Tondo, A.; Spinelli, V.; Ricci, L.; Pasha, A.; Bruno, G.; Buonvicino, D.; Bigagli, E.; Vignoli, M.; et al. β 3-Adrenoreceptors Control Mitochondrial Dormancy in Melanoma and Embryonic Stem Cells. *Oxidative Med. Cell. Longev.* **2018**, *2018*, 6816508. [[CrossRef](#)]
10. Uhlén, M.; Fagerberg, L.; Hallström, B.M.; Lindskog, C.; Oksvold, P.; Mardinoglu, A.; Sivertsson, Å.; Kampf, C.; Sjöstedt, E.; Asplund, A.; et al. Tissue-Based Map of the Human Proteome. *Science* **2015**, *347*, 1260419. [[CrossRef](#)]
11. Dal Monte, M.; Calvani, M.; Cammalleri, M.; Favre, C.; Filippi, L.; Bagnoli, P. β -Adrenoceptors as drug targets in melanoma: Novel preclinical evidence for a role of β 3-adrenoceptors. *Br. J. Pharmacol.* **2019**, *176*, 2496–2508. [[CrossRef](#)] [[PubMed](#)]
12. Michel, L.Y.M.; Farah, C.; Balligand, J.-L. The Beta3 Adrenergic Receptor in Healthy and Pathological Cardiovascular Tissues. *Cells* **2020**, *9*, 2584. [[CrossRef](#)] [[PubMed](#)]

13. Filippi, L.; Pini, A.; Cammalleri, M.; Bagnoli, P.; Dal Monte, M. β 3-Adrenoceptor, a novel player in the round-trip from neonatal diseases to cancer: Suggestive clues from embryo. *Med. Res. Rev.* **2022**, *42*, 1179–1201. [[CrossRef](#)] [[PubMed](#)]
14. Dessy, C.; Moniotte, S.; Ghisdal, P.; Havaux, X.; Noirhomme, P.; Balligand, J. Endothelial Beta3-Adrenoceptors Mediate Vasorelaxation of Human Coronary Microarteries Through Nitric Oxide and Endothelium-Dependent Hyperpolarization. *Circulation* **2004**, *110*, 948–954. [[CrossRef](#)] [[PubMed](#)]
15. Ristori, C.; Filippi, L.; Dal Monte, M.; Martini, D.; Cammalleri, M.; Fortunato, P.; la Marca, G.; Fiorini, P.; Bagnoli, P. Role of the Adrenergic System in a Mouse Model of Oxygen-Induced Retinopathy: Antiangiogenic Effects of beta-Adrenoreceptor Blockade. *Investig. Ophthalmol. Vis. Sci.* **2011**, *52*, 155–170. [[CrossRef](#)]
16. Selvam, S.; Kumar, T.; Fruttiger, M. Retinal vasculature development in health and disease. *Prog. Retin. Eye Res.* **2018**, *63*, 1–19. [[CrossRef](#)]
17. Smith, L.E.H.; Wesolowski, E.; McLellan, A.; Kostyk, S.K.; D'Amato, R.J.; Sullivan, R.; D'Amore, P.A. Oxygen-induced retinopathy in the mouse. *Investig. Ophthalmol. Vis. Sci.* **1994**, *35*, 101–111.
18. Orlando, I.M.; Lafleur, V.N.; Storti, F.; Spielmann, P.; Crowther, L.; Santambrogio, S.; Schödel, J.; Hoogewijs, D.; Mole, D.R.; Wenger, R.H. Distal and proximal hypoxia response elements cooperate to regulate organ-specific erythropoietin gene expression. *Haematologica* **2019**, *105*, 2774–2784. [[CrossRef](#)]
19. Krueger, K.; Catanese, L.; Sciesielski, L.; Kirschner, K.; Scholz, H. Deletion of an intronic HIF-2 α binding site suppresses hypoxia-induced WT1 expression. *Biochim. Biophys. Acta Gene Regul. Mech.* **2019**, *1862*, 71–83. [[CrossRef](#)]
20. Binó, L.; Procházková, J.; Radaszkiewicz, K.A.; Kučera, J.; Kudová, J.; Pacherník, J.; Kubala, L. Hypoxia favors myosin heavy chain beta gene expression in an Hif-1alpha-dependent manner. *Oncotarget* **2017**, *8*, 83684–83697. [[CrossRef](#)]
21. Strowitzki, M.J.; Cummins, E.P.; Taylor, C.T. Protein Hydroxylation by Hypoxia-Inducible Factor (HIF) Hydroxylases: Unique or Ubiquitous? *Cells* **2019**, *8*, 384. [[CrossRef](#)] [[PubMed](#)]
22. Cammalleri, M.; Monte, M.D.; Locri, F.; Pecci, V.; De Rosa, M.; Pavone, V.; Bagnoli, P. The urokinase-type plasminogen activator system as drug target in retinitis pigmentosa: New pre-clinical evidence in the rd10 mouse model. *J. Cell. Mol. Med.* **2019**, *23*, 5176–5192. [[CrossRef](#)] [[PubMed](#)]
23. Cammalleri, M.; Monte, M.D.; Amato, R.; Lapi, D.; Bagnoli, P. Novel Insights into Beta 2 Adrenergic Receptor Function in the rd10 Model of Retinitis Pigmentosa. *Cells* **2020**, *9*, 2060. [[CrossRef](#)] [[PubMed](#)]
24. Martini, D.; Monte, M.D.; Ristori, C.; Cupisti, E.; Mei, S.; Fiorini, P.; Filippi, L.; Bagnoli, P. Antiangiogenic effects of β 2-adrenergic receptor blockade in a mouse model of oxygen-induced retinopathy. *J. Neurochem.* **2011**, *119*, 1317–1329. [[CrossRef](#)]
25. Schödel, J.; Oikonomopoulos, S.; Ragoussis, J.; Pugh, C.W.; Ratcliffe, P.J.; Mole, D.R. High-resolution genome-wide mapping of HIF-binding sites by ChIP-seq. *Blood* **2011**, *117*, e207–e217. [[CrossRef](#)]
26. Mole, D.R.; Blancher, C.; Copley, R.R.; Pollard, P.J.; Gleadle, J.M.; Ragoussis, J.; Ratcliffe, P.J. Genome-wide Association of Hypoxia-inducible Factor (HIF)-1 α and HIF-2 α DNA Binding with Expression Profiling of Hypoxia-inducible Transcripts. *J. Biol. Chem.* **2009**, *284*, 16767–16775. [[CrossRef](#)]
27. Kaluz, S.; Kaluzová, M.; Stanbridge, E.J. Rational design of minimal hypoxia-inducible enhancers. *Biochem. Biophys. Res. Commun.* **2008**, *370*, 613–618. [[CrossRef](#)]
28. Yang, J.; Yan, R.; Roy, A.; Xu, D.; Poisson, J.; Zhang, Y. The I-TASSER Suite: Protein structure and function prediction. *Nat. Methods* **2015**, *12*, 7–8. [[CrossRef](#)]
29. Fiser, A.; Sali, A. ModLoop: Automated modeling of loops in protein structures. *Bioinformatics* **2003**, *19*, 2500–2501. [[CrossRef](#)]
30. Park, H.; Lee, G.R.; Heo, L.; Seok, C. Protein Loop Modeling Using a New Hybrid Energy Function and Its Application to Modeling in Inaccurate Structural Environments. *PLoS ONE* **2014**, *9*, e113811. [[CrossRef](#)]
31. Ceroni, A.; Passerini, A.; Vullo, A.; Frascioni, P. DISULFIND: A disulfide bonding state and cysteine connectivity prediction server. *Nucleic Acids Res.* **2006**, *34*, W177–W181. [[CrossRef](#)] [[PubMed](#)]
32. Páll, S.; Hess, B. A flexible algorithm for calculating pair interactions on SIMD architectures. *Comput. Phys. Commun.* **2013**, *184*, 2641–2650. [[CrossRef](#)]
33. Darden, T.; York, D.; Pedersen, L. Particle mesh Ewald: An $N \cdot \log(N)$ method for Ewald sums in large systems. *J. Chem. Phys.* **1993**, *98*, 10089–10092. [[CrossRef](#)]
34. Hoover, W.G. Canonical dynamics: Equilibrium phase-space distributions. *Phys. Rev. A* **1985**, *31*, 1695–1697. [[CrossRef](#)] [[PubMed](#)]
35. Parrinello, M.; Rahman, A. Polymorphic transitions in single crystals: A new molecular dynamics method. *J. Appl. Phys.* **1981**, *52*, 7182–7190. [[CrossRef](#)]
36. Abraham, M.J.; Murtola, T.; Schulz, R.; Páll, S.; Smith, J.C.; Hess, B.; Lindahl, E. GROMACS: High performance molecular simulations through multi-level parallelism from laptops to supercomputers. *SoftwareX* **2015**, *1–2*, 19–25. [[CrossRef](#)]
37. Yan, Y.; Tao, H.; He, J.; Huang, S.-Y. The HDock server for integrated protein-protein docking. *Nat. Protoc.* **2020**, *15*, 1829–1852. [[CrossRef](#)]
38. Yan, Y.; Zhang, D.; Zhou, P.; Li, B.; Huang, S.-Y. HDock: A web server for protein-protein and protein-DNA/RNA docking based on a hybrid strategy. *Nucleic Acids Res.* **2017**, *45*, W365–W373. [[CrossRef](#)]
39. Yan, Y.; Wen, Z.; Wang, X.; Huang, S.-Y. Addressing recent docking challenges: A hybrid strategy to integrate template-based and free protein-protein docking. *Proteins Struct. Funct. Bioinform.* **2017**, *85*, 497–512. [[CrossRef](#)]
40. Huang, S.-Y.; Zou, X. A knowledge-based scoring function for protein-RNA interactions derived from a statistical mechanics-based iterative method. *Nucleic Acids Res.* **2014**, *42*, e55. [[CrossRef](#)]

41. Huang, S.-Y.; Zou, X. An iterative knowledge-based scoring function for protein-protein recognition. *Proteins Struct. Funct. Bioinform.* **2008**, *72*, 557–579. [[CrossRef](#)] [[PubMed](#)]
42. Case, D.A.; Ben-Shalom, I.Y.; Brozell, S.R.; Cerutti, D.S. *AMBER 2018*; University of California: San Francisco, CA, USA, 2018.
43. Wang, J.; Wolf, R.M.; Caldwell, J.W.; Kollman, P.A.; Case, D.A. Development and testing of a general amber force field. *J. Comput. Chem.* **2004**, *25*, 1157–1174. [[CrossRef](#)] [[PubMed](#)]
44. Wu, D.; Potluri, N.; Lu, J.; Kim, Y.; Rastinejad, F. Structural integration in hypoxia-inducible factors. *Nature* **2015**, *524*, 303–308. [[CrossRef](#)] [[PubMed](#)]
45. Humphrey, W.; Dalke, A.; Schulten, K. VMD: Visual molecular dynamics. *J. Mol. Graph.* **1996**, *14*, 33–38. [[CrossRef](#)]
46. Pettersen, E.F.; Goddard, T.D.; Huang, C.C.; Couch, G.S.; Greenblatt, D.M.; Meng, E.C.; Ferrin, T.E. UCSF Chimera—a visualization system for exploratory research and analysis. *J. Comput. Chem.* **2004**, *25*, 1605–1612. [[CrossRef](#)]
47. Hoppe, G.; Yoon, S.; Gopalan, B.; Savage, A.R.; Brown, R.; Case, K.; Vasanthi, A.; Chan, E.R.; Silver, R.B.; Sears, J.E. Comparative systems pharmacology of HIF stabilization in the prevention of retinopathy of prematurity. *Proc. Natl. Acad. Sci. USA* **2016**, *113*, E2516–E2525. [[CrossRef](#)]
48. Sears, J.E.; Hoppe, G.; Ebrahim, Q.; Anand-Apte, B. Prolyl hydroxylase inhibition during hyperoxia prevents oxygen-induced retinopathy. *Proc. Natl. Acad. Sci. USA* **2008**, *105*, 19898–19903. [[CrossRef](#)]
49. Messeguer, X.; Escudero, R.; Farre, D.; Núñez, O.; Martinez, J.; Albà, M. PROMO: Detection of known transcription regulatory elements using species-tailored searches. *Bioinformatics* **2002**, *18*, 333–334. [[CrossRef](#)]
50. Farré, D.; Roset, R.; Huerta, M.; Adsuara, J.E.; Roselló, L.; Albà, M.M.; Messeguer, X. Identification of patterns in biological sequences at the ALGGEN server: PROMO and MALGEN. *Nucleic Acids Res.* **2003**, *31*, 3651–3653. [[CrossRef](#)]
51. Ortiz-Barahona, A.; Villar, D.; Pescador, N.; Amigo, J.; Del Peso, L. Genome-wide identification of hypoxia-inducible factor binding sites and target genes by a probabilistic model integrating transcription-profiling data and in silico binding site prediction. *Nucleic Acids Res.* **2010**, *38*, 2332–2345. [[CrossRef](#)]
52. Pisani, F.; Cammalleri, M.; Monte, M.D.; Locri, F.; Mola, M.G.; Nicchia, G.P.; Frigeri, A.; Bagnoli, P.; Svelto, M. Potential role of the methylation of VEGF gene promoter in response to hypoxia in oxygen-induced retinopathy: Beneficial effect of the absence of AQP. *J. Cell. Mol. Med.* **2017**, *22*, 613–627. [[CrossRef](#)] [[PubMed](#)]
53. Balligand, J.-L. Cardiac salvage by tweaking with beta-3-adrenergic receptors. *Cardiovasc. Res.* **2016**, *111*, 128–133. [[CrossRef](#)] [[PubMed](#)]
54. Michel, L.Y.M.; Balligand, J.-L. New and Emerging Therapies and Targets: Beta-3 Agonists. In *Heart Failure*; Springer: Cham, Switzerland, 2016; pp. 205–223.
55. Chen, J.; Joyal, J.-S.; Hatton, C.J.; Juan, A.; Pei, D.T.; Hurst, C.G.; Xu, D.; Stahl, A.; Hellström, A.; Smith, L.E.H. Propranolol Inhibition of β -Adrenergic Receptor Does Not Suppress Pathologic Neovascularization in Oxygen-Induced Retinopathy. *Investig. Ophthalmol. Vis. Sci.* **2012**, *53*, 2968–2977. [[CrossRef](#)] [[PubMed](#)]
56. Pini, A.; Fazi, C.; Nardini, P.; Calvani, M.; Fabbri, S.; Guerrini, A.; Forni, G.; La Marca, G.; Rosa, A.C.; Filippi, L. Effect of Beta 3 Adrenoreceptor Modulation on Patency of the Ductus Arteriosus. *Cells* **2020**, *9*, 2625. [[CrossRef](#)]
57. Calvani, M.; Bruno, G.; Dal Monte, M.; Nassini, R.; Fontani, F.; Casini, A.; Cavallini, L.; Becatti, M.; Bianchini, F.; De Logu, F.; et al. β 3-Adrenoceptor as a potential immuno-suppressor agent in melanoma. *Br. J. Pharmacol.* **2019**, *176*, 2509–2524. [[CrossRef](#)]
58. Dengler, V.L.; Galbraith, M.; Espinosa, J.M. Transcriptional regulation by hypoxia inducible factors. *Crit. Rev. Biochem. Mol. Biol.* **2014**, *49*, 1–15. [[CrossRef](#)]
59. Monte, M.D.; Evans, B.A.; Arioglu-Inan, E.; Michel, M.C. Upregulation of β 3-adrenoceptors—a general marker of and protective mechanism against hypoxia? *Naunyn-Schmiedeberg's Arch. Pharmacol.* **2020**, *393*, 141–146. [[CrossRef](#)]
60. Dixon, T.M.; Daniel, K.W.; Farmer, S.; Collins, S. CCAAT/Enhancer-binding Protein α Is Required for Transcription of the beta 3-Adrenergic Receptor Gene during Adipogenesis. *J. Biol. Chem.* **2001**, *276*, 722–728. [[CrossRef](#)]
61. Schödel, J.; Mole, D.R.; Ratcliffe, P.J. Pan-genomic binding of hypoxia-inducible transcription factors. *Biol. Chem.* **2013**, *394*, 507–517. [[CrossRef](#)]
62. Xia, X.; Kung, A.L. Preferential binding of HIF-1 to transcriptionally active loci determines cell-type specific response to hypoxia. *Genome Biol.* **2009**, *10*, R113. [[CrossRef](#)]
63. Sokkar, P.; Sathis, V.; Ramachandran, M. Computational modeling on the recognition of the HRE motif by HIF-1: Molecular docking and molecular dynamics studies. *J. Mol. Model.* **2011**, *18*, 1691–1700. [[CrossRef](#)] [[PubMed](#)]
64. Bracken, C.P.; Whitelaw, M.L.; Peet, D.J. The hypoxia-inducible factors: Key transcriptional regulators of hypoxic responses. *Cell Mol. Life Sci.* **2003**, *60*, 1376–1393. [[CrossRef](#)] [[PubMed](#)]
65. Lisy, K.; Peet, D. Turn me on: Regulating HIF transcriptional activity. *Cell Death Differ.* **2008**, *15*, 642–649. [[CrossRef](#)] [[PubMed](#)]
66. Dal Monte, M.; Filippi, L.; Bagnoli, P. Beta3-adrenergic receptors modulate vascular endothelial growth factor release in response to hypoxia through the nitric oxide pathway in mouse retinal explants. *Naunyn-Schmiedeberg Arch. Pharmacol.* **2013**, *386*, 269–278. [[CrossRef](#)] [[PubMed](#)]
67. Monte, M.D.; Cammalleri, M.; Mattei, E.; Filippi, L.; Bagnoli, P. Protective Effects of 1/2 Adrenergic Receptor Deletion in a Model of Oxygen-Induced Retinopathy. *Investig. Ophthalmol. Vis. Sci.* **2014**, *56*, 59–73. [[CrossRef](#)]
68. Hoffmann, C.; Leitz, M.R.; Oberdorf-Maass, S.; Lohse, M.J.; Klotz, K.-N. Comparative pharmacology of human β -adrenergic receptor subtypes—characterization of stably transfected receptors in CHO cells. *Naunyn-Schmiedeberg's Arch. Pharmacol.* **2004**, *369*, 151–159. [[CrossRef](#)]

69. Cernecka, H.; Sand, C.; Michel, M.C. The Odd Sibling: Features of β 3-Adrenoceptor Pharmacology. *Mol. Pharmacol.* **2014**, *86*, 479–484. [[CrossRef](#)]
70. Vij, M.; Drake, M.J. Clinical use of the β 3 adrenoceptor agonist mirabegron in patients with overactive bladder syndrome. *Ther. Adv. Urol.* **2015**, *7*, 241–248. [[CrossRef](#)]
71. Gauthier, C.; Langin, D.; Balligand, J.-L. Beta3-Adrenoceptors in the cardiovascular system. *Trends Pharmacol. Sci.* **2000**, *21*, 426–431. [[CrossRef](#)]
72. Gericke, A.; Böhmer, T.; Michel, M.C. β 3-Adrenoceptors: A drug target in ophthalmology? *Naunyn-Schmiedebergs Arch. Pharmacol.* **2013**, *386*, 265–267. [[CrossRef](#)]
73. Steinle, J.; Booz, G.W.; Meininger, C.; Day, J.N.E.; Granger, H.J. Beta3-Adrenergic Receptors Regulate Retinal Endothelial Cell Migration and Proliferation. *J. Biol. Chem.* **2003**, *278*, 20681–20686. [[CrossRef](#)] [[PubMed](#)]
74. Steinle, J.J.; Zamora, D.O.; Rosenbaum, J.T.; Granger, H.J. Beta3-Adrenergic receptors mediate choroidal endothelial cell invasion, proliferation, and cell elongation. *Exp. Eye Res.* **2005**, *80*, 83–91. [[CrossRef](#)] [[PubMed](#)]
75. Topcuoglu, M.; Aslan, F. Evaluation of the Effect of a Novel Beta3-Adrenergic Agonist on Choroidal Vascularity. *Investig. Ophthalmol. Vis. Sci.* **2021**, *62*, 17. [[CrossRef](#)] [[PubMed](#)]

In vitro models of retinal diseases

Martina Lucchesi, Silvia Marracci

Department of Biology, University of Pisa, Pisa, Italy

Correspondence to: Martina Lucchesi; Silvia Marracci. General Physiology Unit, via S. Zeno 31, 56127 Pisa, Italy.

Email: martina.lucchesi@student.unipi.it; silvia.marracci@unipi.it.

Background: Continuous and primary *in vitro* cultures are largely used to study cellular mechanisms occurring in several pathologic-like or pathological conditions. Continuous cell lines allow to perform long-lasting experiments since they do not undergo senescence.

Methods: The immortalized Moorfields/Institute of Ophthalmology-Müller 1 (MIO-M1) cell type represents a valuable model to analyze the mechanistic pathways characterizing Müller glial cells, both in health and in disease. MIO-M1 can be used to dissect the response of these glial cells following treatments which mimic pathological condition. For instance, MIO-M1 are useful to study the response of this cell type to stress condition as the case of oxidative stress (OS) (cultured with hydrogen peroxide), pathological neovascularization (cultured with VEGF), hypoxic or hyperoxic condition (cultured in low or high oxygen chamber). On the other hand, primary cultures allow to specifically analyze cellular responses without the interference of the whole organ, although the experimental treatment is performed *in vivo*. Primary Müller cells can be used to perform electrophysiological analyses of different cell sites.

Discussion: We describe how to manage MIO-M1 cells and how to analyze their response to different stress conditions; moreover, we report how to isolate and identify primary Müller cells and how to perform patch clamp and single cell recordings on them.

Keywords: Müller cells; Moorfields/Institute of Ophthalmology-Müller 1 (MIO-M1); primary culture

Received: 30 July 2021. Accepted: 05 November 2021.

doi: 10.21037/aes-21-36

View this article at: <https://dx.doi.org/10.21037/aes-21-36>

Introduction

Accumulating evidence has progressively highlighted the essential functions of glial cells, which can no longer be thought of as the “silent supporters” of neurons. Within the vertebrate retina, which is responsible for visual perception, Müller cells are the principal glial cells. These cells are radially organized across the entire retinal thickness as originally shown by Cajal through Golgi staining in 1892. This localization is designed for them to play major supporting roles: indeed, these glial cells constitute an anatomic-functional connection between retinal neurons and blood vessels, vitreous body, and subretinal space (1). Müller cells are deeply involved in the generation of the electroretinogram, highlighting their significant role in both retinal physiological and pathological responses. In addition, they are the major producer of retinal vascular endothelial

growth factor (VEGF), providing a crucial contribution to retinal angiogenesis during physiological development but also exacerbating pathological neovascularization (2).

In vitro model systems including Müller primary cultures as well as immortalized cell lines, have been developed; these systems represent useful tools to investigate the physiological and pathological events that occur within the retina under different stress conditions.

Methods

Moorfields/Institute of Ophthalmology-Müller 1 (MIO-M1)

Limb *et al.* described for the first time the isolation protocol of Müller cells from human retina, and they called this spontaneously immortalized cell line MIO-M1 (3). Nowadays, MIO-M1 are widely used to investigate the

Table 1 MIO-M1 density at confluence

Flask/dish type	Cell density at confluence
T75 flask	2.7×10^6
TC 100 Petri dish	1.5×10^6

2.7×10^6 MIO-M1 cells reach 100% confluence in a TC 75 flask.
 1.5×10^6 MIO-M1 cells reach 100% confluence in a TC 100 Petri dish. MIO-M1, Moorfields/Institute of Ophthalmology-Müller 1.

Table 2 Number of seeding cells

Dish type	Number of seeding cells for time course experiments		
	24 h	48 h	72 h
TC 100 mm Petri dish	1.0×10^6	7.25×10^5	5.89×10^5
TC 60 mm Petri dish	4.0×10^5	2.77×10^5	2.25×10^5

MIO-M1 cells number we suggest seeding in TC 100 mm or 60 mm Petri dishes for each point of the time course experiments. MIO-M1, Moorfields/Institute of Ophthalmology-Müller 1.

role of Müller cells in retinal diseases. For example, their response to hyperoxic or hypoxic exposure (when they are cultured in high or low oxygen tension, respectively), can give insights into their involvement in retinopathy of prematurity (ROP). Furthermore, it can be intriguing to analyze MIO-M1 response following stress conditions, as the case of oxidative stress (OS) (when they are cultured with H_2O_2) or pathological neovascularization (when they are cultured with VEGF). Below, we describe how to manage MIO-M1 cell lines and how to realize the previous mentioned experimental conditions.

Recipes

Complete cell culture medium:

- ❖ Dulbecco's modified Eagle's medium (DMEM) high glucose (4.5 g/L) (Merck, Darmstadt, Germany, catalog number: D5671).
- ❖ 1% Glutamine (Merck, catalog number: G7513).
- ❖ 10% Foetal bovine serum (FBS) (Merck, catalog number: F4135).
- ❖ 1% penicillin-streptomycin (PS) (Merck, catalog number: P4333).

Starvation medium:

- ❖ DMEM high glucose (4.5 g/L).
- ❖ 1% Glutamine.
- ❖ 0.1% FBS.
- ❖ 1% PS.

Culture of MIO-M1

MIO-M1 cells grow at 37 °C, 5% CO_2 in humidified conditions. The cells must be seeded in flasks T75 (Sartstedt, Nümbrecht, Germany, catalog number: 83.3911.002) or petri dishes (Sartstedt, catalog number: 83.3902) and maintained until they reach a subconfluent density. When cell density is about 75%, MIO M1 can be expanded or frozen, according to canonical cell culture protocols. In *Table 1*, MIO-M1 cell number at confluence are reported.

Hyperoxia experiments

Hyperoxic condition should be performed at 75% oxygen and 5% CO_2 . Normoxic condition (atmospheric oxygen tension and 5% CO_2) is used as a control. Experiments in hyperoxia should be performed following a time course, e.g., 24/48/72 h. At least three independent experiments for each condition (normoxia and hyperoxia) must be used to perform statistical analysis. The suggested cells seeding density is reported in *Table 2*.

- ❖ On the first day, seed the suggested number of MIO-M1 cells in complete cell culture medium.
- ❖ The following day, remove the medium from the dish.
- ❖ Add MIO-M1 starvation medium.
- ❖ After 24 h, remove the starvation medium.
- ❖ Add complete cell culture medium.
- ❖ Incubate the cells in hyperoxic condition, leaving the control cells in normoxia.

After 24/48/72 h proceed with subsequent analyses.

Hypoxia experiments

Hypoxic condition should be performed at 1% oxygen and 5% CO_2 . Normoxic condition is used as a control (see above). Experiments in hypoxia should be performed following a time course, e.g., 24/48/72 h. At least three independent experiments for each condition (normoxia and hypoxia) must be used to perform statistical analysis. The suggested cells seeding density is reported in *Table 2*.

- ❖ On the first day, seed the suggested number of MIO-M1 cells in complete cell culture medium.
- ❖ The next day, remove the medium from the dish.
- ❖ Add MIO-M1 starvation medium.
- ❖ After 24 h, remove the starvation medium.
- ❖ Add complete cell culture medium.
- ❖ Incubate the cells in hypoxic condition, leaving the control cells in normoxia.

After 24/48/72 h proceed with subsequent analyses.

Induction of OS

H₂O₂ is commonly used to induce OS on cultured cells. It has been demonstrated that MIO-M1 cells proliferation/ viability and morphology remain unaltered at H₂O₂ concentration of 100, 200 or 400 μM, while higher concentrations result in dramatic loss of cell viability and alter morphology (4).

- ❖ On the first day, seed the suggested number of cells in complete cell culture medium.
- ❖ The next day, remove the medium from the dish.
- ❖ Add the starvation medium.
- ❖ After 24 h, remove the starvation medium.
- ❖ Add OS medium.
- ❖ After 24 h proceed with subsequent analyses.

To maximize H₂O₂ effect, treat the cells with 5 μM ML385 (Bio-Techne, Minneapolis, MN, USA, catalog number: 6243), an inhibitor of Nrf2.

Culture with VEGF

To mimic the conditions of pathological angiogenesis, treat MIO-M1 cells with recombinant human VEGF (Merck, St. Louis, MO, USA, catalog number: SRP3182) diluted 1–5 ng/mL in complete growth medium (VEGF medium) as shown in (4).

- ❖ On the first day, seed the suggested number of cells in complete cell culture medium.
- ❖ The following day, remove the medium.
- ❖ Add the starvation medium.
- ❖ After 24 h, remove the starvation medium.
- ❖ Add VEGF medium.
- ❖ After 24 h proceed with subsequent analyses.

Molecular analyses

Once mimicked a given pathological condition (e.g., ROP ischemic phase by means of hyperoxia, ROP neovascularization phase by means of hypoxia, etc.), it is interesting to investigate whether and which molecular pathways are altered compared to untreated controls. Here, we briefly report protocols regarding qPCR, Western Blot analysis, viability assay (e.g., Trypan blue assay and MTT assay), cell cycle analysis and Reactive Oxygen Species (ROS) detection.

qRT-PCR

Perform total RNA extraction using RNeasy Micro Kit (Qiagen, Hilden, Germany, catalog number: 74104). Use Nanodrop™ spectrophotometer (NanoDrop products, Wilmington, CA, USA) for RNA quantification, and random hexamers (Qiagen, QuantiTect® Reverse Transcription

Kit, catalog number: 205313) for cDNA synthesis. Use SsoAdvanced Univ SYBR Grn Suprmix (Biorad, CA, USA, catalog number: 1725274) for qRT-PCR reactions. Perform data analysis using the comparative 2^{-ΔΔCt} method for relative quantification (5).

Western blot

Use RIPA Lysis Buffer System (Santa Cruz, Dallas, Texas, USA, catalog number: sc-24948) for protein extraction; assess protein concentration through Micro BCA™ Protein Assay Kit (ThermoFisher, Massachusetts, USA, catalog number: 23235). Carry out Western Blot analysis on 15 μg protein using 4–20% Mini-PROTEAN® TGX™ Precast Protein Gels, 10-well (Biorad, catalog number: 4561093) and Trans-Blot Turbo Midi NC Transfer Packs (Biorad, catalog number: 1704159). Use Clarity Western ECL Substrate (Biorad, catalog number: 1705061) to visualize the signal that will be analyzed with Image Lab Software (Biorad).

Cell viability assays

(I) Trypan blue exclusion assay

Detach MIO-M1 cells with trypsin-EDTA. Add 50% Trypan blue (3Z,3'Z)-3,3'-[(3,3'-dimethylbiphenyl-4,4'-diyl)di(1Z)hydrazin-2-yl-1-ylidene]bis(5-amino-4-oxo-3,4-dihydronaphthalene-2,7-disulfonic acid) (Sigma-Aldrich, catalog number: T8154). Perform cell count using TC20 Automated Cell Counter (Biorad, catalog number: 1450102) and Cell Counting Slides Dual-Chamber for TC10™/TC20™ Cell Counter (Biorad, catalog number: 1450011). At least three counts for each sample must be performed for statistical analysis.

(II) MTT assay

Seed MIO-M1 cells onto 96-well flat bottom microplates. When cells are 60–70% confluent, evaluate their viability with Cell Proliferation Kit I MTT assay (Roche, Monza, Italy, catalog number: 11465007001), in accordance with the manufacturer's protocol. Use Ultra Microplate reader (Bio-Tek Instruments Inc., Winooski, VT, USA) to measure absorbance at 570 nm.

Cell cycle analysis

Seed MIO-M1 cells onto 10 mm plates. Detach the cells with Trypsin-EDTA, fix and stain them in propidium iodide solution, according to the protocol described in reference (6).

ROS determination

(I) ROS determination with the Fluorescent Probe 2',7'-Dichlorofluorescein diacetate (DCF)

Seed MIO-M1 cells in 96 well-black plates with flat bottom (Sigma-Aldrich, catalog number: 35845) and wash them

with PBS 1X, incubate with 15 μm DCF (Sigma-Aldrich, catalog number: 35845) and quantify ROS production following the protocol described in (7).

(II) Flow cytometry analysis of MitoSOX signal

Stain MIO-M1 cells with 1 μm MitoSOX Red (Thermo Fisher Scientific, catalog number: M36008) for 40 min at 37 °C following manufacturer's instructions. After staining, cells can be analyzed by flow cytometry as described in (7).

Immunocytochemistry

MIO-M1 cells can be characterized through immunocytochemistry using the Glutamine Synthetase (GS) as a specific marker for Müller cells (8). In addition, a widely used target to examine pathological-like general responses of these cells following stress is the Glial Fibrillary Acidic Protein (GFAP). GFAP is a cytoskeletal protein used as a marker of reactive gliosis, and abundantly expressed in Müller cells under stress conditions (9). Below, we describe the protocol to perform immunocytochemistry analysis of MIO-M1 cells:

- ❖ Plate MIO-M1 cells onto 24×24 slides (Bio Optica, Milano, Italy, catalog number: 09-02424) with complete cell culture medium and allow them to attach.
- ❖ Remove medium and wash the slides with PBS 1X.
- ❖ Fix the cells by incubating the slides for 20 min at –20 °C with cold methanol (Carlo Erba, Milan, Italy, catalog number: 414816) plus 5% Acetic acid glacial Baker analyzed™ (ThermoFisher, catalog number: 6052).
- ❖ Rinse with PBS 1X three times for 5 min.
- ❖ Permeabilize and block into a humidified chamber at RT in 0.1% triton with 5% bovine serum albumin (BSA) fraction V (Merck, catalog number: 10735086001) for 1 h and cover the slides with parafilm (Merck, catalog number: P7668).
- ❖ Incubate the slides overnight with the primary antibody in a humidified chamber at 4 °C and cover them with parafilm.
- ❖ Rinse the slides three times for 5 min with PBS 1X.
- ❖ Incubate them for 1 h with the properly conjugated secondary antibody into a dark humidified chamber.
- ❖ Rise them three times for 10 min with PBS 1X in the dark.
- ❖ Coverslip the slides with the Fluoroshield™ with DAPI mounting medium (Merck, catalog number: slcc8448).

Figure 1A shows MIO-M1 cells stained with anti-GS

antibody (Abcam, Cambridge, United Kingdom, catalog number: ab228590) diluted 1:1,000. The secondary antibody is a Goat Anti-Rabbit IgG H&L (Alexa Fluor® 488) (Abcam, catalog number: ab150077).

Figure 1B shows MIO-M1 cells stained with monoclonal anti-GFAP antibody (Merck, catalog number: G3893) diluted 1:100, after 24 h hypoxia. The secondary antibody is a Goat Anti-Rabbit IgG H&L (Alexa Fluor® 488) (Abcam, catalog number: ab150077).

Primary cultures of isolated Müller cells

Primary cultures are widely used to investigate the molecular pathways involved in both physiological and pathological conditions, while maintaining the functional properties the cells showed within the organ they come from. Moreover, primary cultures allow us to evaluate the direct effects on cells of either synthetic or natural compounds to be used as drugs in therapy. Particularly, isolation of primary Müller cells offers the invaluable possibility to analyze status and responses of the major retinal glia lineage within diseased retinas. For example, it is possible to isolate Müller cells from diabetic animals, OIR mice, retinal degeneration 10 (RD10) mice, glaucoma rat models and so on. Here, we report the protocol to isolate primary Müller cells from the mouse retina according to (10):

- ❖ Dissect mouse retina.
- ❖ Incubate the retina in papain and DNase solution (Worthington Papain Kit Worthington Biochemical, catalog number: K003150).
- ❖ Cut the retina into small pieces and incubate at 37 °C with gentle shaking for 1h until the solution becomes clear.
- ❖ Dissociate the mixture with a 5 mL pipette for 2–3 times.
- ❖ Centrifuge the cellular suspension at 300 Relative Centrifugal Force (RCF) for five minutes at room temperature.
- ❖ Mix the medium (DMEM supplemented with 10% FBS, 1% PS) in a tube with sterile EBSS, reconstituted albumin-ovomucoid inhibitor solution, DNase I solution.
- ❖ Remove the supernatant and resuspend the cell pellet in medium mix.
- ❖ Add the albumin-inhibitor solution and centrifuge at 70 RCF for 6 minutes at room temperature.
- ❖ Remove the supernatant and resuspend the pelleted

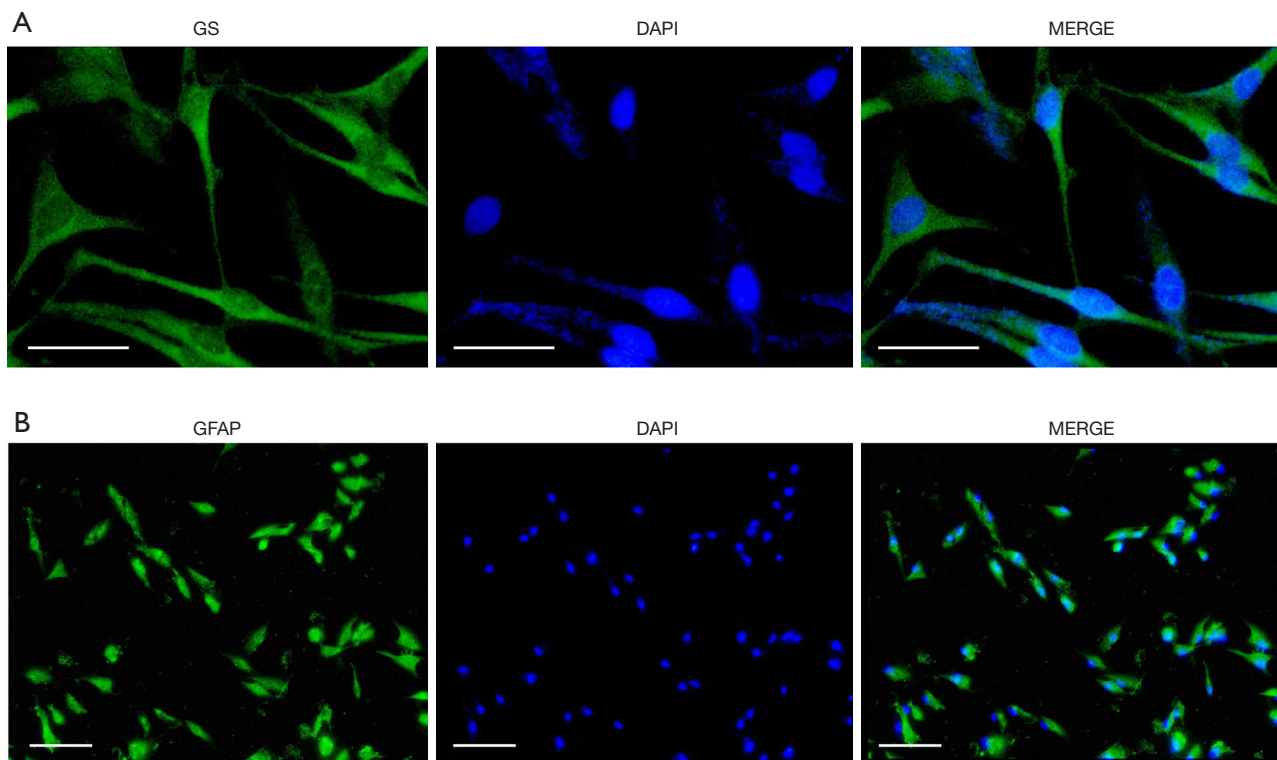


Figure 1 Immunostaining of MIO-M1 cells. (A) Untreated MIO-M1 glia was stained with 1:100 anti-GS antibody; nuclei are DAPI-stained. Scale bars = 50 μm . (B) Twenty-four hours hypoxic MIO-M1 cells were stained with 1:100 monoclonal anti-GFAP antibody; nuclei are stained with DAPI. Scale bars = 150 μm . MIO-M1, Moorfields/Institute of Ophthalmology-Müller 1.

cells in culture medium.

- ❖ Culture the dissociated cells in 0.1% gelatin-coated dish at 5.5% CO_2 and 37 $^\circ\text{C}$.
- ❖ Change the medium every 5 days until cells are confluent.
- ❖ Pass cells at 1:1 ratio to a fresh dish gelatin-coated dish.
- ❖ Adherent Müller glial cells reach more than 95% purity after 2 passages since other retinal neural cells do not survive under such a culture condition.

Once isolated, Müller cells can be roughly recognised based on their typical bipolar morphology: they show two main cellular processes, both arising from the central soma (Figure 2). *In vivo*, their inner process forms an endfoot at the inner limiting membrane which borders the retina to the vitreous humour; instead, their outer process forms close contacts to the photoreceptors (11).

Immunocytochemistry of isolated Müller cells

Once isolated, primary Müller cells can be identified using

GS which is expressed throughout their length (8). Below, we report the immunocytochemistry protocol to perform GS staining on isolated Müller cells, according to (12):

- ❖ Plate primary Müller cells onto glass slides.
- ❖ Remove medium and wash the slides with PBS 1X.
- ❖ Fix them for 20 minutes in 4% paraformaldehyde at room temperature (RT) in a humidified chamber.
- ❖ Block cells with 3% BSA in PBS 1X for 1 h in a humidified chamber.
- ❖ Incubate them with anti-GS antibody overnight at 4 $^\circ\text{C}$.
- ❖ Wash three times with PBS 1X added with 0.1% Tween-20.
- ❖ Incubate the slides with the secondary antibody in a dark humidified chamber.
- ❖ The nuclei can be stained with 1:1,000 4',6-diamidino-2-phenylindole (DAPI) for 5 minutes.
- ❖ Müller glia can be visualized through a confocal microscope.

Figure 3 shows immunocytochemistry on primary Müller

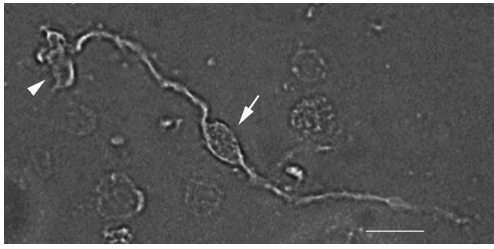


Figure 2 Phase Contrast microscopy of primary mouse Müller cell. White arrow indicates cell body. White arrowhead points out cell endfoot. Scale bar = 50 μm .

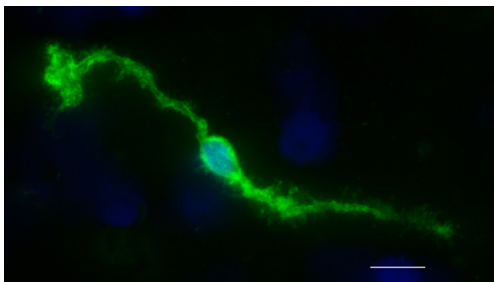


Figure 3 GS staining of primary mouse Müller cell. Murine primary Müller cell was stained with 1:500 anti-GS antibody; nuclei were DAPI-stained. Scale bar = 50 μm . GS, Glutamine Synthetase.

cells isolated from the mouse retina using anti-GS antibody (Abcam, Cambridge, United Kingdom, catalog number: ab228590) diluted 1:500. The secondary antibody is a Goat Anti-Rabbit IgG H&L (Alexa Fluor[®] 488) (Abcam, catalog number: ab150077).

Whole-cell patch clamp on isolated Müller cells

Müller cells are deeply involved in controlling osmotic and ionic homeostasis of retinal extracellular environment. To this purpose, they express a variety of ion channels including the glial Inwardly Rectifying K⁺ (Kir) channels. Kir channels have a high opening likelihood and, thus, a large macroscopic conductance at the resting membrane potential. These channels are open in resting Müller glia and play an important role in the spatial buffering of potassium ions and in retinal osmoregulation (13). Kir 4.1 is the main responsible for the negative resting membrane potential (approximately -80 mV), which is near to the equilibrium potential of K⁺ ions (14). Several homeostatic functions of Müller cells, as potassium buffering itself and neurotransmitter uptake, depend on this negative

membrane potential (1). Müller cells are known to show altered membrane properties in many pathological conditions; whole-cell patch technique is a worthwhile tool to analyze these possible changes in primary Müller cells derived either from diseased animals or treated ones (15). In fact, electrophysiological studies on the retina, particularly on Müller cells, were firstly performed by recording the electroretinogram (ERG) or by using intracellular electrodes or K⁺-selective electrodes; these methods only allowed to draw indirect conclusion about Müller cells physiology, for example by observing alterations in the ERG following blockage of glial K⁺ conductance. Instead, whole-cell patch clamp technique enables a more specific investigation of the functionality of channels and receptors on individual cells. This technique was used for investigating Müller cell functions involving electrophysiological properties in different vertebrate species (9). Importantly, whole-cell patch clamp technique can be used to record current signals from different parts of a neuron as well as from a small network of interconnected neurons. Up to date, whole-cell patch clamp recordings have been performed on different neuronal cell types, including retinal ones (16,17).

Below, we report the protocols to perform patch clamp on primary Müller cells isolated from mouse and from rat:

- ❖ To perform patch clamp recordings from Müller cells isolated from mouse, use borosilicate glass patch pipettes (GB150-8P, Science Products, Hofheim, Germany). Their resistance should be 5–7 M Ω when filled with the intracellular solution reported in (15). To perfuse the recording chamber, use the extracellular solution as described in (15). Record membrane currents of isolated Müller cells in the voltage clamp mode, according to (15).
- ❖ To perform patch clamp recordings from Müller cells isolated from rats, use a patch clamp amplifier (EPC10; HEKA Elektronik, Lambrecht, Germany). The resistance of pipette is 8–10 M Ω when filled with recording solution described in (18). The content of external medium is reported in (18). Kir currents can be evoked through hyperpolarized voltage pulses from a holding potential of -80 mV in increments of 20 mV, according to (18).

Single channel recordings

Single channel recording can be performed on Müller cells in order to specifically examine single-channel properties, as the ones of a Kir4.1 channel, for example. Single-channel patch recordings can be carried out with borosilicate

glass pipettes. The content of both the internal solution contained in pipettes, and the bathing solution are reported in (19). Data must be recorded at 5 kHz and low-passed at 1 kHz using an Axon 200B amplifier, according to (19).

Discussions

In summary, both MIO-M1 cells and isolated Müller cells represent valuable *in vitro* model systems to investigate biological, molecular and electrophysiological properties of a fundamental component of retina. The glial retinal cells, either in healthy or pathological condition. The choice of the model depends on the experimental settings and requirements. Indeed, primary cultures are limited by restricted lifespan since cells, once isolated, undergo senescence and death: no long-lasting studies can be performed on them, differently from continuous MIO-M1 cell line. However, primary Müller cells can be directly isolated from disease animal models, also upon *in vivo* treatment of the models with drugs to be tested.

Acknowledgments

The authors would like to thank Prof. Dario Rusciano (Sooft Italia, Catania, Italy), Prof. Massimo Dal Monte (University of Pisa, Italy) for introducing us into the interesting topics concerning retinal studies. We are grateful to Dr. Maurizio Cammalleri (University of Pisa, Italy) for his expert assistance in the immunocytochemistry and electrophysiological fields.

Funding: None.

Footnote

Provenance and Peer Review: This article was commissioned by the Guest Editor (Dario Rusciano) for the series “Preclinical Models in Ophthalmic Research” published in *Annals of Eye Science*. The article has undergone external peer review.

Conflicts of Interest: Both authors have completed the ICMJE uniform disclosure form. (available at <https://dx.doi.org/10.21037/aes-21-36>). The series “Preclinical Models in Ophthalmic Research” was commissioned by the editorial office without any funding or sponsorship. The authors have no other conflicts of interest to declare.

Ethical Statement: The authors are accountable for all

aspects of the work in ensuring that questions related to the accuracy or integrity of any part of the work are appropriately investigated and resolved.

Open Access Statement: This is an Open Access article distributed in accordance with the Creative Commons Attribution-NonCommercial-NoDerivs 4.0 International License (CC BY-NC-ND 4.0), which permits the non-commercial replication and distribution of the article with the strict proviso that no changes or edits are made and the original work is properly cited (including links to both the formal publication through the relevant DOI and the license). See: <https://creativecommons.org/licenses/by-nc-nd/4.0/>.

References

1. Reichenbach A, Bringmann A. New functions of Müller cells. *Glia* 2013;61:651-78.
2. Li X, Liu J, Hoh J, et al. Müller cells in pathological retinal angiogenesis. *Transl Res* 2019;207:96-106.
3. Limb GA, Salt TE, Munro PM, et al. In vitro characterization of a spontaneously immortalized human Müller cell line (MIO-M1). *Invest Ophthalmol Vis Sci* 2002;43:864-9.
4. Rossino MG, Lulli M, Amato R, et al. Oxidative Stress Induces a VEGF Autocrine Loop in the Retina: Relevance for Diabetic Retinopathy. *Cells* 2020;9:1452.
5. Schmittgen TD, Livak KJ. Analyzing real-time PCR data by the comparative C(T) method. *Nat Protoc* 2008;3:1101-8.
6. Agnarelli A, Natali M, Garcia-Gil M, et al. Cell-specific pattern of berberine pleiotropic effects on different human cell lines. *Sci Rep* 2018;8:10599.
7. Garcia-Gil M, Turri B, Gabriele M, et al. Protopine/Gemcitabine Combination Induces Cytotoxic or Cytoprotective Effects in Cell Type-Specific and Dose-Dependent Manner on Human Cancer and Normal Cells. *Pharmaceuticals (Basel)* 2021;14:90.
8. Riepe RE, Norenburg MD. Müller cell localisation of glutamine synthetase in rat retina. *Nature* 1977;268:654-5.
9. Grosche J, Härtig W, Reichenbach A. Expression of glial fibrillary acidic protein (GFAP), glutamine synthetase (GS), and Bcl-2 protooncogene protein by Müller (glial) cells in retinal light damage of rats. *Neurosci Lett* 1995;185:119-22.
10. Liu X, Tang L, Liu Y. Mouse Müller Cell Isolation and Culture. *Bio Protoc* 2017;7:e2429.
11. Pannicke T, Ivo Chao T, Reisenhofer M, et al.

- Comparative electrophysiology of retinal Müller glial cells-A survey on vertebrate species. *Glia* 2017;65:533-68.
12. Wang J, He C, Zhou T, et al. NGF increases VEGF expression and promotes cell proliferation via ERK1/2 and AKT signaling in Müller cells. *Mol Vis* 2016;22:254-63.
 13. Newman EA, Frambach DA, Odette LL. Control of extracellular potassium levels by retinal glial cell K⁺ siphoning. *Science* 1984;225:1174-5.
 14. Newman EA. Membrane physiology of retinal glial (Müller) cells. *J Neurosci* 1985;5:2225-39.
 15. Reisenhofer M, Pannicke T, Reichenbach A, et al. Characteristics of Müller glial cells in MNU-induced retinal degeneration. *Vis Neurosci* 2016;33:E013.
 16. Petrucci C, Resta V, Fieni F, et al. Modulation of potassium current and calcium influx by somatostatin in rod bipolar cells isolated from the rabbit retina via sst2 receptors. *Naunyn Schmiedebergs Arch Pharmacol* 2001;363:680-94.
 17. Matsumoto H, Sugio S, Seghers F, et al. Retinal Detachment-Induced Müller Glial Cell Swelling Activates TRPV4 Ion Channels and Triggers Photoreceptor Death at Body Temperature. *J Neurosci* 2018;38:8745-58.
 18. Yang Z, Huang P, Liu X, et al. Effect of adenosine and adenosine receptor antagonist on Müller cell potassium channel in Rat chronic ocular hypertension models. *Sci Rep* 2015;5:11294.
 19. Ruiz-Ederra J, Zhang H, Verkman AS. Evidence against functional interaction between aquaporin-4 water channels and Kir4.1 potassium channels in retinal Müller cells. *J Biol Chem* 2007;282:21866-72.

doi: 10.21037/aes-21-36

Cite this article as: Lucchesi M, Marracci S. *In vitro* models of retinal diseases. *Ann Eye Sci* 2021.